LOAD FREQUENCY REGULATION IN MULTI-SOURCE MULTI-AREA POWER SYSTEM USING MEMETIC OPTIMIZATION STRATEGY WITH ENERGY STORAGE DEVICE

A Thesis Submitted For the Award of the Degree of

DOCTOR OF PHILOSOPHY

in

Electrical Engineering

By

ARDHALA BALA KRISHNA

11815013

Under the Supervision of

Dr. Sobhit Saxena
Professor
School of Electronics and Electrical Engineering
LOVELY PROFESSIONAL UNIVERSITY
Phagwara, 144402

Dr. Vikram Kumar Kamboj
Professor
School of Electronics and Electrical Engineering
LOVELY PROFESSIONAL UNIVERSITY
Phagwara, 144402

LOVELY PROFESSIONAL UNIVERSITY

PUNJAB

DECEMBER 2022

Dedicated to my Grand parents

Ardhala Radha Krishna Murthy and Ardhala Seetha Mahalakshmi

&

Parents

Ardhala Siva Ramaiah and Ardhala Sivamma

DECLARATION

I declare that the thesis entitled "LOAD FREQUENCY REGULATION IN MULTI-SOURCE MULTI-AREA POWER SYSTEM USING MEMETIC OPTIMIZATION STRATEGY WITH ENERGY STORAGE DEVICE" has been prepared by me under the supervision of Dr. Sobhit Saxena, Professor, School of Electronics and Electrical Engineering, Lovely Professional University, India and Dr. Vikram Kumar Kamboj, Professor and Head of Department, School of Electronics and Engineering, Lovely Professional University, India. is an authentic record of my own work carried out during a period from August 2018 to December 2022. No part of this thesis has formed the basis for the award of any degree or fellowship previously.

A. Bala Krishna
School of Electronics and Electrical Engineering
Lovely Professional University, Punjab
Phagwara –144411
Place: Phagwara
Date: 17th December 2022

THESIS CERTIFICATE

This is to certify that the thesis entitled "LOAD FREQUENCY REGULATION IN MULTI-SOURCE MULTI-AREA POWER SYSTEM USING MEMETIC OPTIMIZATION STRATEGY WITH ENERGY STORAGE DEVICE" submitted by **ARDHALA BALA KRISHNA** to the Lovely Professional University, Punjab for the award of the degree of Doctor of Philosophy is a bonafide record of research work carried out by his under my supervision. The contents of this thesis, in full or in parts, have not been submitted to any other Institute or University for the award of any degree or diploma.

Dr. Sobhit Saxena
Professor,
School of Electronics and Electrical Engineering
LOVELY PROFESSIONAL UNIVERSITY
Phagwara, 14411
Date: December 2022

Dr. Vikram Kumar Kamboj
Professor,
School of Electronics and Electrical Engineering
LOVELY PROFESSIONAL UNIVERSITY
Phagwara, 144411
Date: December 2022

ACKNOWLEDGEMENTS

This thesis would not have been possible without the support of glorious people who motivated me during my doctoral study. I am thankful from my bottom of my heart toward the numerous persons who assisted me while conducting this study.

First of all, I would like to thank my supervisors, **Dr. Sobhit Saxena, Professor, School of Electronics and Electrical Engineering, Lovely Professional University, India, and Dr. Vikram Kumar Kamboj, Professor and Head of the Electrical Department, School of Electronics and Electrical Engineering, Lovely Professional University, India** for their worthy guidance, support, and suggestions, in every step of this research project during my Ph.D. journey. Dr. Sobhit Saxena and Dr. Vikram Kumar Kamboj has an optimistic personalities with helpful nature, they always made them self-ready to clarify my doubts and it was a great opportunity to work under their supervision. They always shed light whenever I was feeling stuck in my path of research ambitions.

I would like to express my gratitude toward the entire Lovely Professional University family for providing suitable infrastructure and environment for completing my research work in a time-bound manner. Also, I like to thank the Division of Research & Development and School of Electronics and Electrical Engineering for their help and encouragement in my entire Ph.D. journey.

I feel heartfelt thanks to my Parents for their blessings. I am really thankful to my wife Ardhala Sri Dhana Lakshmi, who has always been encouraging and co-operative to me during the difficult period of my research work. I feel a sense of apology to my daughters Lishitha Naga Sri and Chaithreshwari to whom I could not provide their due share of love, attention, and proper care during the period of research work.

Finally, I like to thank almighty God who helped me to achieve such a big milestone.

Date: 17th December, 2022 **A. Bala Krishna**

ABSTRACT

Frequency regulation is the most critical aspect in the electric power system due to rapidly increasing power requisition demand, because of its growing size, formation of microgrids, new emerging uncertainties, evolving Renewable Energy Sources (RESs), environmental constraints, and the complexity of power system. Frequency fluctuations are caused by a sudden mismatch among electric power consumption and origination, inadequate generation reserve, poor synchronizing of protection and control units, or shortcomings in equipment response. The regulation of energy interchanges/origination and frequency with near control regions as per scheduled limits is termed as "automatic generation control" (AGC) and "load frequency regulation" (LFR).

With the passage of time, existing modern interlinked power systems migrated to deregulated manner. Deregulation in the existing conventional electric power systems recreates the energy companies around the globe and novel business companies, like TRANSCOs (energy transferring units), DISCOs (energy distribution units), independent system operator (ISO) and GENCOs (energy origination or generation units), have been formed in an open competitive market. The novel and augmented units have their responsibilities of maintaining protection, stability, and assurance under modest and regulation environment. However, introduction of novel units in the established electric power system network complicates the operation of the entire network. In today's novel electrical market scenario, frequency regulation has become hugely essential to ensure power security and stability. Additionally, increased the integration of the distributed generators (small-hydro, PV, etc.) into the established electric networks poses to sever frequency stabilizations issues, raising concerns among power system regulators and operators. Switching RES with established originating units (nuclear – gas – hydro – thermal) minimizes the inertia of the electric power system. Thus, the frequency stabilization became an important factor in the ages of renewable energy and smart grid, that should be resolved to integrate more RES premised origination/generation into the existing electric power system networks. The analysis on LFR challenges in modern and deregulated power system (DPS) networks are reported. These issues in novel electric DPS motivated investigators to aim at efficacious control methodologies for ensuring LFR in the DPS.

Investigators all over the globe attempting to resolve the LFR challenge in the electric power system network operation utilizing various optimization control methodologies. Majority of the modern LFR methodologies facilitate model premised controllers that are extremely premise models are taken to consideration, and thus are unsuitable for huge size electric power system networks with undefine, uncertain, and non-linearities parameters. As a result, the implementation of advanced LFR networks that are adaptive and flexible among modern ones seems to be a tempting methodology.

Various heuristics and conventional regulation methodologies are recent times applied to resolve the established LFR challenge in the electric power system. In recent times different soft computing methodologies premised various controllers and optimizers that have been developed by several investigators to stabilize the LFR of the electric power system network. The existing works depicts the kind of evolutionary optimizer methodologies and controllers applied to optimize the parameters of the controllers, have a significant impact on a variety of features of modern and DPS network.

In addition, the energy storage devices (ESD) have a huge promise towards assisting LFR in the electric power system by keeping the power balance and ensuring the grid frequency under abrupt interruptions. In recent years, significant progress has been done in the field of frequency response delivery using ESD. Existing studies depicts the ESD on flexible AC transmission system's (FACTS) like Capacitive Energy Storage (CES), Redox Flow Batterie's (RFB), and Superconducting Magnetic Energy Storage (SMES) seems to be very efficacious in dampening the unpredicted load instabilities by absorbing or adding the requisite level of power into the grid network. ESD has been mostly used, due to its rapid reaction capability, and facilitate electric power system frequency regulation in a considerably shorter timescale than modern network resources and thus, fulfil the LFR requisition.

Furthermore, utility generation is changing away from huge, centralized power origination units and toward a variety of small-scale plants and RESs. Recent days, RESs origination is proving to be a very promising source of energy. However, the intermittency nature of RESs such as wind and PV (solar) creates significant economic and technical challenges that must be addressed. For improving system overall performance and dependability, backup in the form of energy storage is essential to overcome RESs intermittency. Energy storage can be used to counteract the

unpredictable nature of renewable energy generation. One of the most adaptable and promising technological is the battery energy storage system. In general, when the electricity from the RESs varies, the batteries of Electric vehicles (EVs) (EVs with batteries on the wheels) can be used to supply energy. As a result, EVs provide LFR and power balance among the interlinked DPS. EVs assist to minimize CO_2 emissions by being a clean source of energy.

Recent research from the investigators indicates that the evolutionary optimization search methodologies, the kind of controller applied to optimize the parameters of the controller, and ESD have a role in the frequency stability of the complex electric power systems. The CES unit in conjunction with a thyristor-controlled phase shifter (TCPS) behavior and furtherly, EV with PV source behavior also studied in the LFR of conventional power systems. As a result, it's crucial to examine their behavior in multisource, multi-area DPS. In addition, there has been no attempt to develop the hybrid memetic Slime mould-pattern search optimizer (SMA-PS) for optimizing the gain parameters of the proportional -integral (PI) controller for two area hydro-thermal-gas (H – T – G) multi-sources till now. As a result, in this research, an effort was made to investigate LFR in two area DPS using a hybrid memetic HHO-PS optimizer tuned PI controller, and hybrid memetic SAM-PS optimizer tuned PI controller with CES/TCPS and EV/PV units.

This research includes the LFR in multi area, tie line interlinked DPS and necessity to the global markets in aspects of complexity of the challenge, minimizing settling time and time complexity of the system. LFR has a vital role in DPS network for providing better quality of power generation and distribution for the industries and urban regions, this attracts people from last few decades to do research on LFR challenge. Additionally, discusses the basic theme and societal need of AGC and LFR challenges effect at modern market.

This chapter explores the recent outcomes and advancements in LFR of the DPS. The investigators are previously implemented several control methodologies and invented various metaheuristics, moderate algorithms, and hybrid metaheuristics, and additionally several ESD and FACTS controllers are implemented and integrated to balance the LFR of the DPS. This chapter included the comprehensive report on previous academician’s report with advancements and demerits on several optimizers with the effect of ESD and FACTS units. Additionally, effect of EV with RES on the DPS also discussed.

This chapter suggested a different possible solutions of hybrid memetic optimization search algorithms to resolve the LFR of the multi area tie line interlinked DPS network. In recent times various methodologies are introduced to simplify and mitigate the time complexity of the LFR of multi area tie line interlinked DPS network. but the existing methodologies still must improve for the best possible outcomes, and few of them are offering local optimum trapping challenges. As per No free lunch theorem (NFL), each optimizer doesn't offer and suitable to every optimization challenge. As per NFL, new methodologies need to augment to resolve the complex optimal problems. In this chapter hybrid memetic optimizers are introduced as a solution to resolve the complexity in a LFR challenge, and a hybrid memetic Harris hawks and pattern search (HHO-PS), and Slime mould and pattern search (SMA-PS) optimization algorithms are suggested and discussed in detail. Here, to form hybrid memetic HHO-PS and SMA-PS optimizers, firstly Harris hawk's optimizer (HHO) solution was carried out and at the termination end pattern search (PS) operators was integrated to carry the solution of HHO, and secondly, Slime mould algorithm (SMA) solution was carried out and at the termination end pattern search (PS) operators was integrated to carry the solution of SMA. To test the efficacy of the suggested HHO-PS and SMA-PS optimizers, heuristics procedure is applied to find the efficacy of the suggested optimizers. The suggested optimizers are evaluated with the help of twenty-three benchmarks and nine constrained optimal engineering designs. And later the outcomes are analyzed with classic HHO, SMA and other novel augmented recent search algorithms. The outcomes reveals that the hybrid memetic HHO-PS optimizer performs effective results over classic HHO and SMA optimizers and other metaheuristics optimizers. Overall, hybrid memetic SMA-PS optimizer performs efficacious results over hybrid memetic HHO-PS optimizer in terms of fastest convergence rate, and statistical outcomes. As a result, hybrid memetic HHO-PS optimizer and hybrid memetic SMA-PS optimizer are carried out as a solution to LFR multi area network.

The ensuring chapter focuses on the solution to the LFR of the two-area tie line interlinked deregulated power system (DPS). This chapter expresses the hybrid memetic HHO-PS and SMA-PS optimizers used to tune the proportional integral (PI) controller and, to resolve the LFR of the two-area hydro – thermal – gas (H – T – G) origination sources with tie line interlinked DPS to get the optimal gain values of the designed PI controller to meet the load demand at different contract scenarios. Here, to form hybrid memetic SMA-PS optimizer, SMA and PS are combined recursively. A non-convex, mixed integer, and non-linear of the LFR of DPS optimization

challenge is tackled by using hybrid memetic HHO-PS and SMA-PS optimizers for two-area H – T – G origination source. By performing LFR of the two-area system by using suggested hybrid memetic optimizers tuned PI controller and other classic HHO, and SMA tuned PI controller's, the efficacy of the hybrid memetic SMA-PS optimizer tuned PI controller was confirmed. According to the comparative analysis at POOLCO, Bilateral, and Contract violation methods, the hybrid memetic SMA-PS tuned PI controller outperforms other hybrid memetic HHO-PS tuned PI controller and classic HHO, and SMA optimizers tuned PI controller in terms of settling time of the tie line error, frequency fluctuation, and six origination sources (GENCO 1 – 6). And also, To prove the robustness and efficacy of suggested hybrid memetic HHO-PS and SMA-PS optimizers controller with the developed DPS network, its dependent factors of *governor* time constant (T_{sg}) and *inertia* constant H, which leads to change the load constant (T_{ps}) are regularized from nominal values in the range of $\pm 25\%$. And the analysis reveals that the suggested hybrid memetic SMA-PS premised PI controller outperforms the other.

In the next chapter, hybrid memetic SMA-PS optimizer tuned PI controllers are extended to resolve LFR of the two-area H – T – G origination sources with tie line interlinked DPS with integrating capacitive energy storage (CES) in each area and thyristor-controlled phase shifter (TCPS) at the tie line of the DPS. Here, CES is used to boost the performance of DPS, the frequency fluctuation at each area utilized as an input to the CES. Hence, CES stores the exceeding energy in grid system of each area and during unexpected load disruption, it discharges, and it banked energy into the grid. TCPS is used as a tie line error control device at the interlinked tie line in DPS. TCPS is utilized to dampening the transmission line power deviations from inter area oscillations among tie line interlinked LFR of the DPS. By using the TCPS, it provides the DPS maximum dependability and consistency by allowing for available power scheduling under a variety of (changing) operating conditions. Simulation outcomes reveals that the suggested, hybrid memetic HHO-PS and SMA-PS optimizers tuned PI controllers have a perspective outcome to resolve the LFR of two area interlinked DPS with integrating CES/TCPS units. From the outcomes of the LFR of two area interlinked DPS, hybrid memetic SMA-PS optimizer tuned PI controller performs greater efficacious results over hybrid memetic HHO-PS, classic HHO, and SMA optimizers tuned PI controllers in terms of the settling time of the tie line error, frequency fluctuation, and six origination sources (GENCO 1 – 6). Additionally, sensitivity analysis was carried out for the

developed DPS network with CES, dependent factors of H and Tsg parameters are changed from its nominal value as ±25% to prove the robustness and excellence of the suggested electric system. The analysis validated the developed DPS network with CES performs stable performance and the suggested hybrid memetic SMA-PS premised PI controller depicts better efficacious results than other.

The following chapter ensures the hybrid memetic HHO-PS and SMA-PS optimizers tuned PI controllers furtherly extends to solve the developed LFR of two area interlinked DPS with integrating CES/TCPS units and additionally, PV is added as an energy originating source, and EV as the energy origin and restoring unit at each area of the LFR of two area interlinked DPS. Here, PV unit included as a RES, but the integration of the PV in each area causes frequency fluctuation of the grid at DPS network. And therefore, EV is introduced as a RES causing fluctuation control unit. Here, EV having the two inputs, first one is the suggested optimizer tuned PI controller as input signal and second is the fluctuation of each area DPS network. Hence, the simulation outcomes depict the suggested optimizers have prospective to resolve the two area LFR of the DPS with PV/EV sources as energy origination and storing/discharge units. And, it has established that hybrid memetic SMA-PS optimizer tuned PI controller outperforms the hybrid memetic HHO-PS, classic HHO, and SMA optimizers tuned PI controllers in terms of time complexity and settling time. Furthermore, sensitivity analysis was done by exchange the parametric values of H and Tsg as ±25%, to prove the robustness and stability of the developed DPS network with CES and EV. And hence the simulation outcomes proved that the proposed hybrid memetic SMA-PS optimized PI regulator outperforms other.

All the findings and major conclusions of the research conducted for the developed study are obtained from the above. The inclusion and utilization of the hybrid memetic HHO-PS and SMA-PS optimizers tuned PI controllers for the two-area tie line interlinked DPS network with CES/TCPS and PV/EV units' studies are systematically summarized and presented. Suggestions for the future investigation work also noted.

TABLE OF CONTENTS

LIST OF FIGURES

LIST OF TABLES

LIST OF ABBREVIATIONS AND SYMBOLS

LFR	Load Frequency Regulation
CES	Capacitive Energy Storage
TCPS	Thyristor Controller Phase Shifter
PV	Photo Voltaic
H – T – G	Hydro, Thermal, And Gas
HHO	Harris Hawks Optimizer
SMA	Slime Mould Algorithm
PS	Pattern Search Optimizer
HHO-PS	Harris Hawks Optimizer – Pattern Search Algorithm
SMA-PS	Slime Mould Algorithm – Pattern Search Algorithm
EV	Electric Vehicle
MA	Metaheuristic Algorithm
RES	Renewable Energy Source
AGC	Automatic Generation Control
FACTS	Flexible Alternating Current Transmission System
FP-PID	Fuzzy-Proportional – Proportional Integral Derivative Controller
FPIDN – FOPIDN	Fuzzy-Proportional Integral Derivative Including Filter (PIDN)-Fractional Order PIDN Controller
BFA	Bacterial Foraging Algorithm
ANFIS	Adaptive Neuro-Fuzzy Inference System
GRC	Generation Rate Constraint
GSA	Gravitational Search Algorithm
GWO-PS	Grey Wolf Optimizer – Pattern Search Optimizer
2DOF-PID	2-Degree Order of Freedom – Proportional Integral Derivative Controller
PSO-PS	Particle Swarm Optimizer – Pattern Search Optimizer
PSO-FA-GSA	Particle Swarm Optimizer – Fruitfly Algorithm – Gravitational Search Algorithm
PI	Proportional Integral Controller
PID	Proportional Integral Derivative Controller
Hgfa	Hybrid Gravitational Search Algorithm – Fruitfly Algorithm

JO	Jaya Optimizer
TID	Tilt Integral Derivative Controller
GA-PSO	Genetic Algorithm Integrated With PSO
SCA	Sine Cosine Algorithm
ES	Energy Storage
SMES,	Superconducting Magnetic Energy Storage
UPFC	Unified Power Flow Controller
SSSC	Static Synchronous Series Compensator
IPFC	Inter Line Ppower Flow Controller
MVO	Multi Verse Optimizer
UC	Ultra-Capacitor
CAES	Compressed Air Energy Storage
GRB	Generation Rate Band
MAPS	Multi Area Power Sysetm
WOA	Whale Optimization Algorithm
FOFPID	Fractional Order Fuzzy PID
TLBO	Teacher Learning Based Algorithm
RFB	Redox Flow Battery
FLC	Fuzzy Logic Controller
AEO	Artificial Ecosystem Optimizer
PEV	Parking Electric Vehicle
WDO	Wind-Driven Optimization
STPP	Solar-Thermal Power Plant
FPIC	Fuzzy Premised PI Controller
BELBIC	Brain Emotional Learning-Based Intelligent Controller,
BM	Benchmarks
PSA	Photon Search Algorithm
TSA	Tunicate Swarm Algorithm
PO	Political Optimizer
ABC	Artificial Bee Colony Optimizer
SSA	Social Spider Algorithm

BRO	Battle Royal Optimizer
EO	Electro Search Optimization
VCS	Virus Colony Search
TSO	Transient Search Optimizer
CSS	Charged System Search
DGCO	Dynamic Group Based Cooperative Optimizer
BIA	Billiards Inspired Optimization
EFO	Electromagnetic Filed Optimization
LFD	Lévy Flight Distribution Optimizer
GBO	Gradient Based Optimizer
TS	Tabu Search
EP	Evolutionary Programming
MFO	Moth Flame Optimizer
HS	Harmony Search
GSO	Group Search Optimizer
CS	Cuckoo Search
ISA	Interior Search Algorithm
BBO	Biogeography Based Optimization
AMO	Animal Migration Optimization
CFO	Central Force Optimization
TSA	Tree Seed Algorithm
SFS	Stochastic Fractal Search
ESA	Emperor Penguin and Salp Swarm Algorithm
PSOSCALF	Particle Swarm Optimizer – Sine Cosine Algorithm – Levi Flight
OAGO	Orthogonally Designed Adapted Grasshopper Optimization
IFDOA	Improved Fitness-Dependent Optimizer Algorithm
SA-DABC	Self-Adaptive Differential Artificial Bee Colony
AEBO	Artificial Ecosystem-Based Optimization
ICLBO	Imperialist Competitive Learner-Based Optimization
RSHO	Refined Selfish Herd Optimizer
HC- PSOGWO	Hybrid Crossover Oriented PSO And GWO

MSESCA	Multi Strategy Enhanced Sine Cosine Algorithm
I-GWO and Ex-GWO	Incremental GWO and Expanded GWO
MHTSA	Multi-objective Heat Transfer Search Algorithm
EP	energy of prey
WSA	Wind stride algorithm
UM	uni-modal
MM	multimodal
FD	fixed dimensions
CE	Constrained engineering
SHO	Spotted hyena optimizer
HGSO	Henry gas solubility optimizer
MBA	Mine blast algorithm
ACO	Ant colony optimizer
DPS	Deregulated power system
DISCOs	Distributing company's
POOLCO	An individual power pool company
GENCOs	Generation company's
SOC	State of charge
DPM	Disco Participation Matrix
CPF	Contract participation factor
APF	Area participation factor
ISO	Independent system operators
ACE	Area control error
ITAE	Integral Time Absolute Error

LIST OF SYMBOLS

B_1, B_2	Frequency bias constant of area-1 & 2
δ_1^0, δ_2^0	Power angles of equivalent machines of the two areas.
$\Delta\phi$	Angle of the phase shifter.
k_ϕ	Stabilization gain
T_{gh}	Electric governor gain
K_i, K_p	Integral and proportional gains of the system
Δp_{D2}, Δp_{D1}	Local area-2 & area-1 loads
Δp_{l4}, Δp_{l3}, Δp_{l2}, Δp_{l1}	Per unit (pu) loads of DISCOs 1 to 4.
Δp_{Gci}	Produced steady state set out limit power
k_r	Gain constant
T_r	Turbine time constant
T_{sg}	Governor time constant.
T_{rs}	Hydro turbine speed governor reset time
T_{rh}	Hydro turbine speed governor transient droop time constant
T_{cd}	Compressor dicharge system time
X_g , Y_g	Governor servo time and droop time constants
B_g, Cg	Valve positioner time constants
T_f	Fuel dynamics of turbine
T_{cr}	Turbine compressor discharge
$\Delta F_i(s)$	i^{th} area frequency fluctuation
T_w	Time constant for water
T_{TCPS}	Time constant of TCPS device
K_{ces}	CES gain constant
T_{ces}	CES time constant
T_{12}	Tie line synchronizing coefficient
Δp_{Gi}	*i*th GENCO generated power change
Δp_{Li}^{uc}	Unagreed DISCO of the *i*th area power demand
Δp_{lj}	Demand load of jth DISCO

λ, Y, X, Z	Uncontracted, state, control, and disturbance load vectors
f_{ul}	Upper limit of EV dead band
f_{ll}	Lower limit of EV dead band
ΔP_{AG}^{max}	Maximum power outputs of electric vehicle fleets
ΔP_{AG}^{min}	Minimum power outputs of electric vehicle fleets
R_{AG}	Aggregate model droop coefficient
K_{EVi}	EV gain value
T_{EVi}	Battery time constant of EV
ΔP_{EVi}	Incremental generation change of EV
N_{EV}	Number of electric vehicles
K_{PV}	Gain value of PV
T_{PV}	Time constant of PV
ϕ	Solar insolation in kw/m^2
S	Size of the PV array in m^2
T_a	Ambient temperature in °C
$A_P(x)$	Average position of hawks
H	Size of the hawks
A_j	Location of the hawks
$A(x+1)$	Following iteration of the hawk's position vector
A_{rand}	One of the existing hawks was chosen at random.
A_{rabbit}	Prey position (best agent).
t_1, t_2, t_3, t_4, and R	Random numbers within [0, 1].
D, B_{UB}, B_{LB}	Dimension, upper and lower bounds of the variables
x, D	Iteration counter, Max. iterations
EP_0, EP	Initial state of energy, escaping energy of prey
$A(x)$	Current position vector of the hawks.
LF	Levi's flight
$\overrightarrow{vc}$ and $\overrightarrow{vb}$	Parameters values of slime mould
$\overrightarrow{W}$	Slime Mould weight

$\vec{S}$	Slime Mould location
$\overrightarrow{S_A}$ and $\overrightarrow{S_B}$	Two individuals chosen at random from the population in Slime Mould,
$\overrightarrow{S_b}$	Location of the individual with the maximum odour concentration
DF	The best fitness obtained in all iterations by Slime Mould
$SmellIndex$	The sequence of fitness value of Slime Mould
r	Replicates the random value
wF	Replicates the worst fitness value

LIST OF PUBLICATIONS AND PARTICIPATING CONFERENCES FROM THE THESIS

1. LIST OF PUBLICATIONS

[1] A. B. Krishna, S. Saxena, and V. K. Kamboj, "A novel statistical approach to numerical and multidisciplinary design optimization problems using pattern search inspired Harris hawks optimizer," *Neural Comput. Appl.*, 2021, doi: 10.1007/s00521-020-05475-5.

[2] A. Bala Krishna, S. Saxena, and V. K. Kamboj, *hSMA-PS: a novel memetic approach for numerical and engineering design challenges*, no. 0123456789. Springer London, 2021.

[3] A. B. Krishna, S. Saxena, V. K. Kamboj, and C. Verma, "A memetic metaheuristics search algorithm for load frequency regulation in multi area power system," *2020 Int. Conf. Decis. Aid Sci. Appl. DASA 2020*, pp. 163–167, 2020, doi: 10.1109/DASA51403.2020.9317189.

[4] A. B. Krishna, S. Saxena, and V. K. Kamboj, "Mathematical Formulation of Load Frequency Control for Multi-area Multi-source Realistic Power System Considering Energy Storage Devices," 2021.

2. LIST OF CONFERENCES ATTENDED

S.NO	CONFERENCE NAME	YEAR OF PARTICIPATION
1	International conference on Advances in Sustainable Technologies (ICAST 2020), 2020, LPU, Punjab	2020
2	International Conference on Decision Aid Sciences and Application (DASA), 2020, BAHRAIN.	2020

Chapter-1

INTRODUCTION

1.1 INTRODUCTION

An electrical system network job is to origin and distribute electrical energy to various users in a reliable and secure way. Consumers are typically categorized into three categories based on the characteristics of distinct consuming units: residential, industry, and commercial. Because of the ever-increasing demand for electric power, the electric power industry has recently faced several problems. This may be addressed by reorganizing industries, which will improve the efficiency and quality of the power system's functioning. The electric utility strives to launch innovative concepts for enhancing services under deregulation, which saves money and improves profit. In India, there are five primary grid systems: Northern grid, Eastern grid, Western grid, and Northeastern grids, as well as the Southern Grid. These grids are linked together using HVDC interlinks, because the flow of electricity between the grids regulated separately, the five grids can function independently.

India's total installed power generating capacity was 3,84,116 MW as of June 06, 2021 (as per (CEA) Central Electricity Authority). The state sector contributes 1,03,876 MW, the central sector contributes 96,837MW, and the private sector contributes 1,83,403 MW. Here, the private sector plays a significant role in increasing India's overall power producing capacity.

Thermal power plants continue to be India's primary source of electric electricity. Oil premised, lignite premised, coal premised, and gas premised power plants are among the thermal power plants. As of June 2021, total thermal (thermal premised power generations are coal, gas, lignite, and diesel) power generation was 2,34,058 MW.

The conventional electrical energy generation target for the years 2021-2022 has been set at 1356 billion units (BU). i.e., a 9.83 percent increase over the previous year's real conventional generation of 1234.608 BU (2020-2021). The conventional generation in 2020-2021 was 1234.608 BU, down from 1250.784 BU in 2019-20, reflecting a 1.29 percent decrease.

As per data from MNRE, on the date of 31-12-2019, 85908.37 MW grid connected RES (Renewable Energy Sources, as per MNRE) cumulative power was available. Although, as of June 2021, total RES power generation was 96,956 MW. From here onwards, we could understand that generation of RES has been increased 11 percent in a short time.

Novel electric power system network consists different energy originating units like hydro, biomass, thermal, nuclear etc. Furtherly, the electric power demand fluctuates regularly in a day. As a result, the originated units should need to meet the load demand regularly and obtain the minimal power fluctuation as possible. The entire process of making the smart decision, is termed as Load Frequency regulation (LFR) and the originating units has been planned to connect to electric system network, is known as matching the power demand.

LFR with respect to electric system optimal process refers to the determining the OFF/ON scheduling of the energy producing units to reduce the power flow fluctuation over a particular time horizon. Power generating units couldn't be turned on promptly to reach and fulfil the electricity demand. Therefore, the electric power origination and absorption need to plan accordingly to meet the origination and load demand for minimizing the negative effects of malfunctions and failures under bad conditions.

1.2 AUTOMATIC GENERATION CONTROL

Automatic generation control (AGC) is a tactic for regularizing the power origin output of numerous generators at separate power origin units in response to changes in the load in an electric power system network. Because an electric system always requires the origination and load be precisely balanced, and generator output must be adjusted often. The system frequency has been used to determine the balance; if it is growing, more power is being created than is being utilized, causing all the machines in the system to accelerate. When the system frequency falls, more demand is placed on the system than the system's instantaneous generating capacity can handle, causing all generators to slow down.

1.3 LOAD FREQUENCY REGULATION

Load–frequency regulation (LFR) is crucial in the design and operation of electric power system network. Any electric system with the basic regulating challenge of matching real energy origination to load, losses are included., is referred to as LFR. By adjusting the generators' energy outputs to fit changeable load demands. In an electrical network, the LFR's goal is to keep grid stability inside limitations and tie-line power (TLP) flows within predetermined tolerances. A well-built and managed electric power system must be able to cope with fluctuations in load and system interruptions, as well as keep proper frequency and voltage while providing a suitable high degree of system reliability.

The set reference range of a network deviates out of its specified value when it is disturbed. As a result, there is an unfavorable deviation from the operating point, such as nominal system frequency and scheduled power transfer to other places.

AGC regulation, excitation position control, and parameter variation/uncertainty control performance and varied load characteristics have all been addressed by various researchers at different times. Since the modern electrical system is so complex, any disturbance might produce large-scale oscillations, ending in a total blackout. Sophisticated controlling approaches such as varying control scheme, structural control, optimal control, resilience, and intelligent control were used to overcome the LFR problem. In general, LFC control strategies as follows:

Primary control

The aim of the primary control is to meet the power origination and demand of load, as a result if the load suddenly changes its prescribed value, the power originating units adjust themselves with increase/decrease of power until the frequency fluctuation settles its nominal value. The following were the operating characteristics

- Automatic energy origination and control system
- Responding time within seconds.

Secondary control

This method is used to balance the energy originating outcomes and demand of load by interchanging the power among various areas through interlinked tie line power and energy absorption/restored FACTS units.

Tertiary control

This control topology has to use manually, to maintain the electric system frequency fluctuation at nominal and acceptable value. At the tertiary end of the LFR of electric system a small-scale energy originating units are connected among tie line and grid to meet the electric system nominal value.

1.4 MULTI-SOURCE POWER SYSTEM

In modern days, a minute's born baby has been starting his/her first exercise with utilization of electricity without her mother feed. Here, situation of human living explains that utilization of electricity and its necessity to industrial and commercial areas. Due to that utilization of large

scale of energy, it requires huge interconnections to the electric power system, which may cause to complexity in the electric system. For power frequency controlling and reducing the size of system previously researchers were introducing multi area power system in deregulation mode. Deregulated electricity networks are often massive in scale, with a vastly complex structure that includes thousands of distribution plants (load centers), producing units, and interconnections.

In a multi area deregulated electric network, each area is interconnected through the tie line of a power system which maintain the frequency errors and voltage fluctuations of each region within inside the reference limit and controlling the inter area TLP exchanges within limits. Previously researchers are incorporated fast energy storage units and various FACTS units to maintain scheduled limits.

Originally, a two-area multi-source electric network is considered and is engaged to optimize for a converted objective function. The comparison is built using various performance standards. Variations in the power frequency in distributed areas are often, controlled with a coordinated multi-area power system in realistic deregulation. High variation of generation poses questionable to the protection frequency management of power systems, especially in terms of shortage of power.

Now-a-days with large scale interconnections, huge nonentities, and bigger proportions the power system networks are renowned. But, in deregulation mode will incredibly rises the energy exchange among areas and modulate the way of interring area power exchanges and the electric network will be employed. The main aim of deregulation is to overcome the monopoly of generation, transmission, distribution, and safeguard of the electric power and create healthy competition. The idea and technique of outlining and operation started over the past decades and reinventing to change and meet the challenges dad by day.

1.5 OUTLINES OF THE DISSERTATION

The current research project aims to investigate novel techniques for describing, extending, and initiating optimal Load Frequency regulation approaches for multiarea issues involving several physical and structural constraints evident in the input-output characteristics of thermal, hydro, and gas generating units. Conventional and non-conventional search techniques are investigated to tackle the multi-area Load Frequency regulation issue. CES with TCPS devices,

which are considered energy storage devices, to stabilize the LFR. Later, to address complexity, an electrical vehicle with a renewable energy source is introduced to the deregulated system.

The memetic optimizer was developed with the combination of global with local search method to avoid the local minima trap of the global optimizer. The present study's work has been structured in this thesis in the following manner.

Chapter-1 introduces the need of electricity for modern day needs, current Indian electricity origination with statistics and inclusion of RES with replacement into the current Indian market originators. And Fundamentals of AGC and LFR, as well as their importance in today's electrical power systems. This chapter looks at LFR strategies at the initial and termination ends of the electric network. Multi source originators in multi area deregulated electric network challenges and necessity in modern electric network. Additionally, declares the outlines of the overall research of the proposed work.

Chapter-2 discusses the several authors/investigators have had a significant impact on the problem of load frequency regulation and automatic generation control in this chapter. Academicians are expected to apply a variety of approaches to a variety of problems, and they can do so effectively. Not only are new optimizers being developed, but hybrid algorithms are also being investigated to address any inefficiencies in current techniques. This chapter looks at a literature review of different approaches that have been successfully used to a variety of problems involving load frequency control. This chapter includes a broad review of recent LFR research articles, as well as the merits and downsides of various algorithms used to solve various types of optimization issues.

Chapter-3 organizes several approaches for resolving the LFR problem. Because LFR is such a large, non-linear, mixed integer problem, the endeavor to find the best schedule of dedicated producing units is energizing. The technique of Load Frequency Control necessitates a continuous matching of resource and requirement in accordance with established operating rules. In this chapter, pattern search inspired Harris hawk’s optimizer (HHO-PS), and Slime mould algorithm integrated with pattern search algorithm (SMA-PS) are examined to resolve twenty-three benchmarks and nine engineering optimal design problems. The comparative outcomes reveals that the proposed SMA-PS algorithm performs superior efficacy than other metaheuristics. The efficiency of the SMA-PS approach will be deliberated in future study for optimal response to many additional industrial issues.

Chapter-4 represents the mathematical modelling, and transfer function model for the two-area hydro, thermal, and gas generating sources with tie line power exchange in a deregulated electric power system was developed. In this model each area consists of two DISCOs with each having power demand of 0.005 pu MW along with three generating units. Overall, the proposed system having four DISCOs and six generating units. Each area having a power demand of 0.01 pu MW. The power system frequency and tie-line power fluctuate and settle with optimization method tuned PI controller in each Area. The proposed SMA-PS algorithm tuned PI controller was evaluated with all possible contract scenarios in a deregulated system. The outcomes are verified with HHO-PS, HHO, and SMA optimizers tuned PI controller, the comparative analysis reveals that the proposed SMA-PS tuned PI controller produces greater results than other optimizers.

Chapter-5 presents the mathematical and transfer function model for the LFR of two area hydro, thermal, and gas generating sources with CES/TCPS units in a deregulated electric power system was developed. The developed system verified with all possible transaction methods. The effect of CES/TCPS units in a deregulated power system was performed and the outcomes reveal that in the form of frequency responses in each area and tie line power exchange frequency changes have been dampen extraordinarily within a short settling time, peak overshoot, and under shoot responses. SMA-PS tuned PI controller method outperforms the other methodologies in a proposed deregulated power system with CES/TCPS units.

Chapter-6 presents the transfer function model of Electric vehicle model has been developed with primary frequency control with battery charger model. And later along EV, PV (solar) cell mathematical model was developed, both are integrated in each area grid. After, integrating EV/PV model in a proposed power system with CES/TCPS units, the frequency response in each area and tie line power oscillations reduced efficiently with compared to previous chapter models. Therefore, SMA-PS tuned PI controller method outperforms the other methodologies in a proposed deregulated power system with integrating EV/PV units.

Chapter-7 summarize the essential findings of the study conducted in preparation for the current thesis. The contributions and use of integrated modern and hybrid methods for LFR of two-area hydro, thermal, and gas producing sources with integrated FACTS devices, as well as the addition of EV/PV to the grid system operation analysis, are given and summarized in detail. There are also several suggestions for future study activities also mentioned.

Chapter-2

LITERATURE REVIEW

2.1 INTRODUCTION

LFR is a significant optimal control issue that is utilized to determine the best time to operate the producing units to satisfy the restriction requirements while also meeting the needed load demand. Over the past few years, LFR has attracted a great deal of researchers. Most researchers have looked at the multi-area DPS network of LFR issue solution. The researchers are eager to use Electric vehicle, renewable energy sources, FACTS regulators, and novel methodology to address the LFR problem. Also, Electric vehicle application takes hottest theme globally to fulfil the universal needs. The researchers are effectively solving challenges by using diverse strategies to a variety of issues. To address any shortcomings in the current methods, effort is being done to discover an efficient DPS network with new algorithms as well as hybrid versions of the algorithms. This chapter examines the literature review of several strategies that have been effectively used to address various tough difficulties, such as the multi area LFR of DPS network with FACTS regulators and EVs problem.

2.2 REVIEW OF LITERATURES

Utility companies require AGC and LFR to properly match the energy needs at any time. Controlling TLP flow is another crucial goal of AGC. A useful indicator of an imbalance among power origination and load is electric network frequency regulation. A variation in electric network frequency regulation will signal a mismatch among the power being created and the power being consumed. These will result in a rise or fall in the turbine's speed. As a result, the electric network frequency regulation will differ from the planned frequency. The LFR of multi area DPS network is configured to organize power temporarily to maintain changes in electric network frequency within predetermined schedule bounds. The literature was done on the eve of the LFR of tie line connected multi area electric system with the energy absorption and restoration nature FACTS units and later with the small-scale energy originated units as RES and Electric vehicle units.

2.2.1 Review of Literatures on Optimization Algorithms with controllers

Rajiv et al., 2021 [1] used Grass hopper optimizer for tuning the parameters of FP-PID controller in three area multi source (hydro, steam, thermal, and wind) electric power system

network. In the light of changing system characteristics and random load disturbance, the proposed method is competitively better, resilient, and stable than other methodologies in terms of settling time.Yogendra et al., 2021 [2] proposed a new control approach to successfully deal the AGC issue of interconnected electric power system network, an Imperialist competitive methodology premised new cascade (FPIDN)-fractional order PIDN (FPIDN-FOPIDN) regulating controller is proposed. With large variations in developed system characteristics, load patterns, and GRC values, the suggested controller demonstrates steady performance. Furthermore, increased GRC results in improved reactions with lower peak deviation and settling time by using the developed controller than existing controller tactics.

Hakimuddin et al., 2020 [3] introduced Bacterial foraging algorithm (BFA) premised PID controller structure to optimize the energy generation in a two area AGC electric power system network. The obtained findings displays that the dynamic responses of a system with a BFA tuned AGC controller are superior to GA premised AGC controller.Rajesh et al., 2019 [4] introduced a fuzzy assisted PID structured controller for AGC of 5 area power systems is tuned using the hIFA-PS method. It has been proven that enhanced FA outperforms original FA. Later the enhanced FA was integrated with the local search Pattern search optimizer to tune the controller's settings. When compared to hIFA-PS tuned I/PI/PID controllers, the hIFA-PS tuned fuzzy aided PID structure provides a substantial improvement in system dynamic response.Prakash et al., 2018 [5] used an ANFIS to regulate the automated load frequency control (ALFC) of a multi-generation hybrid linked power system with six uneven regions. The suggested ANFIS controller outperforms the traditional PI controller and ANN controller for tie-line power and frequency deviation in all six regions of an interconnected hybrid power system when compared to ANN, ANFIS, and PI premised methodologies.

Ali 2020 [6] presented a four area interconnected electric power system network with different contract scenarios having hydro, thermal units with reheat turbine, gas, diesel energy origination power units as energy generating sources. MVCS optimizer premised PID controller used to optimize the application of proposed AGC model. The results show, at various contract methodologies the proposed MVCS optimizer performs superior over other existing heuristics methodologies. Rout et al., 2021 [7] developed four area multi source electric system with GSA premised PID controller. The suggested has reduced overshoot, a faster settling time, and the capacity to efficiently dampen transient oscillation is efficient and durable. GSA-PID controller demonstrated all these characteristics, making it the best LFC design for controlling complicated multi-area interconnections. Hota et al., 2016 [8] introduced

a four area gas, thermal source electric power system network with DE optimizer tuned PID controller. The analysed outcomes demonstrate, DE-PID controller performs superior over GA-PID controller.

Soni et al., 2016 [9] introduces a two area electric system with hybrid GWO-PS tuned 2DOF-PID controller for LFR challenge. The suggested optimised controller performs significantly better in terms of dynamic responsiveness over PSO tuned fuzzy PI, and PSO-PS tuned PI controllers. Soni et al., 2020 [10] presents a hybrid GWO-PS tuned FOPID controller for three area tie line interconnected hydro, thermal units as generating sources in the electric power system network. The obtained results depict proposed hybrid GWO-PS premised FOPID controller performs superiority over hybrid BFOA-PSO-ANFIS and hGWO- PS optimised 2DOF-PID controller methodologies. Chandra et al., 2016 [11] In a deregulated environment, the Firefly algorithm was utilised to optimise a FPID regulating controller with a derivative filter for LFR of a four-area reheat thermal network. According to the findings, the developed controller is durable, and the suggested controller's optimal gains do not need to be reset even when the system is subjected to a broad range of loading conditions and system characteristics.

Gupta et al., 2021 [12] designed a hybrid PSO-FA-GSA optimizer premised PID controller for a two-area hydro, thermal, gas (H – T – G) originating sources tie line integrated electric power system network. The augmented hybrid search optimizer performs greater efficacy in terms of settling time and TLP error over individual FA, PSO, GSA algorithm methodologies. Deepak et al., 2021 [13] augmented a new hybrid memetic GSA-FA optimizer premised PI controller to address the LFR and tie line power flow problems on two area hydro, thermal electric power system network. In these two case studies were performed, when compared to PSO, GA, GSA, and FA methodologies tie line power are reduced by almost 15% in case study I and nearly 50% in case study II when the suggested hGFA methodology is used.

Chittaranjan et al., 2019 [14] developed two versions of modified jaya optimizer with one is linear weight (LW) variation (Scheme-1) and another is a fuzzy variation (Scheme-2). Out these two fuzzy premised JO performs superior over other case. Further, in a multi-area wind integrated power system, modified JO is used to optimise the integral gains of tie-line power and AGC in real time and later, in the New England 39-bus test system, on a real-time embedded platform. During various power system disturbances, it is found that the adaptive Jaya algorithm-based controller is more stable and offers superior frequency responses in terms of shorter settling time and smaller amplitude of dips/peaks. Delassi et a., 2018 [15] designed

an order of Fractions on AGC of a three-area reheat-thermal network, a PIλD controller with an integral fraction action and a simple filtered derivative action is studied. Differential evolution optimizer was utilised to tune the PIλD controller gains. The proposed methodology shows superior over GA in terms of load disturbance and tie line power (TLP). Vijay et al., 2017 [16] used a multi agent system method, an intelligent PI controller for LFC in a smart grid context with changes in communication topology was proposed. As a result, this study focuses on the multi agent system communication infrastructure approach and its application to LFC in smart grid.

Topno et al., 2016 [17] a two-area thermal electric network, with a tilt ID regulating controller (TID) is introduced. An interior point approach was used to get the best value for the suggested TID controller parameters. The dynamic responses of several controllers are compared, revealing that the TID controller outperforms the PID controller. Kouba et al., 2017 [18] To tackle the LFC challenge, a novel hybrid Genetic Algorithm integrated with PSO (GA-PSO) is created. Later, different approaches are used to optimize the PID controller settings of the studied LFC model. The suggested hybrid GA-PSO algorithm premised PID controller is tested on a two-area, and three-area tie line interconnected system model. And hence the suggested methodology performs superior outcomes over other methodologies in terms of settling time ($T_{settlingtime}$). Jahan et al., 2018 [19] For the AGC problem, a gravitational search method is utilised to find the best gains for the PIDF (PID plus Filter) controller. For frequency response of the power system under consideration, the GSA-PIDF controller performs better than DE-PIDF and PSO-PIDF controllers in terms of convergence to the optimum solution.

Basavarajappa et al., 2020 [20] introduced a Fuzzy Logic Controller (FLC) to design a decentralized control method for the LFC problem in a two-area inter linked power system. Based on the simulation findings, it is evident that by suggested controller parameters, the system frequency deviation and tie-line real power deviation may be reduced to zero when there are rapid changes in load. Sambaria et al., 2016 [21] for LFC of an isolated system as well as an interconnected power system with non-reheat turbine unit, a fuzzy logic control (FLC) technique is used. The obtained results depict FLC premised electric system performs superior over PID controller premised electric system. Kamel et al., 2019 [22] The SCA approach was used to optimize the PI controller for the LFC problem. The two-area (each area thermal with non-reheating source) linked power system is used for the implementation and design of AGC. For faster steady response of power system, DFIG was introduced. From the

outcomes the developed power system shows SCA-PI controller is suitable for two area power system and the suggested methodology outperforms the other existing optimizers.

Kazem et al., 2015 [23] provides a model for the TCSC-premised damping controller that is premised on Taylor series expansion. By reducing the ITSE performance index, the integral gains of the AGC and TCSC parameters are optimised using the improved particle swarm optimization (IPSO) technique. AGC alone is contrasted with the planned TCSC – AGC coordinated controller. Studying the nonlinearity impacts of GDB and GRC, a two-area linked multi-source electric network system with TCSC situated in series with the TLP is examined. Sensitivity analyses for sinusoidal load perturbation, pulse load perturbation, and uncertainty scenarios in electric network loading state and parameters have been used to evaluate the resilience of the electric network equipped with the designed controller. The improved TCSC – AGC operates adequately in uncertainty situations, according to studies, and is extremely resilient. Farooq et al., 2022 [24] designed a satin bowerbird optimizer SBO tuned cascaded ID-PD regulator based two area hybrid DPS network with SMES and to validate robustness of the network, sensitivity analysis was performed and validated.

Javad et al., 2018 [25], well-known lead-lag structure of the TCSC – AGC premised damping controller is modelled using the Taylor series expansion. The augmented regulator is verified with SSSC – AGC, and TCPS – AGC regulators using two – area realistic multi-source electric network. According to the nonlinear time domain simulations for 0.1 P.U. SLP, the augmented TCSC-AGC regulator has the highest dynamic performance in terms of decreased maximum peak, peak length, and settling time of area frequencies and TLP oscillations. Vaibhav et al., 2001 [26] two area deregulated turbine and governor electric network was augmented and, its optimal regulating parameters were optimized with gradient Newton search algorithm. Rajesh et al 2015[27] integral controller tuned two area deregulated electric network with TLP interlinked TCPS device was developed, and out comes are validated with and without TLP interlinked TCPS.

Rabindra et al., 2016[28] TLBO premised PIDD regulator was utilized to optimize the AGC of multi-area multi-source interlinked network. firstly, two-area interlinked network with GRC is validated. Secondly, G – H – T sources two area interlinked network was verified. And lastly, three unequal area was considering with GRC and GDB verified. The proposed TLBO premised PIDD regulator performs better than existing tactics. Prabha 1993 [29] studied the reaction of power system characteristics, stability challenges, modelling, HVDV transmission,

and small signal stability issues. Ali et al., 2021[30] Levenberg–Marquardt algorithm LMA premised IT2FIS type-2 fuzzy inference system regulator was utilised to tune the 39-bus test system of New England. And the outcomes are validated with the type-1 fuzzy regulator.

2.2.2 Review of Literatures on LFC with CES/ESD

Sobhy et al., 2021 [31] MPA algorithm was used to develop the best PID controller settings for solving the LFC problem. This research presents a current realistic system paradigm that includes system non-linearities, RES uncertainties, and ES unit penetration. Wind, PV, and STPP are the three RES types featured. SMES and BES are two forms of ES units that are considered. The suggested method performs very well when dealing with RES and ES penetration, when output responses fluctuate within permissible ranges as defined by European grid rules. The results clearly demonstrate the impact of ES units on the system's transient responsiveness. Kumar et al., 2021 [32] For a two-area network with a rapid load shift in area-1, IPFC, UPFC, SSSC, TCPS, and SMES are investigated, and the device adjustment features are seen in both areas. Because both regions are connected to a TLP network, if a fast fluctuation in load is seen in one area, the load change in the other area is impacted. SMES is the best of all these devices, although TCPS, SSSC, and UPFC are better in performance increasing order.

Mudi et al., 2020 [33] MVO tuned PID controller has been used for LFC of hybrid electric power system network (solar-thermal sources were used as primary energy generation sources) with various energy storage (DLC double-layer capacitor, UC ultra-capacitor and CAES compressed air energy storage) combinations. The outcomes conclude that the proposed MVO-PID controller outperforms the other heuristic GA-PID controller with combination of solar-thermal power generating, PV, UC, DLC and CAES devices. Prasun et al., 2020 [34] developed a novel MVO tuned cascaded PI-PD controller is used to optimize the two area multi origination AGC electric network with CES unit. When an un-contracted power is included, the dynamic responses show that the system performs satisfactorily. The influence of CD-CES on system performance and dynamic response is described in a clear and concise manner over existing methodologies.

Mahendran et al., 2021 [35] in a MAPS, the authors built a dual-mode-switch-controller-based LFC by taking into account the influence of incremental control action as well as system dynamic limitations including GRC, GDB, with CES. The suggested MS-MA-IPS controller's operations were based on the dual-mode switch to accomplish best results. The switching was

done in relation to a threshold value. The control was switched between PI and MPC based on the switching. The hybrid PSO-DA optimizer was used to optimize the PI controller Kpg and the switch threshold. Kalpana et al., 2020 [36] investigated a hybrid electric power system with a CES unit, consisting of a wind turbine and diesel generators, was examined as a test system to evaluate the proposed Fractional Order Fuzzy PID (FOFPID) controller's performance. The suggested FOFPID controller outperforms both the standard PID controller and the Fuzzy Logic Controller in terms of efficiency.

Paddakapu et al., 2020 [37] introduces various control approaches, AGC of two-area different originators of linked electric network. The optimal gain values of the 2DOF PID/ PID/2DOF PI controllers are obtained using three different optimization techniques: cuckoo, TLBO, and bat algorithm. Furthermore, the two-area restructured system incorporates a mix of ultra-capacitor (UC) with novel FACTS regulating controllers such as and DPFC, SSSC, UPFC, and TCSC to improve electric network stability. In comparison to other examined techniques, the bat search optimizer premised 2DOF-PID regulator with the combination of DPFC and UC provided prolific dynamic results. Dutta et al., 2020 [38] LFC problem is investigated with the help of UC in collaboration with TCPS. Under a bilateral contract scenario, the suggested three-area system is combined with renewables in a deregulated environment. The combined performance of the UC and the TCPS is used to verify the results. UC in one region enhances the LFC in all other areas, and TCPS has a significant influence on tie-line power deviation stabilization. Outcomes proves using an UC in conjunction with TCPS may effectively mitigate frequency oscillations.

Yogendra et al., 2019[39] developed an AGC deregulated two area power system with ICA tuned FPIDF controller initially. Although, the developed network was integrated with CES unit. And hence, FPIDF-CES methodology gives superior results over initial method. Later, the developed controller upgraded as the FPIDF-(1 + PI) controller and CES-RFB units. The FPIDF-(1 + PI) controller provides the best system outcomes by reducing variations in the system frequency/tie line power flow. The use of GDB/GRC has unfavorable outcomes. Compared to changing system parameters, random load perturbation, and system nonlinearities, therefore, FPIDF-(1 + PI) CES-RFB control method is much better, resilient, and stable. Moorthy et al., 2015 [40] designed a ICA tuned integral controller for LFR of two area thermal and hydro originators integrated network. SSSC, in combination with CES, has been proposed to improve the system's dynamic performance in terms of settling time (

$T_{settlingtime}$), overshoot ($P_{overshoot}$), and peak time ($P_{underhoot}$). The results demonstrate that the suggested technique successfully mitigates frequency and TLP variations during a load shift, and that the system with SSSC and CES has a lower performance index than the system without SSSC and CES, indicating that the proposed method is preferable.

Sandeep et al., 2018[41] introduces in the presence of TCPS and CES, an AGC analysis of the two-area G – T – H originating sources with SCA optimally tuned PI controllers was evaluated on three contract scenarios. The outcomes were verified with the PSO premised PI regulating controller, the augmented SCA premised PI controller with TCPS and CES tactic performs greater results over other existing methodologies. Rajendra et al., 2019 [42] LFC for a multi-area multi-source PS with an HVDC link was created. A PID controller is utilized to increase the system's stability, and the hybrid PSO-GSA method is created to optimize the controller's settings. The outcomes were analyzed with the TLBO and DE-based PID optimum controllers, the suggested technique has been shown to be superior. Finally, the work described above is expanded to include a multi-area multi-source PS with damping controllers SSSC and CES. Various disturbances are used to show and investigate the suggested system. When SSSC and CES controllers are introduced to a system with an HVDC link, the findings are more stable than when other elements of the system are studied.

Bhatt et al., 2010 [43] developed a novel craziness based PSO for two area multi source deregulated PS. Further the proposed system tested on integral controller, integral-TCPS, and integral-CES controllers. The outcomes confirm that proposed integral-CES controller performs greater results than other literature studies. Mahto et al., 2017 [44] designed an isolated hybrid PS model with wind turbine generating source and CES device. To demonstrate the superiority of one configuration over the others, a quasi-opposition-based harmony search tuned SF-FLC-PID, SF-FLC-PD, SF-FLC-PI, and SF-FLC controllers were constructed for the transient research under varied input perturbation circumstances. Under load fluctuation conditions, the SF-FLC-PID design is the most successful in suppressing frequency and power deviations. Pappachen et al., 2016 [45] investigated in three scenarios for energy exchange contracts, the implementation of the SMES – TCPS entity in a two-area hydrothermal (H - T) electric network with an ANFIS regulator was examined. Under a deregulated environment, the coordination of the SMES – TCPS unit is successfully used to stabilise the LFC concerns in a two-area H – T system.

Sandeep et al., 2017 [46] augmented a two area G – H – T source deregulated network with CES/DFIG units premised wind turbine damp the electric network oscillations. To validate its robustness, the outcomes are analyzed with CES/TCPS unit in each area. The analyzed outcomes verified that the equipped electric network with CES/DFIG units premised wind turbine outperforms the other. Mathew et al., 2016[47] investigated two forms of energy hosting, namely primary and secondary. And different energy hosting tactics were analyzed with their real-life application. Mohammad et al.,2014[48] validated the SMES unit, its energy density and capacity with CHB cascaded H-bridge multilevel converter for frequency regulation. As per the literature by the authors, first time the case study was done. Sabita et al., 2015 [49] introduces CSA tuned regulator parameters of SMES network in the AGC of a two-area thermal electric network. To prove the proposed fast acting SMES robustness, Sensitivity analysis was performed at different operating conditions to damping out oscillation variations in electric network. Ramesh et al., 2016[50] ACSA premised PI regulator was applied to two area deregulated electric network and its efficacy was validated with integrating ESD's of SMES and RFB separately. Chidambaram et al., 2013[51] introduces a BFOA premised NERC's standards fuzzy logic with conventional control was applied to two area thermal reheat electric network coordinated with RFB and IPFC units to suppress the frequency oscillations.

Yogendra et al., 2017 [52] augmented a ICA premised FOFPID regulator was applied to AGC of single/two-area multi-source G – H – T electric network integrating with RFB. The suggested topology was further extended with and without GRC and GDB on two area networks. Rufer [53] introduces various Energy Storage units history with their Components, ratings, various models of batteries, Supercapacitors. Ravi et al., 2016[54] Opposition premised Harmonic Search (OHS) tactic tuned integral regulator was used to optimize the LFC of the G – H – T sources two are interlinked deregulated electric network with RFB and economic load dispatch also incorporate into this LFC mechanism for the division of economical load among load interchanges.

Egido et al., 2015 [55] investigated on small isolated electric network Frequency stability challenge by Endesa sought to test the most advanced technologies of Li-ion, ultra-capacitors, and flywheel hosting units. The electric network of the Spanish Canary Islands was utilized to validate the bench. Tripathi et al., 1991[56] studied a Lyapunov regulating theorem tuned AGC of a two-area interlinked network with CES units. Appropriate methods for controlling CES devices also introduced. Tripathy et al., 1996[57] wind-Diesel electric network, which operates in isolation from the grid network with and without CES as an energy storage units was studies.

Das et al., 2012[58] GA premised PID regulator utilized to tune the autonomous multi source electric network with ESD units. The outcomes are validated with GA-PI regulator. Anil et al 2022 [59] developed a Black widow optimizer premised PIDF-(1+I) regulator for LFR of diesel, solar, and wind originating resources as1.5 MW smart grid electric network with ultracapacitor and flywheel energy hosting units and developed network efficacy was validated with different optimizers. Biswanath et al., 2022 [60] created an artificial flora optimizer premised CFOPI-FOPDN regulator for LFR-AVR of 3 – area thermal-solar network with RFB as energy hosting unit, the developed network robustness was validated with sensitivity analysis.

2.2.3 Review of Literatures on LFC with Electric Vehicle/RES

Satish et al., 2021 [61] implemented the HHO optimized 2DOFTID controller for the AVR and ALFC loops in a multi-area thermal-CCGT incorporated EV system. In terms of all time-domain indices, the dynamic responses of the system with 2DOFTID controller are superior to those of the PIDF and TID controllers. The impact of EV on the combined AVR and ALFC system has been studied, and it has been discovered that EV is responsible for keeping voltage and frequency variations within specified limits, as well as making the PS more stable with less undershoot, peak overshoot, and dampened oscillations.

Ahmed et al., 2021 [62] presented a modified fractional order cooperative controller optimized by an artificial ecosystem optimizer (AEO) for LFR with EV in a two area electric network. The advantages of both TID and FOPID regulating controllers are combined in the suggested controller. The efficacy of the suggested controller in comparison to traditional controllers (FOPID, PID, and TID), especially given the fluctuating nature of the RES and the EVs' lower penetration levels. The suggested LFR and EV controllers effectively dampen frequency oscillations and manage tie-line power with minimal undershoot /overshoot values and settling time.

Arman et al., 2019 [63] created a lumped model of the EVs and used a TID controller to regulate the available energy in the batteries of EVs in the discharging state using the LFC and SOC signals. The ABCO algorithm used to optimize the TID controller settings in the EV and AGC structures. When compared to PSO and GA optimization techniques, ABCO-based coordinated TID controllers effectively reduced frequency deviations and tie-line power variations.

Gaur et al., 2019 [64] designed a three-region thermal system using PEVs with integration of STPP (solar-thermal power plant) for frequency regulation in each area, WDO (wind-driven optimization) has been fine-tuned in all three control domains, a two-degree-of-freedom proportional–integral–derivative (2DOF-PID) controller was used for robust secondary control. The efficacy of the WDO optimized 2DOF-PID controller is demonstrated by comparing it to a traditional PID controller under nominal and random loading conditions. Under nominal, RLP, and simultaneous perturbation, EVs are found to play a critical role in regulating frequency variations and tie-line power deviation. The system dynamics are significantly better in the presence of EVs/ STPP than in the absence of them, according to the comparison. According to research, when the K_{EV} value approaches 1, EVs become deeply influential in LFC.

Arman et al.,2017 [65] developed a IPSO tuned fuzzy premised PI controller (FPIC) for three area PS with electric vehicles (EVs) each area connected as foremost controllable loads for enhancing the frequency performance after disturbance. The charging and discharging conditions of the electric vehicle are controlled by a PI controller. The FPIC improves frequency performance and tie-line power fluctuation. The efficiency of EVs fitted with the IPSO and FPIC for frequency and tie-line power fluctuations augmentation is demonstrated by outcomes.

Hussein et al., 2021 [66] To stabilize grid frequency, Balloon Effect (BE) relied Harris Hawks Optimizer (HHO) endorsed by a virtual impedance controller was utilized to build an adaptive control tactic for an on-line tuning the I controllers' parameters of the gains for power discharging /charging of plug-in electric vehicles (PEVs) in grid and island mode networks, taking into account high-level penetration of RESs(PV cell considered). The performance of the suggested control strategy modified by HHO based BE, traditional HHO, and CDM for PEVs in the presence of a virtual inertia controller was compared using the results. The outcomes verified that HHO based BE for EVs backed by virtual inertia can effectively damp down the oscillations in the system and ensure resilient performance.

Dutta et al., 2019 [67] In a deregulated environment, developed an emotional controller (Brain Emotional Learning-Based Intelligent Controller, BELBIC) is employed for LFR of a two-area hybrid power system. DG sources like, biomass and solar are integrated into the power grid. Electric cars are utilized to deal with solar power's inconsistency. The simulation outcomes

verified the effectiveness of the emotional controller with PID and FOPID controller and thus emotional controller performs superior to others.

Pushpa et al., 2018 [68] Wind Driven search technique based 2DOF-PID regulator was applied to three region restructured electric network with EV and its efficacy was verified with PID regulator. Kempton et al., 2005[69] studied the response and cost efficacy fleet of light vehicles powered by electricity with vehicle to grid (V2G) tactic. Izadkhast et al., 2015[70] studied the application of PEVs by utilizing a participation factor to stabilize the prime frequency regulation using the ability of energy hosting and instant active energy regulation of rapid switching converters of PEV's.

Jasna et al., 2007 [71] studied an EVs performance, when parked, EVs may power the electric grid (V2G). The economics of grid connected EVs might be improved, which would promote their adoption. V2G electricity may offer a sizable income stream. Additionally, the electrical grid's stability would be increased. Abhishek et al., 2022[72] developed a AOA premised type-2 fuzzy PID regulator for LFC of deregulated electric network with DG and PEVs. To efficacy of the suggested network was proved by using sensitivity analysis performance with 30% variation of network parameters. Dilip et al., 2020 [73] developed a Adaptive Differential Evolution (ADE) optimizer premised PDF plus (1+PI) regulator for LFR of wind, solar, and EVs as originating sources and ESD as flywheel, and battery. To validate the robustness of the system, sensitivity analysis was performed.

2.3 SCOPE OF RESEARCH

According to the literature, considerable attempts are underway for LFR of multi-area multi-source power systems using various meta-heuristics techniques, but no significant attempts to find a global optimizer that combines global with local search capabilities to improve exploration and exploitation. Furthermore, the no free lunch theorem implies that no optimization technique is capable of effectively tackling all sorts of optimization problems. To put it another way, there is always room for development to enhance present approaches and handle maximum optimization issues more effectively.

It was revealed in recent works relevant to optimization algorithms that swarm - based optimization has various limitations that must be addressed. Exploration, which is an inappropriate measure without theoretical guidance, is another major challenge in swarm intelligent algorithms. In practise, it presents a significant difficulty. This sparked our efforts

to develop yet another memetic algorithm for load frequency management in a deregulated multi-area multi-source power system. Further, the multi-area multi-source power system has not been investigated with respect to impact of hybrid and plug-in electric vehicles and RES, which seriously affects the load demand pattern and optimality of the results. The work is therefore justified in persisting the proposed study. The research proposal therefore presents *"Load frequency regulation in multi-source multi-area power system using memetic optimization strategy with energy storage device".*

2.4 RESEARCH OBJECTIVES

The intent of the proposed research is to develop an efficient and powerful hybrid meta-heuristics optimization algorithm, which will provide the reliable and optimal solution for load frequency regulation in multi-area multi-source deregulated power system with due consideration of various energy storage devices. The objectives of the proposed research work are outlined as below:

i. To develop the MATLAB/Simulink based mathematical model for multi-area multi-source power system for load frequency regulation and to study the response of existing classical controller by varying the system operating conditions.

ii. To develop a memetic optimization search algorithm by combing modern global search algorithm with local search algorithm for constrained optimization and engineering optimization problem using memetic algorithm approach and to evaluate the performance of the proposed memetic algorithm for various standard benchmark and engineering optimization problems and determination of superior optimization algorithm out of trial combinations.

iii. To apply the proposed memetic optimizer for load frequency regulation in multi-area multi-source deregulated power system with due consideration of energy storage devices.

iv. To study the impact of renewable energy sources/EV charging and discharging on the proposed power and to compare its performance with other intelligent controllers.

v. To perform sensitivity analysis to judge the robustness of the proposed controller under wide variation in the nominal system initial loading, parameters etc.

2.5 CONCLUSION

This chapter examines the literature review of several strategies that have been effectively used to address various issues of load frequency problem of multi-area power system. The critical reviews of literatures have been done to explore the research gaps of the existing methodologies with respect to load frequency regulation problem of multi-area power system. In the succeeding chapters, hybrid optimization methodologies i.e., SMA-PS and HHO-PS are explored for the optimal solution of load frequency regulation problem with CES, electric vehicles and renewable energy sources.

Chapter-3

HYBRID METHODOLOGIES FOR LOAD FREQUENCY REGULATION

3.1 INTRODUCTION

In several fields of science and engineering, optimization plays a vital role. It is a course in which an acceptable solution to a specific problem is identified via the use of a search tool. With advancements in new technology and inventions, a new era of problem-solving optimization techniques known as meta-heuristics has gained traction in the mathematical community. Meta-heuristic Algorithms (MA) are a type of algorithm that imitates a popular approach for obtaining the best results for a given issue. In an optimization problem, MA pretends to be a seeker of fine requirements. Due to the complexity of MA, hybrid methodologies were implemented with combination of global search and local search optimizers.

The need for electricity is increasing every day. As a result of increases, the supplying and demanding loads have become unbalanced. A strong MA can find the best solution for load frequency regulation (LFR) of multi-area DPS. A memetic MA of HHO-PS and SMA-PS optimizers has been created in the study to handle the LFR challenge of multi-area DPS[74].

To construct a modern meta-heuristic algorithm, researchers look to physics, nature, society, and genetics, for inspiration. In the proposed work, the authors aimed to solve these issues by heuristically integrating two strong algorithms for improved discovery and exploitation, as well as increased search. The following research articles were chosen to investigate the shortcomings of present techniques. Yang studied latest nature premised MA search tactics with diverse applications [75]. This investigation involves in global optimizers are, Slime mould algorithm (SMA) inspired by the natural slime mould's oscillation phase [76], Photon search algorithm PSA driven by physics' understanding of photon characteristics [77], Differential evolution DE It is proposed to minimise potentially non-differentiable and nonlinear continuously space functions [78], TSA tunicate swarm algorithm mimics tunicate swarming behaviour and jet propulsion while navigating and foraging [79], Grey wolf optimizer GWO derived by grey wolves'[80], Sine cosine algorithm SCA created by mathematical functions of sine and cosine parameters [81], Gravitational Search Algorithm GSA relies on mass interaction and the law of gravity [82], PO political optimizer motivated

by the complex political process [83], Artificial Bee Colony optimizer ABC built on the honey bee swarm's clever abilities [84], Harris hawks optimisation HHO motivated by smartest species actions [85], SSA Social spider algorithm concerned with social spiders [86], Rat swarm optimizer RSO inspired by the natural rat-attacking and chasing behaviours [87], BRO battle royal optimizer motivated by digital game of Battle royale [88], Electro search optimisation EO depends on how an atom's electrons travel through their orbits around its nucleus [89], Virus colony search VCS simulate the approaches used by viruses to spread and infect host cells in the cellular environment [90], TSO transient search optimizer is an transient behaviour of switching circuitry with hosting components like capacitor and inductor as an inspiration [91], Multi verse optimizer MVO premised on the mathematical concepts of black, white, and worm holes [92], Charged System Search CSS premised on electrostatics of Coulomb law from and mechanics of Newtonian laws [93], DGCO dynamic group based cooperative optimizer impressed by how swarms of people work together to accomplish their common objectives [94], BIA billiards inspired optimization resembles the game of billiards [95], Electromagnetic filed optimisation EFO amazed by how various polarity electromagnets behave with gold ratio [96],Teacher learning based optimizer TLBO focused on how a teacher's influence affects the production of students in a class [97], LFD Lévy flight distribution optimizer uses the Lévy flight random walk was used as inspiration for examining undiscovered big search areas [98], GBO gradient based optimizer encouraged by the Newton's approach, which uses gradients [99], Tabu search TS utilizes as a combinational optimization technique [100], Evolutionary programming EP presented where the main search operator is a Cauchy mutation rather than a Gaussian mutation [101], Moth flame optimizer MFO influenced by the transverse orienting mechanism of moths in environment [102], Harmony search HS emulating a musician's improvisation [103], Group Search Optimizer GSO influenced by how animals look for things [104], Cuckoo search CS, Genetic algorithm GA studied the complex problems with resemble natural selection [105], Fruit Fly Optimisation FOA was formed by practical use in determining minimal and maximum values [106], Particle swarm optimizer PSO it introduces nonlinearities utilising particle swarm approach. [107], ISA Interior search algorithm motivated by interior decorating and design [108], Biogeography based optimisation BBO mimics the investigation of geographic distribution of living things is known as biogeography [109], AMO Animal migration optimization influenced by the migratory patterns of animals [110], Central Force Optimization CFO influenced by metaphor for the dynamics of gravity [111], TSA Tree seed algorithm For continual improvement, relying on the relationship among trees and their seeds [112], Stochastic Fractal Search

motivated by the growth-related natural phenomena [113], Physarum polycephalum begins its service life when the spore wall splits after 15 to seventy-two incubation hours in a water drop [114], WOA replicates humpback whales' social behaviour [115], WSA influenced by the water strider bug's entire lifespan. [116], GHOA extends it to difficult constructive optimization issues [117], SSA and MSSA augmented to resolve single and multiple objectives [118], WCA influenced by nature and derived from actual observations of how streams and rivers flow into the sea and through water cycle [119], Gandomi et al., studied the optimization challenges of truss and non-truss structural issues [120], Mezura et al., studied an evolutionary premised engineering optimal challenges without considering additional function s[121]. HGSO replicates Henry's law's behaviour to address difficult optimization issues [122], SHO impacted by the spotted hyenas' social interactions and cooperative conduct [123], PSO applied to simple optimal engineering issues [124], ACO motivation from certain ant species' foraging techniques [125], Lagrangian Multiplier [126] and Branch-bound [127] applied to various benchmarks and unit commitment problem, MBA utilizing the idea of the mine bomb detonation [128], BCMO primary concept is to balance people's composite motion qualities in the optimal solutions. [129], PVS takes into account the arithmetic involved in a car overtaking on a two-lane motorway [130], SMS utilizing a simulation analysis of the states-of-matter phenomena [131], SOS replicates the symbiotic interpersonal tactics used by organisms in the environment to survive and grow [132], MMA generalised nonlinear computing and structural optimisation [133] and CS Cuckoo Search optimizer was introduced to addressing optimal design complex tasks [134].

Optimization is a vast research area, and progress is being made at a fast pace. The researchers are investigating a variety of issues to apply certain types of new innovations to complexities and can successfully identify the results. The research is focused on uncovering the most up-to-date methodology, as well as approaches with innovative hybrid forms, to mitigate some of the current methods' drawbacks. The suggested study used existing academic articles to investigate the flaws in present algorithms. Few of memetic optimizers were GWO-PS GWO efficacy was improved with integrating derivative-free search tactic [135][9], PSO-GWO performance was validated with single region unit commitment issue of various originating units [136], GWO-SCA two novel optimizers are integrated and validated on five bio-medical, benchmarks and one sine datasets issues [137], SMA-PSO two novel optimizers are integrated and outcomes verified with standard optimizers [138], PSO-DE PSO efficacy was improved with integrating DE optimizer [139], ESA emperor penguin and Salp Swarm

Algorithm two novel optimizers are integrated and outcomes verified with scalability analysis [140], hHHO-IGWO HHO integrated with hybrid GWO and validated with benchmarks [141], FA-PS FA optimizer integrated at termination end with PS tactic [142], GWO-SMA GWO integrated with novel SMA and validated with benchmarks [143], PSOSCALF firstly PSO was integrated SCA and at termination with LF movements [144], SMA-WOA novel augmented SMA was integrated with WOA and hybrid model was applied to ISP of COVID-19 chest X-ray images [145], Orthogonally-designed Adapted Grasshopper Optimization OAGO was augmented to improve the local trapping of novel GOA [146], Improved Fitness-Dependent Optimizer Algorithm improving the capabilities of the first FDO IFDOA [147], Self-Adaptive differential Artificial Bee Colony SA-DABC combining a self-adaptive mechanisms and several differential search techniques into the ABC framework [148], Improved WOA IWOA developed standard WOA is hybridized with DE [149], Simplified SSA SSSA leader premised search in SSA was analysed and later updated with random search radius tactic [150], Artificial Ecosystem-Based Optimization AEBO inspired by the energy flow in an earthly biosphere [151], Imperialist Competitive Learner-Based Optimization ICLBO ICA was integrated with TLBO optimizer [152], Refined Selfish Herd Optimizer RSHO developed a local optima trap overcome hybrid model with modifications and refinements [153], Hybrid Crossover Oriented PSO and GWO HC- PSOGWO prioritises improved generalisation, search methodology, and diversity [154], Multi Strategy Enhanced Sine Cosine Algorithm MSESCA multi terms control strategies are proposed namely are chaotic local, opposition-premised learning strategy, Cauchy mutation operator, and two operators premised on DE [155], Incremental GWO and Expanded GWO I-GWO and Ex-GWO two novel augmented hybrid versions of GWO are integrated [156], Multi-objective Heat Transfer Search Algorithm MHTSA works on the principles of thermodynamics and heat transfer [157], and hSMA-PS applied to the test efficacy of the proposed electric network [158], hHHO-PS was developed to validate the performance of suggested network [159], ECBO which develops some of the greatest solutions using memory [160], DEAHHO novel HHO tactic was integrated with DE and later Masi entropic function is used in a 1-D histogram predicated multilevel image thresholding technique [161], HHO-SCA novel HHO search method is integrated with novel SCA method and later validated with different CEC BM and optimal engineering designs [162], BF-PSO improved the searching ability while compare with parent optimizers [163], GWO-RES augmented a hybrid version of GWO with integrating random exploratory search tactic and it combines predefined resolution vectors with altered response vectors [164], MALO designed to address the underlying flaws of standard ALO [165], MBFPA validated on several BM and

five constrained optimal engineering designs [166], MSCA validated on limited optimum engineering concepts and various benchmarks [167], GeneAS known as genetic approaches that are both real-coded and binary-coded [168], BWOA chaotic local and Lévy flight are simultaneously implemented into WOA [169], and CMA-ES covariance matrix adaptation was mutated with derandomized evolution strategy to lessen the amount of generations needed to reach the ideal optimal convergence [170].

3.2 GLOBAL OPTIMIZATION ALGORITHMS

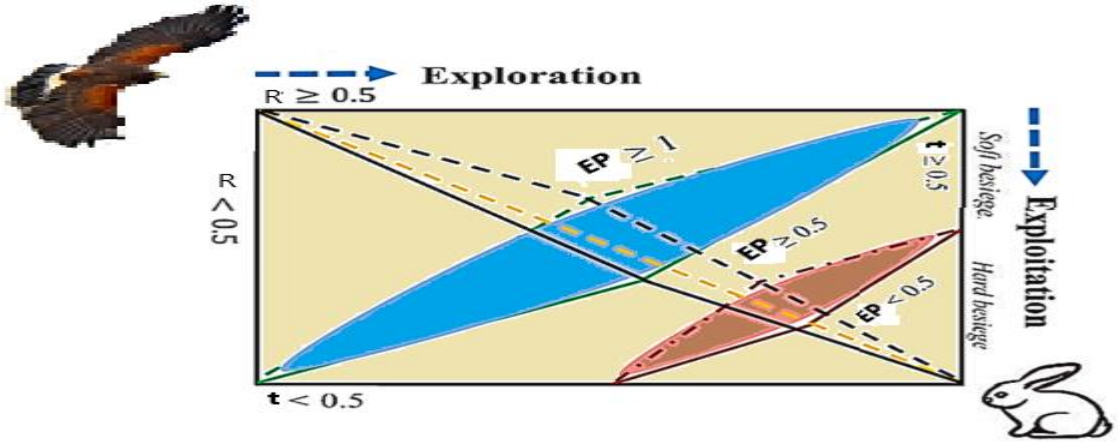

Fig.3.1 Classic HHO main working phases

The algorithm looks for the global optimum by utilizing methods to scan bigger portions of the search area. It is used to solve problems with a minimal number of variables and a high value of discovering the genuine global solution.

3.2.1 Harris Hawks Optimizer

Heidari et al. [38] propose HHO as a swarm intelligence optimizer. To solve different optimal challenges, this initiative simulates the cooperative behaviour of Harris' hawks. Hawks chase their target in a series of actions that include tracking, surrounding, getting close, and eventually striking. The fundamental principle is to run numerous stages in a row to identify the most suitable (optimal) solution. The key HHO stages are depicted in Fig.3.1.

3.2.2.1 Exploitation phase

Over this moment, the hawks hang in various spots at randomly and seek for prey to appear depending on the following:

$$A(x+1) = \begin{cases} A_{rand}(x) - t_1|A_{rand}(x) - 2t_2A(x)| & R \geq 0.5 \\ A_{rabbit}(x) - A_P(x) - t_3(B_{UB} - B_{LB}) & R < 0.5 \end{cases} \quad 3.1$$

Here, $A_P(x)$ has been the average position, and it is determined by

$$A_p(x) = \frac{1}{H}\sum_{j=1}^{H} A_j(x) \quad 3.2$$

Here, H and A_j are the size and location of the hawks, accordingly.

Parameters of the HHO optimizer

$A(x+1)$	Following iteration of the hawk's position vector
A_{rand}	One of the existing hawks was chosen at random.
A_{rabbit}	Prey position (best agent).
t_1, t_2, t_3, t_4, and R	Random numbers within [0, 1].
D, B_{UB}, B_{LB}	Dimension, upper and lower bounds of the variables
x, D	iteration counter, Max. iterations
EP_0, EP	initial state of energy, escaping energy of prey
$A(x)$	Current position vector of the hawks.

3.2.1.2 Exploration to exploitation phase transmission

The optimization technique may now switch from global to local hunting using the escaping energy of prey (EP), which is calculated as:

$$EP = 2EP_0(1 - \frac{x}{D}) \quad 3.3$$

In relation to the value of |EP|, it has been determined to begin the exploration phase (|EP|≥ 1) or to exploit the remedies' neighbour's (|EP | < 1).

3.2.1.3 Exploration phase

The Harris' hawks pull off a surprise assault in this stage, targeting the targeted prey which was found in the previous stage. The hawks will use a strong or mild besiege (trapping) to seize the prey, regardless of what prey responds.

At $R \geq 0.5$ and (|EP|≥ 0.5) (at soft besiege stage), the prey (i.e., rabbit) has enough energy to try to escape by making several random deceptive jumps. The following equations was used to keep updating and simulate this method:

Algorithm-1: HHO search algorithm PSEUDO-CODE

Start-up: Initializing the size of population H, original location, objective function parameters with the no of iterations *D*

Outcome: perform the best possible location of prey 'rabbit' and its objective value of fitness

Setup the original and starting location of hawk's $A_j(j=1,2.....H)$

$while(iter < iter_{\max}$

Compute the possible fitness of H

Set-up A_{rabbit} as the best possible location

For (each of the hawk's (A_j))

Upgrade the migrating strength *J* and origin energy EP_0 ▻ $EP_0 = 2rand\ () -1,\ J = 2(1-rand())$

Upgrade Upgrade EP using eqn (3.3)

$if\ (|EP| \geq 1), then$ ▻ Period of Exploration

Upgrade the location of vector using eqn (2.1)

$if\ (|EP| < 1), then$ ▻ Period of Exploitation

$if\ (t \geq 0.5 and\ |EP| \geq 0.5), then$ ▻ Soft besiege

Upgrade the location of vector using eqn (3.4)

else

$if\ (t \geq 0.5 and\ |EP| < 0.5), then$ ▻ hard besiege

Upgrade the location of vector using eqn (3.6)

else

$if\ (t < 0.5 and\ |EP| \geq 0.5), then$ ▻soft besiege with running quicker drive

Upgrade the location of vector using eqn (3.10)

else

$if\ (t < 0.5 and\ |EP| < 0.5), then$ ▻hard besiege with running quicker drive

Upgrade the location of vector using eqn (3.11)

Return the best possible location A_{rabbit}

$$\mathrm{A(x+1)} = \Delta\mathrm{A(x+1)} - \mathrm{EP|J}A_{rabbit}\mathrm{(x)} - \mathrm{A(x)}| \quad 3.4$$

$$\Delta\mathrm{A(x)} = A_{rabbit}\mathrm{(x)} - \mathrm{A(x)} \quad 3.5$$

The distance between the prey position vector and the present location at instant x is ΔA(x), and the prey leap force is J = 2(1 - r).

When R ≥ 0.5 and |EP | < 1, the prey is fatigued and has a limited power for fleeing in the hard besiege phase. As a result, in this situation, the responses are upgraded using optimal result as defined in Eqn (3.6).

$$A(x+1) = A_{rabbit}(x) - EP|\Delta A(x)| \quad 3.6$$

The solution has the capacity to find out their next move at (R <0.5 and (|EP|≥ 0.5) in the soft besiege with successive fast dive phase, this is done via Eqn (3.7).

$$B = A_{rabbit}(x) - EP|JA_{rabbit}(x) - A(x)| \quad 3.7$$

Levi's flight (LF) is used to upgrade the movement to identify the quick dives:

$$C = B + S * LF(T) \quad 3.8$$

S is a random size 1 * T vector , and T is the problem dimension[75].

$$LF(x) = 0.01 * (x) = 0.01 * \frac{v * \alpha}{|w|^{1/u}}, \alpha = \left(\frac{\delta(1+\rho) * \sin\left(\frac{\pi\rho}{2}\right)}{\delta\left(\frac{1+\rho}{2}\right) * \rho * 2^{\left(\rho-1/2\right)}}\right)^{\frac{1}{\rho}} \quad 3.9$$

Here, w is a standard parameter of 1.5 and v is within random numbers (0,1).

In the following iteration, the methods that affect the hawks' position vector can be stated as follows:

$$A(x+1) = \begin{cases} B & \text{If } F(B) < F(A(x)) \\ C & \text{If } F(C) < F(A(x)) \end{cases} \quad 3.10$$

Here, C and B are achieved by eqns (3.7) & (3.8).

Under the conditions|EP| < 0.5 and R < 0.5, last phase, known as the hard besiege with increasing quick dives, the intended prey has minimal energy to escape, and the solutions must be updated using the following rule:

$$A(x+1) = \begin{cases} B & \text{If } F(B) < F(A(x)) \\ C & \text{If } F(C) < F(A(x)) \end{cases} \quad 3.11$$

Here, C and B are achieved by eqns (3.13) & (3.12).

$$B = A_{rabbit}(x) - EP|JA_{rabbit}(x) - Ap(x)| \quad 3.12$$

$$C = B + S * LF(T) \quad 3.13$$

Here, $A_p(x)$ is calculated with eqn (3.2).

Algorithm replicates the PSEUDO code of HHO optimizer. And fig 2.2 replicates the HHO algorithm flow chart.

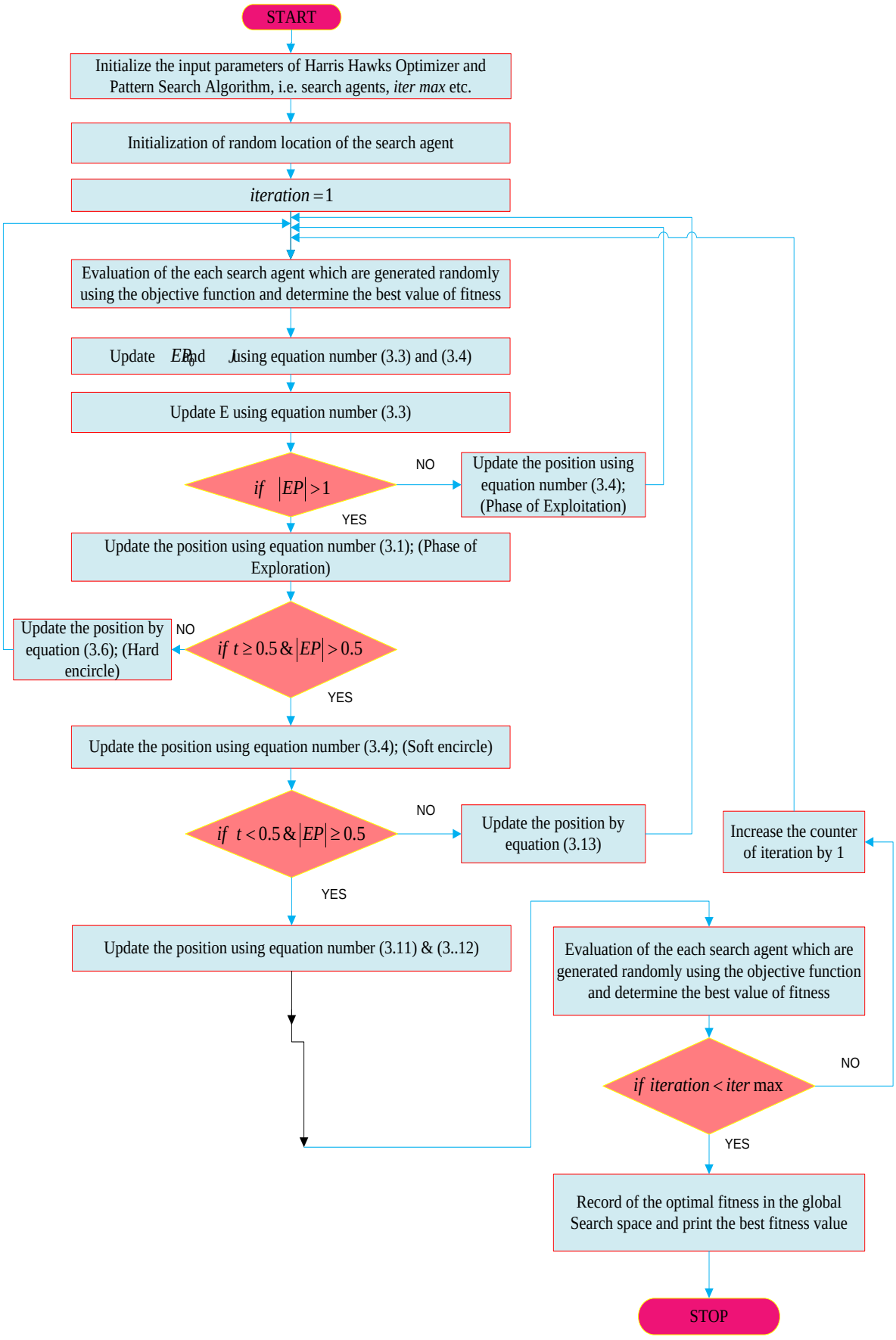

Fig.3.2 Flow chart of the HHO search algorithm

3.2.2 Slime Mould Algorithm

By incorporating weights, SMA is a unique swarm intelligence search algorithm that was recently augmented to imitate the process of slime mould (SM) seeking for the optimum path to food[158]. SM may grow to a size of over 900 square metres if there is adequate food in the environment[114]. Fig 3.3 depicts SM growing crops of morphology.

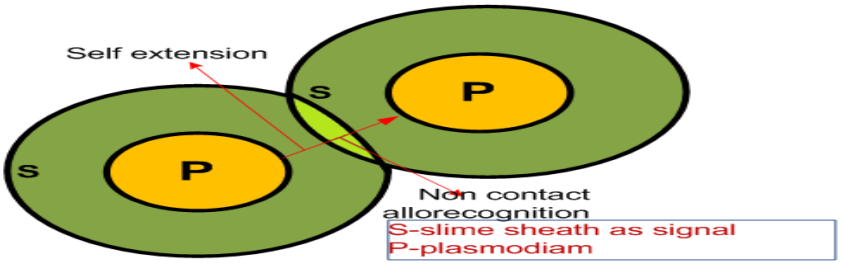

Fig.3.3 Growing crops of SM morphology

- Approach food,
- wrap food, and
- grabble food

these are the three actions involved in this procedure. The SMA will be summarized in this part around these three aspects.

3.2.2.1 Approach food

A SM's ability to acquire food is dependent on the quality of odour in the air. Its strategy of addressing food contraction is described as Eqn (3.14 and 3.15).

$$\overrightarrow{S(\iota+1)} = \overrightarrow{S_b(\iota)} + \overrightarrow{vb} \cdot \left(\vec{W} \cdot \overrightarrow{S_A(\iota)} - \overrightarrow{S_B(\iota)}\right), r < p \qquad 3.14$$

$$\overrightarrow{S(\iota+1)} = \overrightarrow{vc} \cdot \overrightarrow{S(\iota)}, r \geq p \qquad 3.15$$

$\overrightarrow{vc}$ declines linearly from one to zero.

$\overrightarrow{vb}$ is a parameter value between [-a, a]

$\vec{W}$ is the SM weight

where $\vec{S}$ replicates SM location

$\overrightarrow{S_A}$ and $\overrightarrow{S_B}$ are two individuals chosen at random from the population,

$\overrightarrow{S_b}$ replicates the location of the individual with the maximum odour concentration

Eqn. (3.20) is also used to compute a, and while Eqn. (3.16) is used to calculate p.

$$p = \tanh|X(t) - bF| \tag{3.16}$$

DF replicates the best fitness obtained in all iterations.

where $t \in 1,2,\ldots,n$, $S(i)$ replicates the fitness of $\vec{X}$.

Here,

$$\overrightarrow{vb} = [-a, a] \tag{3.17}$$

$$a = \operatorname{arctanh}\left(-\left(\frac{i}{\max\_i}\right) + 1\right) \tag{3.18}$$

$$\overrightarrow{\mathrm{W(SmellIndex(i))}} = \begin{cases} 1 + \mathrm{r} \cdot \log\left(\dfrac{\mathrm{DF} - \mathrm{X(t)}}{\mathrm{DF} - \mathrm{wF}} + 1\right), \text{condition} \\ 1 - \mathrm{r} \cdot \log\left(\dfrac{\mathrm{DF} - \mathrm{X(t)}}{\mathrm{DF} - \mathrm{wF}} + 1\right), \quad \text{others} \end{cases} \tag{3.19}$$

$$SmellIndex = sort(C) \tag{3.20}$$

Here, $SmellIndex$ replicates the sequence of fitness values sorted (ascends in the minimum value problem).

DF replicates the optimal fitness obtained in the current iterative process,

r replicates the random value in the interval of $[0,1]$,

wF replicates the worst fitness value obtained in the iterative process currently, and $condition$ replicates that $S(i)$ ranks first half of the population,

3.2.2.2 Wrap food

During the search, this section computationally models the contraction mode in the SM venous tissue structure. In this scenario, the greater the bio-oscillator-generated wave, the faster

the cytoplasm flows, and the thicker the vein, the greater the food quantity reached by the vein. The behaviour of wrapping food (updating the location of search agent) may be expressed using this approach as Eqn (3.21).

$$\overrightarrow{S^*} = \begin{cases} rand \cdot (U_{\cup B} - U_{LB}) + U_{LB}, rand < z \\ \overrightarrow{S_b(\imath)} + \overrightarrow{vb} \cdot \left(W \cdot \overrightarrow{S(\imath)} - \overrightarrow{S_B(\imath)} \right), r < p \\ \overrightarrow{vc} \cdot \overrightarrow{S(\imath)}, r \geq p \end{cases} \quad 3.21$$

Here,

$rand$ and r replicates the random value in [0,1].

U_{LB} and $U_{\cup B}$ replicates the lower and upper limitations of the search range.

3.2.2.3 Grabble food

The propagation wave is principally responsible for changing the cytoplasmic circulation in the veins, making them seem to have a higher concentration of food. When the quality and quantity of food are large, SM can contact it quicker; when the quality and quantity are poor, SM can reach it more slowly, boosting SM's efficacy in picking the best source of food.

Algorithm-2: SM search algorithm PSEUDO-CODE

Set-up: Initializing the Slime mould parameter variables $Max\_iteration, popsize$

Initializing the initial location of the SM $S_t(t = 1, 2....n)$;

While ($t \leq Max\_iteration$)

Compute the fitness of each SM

$Upgrade\ the\ best\ fitness\ S_b$

Compute the W by Eqn. (3.19).

For $each\ search\ portion$

$Upgrade\ vc, vb, p$;

$Upgrade\ the\ positions\ by$ Eqn. (3.21);

End For

$t = t + 1$

End While

Return $bestfitness, S_b$.

$\overrightarrow{vc}$ oscillates between [-1,1] and tends to zero eventually.

$\overrightarrow{vb}$ changes randomly in-between $[-a, a]$ and gradually approaches zero as the iterations increase.

Here, algorithm 2 replicates the SMA optimizer PSEUDO CODE and fig 3.4 depicts the flow chart of the SMA optimizer.

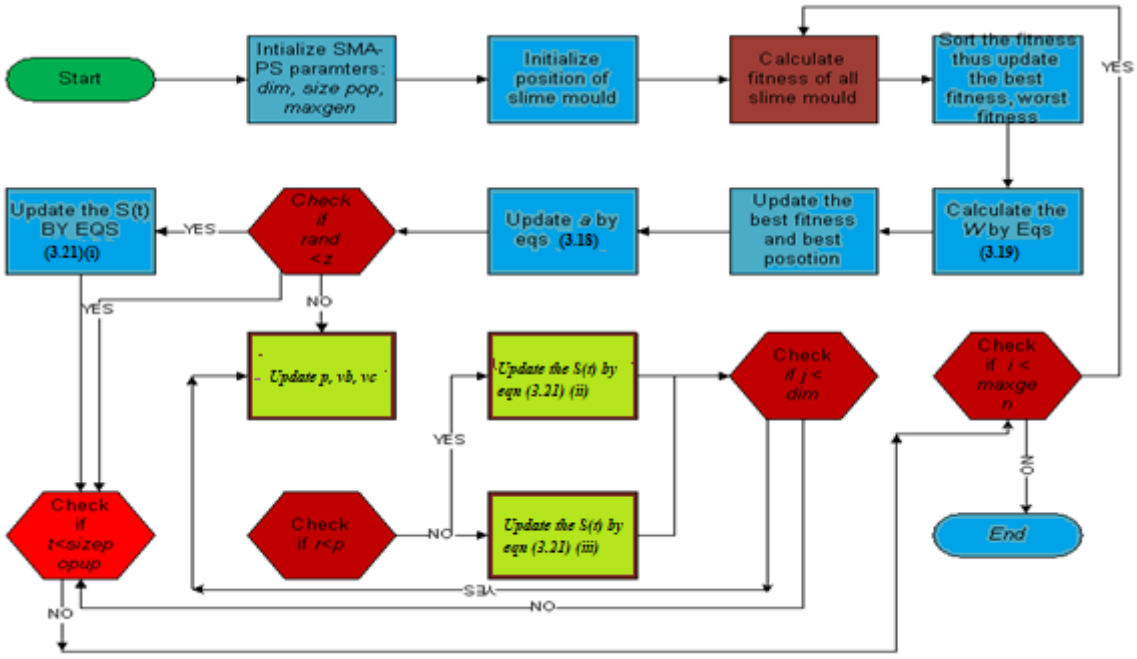

Fig.3.4 SMA optimizer flowchart

3.3 LOCAL SEARCH OPTIMIZER

A local search procedure begins with a current solution and progresses to a neighbour solution repeatedly. This is only feasible if the state space has a neighbourhood relation established. Here, pattern search methodology is introducing as local search optimizer.

3.3.1 Pattern Search Algorithm

Pattern search (PS) strategic approach is a derivative-free way, also termed as a black - box testing tool trick, featuring position-chasing ability and worthiness for optimal solutions, where objectives' task derivatives would be unpleasant or unknown. When carrying out their action, this method necessitates two movements: If the modification is not updated, the exploratory

one quest, which is position pursuit, tries to improve the pathway to be carried; other motion is pattern motion, which has a bigger hunt for reinforcing the path in its motion phase scale. The pattern's motion contains 2 facts: one has been the pre-existing host, and the other is an unnamed location with a better goal function that leads to eqn (3.22) the quest's conclusion. Algorithm 3 illustrates the PS optimizer PSEUDOCODE.

Algorithm-3: PS search algorithm PSEUDO-CODE

$Step-1:$

Initializing the PS optimizer input data i.e

$vector\ disturbance\ tolerance\ (\varphi),\ acceleration\ factor\ (w),\ and\ vector\ disturbance\ (y^{o})$

$Step-2:$

$Initialize\ the\ host\ vector\ of\ disturbance\ y \leftarrow y^{0} and\ select\ the\ beginning\ point\ value.$

$Step-3:$

Upgrade g^{iter} *to* g^{int} *to use exploratory search* g^{int} *to find a strengthened point* g^{iter} *with a stronger objective feature meaning*

$If\ g^{iter} > g^{int}$

$DO\ y \leftarrow \frac{y}{2}$

$If\ g_j < \varphi$

$DO\ g^{final} = g^{int}$

else

$go\ to\ step-3$ and upgrade the best possible vector by using $exploratory$ hunt

else

$DO\ g^{final} = g^{int}, y \leftarrow y^{0} and\ go\ to\ step\ 4$

end

end .

step 4: then, apply black box pattern approach using below steps

step-4 (a): find tentative $g^{(iter+1)}$ by a black box pattern change from $g^{int} to\ g^{iter}$

step-4 (b): find $final\ g^{(iter+1)}$ by an $exploratory$ hunt around tentative $g^{(iter+1)}$

$if\ F\left(g^{(iter+1)}\right) > F\left(g^{iter}\right)$

$DO\ g^{int} \leftarrow g^{iter} and\ go\ to\ step-3$

else

$DO\ g^{int} \leftarrow g^{iter},\ g^{iter} \leftarrow g^{(iter+1)}\ and\ go\ to\ step-4$

end

$$x^{(iter+1)} = x^{(\mathrm{int})} + \upsilon[x^{(iter)} - x^{(\mathrm{int})}] \qquad 3.22$$

The path length improvement vector is multiplied by υ, which is a positive acceleration factor.

Algorithm-4: hybrid memetic HHO-PS search algorithm PSEUDO-CODE

Start-up: Initializing the size of population H, original location, objective function parameters with the no of iterations *D*

Outcome: perform the best possible location of prey 'rabbit' and its objective value of fitness

Setup the original and starting location of hawk's $A_j(j=1,2.....H)$

$while(iter < iter_{\max}$

Compute the possible fitness of H

Set-up A_{rabbit} as the best possible location

For (each of the hawk's (A_j))

Upgrade the migrating strength *J* and origin energy EP_0 ▷ $EP_0 = 2rand\ () -1,\ J = 2(1-rand())$

Upgrade Upgrade *EP* using eqn (3.3)

$if\ (|EP| \geq 1), then$ ▷ Period of Exploration

Upgrade the location of vector using eqn (3.1)

$if\ (|EP| < 1), then$ ▷ Period of Exploitation

$if\ (t \geq 0.5 and\ |EP| \geq 0.5), then$ ▷ Soft besiege

Upgrade the location of vector using eqn (3.4)

else

$if\ (t \geq 0.5 and\ |EP| < 0.5), then$ ▷ hard besiege

Upgrade the location of vector using eqn (3.6)

else

$if\ (t < 0.5 and\ |EP| \geq 0.5), then$ ▷soft besiege with running quicker drive

Upgrade the location of vector using eqn (3.10)

else

$if\ (t < 0.5 and\ |EP| < 0.5), then$ ▷hard besiege with running quicker drive

Upgrade the location of vector using eqn (3.11)

Upgrade the location of the Hawks by using black box PS optimizer (refer algorithm -3 PSEUDO-CODE)

Return the best possible location A_{rabbit}

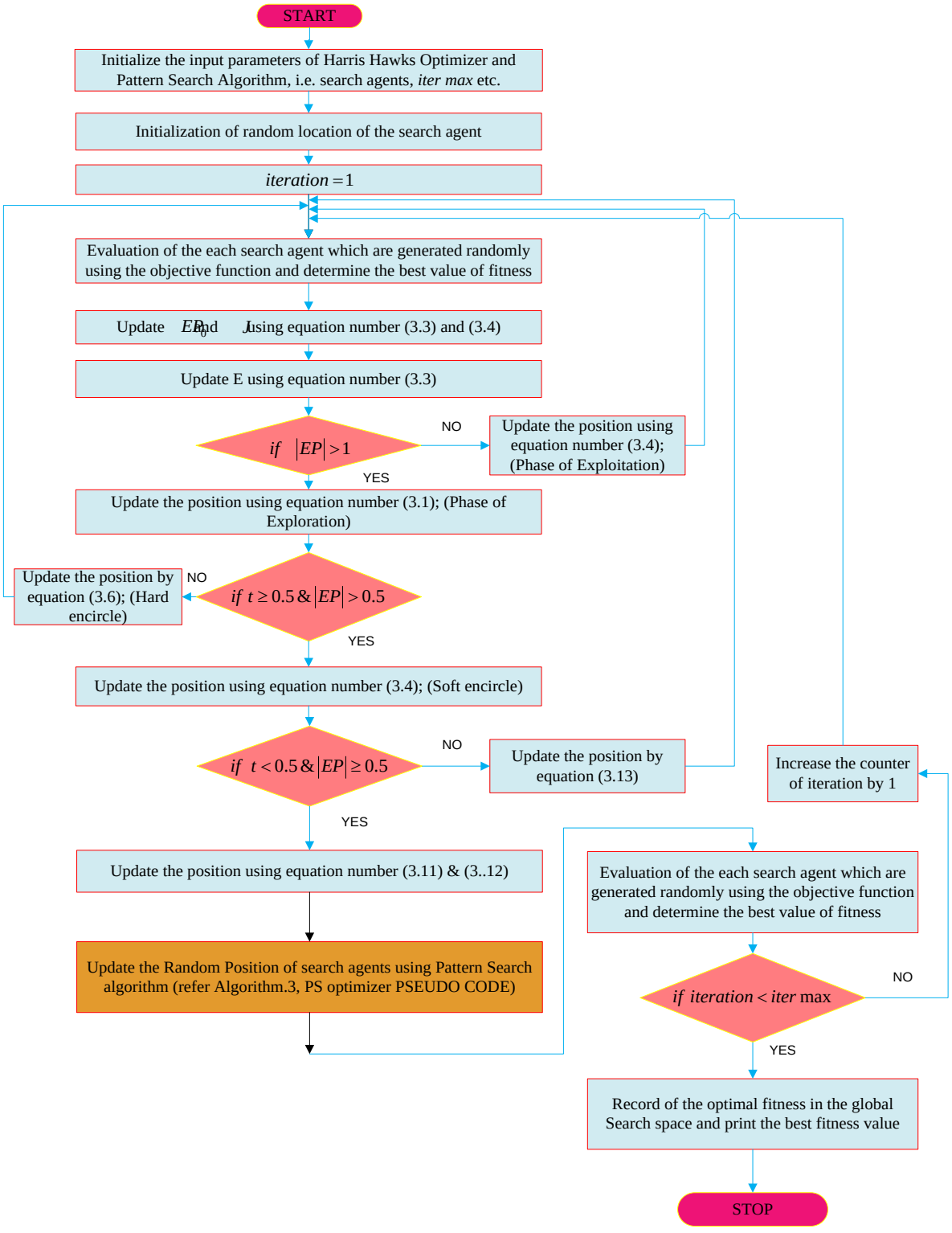

Fig.3.5 HHO-PS algorithm flow chart

3.4 MEMETIC HARRIS HAWKS – PATTERN SEARCH ALGORITHM

The global optimization strategy of the classic HHO method is noteworthy. Yet, it is easy to become caught in local search region for limited engineering and benchmarking optimized issues. The goal of the design template is to recognize the exploration of existing optimization task, and the HHO promising variant has been incorporated using PS method, termed a hybrid HHO-PS algorithm, to speed up the global search of existing HHO and stay it out of the local search area. The effectiveness of the approach optimization task was also tested for a variety of challenges, including 23 conventional benchmark difficulties and nine interdisciplinary engineering design optimum concerns[159]. Here, algorithm 4 depicts the hybrid memetic HHO - PS algorithm pseudo code and fig 5 replicates the hybrid memetic HHO-PS algorithm flowchart

3.5 MEMETIC SLIME MOULD – PATTERN SEARCH ALGORITHM

Algorithm-5: SMA-PS search algorithm PSEUDO-CODE

Set-up: Initializing the Slime mould parameter variables $Max\_iteration, popsize$

Initializing the initial location of the SM $S_t(t=1,2....n);$

While ($t \le Max\_iteration$)

Compute the fitness of each SM

$Upgrade\ the\ best\ fitness\ S_b$

Compute the *W* by Eqn. (3.19).

For $each\ search\ portion$

$Upgrade\ vc, vb, p;$

$Upgrade\ the\ positions\ by$ Eqn. (3.21);

End For

Upgrade the location of the SM by using black box PS optimizer (refer algorithm -3 PSEUDO-CODE)

$t = t+1$

End While

Return $bestfitness, S_b$.

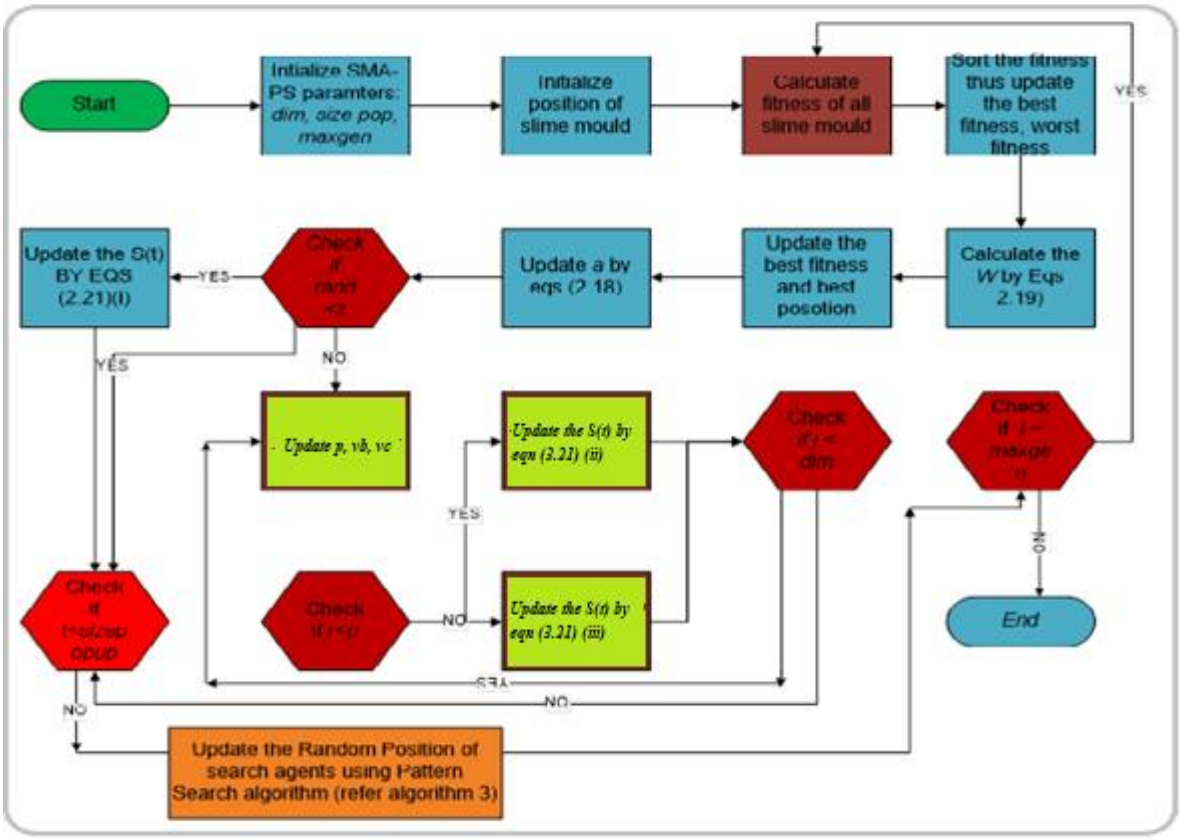

Fig.2.6 SMA-PS algorithm flow chart

Newly augmented SMA is based on the SM oscillation property that occurs naturally. The researchers devised a hybrid version of SMA called the hSMA-PS method to construct a more effective technique to perform discovery through procedure of exploiting for increasing the efficacy of SMA. Here, algorithm 5 depicts the PSEUDOCODE and fig 6 depicts the flowchart for hybrid memetic SMA-PS algorithm.

3.6 TEST SYSTEMS

While evaluating the LFR challenge, several benchmarks (BM) and constrained engineering (CE) optimal challenges considered for find out the efficacy and supremacy of the developed HHO-PS and SMA-PS optimizers.

The basic BM collection includes three primary BM feature classes: and fixed dimensions (FD) (see in fig.3.7 to 3.7b), uni-modal (UM), and multimodal (MM). Tables 3.3, 3.1, and 3.2 illustrate the mathematical formulas for UM, MM, and FD. Figures 3.7, 3.7a, and 3.7b depict its properties. Thirty trail runs are used to test the performance of standard BM functionalities.

3.7 STANDARD BENCHMARK PROBLEMS

Table.3.1 UM standard BM function's

Function's	Dimension's	Range's	f_{min}
$F_1(U) = \sum_{m=1}^{z} U_m^2$	30	[-100, 100]	0
$F_2(U) = \sum_{m=1}^{z} \lvert U_m \rvert + \prod_{m=1}^{z} \lvert U_m \rvert$	30	[-10 ,10]	0
$F_3(U) = \sum_{m=1}^{z} (\sum_{n-1}^{m} U_n)^2$	30	[-100, 100]	0
$F_4(U) = \max_m\{\lvert U_m \rvert, 1 \leq m \leq z\}$	30	[-100, 100]	0
$F_5(U) = \sum_{m=1}^{z-1} [100(U_{m+1} - U_m^2)^2 + (U_m - 1)^2]$	30	[-38, 38]	0
$F_6(U) = \sum_{m=1}^{z} ([U_m + 0.5])^2$	30	[-100, 100]	0
$F_7(U) = \sum_{m=1}^{z} mU_m^4 + \text{random } [0,1]$	30	[-1.28, 1.28]	0

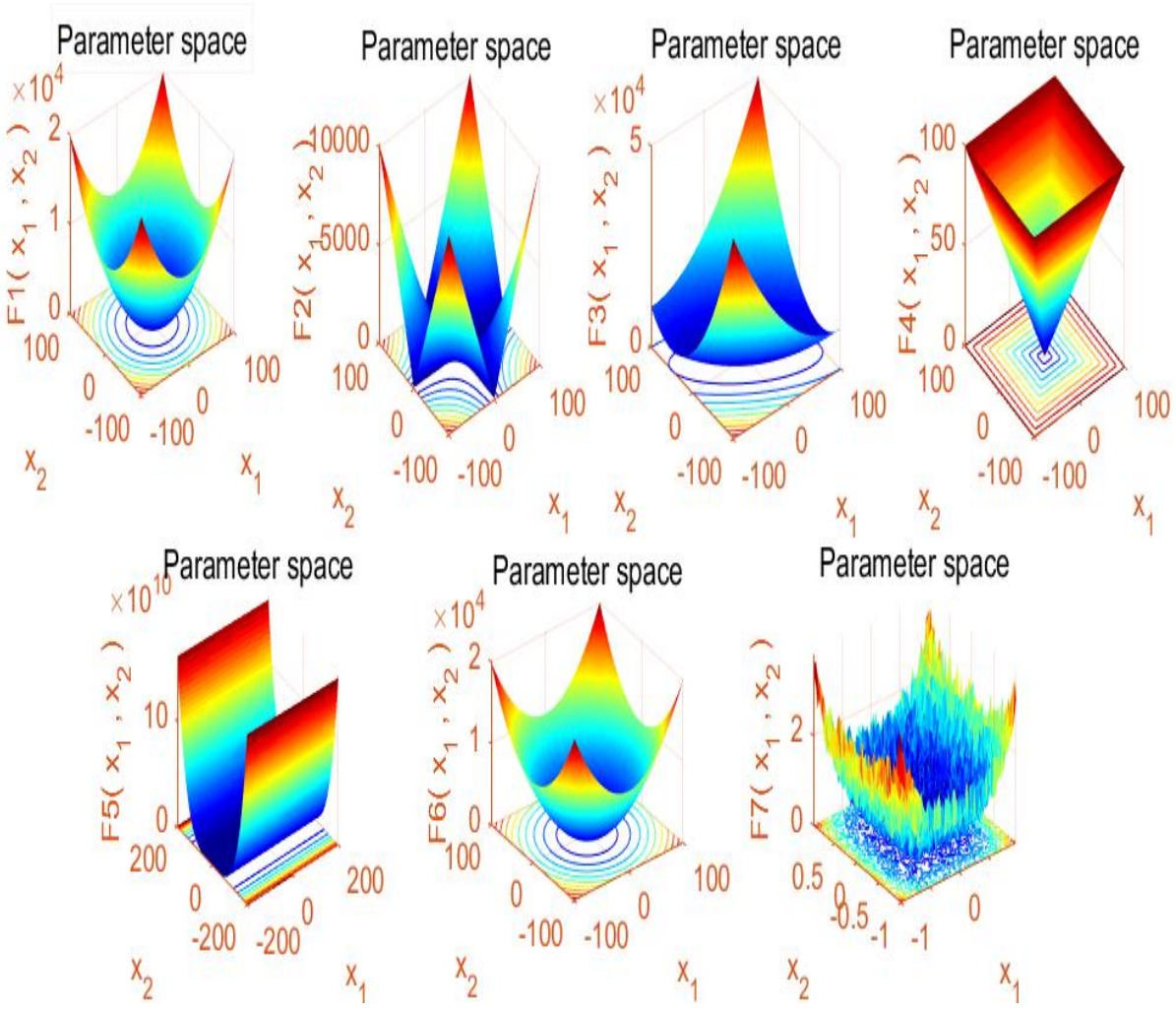

Fig.3.7 3D view of UM standard BM problem's

Table.3.2 MM standard BM function's

Function's	Dim's	Range's	$f_{\min}$
$F_8(\mathrm{U}) = \sum_{\dot{m}=1}^{z} -\mathrm{U}_m \sin(\sqrt{\lvert \mathrm{U}_m \rvert})$	30	-500,500]	-418.98295
$F_9(\mathrm{U}) = \sum_{\dot{m}=1}^{z} [\mathrm{U}_m^2 - 10\cos(2\pi\,\mathrm{U}_m) + 10]$	30	[-5.12,5.12]	0
$F_{10}(\mathrm{U}) = -20\exp\left(-0.2\sqrt{\left(\frac{1}{z}\sum_{\dot{m}=1}^{z}\mathrm{U}_m^2\right)}\right) - \exp\left(\frac{1}{z}\sum_{\dot{m}=1}^{z}\cos(2\pi\mathrm{U}_m)\right) + 20 + \mathrm{d}$	30	[-32,32]	0
$F_{11}(\mathrm{U}) = 1 + \sum_{\dot{m}=1}^{z}\frac{\mathrm{U}_m^2}{4000} - \Pi_{m=1}^{z}\cos\frac{\mathrm{U}_m}{\sqrt{m}}$	30	[-600, 600]	0
$F_{12}(\mathrm{U}) = \frac{\pi}{z}\left\{10\sin(\pi\tau_1) + \sum_{\dot{m}=1}^{z-1}(\tau_m - 1)^2[1 + 10\sin^2(\pi\tau_{m+1})] + (\tau_z - 1)^2\right\} + \sum_{\dot{m}=1}^{z}\mathrm{g}(\mathrm{U}_m, 10,100,4)$ $\tau_m = 1 + \frac{\mathrm{U}_m+1}{4}$ $\mathrm{g}(\mathrm{U}_m, \mathrm{b}, \mathrm{x}, i) = \begin{cases} \mathrm{x}(\mathrm{U}_m - \mathrm{b})^i & \mathrm{U}_m > b \\ 0 & -\mathrm{b} < \mathrm{U}_m < b \\ \mathrm{x}(-\mathrm{U}_m - \mathrm{b})^i & \mathrm{U}_m < -b \end{cases}$	30	[-50,50]	0
$F_{13}(\mathrm{U}) = 0.1\{sin^2(3\pi\mathrm{U}_m) + \sum_{\dot{m}=1}^{z}(\mathrm{U}_m - 1)^2[1 + sin^2(3\pi\mathrm{U}_m + 1)] + (\mathrm{x}_z - 1)^2[1 + sin^2)]$	30	[-50,50]	0

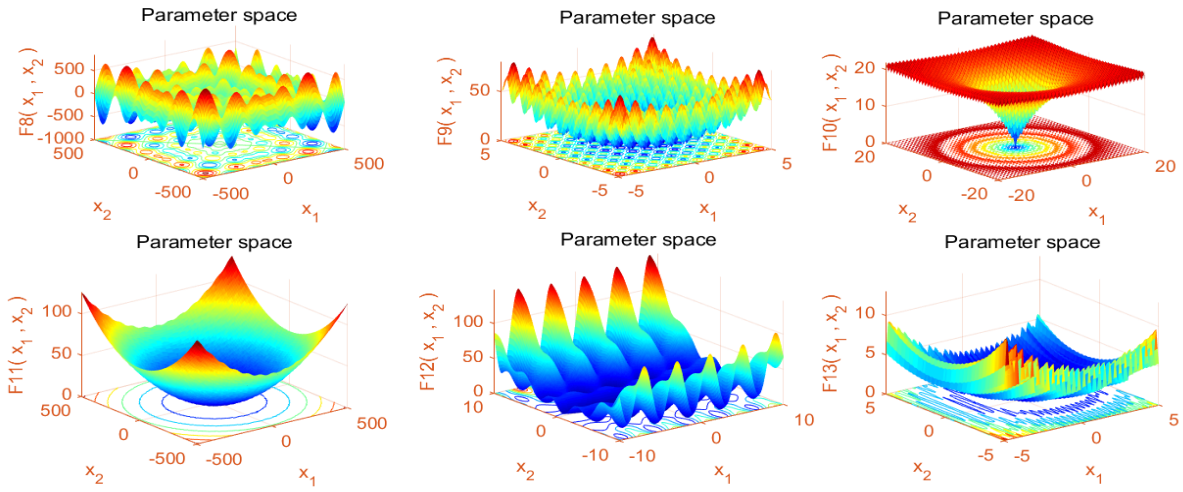

Fig.3.7a 3D view MM standard BM problem's

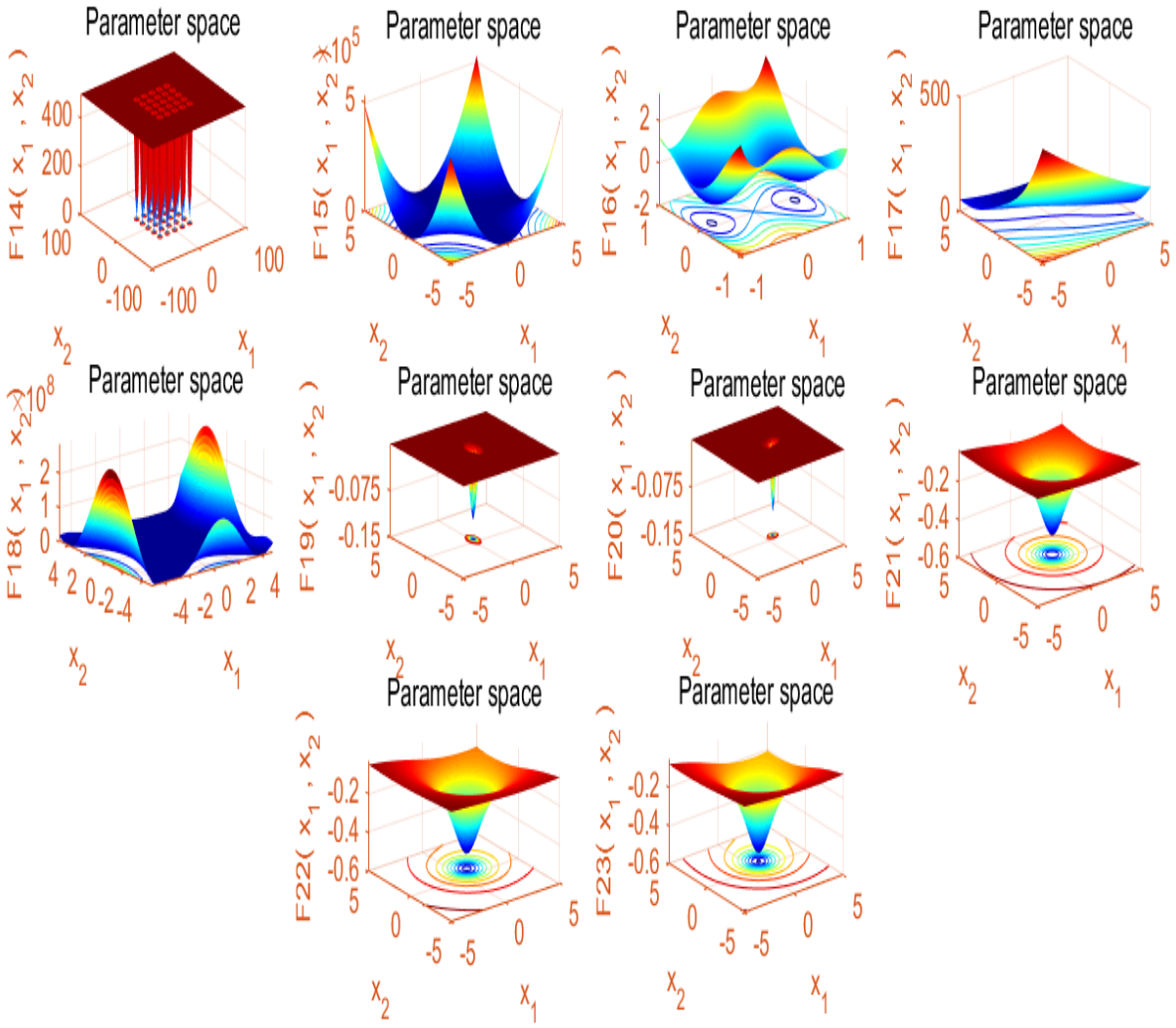

Fig.3.7b 3D view of FD standard BM function's

Table.3.3 FD standard BM function's

Function's	Dim's	Range's	f_{min}
$F_{14}(U) = [\frac{1}{500} + \sum_{n=1}^{2} 5 \frac{1}{n+\sum_{m=1}^{2}(U_m - b_{mn})6}]^{-1}$	2	[-65.536, 65.536]	1
$F_{15}(U) = \sum_{m=1}^{11}[b_m - \frac{U_1(a_m^2+a_m\eta_2)}{a_m^2+a_m\eta_3+\eta_4}]^2$	4	[-5, 5]	0.00030
$F_{16}(U) = 4U_1^2 - 2.1U_1^4 + \frac{1}{3}U_1^6 + U_1U_2 - 4U_2^2 + 4U_2^4$	2	[-5, 5]	-1.0316
$F_{17}(U) = (U_2 - \frac{5.1}{4\pi 2}U_1^2 + \frac{5}{\pi}U_1 - 6)^2 + 10(1-\frac{1}{8\pi})\cos U_1 + 10$	2	[-5, 5]	0.398
$F_{18}(U)=[1+(U_1+U_2+1)^2(19-14\,U_1+3U^2{}_1-14\,U_2+6U_1U_2+3\,U^2{}_2)]$	2	[-2,2]	3

$x[30+(2U_1-3U_2)^2 x(18-32U_1+12\ U^2{}_1+48U_2-36U_1U_2+27\ U^2{}_2)]$			
$F_{19}(U) = -\sum_{m=1}^{4} d_{\ m} \exp\left(-\sum_{n=1}^{3} U_{mn}(U_m - q_{mn})^2\right)$	3	[1, 3]	-3.32
$F_{20}(U) = -\sum_{m=1}^{4} d_{\ m} \exp\left(-\sum_{n=1}^{6} U_{mn}(U_m - q_{mn})^2\right)$	6	[0, 1]	-3.32
$F_{21}(U) = -\sum_{m=1}^{5}[(U - b_m)(U - b_m)^T + d_m]^{-1}$	4	[0,10]	-10.1532
$F_{22}(U) = -\sum_{m=1}^{7}[(U - b_m)(U - b_m)^T + d_m]^{-1}$	4	[0, 10]	-10.4028
$F_{23}(U) = -\sum_{m=1}^{7}[(U - b_m)(U - b_m)^T + d_m]^{-1}$	4	[0, 10]	-10.5363

Table.3.4 parametric tests performance for the optimizers

parameters	No of generations
iteration size for benchmarks (for all included optimizers)	500
No of runs generated by all optimizers	30
Engineering constraints generations	500

Table 3.4 displays the parameters, and no of generations for each constraint. Here, we evaluated the efficacy of the suggested SMA-PS and HHO-PS optimization algorithm with UM (F1-F7), MM (F8-F13) and FD (F14-F23) functions described above with the recent existing methodologies, in terms of Av average, std standard deviation, namely BOA[95], ECBO[160], WOA[115], WSA[116], GOA[117], PSOSCALF[144], DEAHHO[161], HHO[85], and TSA[112]. And the comparative convergence analysed for the suggested HHO-PS and SMA-PS optimizers with novel augmented GWO[80], SSA[118], MVO[92], MFO[102], HHO, SCA[81], SMA, GWO-PS[135], GWO-RES, and PSO[107] optimizers. Performance has been evaluated with the 500 iterations and 30 search agents each BM for the suggested optimizers.

Here, UM BM are used to calculate the global optima (exploitation analysis) for MA. UM comparative analyses with existing MA for the SMA-PS and HHO-PS algorithms are tabulated in table 3.5. here, comparative convergence curves of HHO-PS and SMA-PS optimizer with other existing novel augmented optimizers are displays in fig 3.8.

Table.3.5 UM comparative analysis for suggested optimizers with existing methodologies								
Algorithms	parameters	F1	F2	F3	F4	F5	F6	F7
BOA	Av	1.42E-64	1.32E-38	17.40900	2.17E-15	25.74747	0.075961	0.000436
	Std	4.46E-62	1.87E-37	15.34927	7.07E-12	0.029795	0.003099	0.000730
ECBO	Av	0.014981	0.003078	6676.084	14.72304	618.3821	0.018717	0.077259
	Std	0.009619	0.001012	2308.023	2.376884	519.0368	0.011134	0.019375
WOA	Av	1.42E-43	2.39E-25	43789.54	6.651892	28.21277	0.453929	0.004782
	Std	3.86E-35	2.03E-21	13324.09	4.220696	0.564472	0.220565	0.004616
WSA	Av	1.09E-50	4.89E-28	0.014089	0.000490	32.42146	0	0.006433
	Std	3.99E-50	1.94E-27	0.011180	0.000354	29.52849	0	0.0018394
GOA	Av	8.924014	36.16146	2599.891	5.978819	526.1095	106.3820	0.587710
	Std	7.366225	17.87108	1760.702	2.954771	325.6448	107.8309	0.245901
PSOSCALF	Av	1.11014E-20	4.09460E-11	2.16858E-12	8.47410E-08	21.97646	7.13998E-12	0.00012
	Std	1.8328E-20	5.68981E-11	1.03815E-11	1.23324E-07	0.54774	3.65884E-11	0.00010
DEAHHO	Av	3.3632E-211	6.9024E-106	6.4615E-139	8.0466E-103	0.0366	5.6370E-04	1.3693E-04
	Std	0	4.8610E-105	3.8112E-128	5.6898E-102	0.0525	9.2921E-04	1.5722E-04
HHO	Av	6.1525E-073	1.0849E-039	1.9735E-047	1.6130E-038	0.0387	7.1149E-04	2.3849E-04
	Std	4.0407E-072	3.0364E-039	1.3950E-046	6.9434E-038	0.0595	0.0011	1.8902E-04
TSA	Av	7.78E-56	8.70E-42	3.20E+03	1.36E+00	2.42E+01	2.05E-34	9.47E-03
	Std	1.83E-55	9.00E-42	1.80E+03	6.16E-01	1.06E+01	7.82E-34	2.82E-03
HHO-PS	Av	9.2E-107	8.31E-54	5.03E-20	6.20E-54	2.18E-09	3.95E-14	0.002289
	Std	5E-106	4.46E-53	1.12E-19	1.75E-53	6.38E-10	3.61E-14	0.001193
SMA-PS	Av	6.6232E-307	1.7E-157	0	1.4E-168	2.63E-06	2.49E-12	0.003631
	Std	0	3.9E-157	0	0	1.35E-06	5.53E-12	0.002008

Table 3.6 MM comparative analysis for suggested optimizers with existing methodologies							
Algorithms	parameters	F8	F9	F10	F11	F12	F13
BOA	Av	-11175.9	0	8.88E-16	0	0.005633	0.071574
	Std	1466.041	0	9.86E-32	0	0.001536	0.034192
ECBO	Av	-11911.0	8.42.6.1	0.118860	0.12818	0.078097	0.106004
	Std	211.2423	2.352613	0.155987	0.008800	0.070091	0.097929
WOA	Av	-10562.6	0	4.09E-15	1.11E-16	0.022028	0.502757
	Std	1562.556	0	2.23E-15	0.054574	0.019745	0.218434
WSA	Av	-9354.74	40.56002	1.88E-14	0.016042	1.57E-32	1.35E-32
	Std	653.1757	10.78416	4.52E-15	0.020111	5.57E-48	5.57E-48
GOA	Av	-7286.43	166.6363	12.64091	1.708783	4.627045	3.122240
	Std	500.4084	35.81810	6.554900	0.716727	2.087953	1.279501
PSOSCA	Av	12569.486	0	2.24609E-11	0	8.46465E-14	0.00399
	Std	2.39996E-07	0	2.33547E-11	0	2.79106E-13	0.00928
DEAHHO	Av	-1.2547E+04	0	8.8818E-16	0	2.8911E-05	303031E-04
	Std	84.5581	0	0	0	4.7855E-05	4.8598E-04
HHO	Av	-102354E+04	0	808818-16	0	4.4746E-05	4.1585E-04
	Std	98.2341	0	0	0	9.6436E-05	5.1207E-04
TSA	Av	-1.06E+04	2.54E+01	7.52E-15	2.47E-04	1.57E-32	1.36E-32
	Std	1.15E+03	2.09E+01	1.23E-15	1.35E-03	5.89E-35	3.13E-34
HHO-PS	Av	-12332	0	8.88E-16	0	2.94E-15	1.16E-13
	Std	335.7988	0	0	0	3.52E-15	1.15E-13
SMA-PS	Av	-12569.5	0	8.88E-16	0	1.75E-14	4.01E-13
	Std	3.62E-11	0	0	0	3.88E-14	5.54E-13

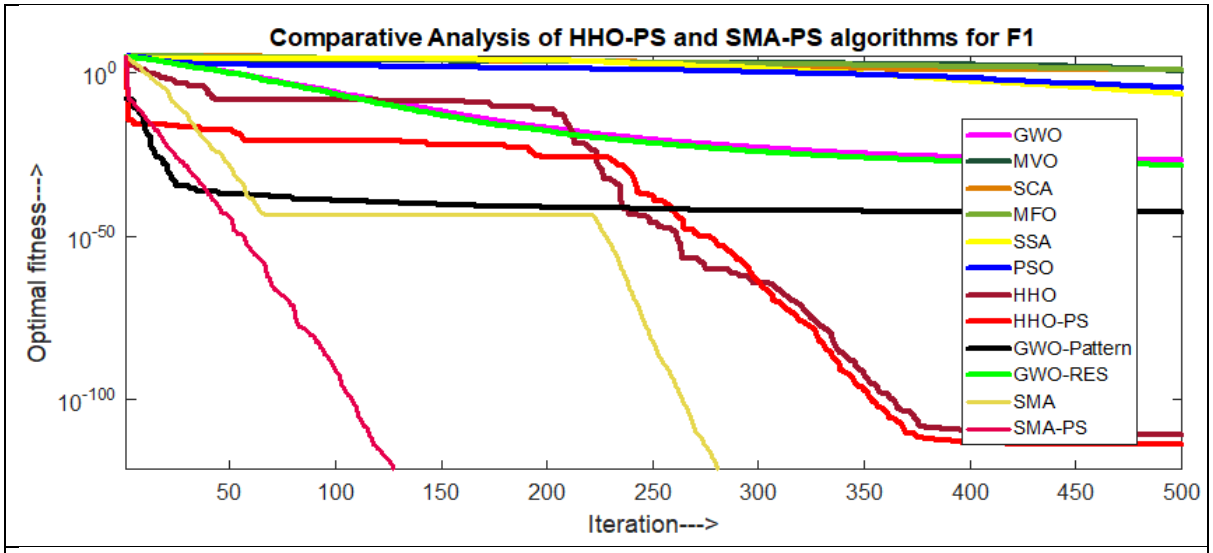
Comparative Analysis of HHO-PS and SMA-PS algorithms for F1
Optimal fitness--->
Iteration--->
GWO
MVO
SCA
MFO
SSA
PSO
HHO
HHO-PS
GWO-Pattern
GWO-RES
SMA
SMA-PS

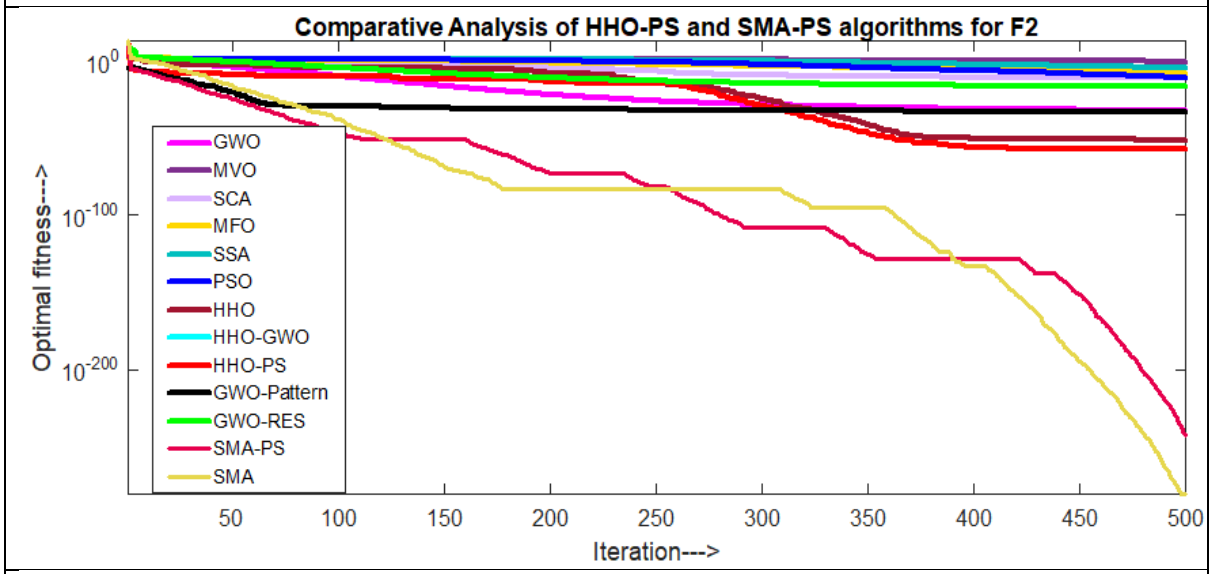
Comparative Analysis of HHO-PS and SMA-PS algorithms for F2
Optimal fitness--->
Iteration--->
GWO
MVO
SCA
MFO
SSA
PSO
HHO
HHO-GWO
HHO-PS
GWO-Pattern
GWO-RES
SMA-PS
SMA

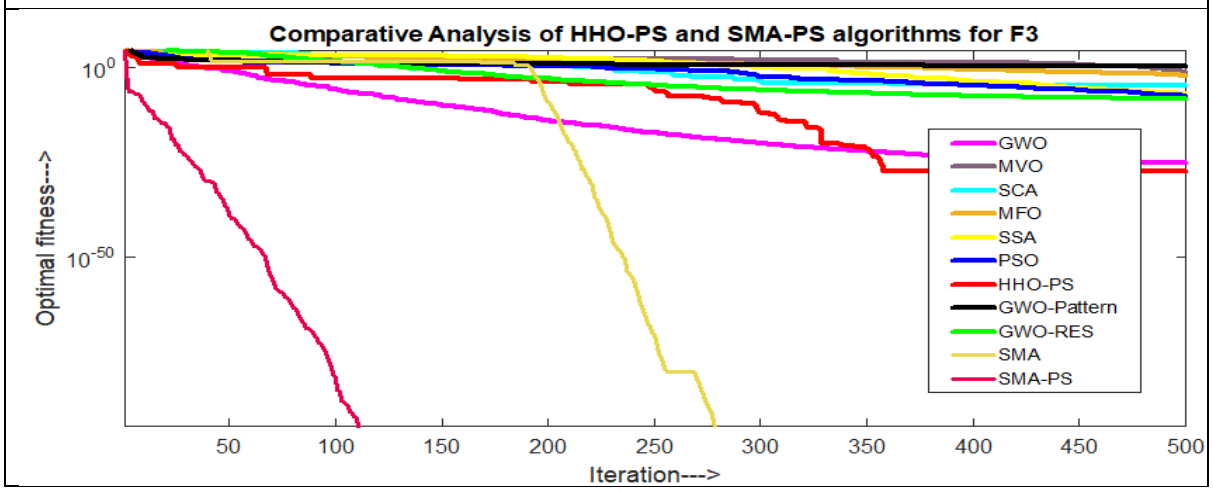
Comparative Analysis of HHO-PS and SMA-PS algorithms for F3
Optimal fitness--->
Iteration--->
GWO
MVO
SCA
MFO
SSA
PSO
HHO-PS
GWO-Pattern
GWO-RES
SMA
SMA-PS

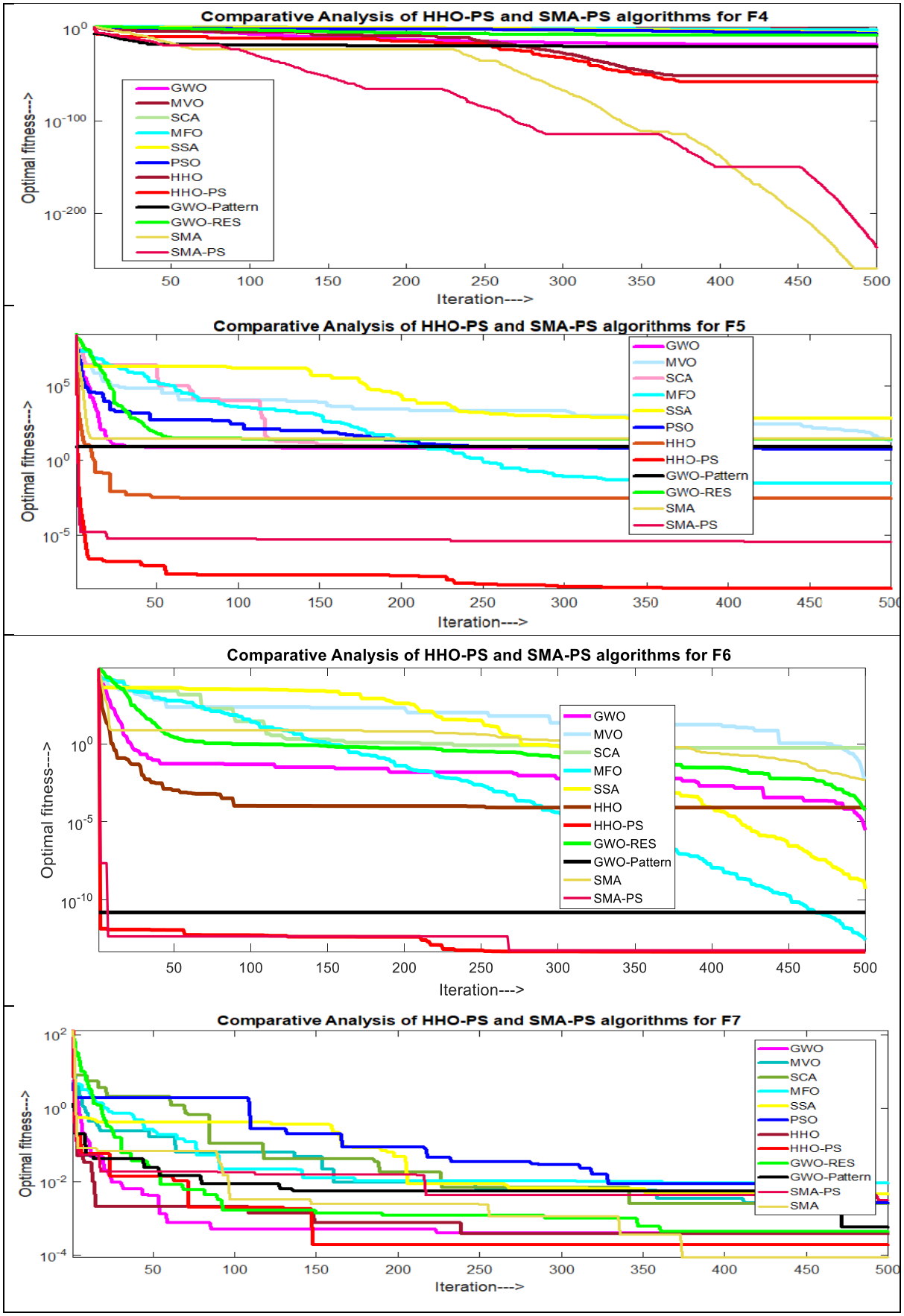

Fig.3.8 UM comparative convergence curves for developed hybrid memetic HHO-PS and SMA-PS optimizers with other novel augmented optimizers.

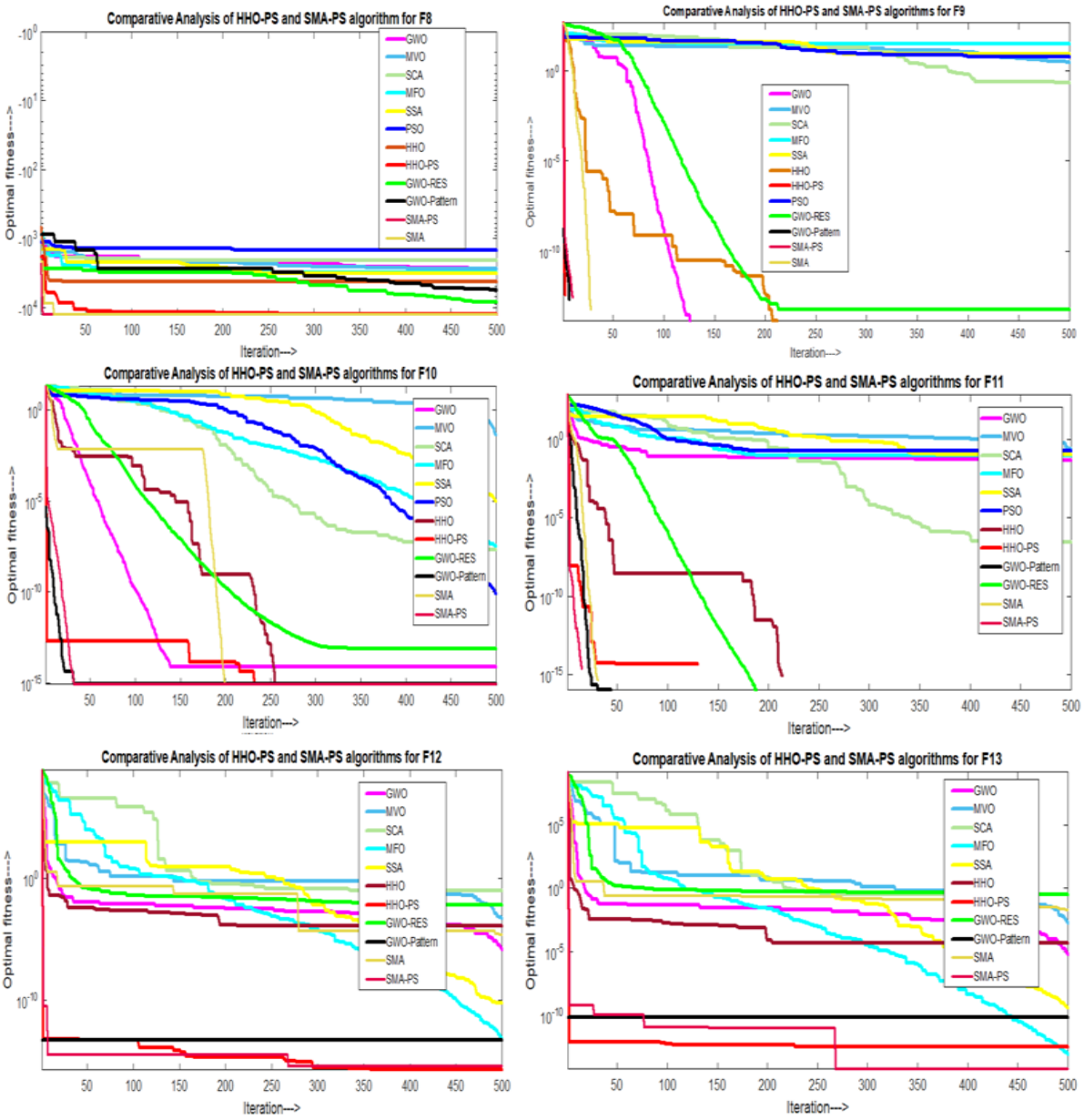

Fig.3.9 MM comparative convergence curves for developed hybrid memetic HHO-PS and SMA-PS optimizers with other novel augmented optimizers.

There are several local minima in MM BM functions (F8-F13) that rise significantly with size. They are also ideal for evaluating exploration (high dimensional) success and the potential to resist local optimism. MM comparative analyses with existing MA for the suggested HHO-PS and SMA-PS algorithms are tabulated in table 3.6. Comparative convergence curves for MM are displays in fig 3.9.

Table.3.7 FD comparative analysis for suggested optimizers with existing methodologies						
Algorithms	parameters	F14	F15	F16	F17	F18

BOA	Av	0.998004	0.000369	-1.03163	0.397887	3.000014
	Std	0.705966	0.000319	1.41E-07	0	3.20E-05
ECBO	Av	0.998004	0.004632	-1.03162	0.397887	3.0000
	Std	0.00000	0.000187	0.000016	0	1.82E-09
WOA	Av	1.4942257	0.000942	-1.03163	0.376981	3.000047
	Std	3.502703	0.000241	1.12E-09	3.57E-05	0.000198
WSA	Av	0.998004	0.000549	-1.03163	0.397887	3
	Std	1.13E-16	0.00032	5.68E-16	0	2.91E-15
GOA	Av	0.998004	0.006711	-1.03163	0.398890	1.92E+01
	Std	5.06E-16	0.013470	2.09E-13	3.98E-06	1.453994
PSOSCA	Av	1.13027	3.13244E-04	-1.0316	0.39788	3
	Std	0.5033.8	2.17489E-05	4.40244E-16	3.66527E-15	5.96540E-13
DEAHHO	Av	0.998	4.3568E-04	-1.0316	3.9789E-01	3
	Std	0	2.7617E-04	2.2430E-16	3.3645E-16	3.5668E-15
HHO	Av	1.1967	4.4421E-04	-1.0316	3.9791E-01	3
	Std	4.4873E-01	3.2096E-04	6.2949E-08	7.0537E-05	8.8360E-06
TSA	Av	9.98E-01	6.29E-04	-1.03E+00	3.98E-01	3.00E+00
	Std	0.00E+00	9.82E-05	6.71E-16	0.00E+00	1.23E-15
HHO-PS	Av	0.998004	0.000307	-1.03163	0.397887	3
	Std	1.57E-16	1.65E-13	1.11E-16	0	2.63E-15
SMA-PS	Av	0.998004	0.000307	-1.03163	0.397887	3
	Std	1.24E-16	5E-10	3.21E-15	2.27E-14	2.08E-14

Table.3.7a FD comparative analysis for HHO-PS and SMA-PS algorithm solutions with existing methodologies (continues……)

Algorithms	parameters	F19	F20	F21	F22	F23
BOA	Av	-3.86281	-3.26854	-8.10257	-9.732711	-10.5300

	Std	2.66E-15	0.08414	2.528422	0.259246	2.686381
ECBO	Av	-3.86278	-3.25066	-6.13871	-6.91297	-8.95150
	Std	4.69E-10	0.057294	3.437738	3.383608	2.928897
WOA	Av	-3.85457	-3.21236	-7.35090	-8.02790	-9.42641
	Std	0.009716	0.082641	2.449949	3.049680	3.195802
WSA	Av	-3.86278	-3.25066	-6.72819	-7.35819	-8.30703
	Std	2.46E-15	0.059241	3.78711	3.609873	3.499898
GOA	Av	-3.54504	-3.28614	-4.88727	-5.19768	-6.71956
	Std	0.433311	0.059569	2.929784	3.385219	3.624282
PSOSCA	Av	-3.86278	-3.27168	-10.15319	-10.40294	-10.53640
	Std	8.31755E-15	0.06371	4.46227E-15	1.80672E-15	4.84794E-15
DEAHHO	Av	-3.8628	-3.2792	-10.1532	-10.4029	-10.5364
	Std	3.1402E-15	5.7648E-02	8.8090E-15	8.0887E-15	9.0185E-15
HHO	Av	-3.8588	-3.0200	-5.1187	-5.2788	-5.2260
	Std	5.62E-03	1.3751E-01	5.7558-01	1.0338	1.0694
TSA	Av	-3.86E+00	-3.32E+00	-1.0E+01	-1.03E+01	-1.05E+01
	Std	2.71E-15	1.37E-15	5.18E-01	3.00E-01	2.70E-05
HHO-PS	Av	-3.86278	-3.322	-10.1532	-10.4029	-10.5364
	Std	2.26E-15	4.35E-15	7.47E-12	7.74E-15	7.69E-15
SMA-PS	Av	-3.86278	-3.322	-10.1532	-10.4029	-10.5364
	Std	2.44E-14	9.06E-13	3.09E-11	6.59E-11	2.33E-11

There are several local minima that increase exponentially with solution space in the FD functions (F14-F23). They are also ideal for assessing the success of discovery and the potential to resist local optima. FD comparative analyses with existing PMH algorithms for the SMA-

PS and HHO-PS algorithms are tabulated in table 3.7 and 3.7a. Convergence comparative curves are displays in fig 3.10.

Between exploitation and exploration, FD functions with several local optima are addressed. SMA-PS and HHO-PS outperforms other search optimizers, as seen in tables 3.7 and 3.7a. SMA-PS and HHO-PS was shown to be able to regulate exploitation and exploration while also avoiding the local optimum. Here, for the FD BM, SMA-PS and HHO-PS optimizers performs similar efficacy outcomes.

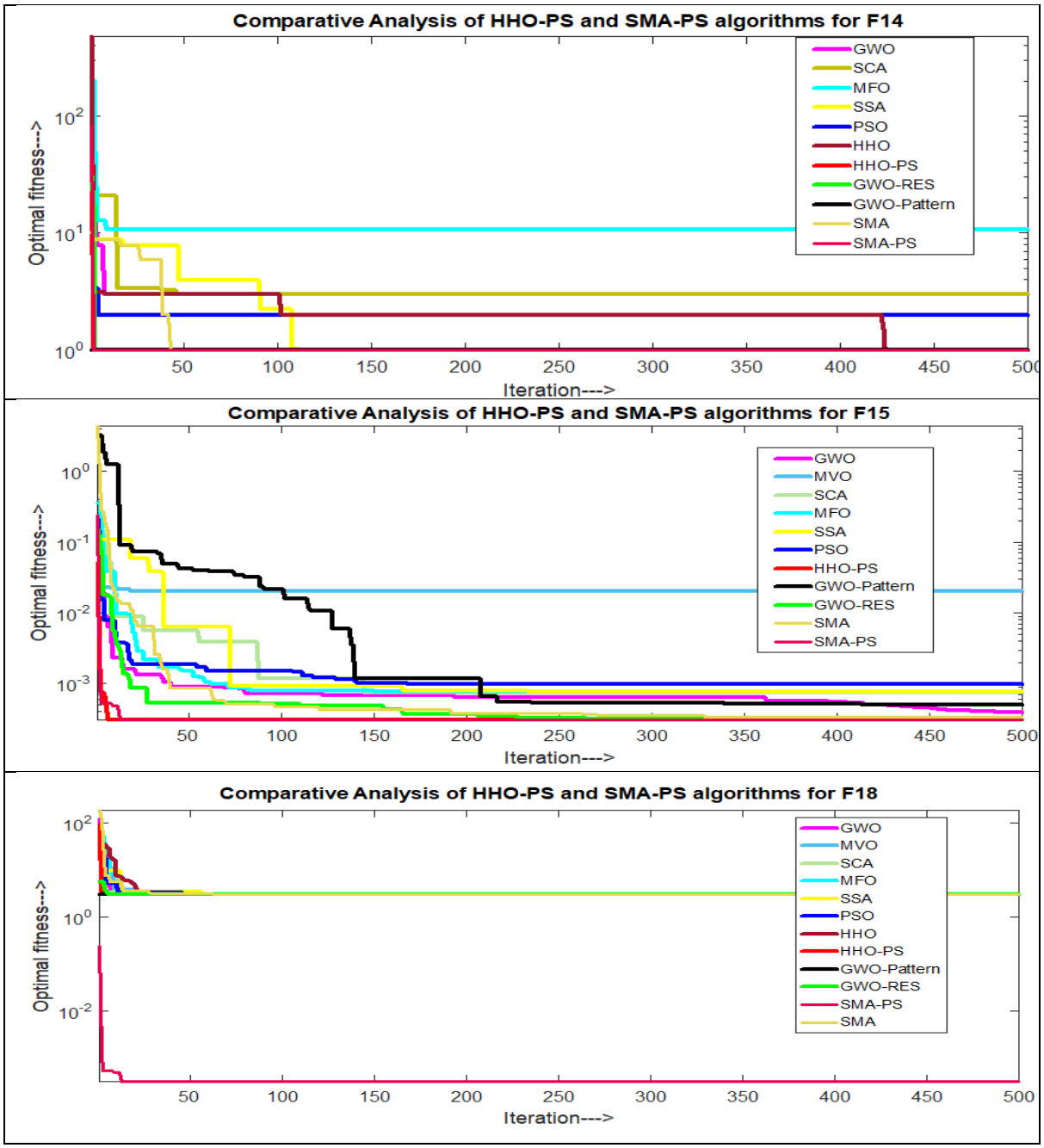

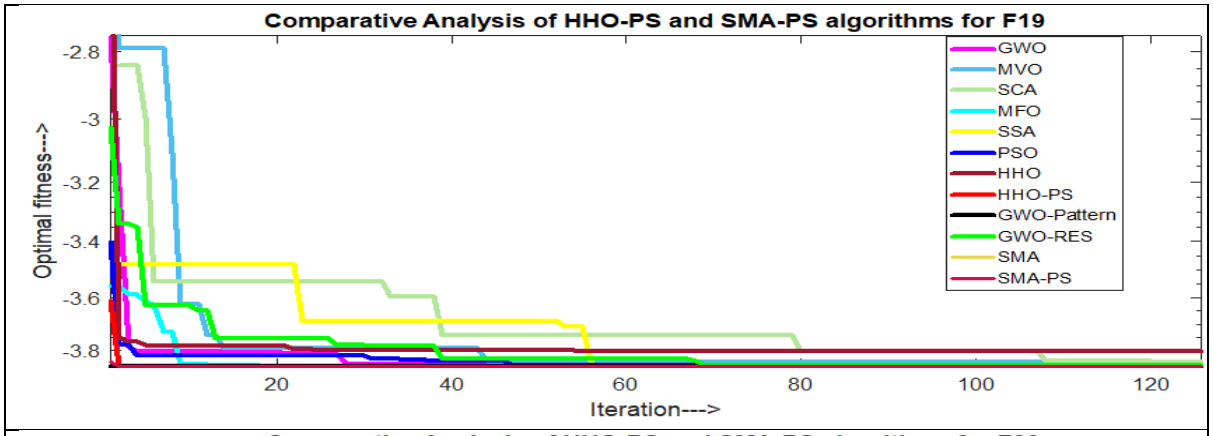
Comparative Analysis of HHO-PS and SMA-PS algorithms for F19
Optimal fitness--->
Iteration--->
GWO
MVO
SCA
MFO
SSA
PSO
HHO
HHO-PS
GWO-Pattern
GWO-RES
SMA
SMA-PS

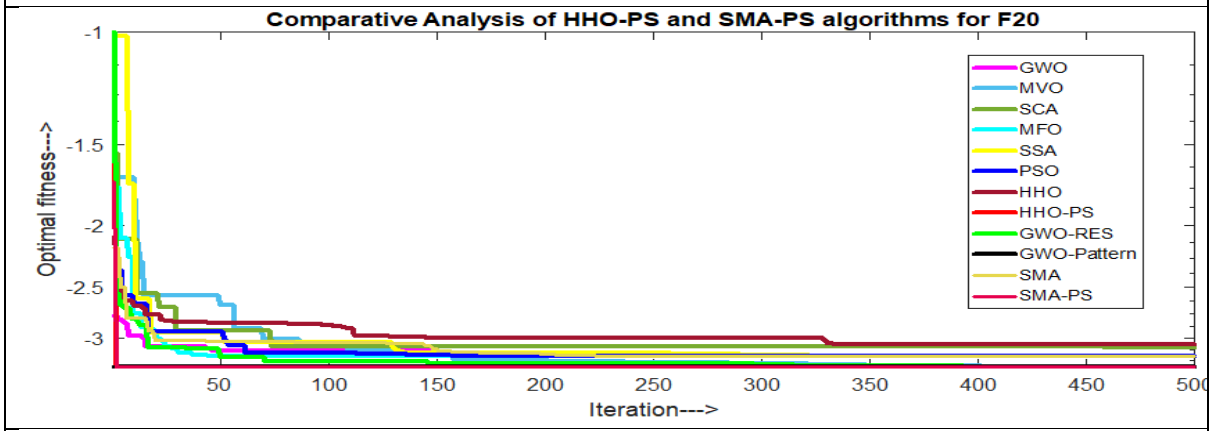
Comparative Analysis of HHO-PS and SMA-PS algorithms for F20
Optimal fitness--->
Iteration--->
GWO
MVO
SCA
MFO
SSA
PSO
HHO
HHO-PS
GWO-RES
GWO-Pattern
SMA
SMA-PS

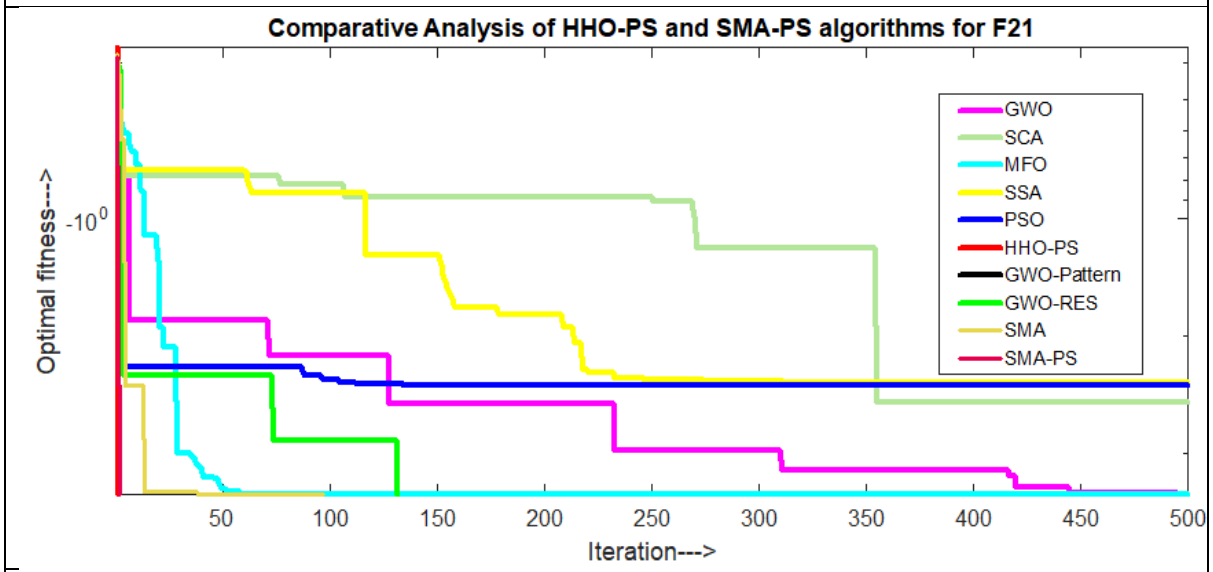
Comparative Analysis of HHO-PS and SMA-PS algorithms for F21
Optimal fitness--->
Iteration--->
GWO
SCA
MFO
SSA
PSO
HHO-PS
GWO-Pattern
GWO-RES
SMA
SMA-PS

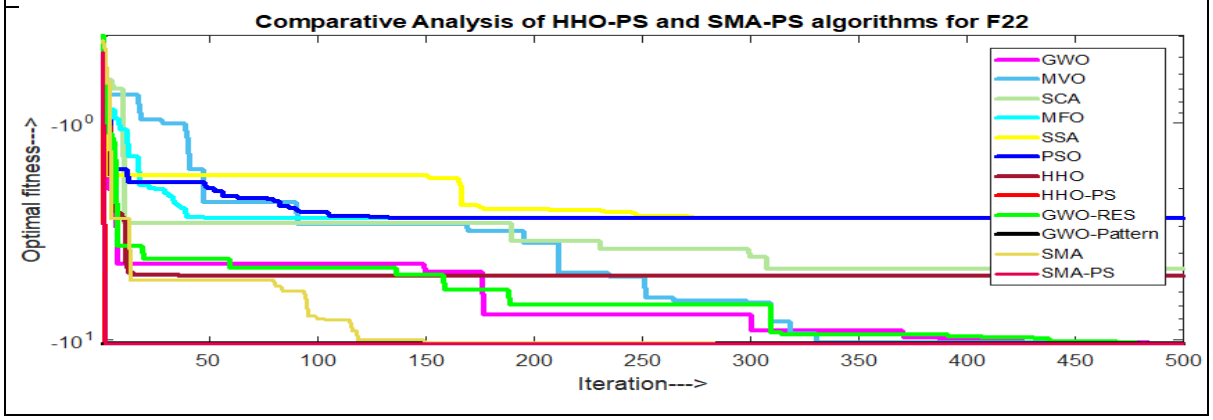
Comparative Analysis of HHO-PS and SMA-PS algorithms for F22
Optimal fitness--->
Iteration--->
GWO
MVO
SCA
MFO
SSA
PSO
HHO
HHO-PS
GWO-RES
GWO-Pattern
SMA
SMA-PS

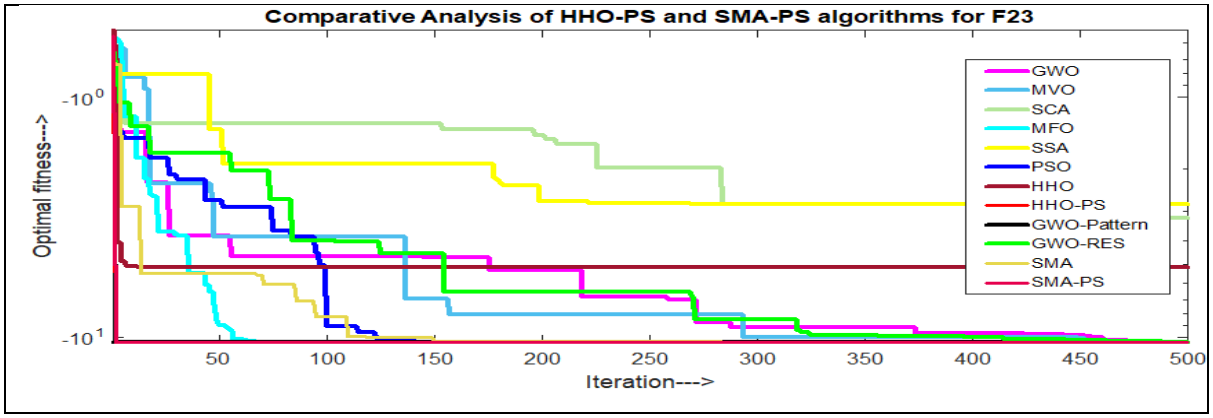

Fig.3.10 FD comparative convergence curves for developed hybrid memetic HHO-PS and SMA-PS optimizers with other novel augmented optimizers.

3.8 ENGINEERING OPTIMIZATION PROBLEMS

This section discusses how the suggested SMA-PS and HHO-PS apply to NINE well-known CE optimum control problems. In past years, overcoming the CE issues using MA has been a well-respected study direction [119] [118]. Earlier, the outputs of the SMA-PS and HHO-PS and were validated using numerous suggested conventional and customized optimizers. The specifics of CE premised designs are shown in Table 3.8. Comparing convergence curves for suggested hHHO-PS and hSMA-PS versus classical HHO and SMA are shown in Fig.3.20.

Table 3.8 Details of CE designs (SPECIAL1-SPECIAL9)

Engineering functions	Design name	Discrete no. of variables	No of constraints	objective
SPECIAL1	Speed reducer problem	7	11	Minimize weight
SPECIAL2	Pressure vessel	4	4	Minimize cost
SPECIAL3	Tension/compression spring design problem	3	4	Minimize weight
SPECIAL4	Welded beam	4	7	Minimize cost
SPECIAL5	Rolling Element Bearing	10	9	Maximize dynamic load
SPECIAL6	Multi disk clutch break (discrete variables)	5	8	Minimize weight
SPECIAL7	Gear Train Design problem	4	1	minimize gear ratio
SPECIAL8	Cantilever beam design	5	1	Minimize weight
SPECIAL9	I beam design	4		minimize vertical deflection

3.8.1 **Design problem of Speed reducer**

The speed reducer optimized strategy is a significantly more difficult problem to solve since it is linked to seven design parameters[120]. In this optimisation issue (see Fig. 3.11), the key goal is minimize the weight of the design[121]. There seem 11 limits in this optimization, as well as 6 continuous variables. Even though this problem has seven parameters for optimization (s_1-s_7). The design and its variables were depicting in fig 3.11. The comparative analysis was depicting in table 3.9. and the mathematical expressions in eqns (3.23 to 3.23k) depicts as follows.

For minimizing,

$$f(\vec{s}) = 0.7854 s_1 s_2 (3.3333 s_3^2 + 14.9334 s_3 - 43.0934) - 1.508 s_1 (s_6^2 + s_7^2) + 7.4777 (s_6^3 + s_7^3) + 0.7854 (s_4 s_6^2 + s_5 s_7^2) \quad 3.23$$

Subjected to,

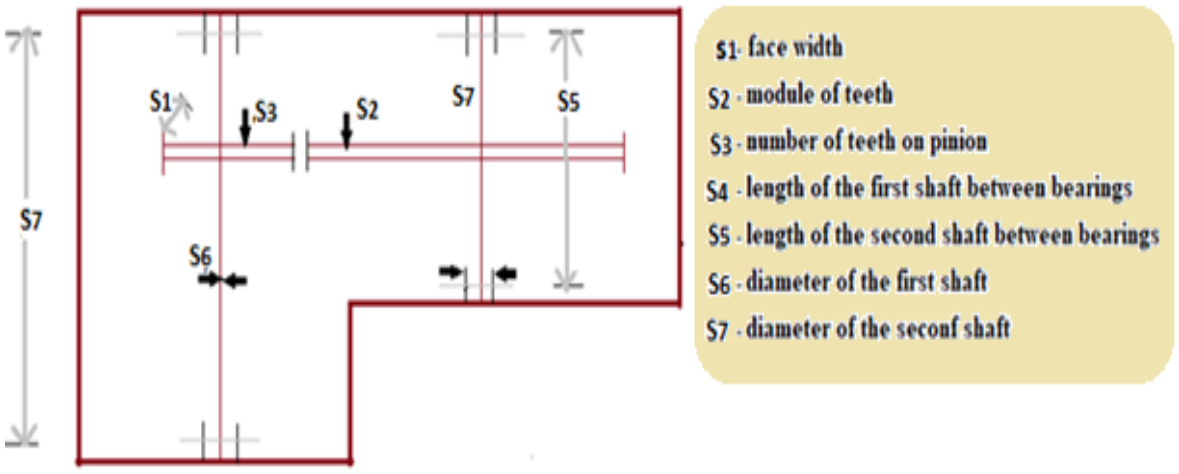

Fig.3.11 speed reducer design problem.

$$r_1(\vec{s}) = \frac{27}{s_1 s_2^2 s_3} - 1 \le 0 \quad 3.23a$$

$$r_2(\vec{s}) = \frac{397.5}{s_1 s_2^2 s_3^2} - 1 \le 0 \quad 3.23b$$

$$r_3(\vec{s}) = \frac{1.93 s_4^3}{s_2 s_3 s_6^4} - 1 \le 0 \quad 3.23c$$

$$r_4(\vec{s}) = \frac{1.93 s_5^3}{s_2 s_3 s_7^4} - 1 \le 0 \quad \text{3.23d}$$

$$r_5(\vec{s}) = \frac{1}{110 r_6^3} \sqrt{\left(\frac{745.0 r_4}{r_2 r_3}\right)^2 + 16.9 \times 10^6} - 1 \le 0 \quad \text{3.23e}$$

$$r_6(\vec{s}) = \frac{1}{85 s_7^3} \sqrt{\left(\frac{745.0 s_5}{s_2 s_3}\right)^2 + 157.5 \times 10^6} - 1 \le 0 \quad \text{3.23f}$$

$$r_7(\vec{s}) = \frac{s_2 s_3}{40} - 1 \le 0 \quad \text{3.23g}$$

$$r_8(\vec{s}) = \frac{5 s_2}{s_1} - 1 \le 0 \quad \text{3.23h}$$

$$r_9(\vec{s}) = \frac{s_1}{12 s_2} - 1 \le 0 \quad \text{3.23i}$$

$$r_{10}(\vec{s}) = \frac{1.5 s_6 + 1.9}{12 s_2} - 1 \le 0 \quad \text{3.23j}$$

$$r_{11}(\vec{s}) = \frac{1.1 s_7 + 1.9}{s_5} - 1 \le 0 \quad \text{3.23k}$$

Where

$$2.6 \le s_1 \le 3.6, 0.7 \le s_2 \le 0.8, 17 \le s_3 \le 28, 7.3 \le s_4 \le 8.3, 7.8 \le s_5 \le 8.3, 2.9 \le s_6 \le 3.9 \, and \, 5 \le s_7 \le 5.5$$

Table.3.9 speed reducer optimal engineering design comparative analysis

Algorithm's		HHO-PS	SMA-PS	HGSO[122]	HHO-SCA[162]	SHO[123]	PSO-DE[139]	MBA
Variables	s_1	3.5	3.5	3.498	3.506119	3.50159	3.50	3.5
	s_2	0.7	0.7	0.71	0.7	0.7	0.7	0.7
	s_3	17	17	17.02	17	17	17	17
	s_4	7.3	7.3	7.67	7.3	7.3	7.3	7.300033
	s_5	7.715321	7.715321	7.810	7.99141	7.8	7.8	7.715772
	s_6	3.350215	3.350215	3.36	3.452569	3.35127	3.350214	3.350218
	s_7	5.286655	5.286655	5.289	5.286749	5.28874	5.2866832	5.286654
Optimal cost		2994.471	2994.472	2997.10	3029.873076	2998.5507	2996.34817	2994.48245

3.8.2 Pressure vessel

The designing of a pressure vessel is utilised to reduce manufacturing costs. There are 4 constraint parameters in this model. It also contains four active limitations. Figure 3.12 shows

the CE design of a pressure vessel[159]. Table 3.10 also contains the analytical results. The following are the mathematical formulas eqns (3.24 to 3.24e).

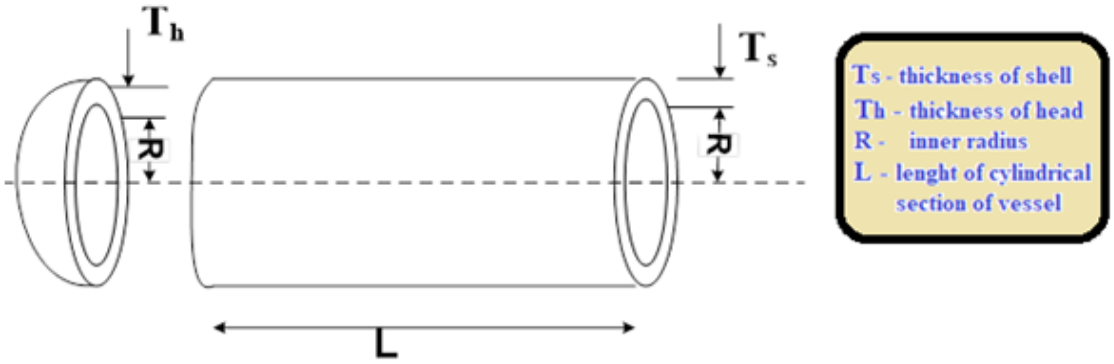

Fig.3.12 design of pressure vessel

Consider:

$$p = [p_1 p_2 p_3 p_4] = [T_s T_h R L_h] \qquad 3.24$$

Minimize,

$$f(p) = 0.6224 p_1 p_3 p_4 + 1.7781 p_2 p_3^2 + 3.1661 p_1^2 p_4 + 19.84 p_1^2 p_3 \qquad 3.24a$$

Subjected to

$$r_1(p) = -p_1 + 0.0193 p_3 \le 0 \qquad 3.24b$$

$$r_2(\vec{y}) = p_3 + 0.00954 p_3 \le 0 \qquad 3.24c$$

$$r_3(p) = -\pi p_3^2 p_4 - \frac{4}{3}\pi p_3^3 + 1296000 \le 0 \qquad 3.24d$$

$$r_4(p) = p_4 - 240 \le 0 \qquad 3.24e$$

Variable range, $0 \le p_1 \le 99$

$$0 \le p_2 \le 99$$

$$10 \le p_3 \le 200$$

$$10 \le p_4 \le 200$$

Table.3.10 analytical results for pressure vessel design

Algorithms		HHO-PS	SMA-PS	GSA [82]	PSO[148]	GA [124]	SHO[123]	HHO[85]	MFO[102]	ACO [125]	Lagrangian Multiplier[126]	Branch-bound [127]
variables	T_s	0.778169	0.8125	1.125	0.8125	0.778210	0.81758383	0.8125	0.8125	0.8125	1.125	1.125
	T_h	0.384649	0.4345	0.625	0.4375	0.384889	0.4072927	0.4375	0.4375	0.4375	0.625	0.625
	R	40.31963	42.0892	55.9887	42.0913	40.315040	42.0917457 6	42.098445	42.0981	42.1036	58.291	47.7
	L	199.9999	176.7587	84.4542	176.7465	200.00000	176.7196352	176.636596	176.641	176.5727	43.69	117.701
Optimum Cost		5885.762	5885.334	8538.84	6061.078	6288.745	5885.5773	6000.46259	6059.7143	6059.089	7198.043	8129.1

3.8.3 Compression spring engineering design

Figure 3.13 shows a compression spring, which is a mechanical engineering design [128] [164]. The basic goal of this sort of challenge is to reduce the spring weight as much as possible and having three design variables as shown in fig 3.13. Table 3.11 compares the findings to those of other approaches. The following eqns (3.25 to 3.26d) are the formula.

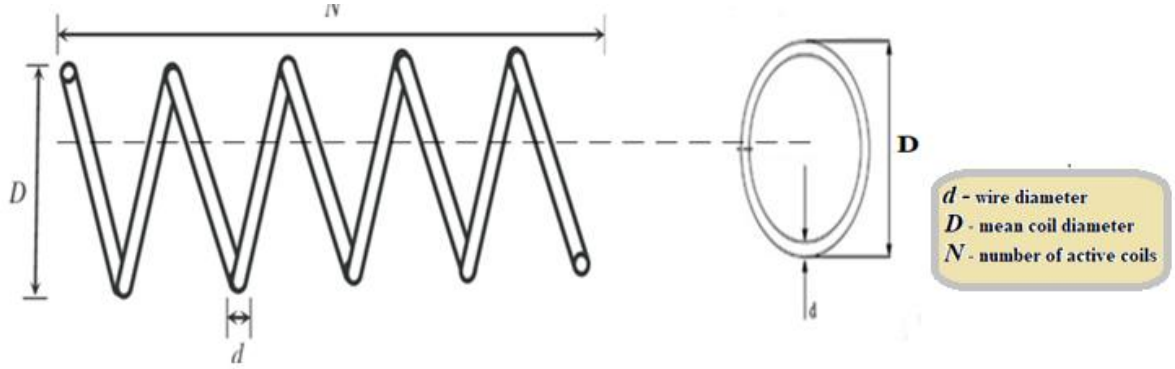

Fig.3.13 Compression Spring Design

Consider, $t = [t_1 t_2 t_3] = [drDmNc]$, 3.25

Minimize $f(t)=(t_3+2)t_2t_1^2$, 3.26

Subjected $g_1(t)=1-\frac{t_2^3t_3}{71785t_1^4}\le 0$, 3.26a

$g_2(t)=\frac{4t_2^2-t_1t_2}{12566(t_2t_1^3-t_1^4)}+\frac{1}{5108t_1^2}\le 0$, 3.26b

$g_3(t)=1-\frac{140.45_1}{t_2^2t_3}t\le 0$, 3.26c

$g_4(t)=\frac{t_1+t_2}{1.5}-1\le 0$, 3.26d

Variables ranges are $0.005\le t_1\le 2.00$, $0.25\le t_2\le 1.30$, $2.00\le t_3\le 15.0$

Table.3.11 Compression Spring comparative analysis

Algorithm's		HHO-PS	SMA-PS	HGSO	HHO	MFO	GWO	GSA	PSO
variables	d	0.051612	0.051144	0.0518	0.051796393	0.051994457	0.0516	0.0503	0.0517
	D	0.354869	0.343751	0.3569	0.359305355	0.36410932	0.3567	0.3237	0.3576
	N	11.39821	12.0955	11.2023	11.138859	10.868421862	11.2889	13.5254	11.2445
Optimum weight		0.012665	0.012665	0.0126	0.012665443	0.0126669	0.01267	0.0127	0.01267

3.8.4 Welded Beam Design

The fundamental goal of welded bam design is to reduce the welded beam's manufacturing costs. Figure 3.14[128] [164] displays the welded beam optimum design and associated factors. The comparison analysis is provided in Table 3.12. The mathematical equations (3.27 to 3.28g) are as follows.

Consider.

$w=[w_1w_2w_3w_4]=[hltb]$, 3.27

Minimize,

$$f(w) = 1.10471 w_1^2 w_2 + 0.04811 w_3 w_4 (14.0 + w_2) \quad 3.28$$

Subject to

$$g_1(w) = \tau(w) - \tau_{\text{maxi}} \le 0, \quad 3.28a$$

$$g_2(w) = \sigma(w) - \sigma_{\text{maxi}} \le 0 \quad 3.28b$$

$$g_3(w) = \delta(w) - \delta_{\text{maxi}} \le 0 \quad 3.28c$$

$$g_4(w) = w_1 - w_4 \le 0 \quad 3.28d$$

$$g_5(w) = P_i - P_c(w) \le 0 \quad 3.28e$$

$$g_6(w) = 0.125 - w_1 \le 0 \quad 3.28f$$

$$g_7(w) = 1.10471 w_1^2 + 0.04811 w_3 w_4 (14.0 + w_2) - 5.0 \le 0 \quad 3.28g$$

Variable range $0.1 \le w_1 \le 2$, $0.1 \le w_2 \le 10$, $0.1 \le w_3 \le 10$, $0.1 \le w_4 \le 2$,

Here,

$$\tau(w) = \sqrt{(\tau')^2 + 2\tau'\tau'' \frac{w_2}{2R} + (\tau'')^2},$$

$$\tau' = \frac{P_i}{\sqrt{2} w_1 w_2}, \tau'' = \frac{MR}{J}, M = P_i\left(L + \frac{w_2}{2}\right),$$

$$R = \sqrt{\frac{w_2^2}{4} + \left(\frac{w_1 + w_3}{2}\right)^2},$$

$$J = 2\left\{\sqrt{2} w_1 w_2 \left[\frac{w_2^2}{4} + \left(\frac{w_1 + w_3}{2}\right)^2\right]\right\}$$

$$\sigma(w) = \frac{6 P_i L}{w_4 w_3^2}, \delta(w) = \frac{6 P_i L^3}{E w_2^2 w_4}$$

$$P_c(w) = \frac{4.013 E \frac{\sqrt{w_3^2 w_4^6}}{36}}{L^2}\left(1 - \frac{w_3}{2L}\sqrt{\frac{E}{4G}}\right)$$

$$P_i = 6000 lb, L = 14 in, \delta_{\max i} = 0.25 in, E = 30 \times 1^6 \, psi, G = 12 \times 10^6 \, psi,$$
$$\tau_{\text{maxi}} = 13600 \, psi, \sigma_{\text{maxi}} = 3000 \, psi$$

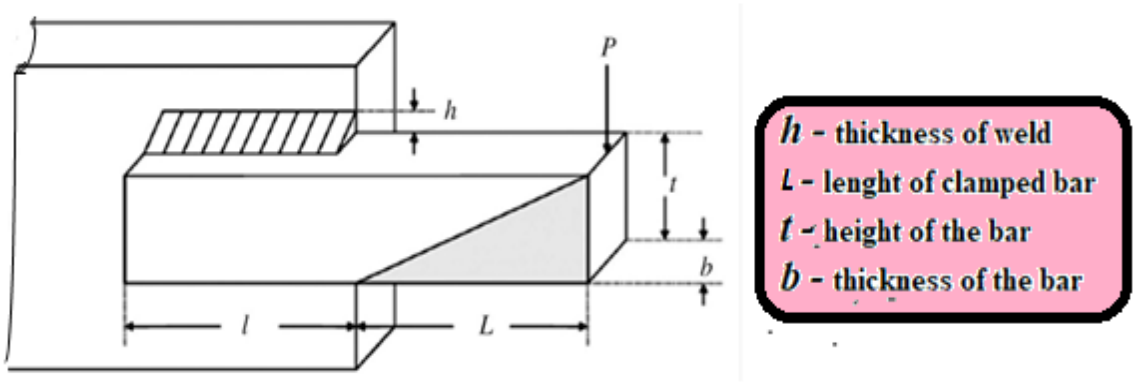

Fig.3.14 Design of Welded Beam.

Table.3.12 welded beam Comparative findings

Algorithms		hSMA-PS	hHHO-PS	HHO-SCA[162]	BCMO[129]	MALO[165]	SMA[76]
variables	h	0.205739	0.210108	0.190086	0.2057296526	0.205670	0.2054
	l	3.470332	3.41438	3.696496	3.4704890037	3.247600	3.2589
	t	9.036524	8.941964	9.386343	9.0366223562	9.060900	9.0384
	b	0.205739	0.210108	0.204157	0.2057297169	0.20567	0.2058
Optimal Cost		1.724899	1.725192	1.779032249	1.724852	1.698100	1.69604

3.8.5 Rolling Element Bearing Design

The goal of this design feature is to maximise the dynamic load bearing capability of the rolling element, as shown in fig.3.15 [89]. This engineering design challenge comprises 10 different choice numbers: (i) Pitch diameter (DIM_P), (ii) Ball diameters (DIM_B), (iii) Numbers of balls (Nb), (iv) outside and inner raceway curvature coefficients The additional five factors (KDmin, KDmax, ε, e and f) only have a little impact on the interior layout. Excluding the discrete number of balls, it has continuous components. The task involves nine nonlinear restrictions on kinematic circumstances and production parameters. The comparative analysis was depicting in table 3.13. the mathematical expressions as follows eqns (3.29 to 3.30i).

Maximizing.

$$C_D = f_c N^{2/3} DIM_B^{1.8} \qquad 3.29$$

if $DIM \le 25.4mm$

$$C_D = 3.647 f_C N^{2/3} DIM_B^{1.4} \quad 3.30$$

if $DIM \geq 25.4mm$

Subjected to;

$$b_1(x) = \frac{\theta_0}{2\sin^{-1}\left(\frac{DIM_B}{DIM_{MAX}}\right)} - N + 1 \geq 0 \quad 3.30a$$

$$b_2(x) = 2DIM_B - K_{DIM_{MIN}}(DIM - \dim) \geq 0 \quad 3.30b$$

$$b_3(x) = K_{DIM_{MAX}}(DIM - \dim) \geq 0 \quad 3.30c$$

$$b_4(x) = \beta B_W - DIM_B \leq 0 \quad 3.30d$$

$$b_5(x) = DIM_{MAX} - 0.5(DIM + \dim) \geq 0 \quad 3.30e$$

$$b_6(x) = (0.5 + re)(DIM + \dim) \geq 0 \quad 3.30f$$

$$b_7(x) = 0.5(DIM - DIM_{MAX} - DIM_B) - \alpha DIM_B \geq 0 \quad 3.30g$$

$$b_8(x) = f_I \geq 0.515 \quad 3.30h$$

$$b_9(x) = f_0 \geq 0.515 \quad 3.30i$$

Where,

$$f_c = 37.91\left[1 + \left\{1.04\left(\frac{1-\varepsilon}{1+\varepsilon}\right)^{1.72}\left(\frac{f_I(2f_0 - 1)}{f_0(2f_I - 1)}\right)^{0.41}\right\}^{10/3}\right]^{-0.3} \times \left[\frac{\varepsilon^{0.3}(1-\varepsilon)^{1.39}}{(1+\varepsilon)^{1/3}}\right]\left[\frac{2f_I}{2f_I - 1}\right]^{0.41}$$

$$\theta_0 = 2\pi - 2\cos^{-1}\left(\frac{\left[\left\{(DIM - \dim)/2 - 3(t/4)\right\}^2 + \left(DIM/2 - t/4 - DIM_B\right)^2 - \left\{\dim/2 + t/4\right\}^2\right]}{2\left\{(DIM - \dim)/2 - 3(t/4)\right\}\left\{D/2 - t/4 - DIM_B\right\}}\right)$$

$$\varepsilon = \frac{DIM_B}{DIM_{MAX}},\ f_I = \frac{R_I}{DIM_B},\ f_0 = \frac{R_0}{DIM_B},\ t = DIM - \dim - 2DIM_B$$

$$DIM = 160, \dim = 90, B_W = 30, R_I = R_0 = 11.033$$

$$0.5(DIM + \dim) \leq DIM_{MAX} \leq 0.6(DIM + \dim), 0.15(DIM - \dim) \leq DIM_B \leq 0.45(DIM - \dim), 4 \leq N \leq 50$$

$$0.515 \leq f_I \text{ and } f_0 \leq 0.6$$

$$0.4 \leq K_{DIM_{MIN}} \leq 0.5, 0.6 \leq K_{DIM_{MAX}} \leq 0.7, 0.3 \leq re \leq 0.1, 0.02 \leq re \leq 0.1, 0.6 \leq \beta \leq 0.85$$

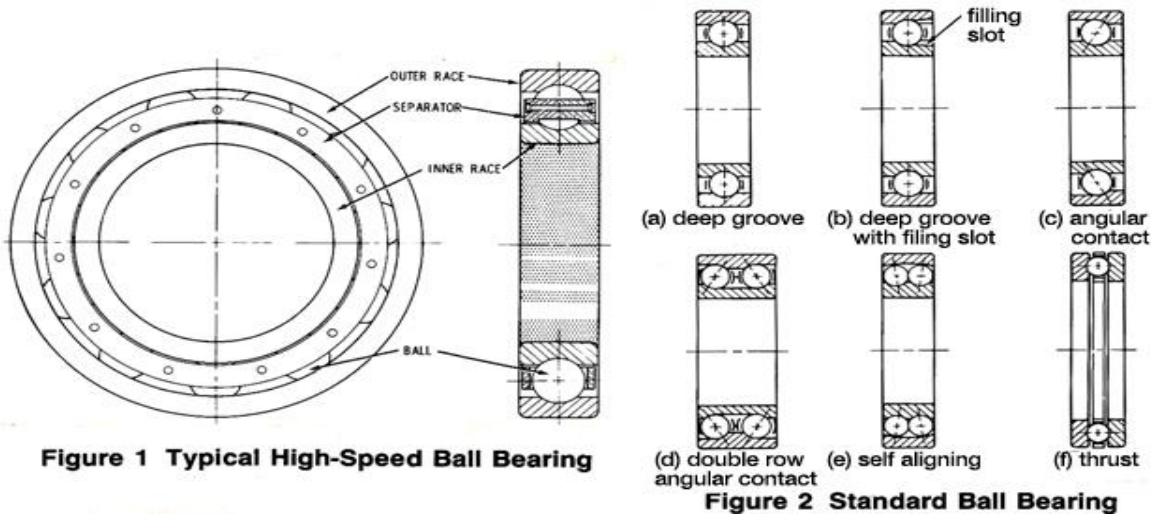

Figure 1 Typical High-Speed Ball Bearing

Figure 2 Standard Ball Bearing

Fig.3.15 Rolling element bearing problem

Table.3.13 Rolling element bearing comparative results

Algorithms		SMA-PS	HHO-PS	SHO[123]	HHO[85]	WCA[119]	PVS[130]
variables	*r*1	125.7234255	126.3365	125	125.00	125.721167	125.719060
	*r*2	21.42285806	21.03971	21.40732	21.00	21.42300	21.425590
	*r*3	11.00138214	11.19893	10.93268	11.092073	1.001030	11.000000
	*r*4	0.515	0.5150	0.515	0.51500	0.515000	0.515000
	*r*5	0.515	0.5150	0.515	0.51500	0.515000	0.515000
	*r*6	0.49206789	0.4	0.4	0.4000	0.401514	0.400430
	*r*7	0.7	0.607449	0.7	0.6000	0.659047	0.680160
	*r*8	0.3	0.3	0.3	0.3000	0.300032	0.300000
	*r*9	0.030435006	0.02938	0.2	0.050474	0.040045	0.079990
	*r*10	0.638555041	0.6	0.6	0.600	0.600000	0.700000
Optimum weight		-85539.1	- 85502.8	85054.532	83011.88329	85538.48	81859.741210

3.8.6 Multi disk clutch break (discrete variables)

For weight reduction, a multidisc-clutch brake design (see in fig 3.16) was adopted. The outer radius of the surface (Ro), the friction surface (Sf), the actuation of force (Fac), the thickness of the discs (Th), and the radius of the inner surface (Rin), count are among the five variables and eight limitations. Table 3.14 shows comparison of the Multiple disc clutch brake problem with other approaches. The mathematical expressions as following in eqns (3.31 to 3.31e).

Minimizing

$$f\left(R_{in}, R_O, S_f, Th\right) = \pi Th\gamma\left(R_0^2 - R_{in}^2\right)\left(S_f + 1\right) \qquad 3.31$$

Where,

$$R_{in} \in 60,61,62....80; R_o \in 90,91,.....110; Th \in 1,1.5,2,2.5,3; F_{ac} \in 600,610,620,1000; S_f \in 2,3,4,5,6,7,8,9$$

Subjected to;

$$b(x_1) = R_0 - R_{in} - \Delta R \geq 0 \qquad 3.31a$$

$$b(x_2) = L_{MAX} - (S_f + 1)(Th + \alpha) \geq 0 \qquad 3.31b$$

$$b(x_3) = PM_{MAX} - PM_{\pi} \geq 0 \qquad 3.31c$$

$$b(x_4) = PM_{MAX} Y_{MAX} + PM_{\pi} Y_{SR} \geq 0 \qquad 3.31d$$

$$b(x_5) = Y_{SR_{MAX}} - Y_{SR} \geq 0 \qquad 3.31e$$

Table.3.14 Comparative results for multiple clutch design

Algorithms		SMA-PS	HHO-PS	HHO[85]	WCA[119]	MBFPA[166]	PVS[130]
variables	x_1	70	76.594	69.999999	70.00	70	70
	x_2	90	96.59401	90.00	90.00	90	90
	x_3	1.5	1.5	1.00	1.00	1	1
	x_4	1000	1000	1000.00	910.000	600	980
	x_5	2.312782	2.13829	2.312781994	3.00	2	3
Optimum fitness		0.389653	0.389653	0.259768993	0.313656	0.235242457900804	0.31366

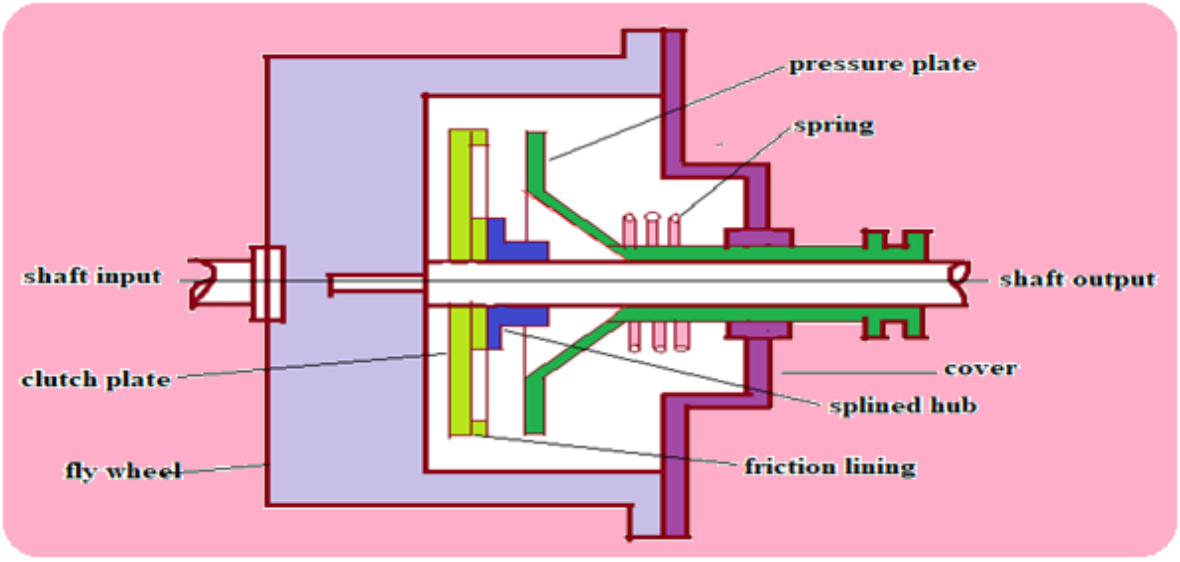

Fig.3.16 Multidisc clutch break design

$$b(x_6) = t_{MAX} - t \geq 0$$

$$b(x_7) = DC_h - DC_f \geq 0$$

$$b(x_8) = t \geq 0$$

$$PM_{\pi} = \frac{F_{ac}}{\Pi\left(R_0^2 - R_{in}^2\right)}$$

Where,

$$Y_{SR} = \frac{2\pi n\left(R_0^3 - R_{in}^3\right)}{90\left(R_0^2 - R_{in}^2\right)}$$

$$t = \frac{i_x \pi n}{30\left(DC_h + DC_f\right)}$$

3.8.7 Gear Train Design

The gear train design is presented in Fig.3.17, and four variables have been tweaked to reduce the teeth ratio and scalar value [128]. As a result, the number of teeth on each gear is included in the decision variable. Table 3.15 shows the analysing solutions using available optimization methods. The following eqns (3.32 to 3.33) are the mathematical expressions.

Let, considering.

$$\vec{t} = \left[t_1 t_2 t_3 t_4\right] = \left[M_A M_B M_C M_D\right] \qquad 3.32$$

Minimizing.

$$f(t)=\left(\frac{1}{6.931}-\frac{t_3 t_4}{t_1 t_4}\right)^2 \qquad 3.33$$

Subjected to; $12 \le t_1, t_2, t_3, t_4 \le 60$

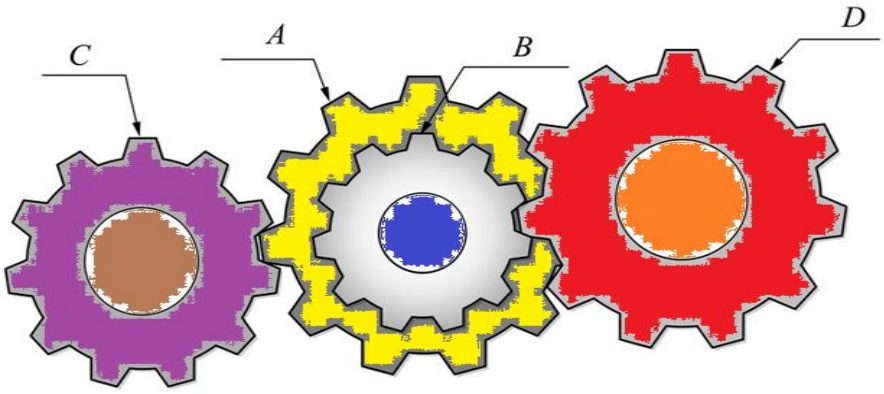

Fig.3.17 gear train design

Table.3.15 Gear Train challenge Comparative analysis

Algorithm		SMA-PS	HHO-PS	HHO-SCA	MFO	MSCA[167]	GeneAS [168]	Kannan and Kramer [168]	Sandgren [168]
Optimal values for variables	*t*1	49	38.765	58.22844	43	49	50	41	60
	*t*2	19	13.21351	57.73199	19	16	33	33	45
	*t*3	16	13.21351	40.41797	16	19	14	15	22
	*t*4	43	31.21711	12	49	43	17	13	18
Optimum fitness		2.7009 E-012	0	0	2.7009e-012	2.79009E-12	0.144242	0.144124	0.146667

3.8.8 Cantilever Beam Design

The development of a cantilever beam is a structural engineering challenge in which the major focus is on minimising beam weight, as seen in Fig 3.18. This layout is made up of five different constituent shapes [164]. This is governed by only one factor, and the design layout is made

up of five variables, the majority of which are stable, such as the thickness of the beam. The movement of the vertically limitation should be addressed all through finished problem. Here table 3.16 depicts the analysis of cantilever design. The mathematical expressions (3.34 to 3.35) as follows.

Consider, $c = [c_1 c_2 c_3 c_4 c_5]$

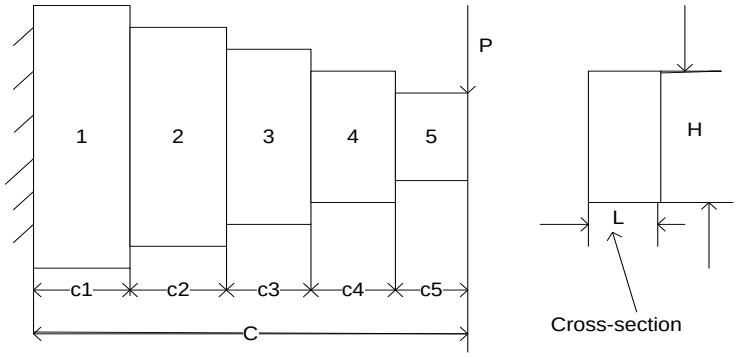

Fig.3.18 Cantilever beam design

Minimize

$$f(c) = 0.06224(c_1 + c_2 + c_3 + c_4 + c_5), \qquad 3.34$$

Subject to

$$g(c) = \frac{61}{c_1^3} + \frac{27}{c_2^3} + \frac{19}{c_3^3} + \frac{7}{c_4^3} + \frac{1}{c_5^3} \leq 1 \qquad 3.35$$

Variable range $0.01 \leq c_1, c_2, c_3, c_4, c_5 \leq 100$

Table.3.16 Cantilever Beam Comparative analysis

Algorithm's		SMA-PS	HHO-PS	HHO-SCA[162]	SMA[76]	MFO[102]	ALO[131]	SOS[132]	MMA[133]
variables	$c1$	5.995189	5.978829	5.937725	6.017757	5.984871773 2166	6.0181	6.0188	6.01
	$c2$	4.809669	4.876628	4.85041	5.310892	5.316726924 29783	5.3114	5.3034	5.3

	$c3$	4.441805	4.464572	4.622404	4.493758	4.49733258583062	4.4884	4.4959	4.49
	$c4$	3.486532	3.479744	3.45347	3.501106	3.51361646768954	3.4975	3.499	3.49
	$c5$	2.213005	2.139358	2.089114	2.150159	2.16162029338550	2.1583	2.1556	2.15
Optimum weight		1.303321	1.303251	1.30412236	1.339957	1.33998808597181	1.33995	1.33996	1.34

3.8.9 I beam design

The goal of this engineering challenge is to reduce the I-vertical beam's divergence by altering four variables as illustrated in Figure 3.19.the comparative analysis depicts in table 3.18. the mathematical expressions (3.36 to 3.37) are as follows.

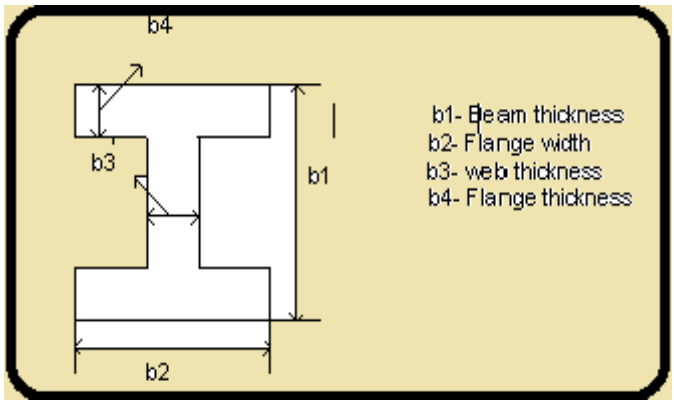

Fig.3.19 I beam optimal design

$$\vec{\imath} = [i_1, i_2, i_3, i_4\,] \tag{3.36}$$

$$f(\vec{\imath}) = \frac{5000}{\frac{i_3(i_1 - 2i_4)^3}{12} + \frac{i_2 l_4^3}{6} + 2i_2 i_4 \frac{(i_1 - 2i_4)^2}{4}} \tag{3.37}$$

Subject to,

$$g(\vec{\imath}) = 2i_2 i_3 + i_3(i_1 - 2i_4) \leq 0$$

$$10 \leq i_1 \leq 80$$

$$10 \leq i_2 \leq 50$$

$$0.9 \leq i_3 \leq 5$$

$$0.9 \leq i_4 \leq 5$$

Table.3.17 I beam design Comparative results							
Algorithms		SMA-PS	HHO-PS	BWOA[169]	SMA[76]	CS[134]	SOS[132]
variables	*i*1	50	50.00	50.00	49.998845	50.0000	50.0000
	*i*2	80	80.00	80.00	79.994327	80.0000	80.0000
	*i*3	1.764706	1.764706	1.76470588	1.764747	0.9000	0.9000
	*i*4	5	5.00	5.00	4.999742	2.3217	2.3218
Optimum fitness		0.006626	0.006626	0.00625958	0.006627	0.0131	0.0131

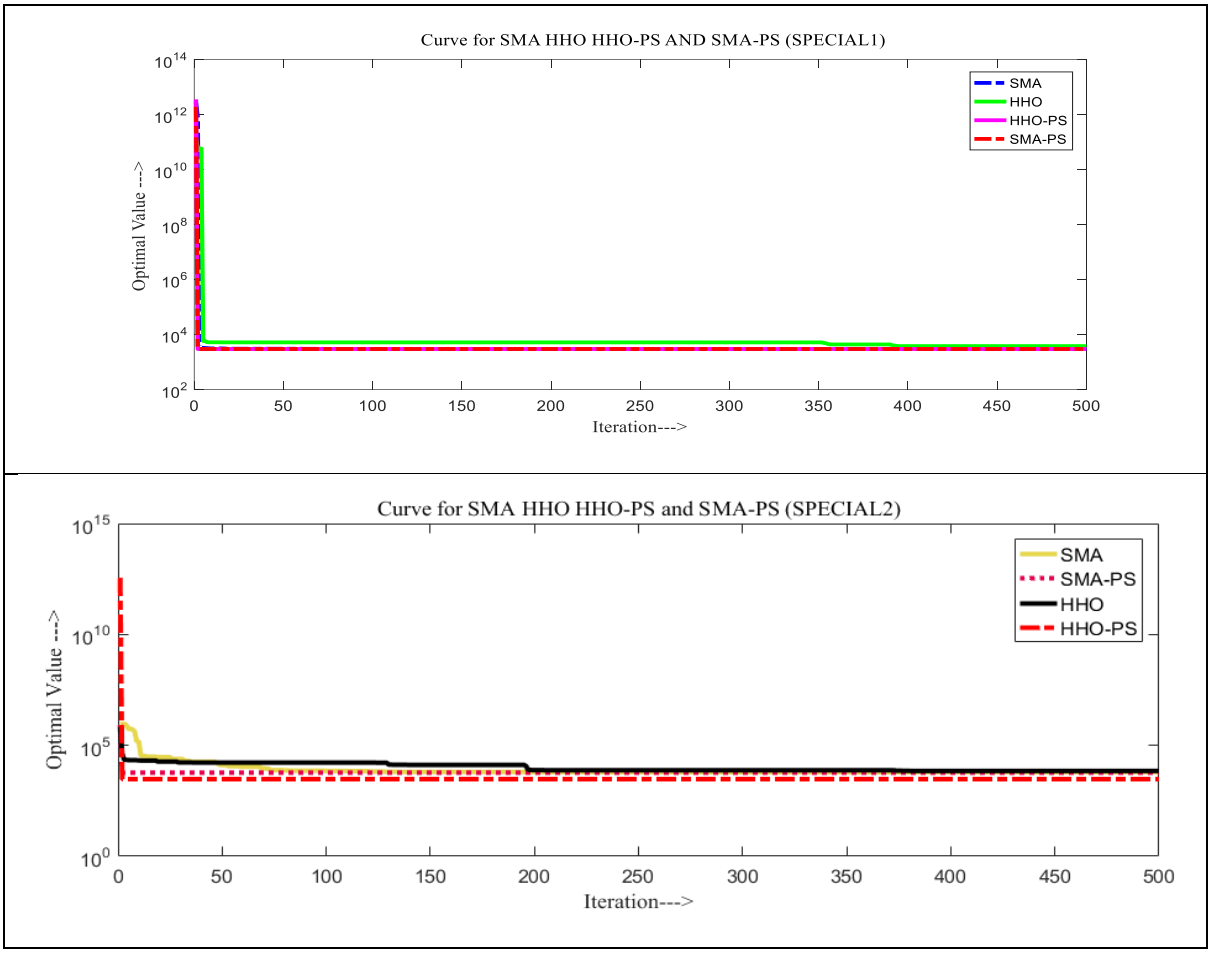

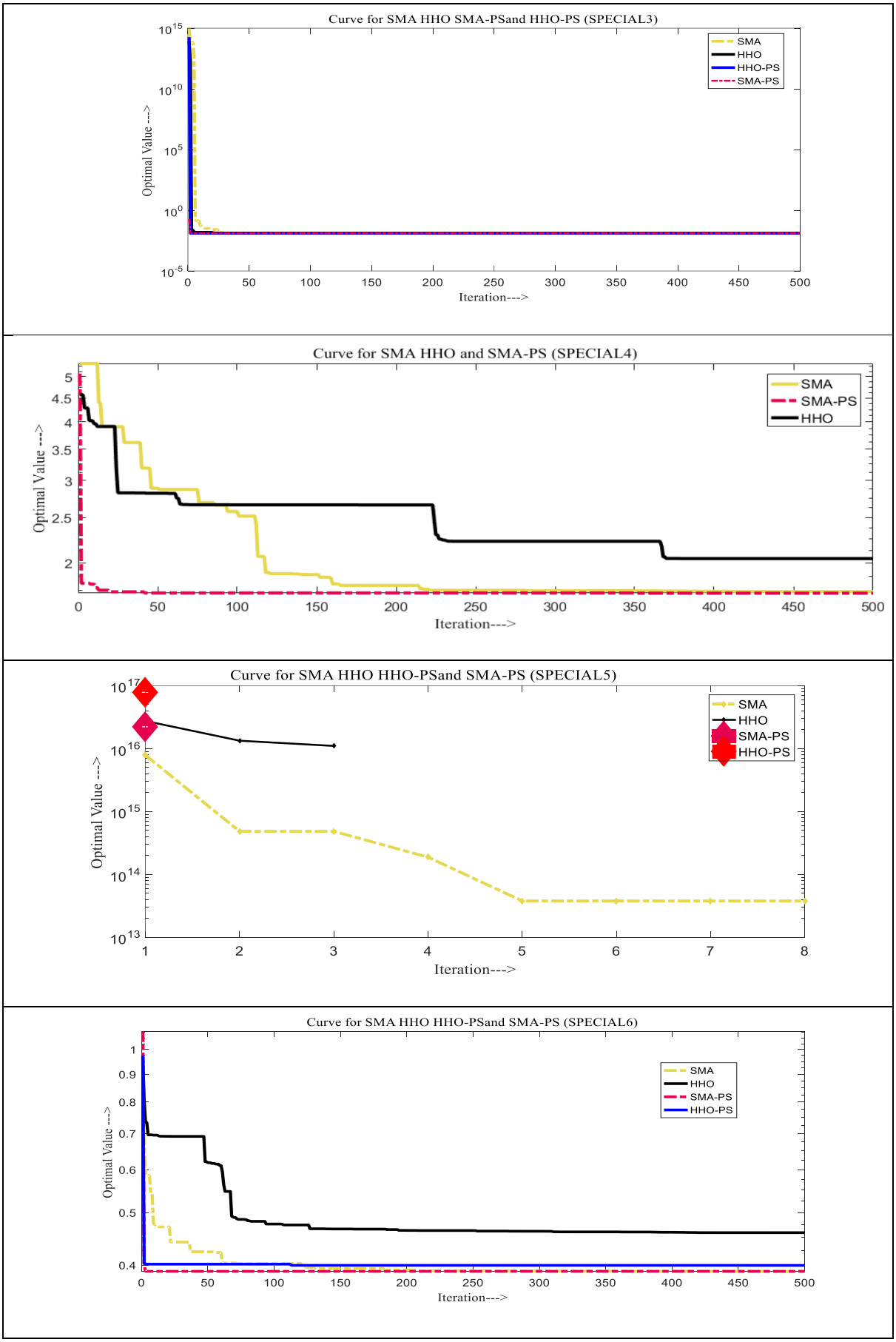
Curve for SMA HHO SMA-PSand HHO-PS (SPECIAL3)
Optimal Value --->
Iteration--->
SMA
HHO
HHO-PS
SMA-PS
Curve for SMA HHO and SMA-PS (SPECIAL4)
Optimal Value --->
Iteration--->
SMA
SMA-PS
HHO
Curve for SMA HHO HHO-PSand SMA-PS (SPECIAL5)
Optimal Value --->
Iteration--->
SMA
HHO
SMA-PS
HHO-PS
Curve for SMA HHO HHO-PSand SMA-PS (SPECIAL6)
Optimal Value --->
Iteration--->
SMA
HHO
SMA-PS
HHO-PS

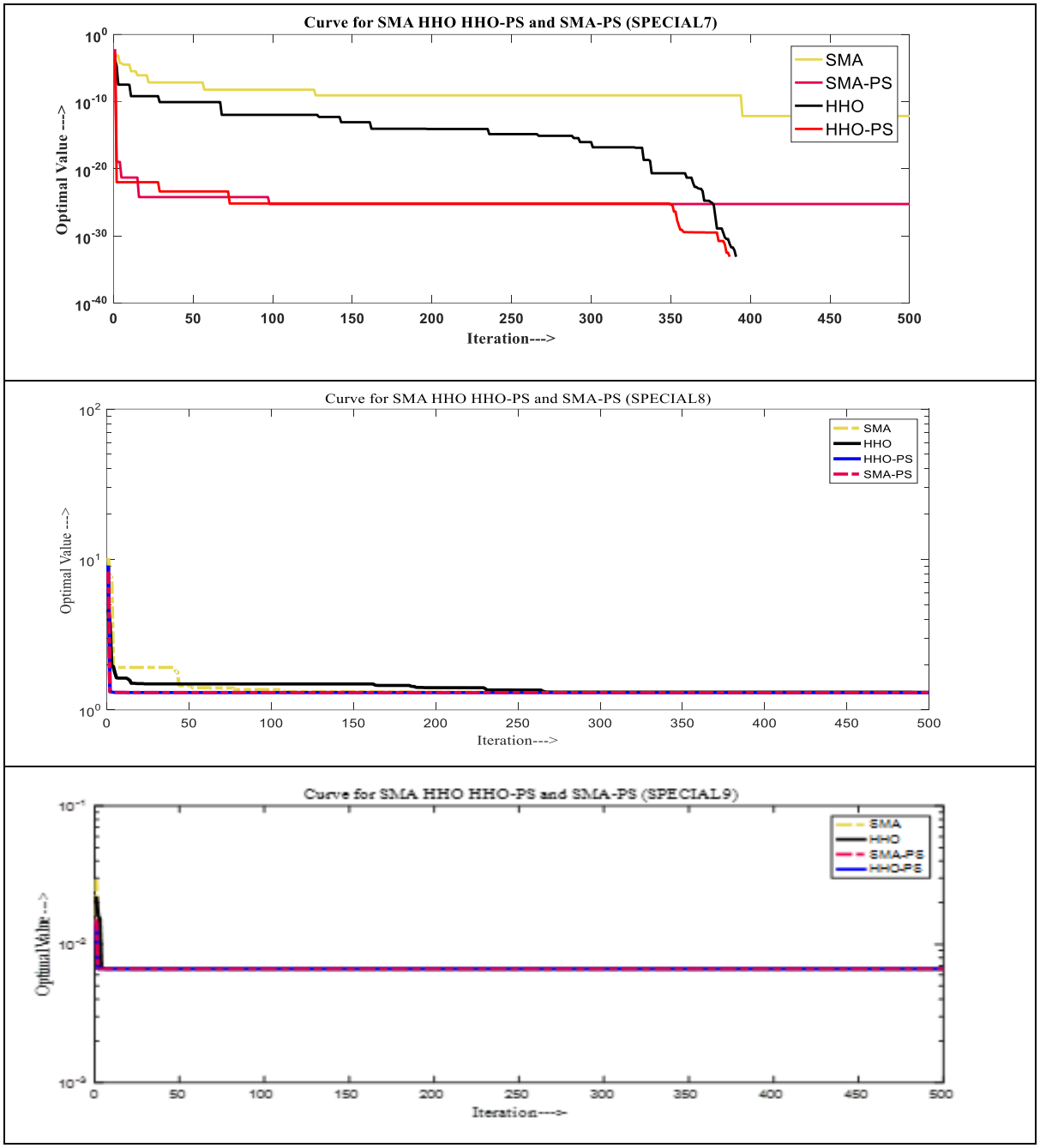

Fig.3.20 comparative convergence curves (SPECIAL1 – SPECIAL9).

3.9 RESULTS AND DISCUSSIONS

The UM (F1-F7) BM functions only has global optimums, those were utilised to determine the exploitation of methodologies. Table 3.5 shows that SMA-PS was most efficient heuristic algorithm for F3, F4, and F1 BM, but it performed similarly to HHO-PS for F7, F6, F5, and F2. The reason for this is that SMA-PS uses two different exploitation strategies for each cycle. The first method focuses on finding the solution, whereas the second method focuses on finding the best solution. Another important feature was the balancing among exploitation and exploration. Over other metaheuristics, SMA-PS starts the exploitation strategic changes in

iteration, and such participation in the exploitation population grows with time. This explains why SMA-PS beat other HHO, SMA, HHO-PS models in various UM BM characteristics (see in fig 3.8).

The MM functions (F8-F13) were chosen for they contain a lot of local optima, and unlike the UM forms, the range of specifications variable goes up exponentially with complexity. SMA-PS is particularly efficient versus other HHO, SMA, HHO-PS, and other optimizers, as demonstrated in Table 3.6. from fig 3.9, SMA-PS outperforms for F13 BM function and for remaining BM (F8-12) it shows very competitive results over other recent MA.

Exploration and exploitation resolve FD (F14-F23) functions, which have many local optima. Tables 3.7 and 3.7a show that SMA-PS is a powerful search optimizer when compared to other query metaheuristics. The test results revealed that SMA-PS can strike a balance between exploitation and exploration while avoiding the local optimum. From the fig 3.10, the comparative convergence curves illustrate that HHO-PS and SMA-PS shows comparative outcomes to each other.

While, in case of engineering constraints SMA-PS and HHO-PS performs almost equal results for the all nine engineering constraints except Pressure vessel (special-2), Welded beam (special-4), and Multi disk clutch break (special-6) constraints. For the Special 2, 4, and 6 constraints SMA-PS performs greater efficacy results in terms of their fitness evaluation. From the outcomes we can conclude that SMA-PS is been the superior one among HHO-PS, HHO, SMA and other recent well-known MA optimizers.

3.10 CONCLUSION

This research suggested a hybrid memetic optimization search methods HHO-PS and SMA-PS optimizers, for both (HHO, and SMA) PS optimizers was driven at the termination end to HHO, and SMA. The effectiveness of the recommended searching algorithms of avoidance of local optima, exploration, exploitation, and convergence was determined using twenty-three BM. BOA, ECBO, WOA, WSA[116], GOA, PSOSCALF, DEAHHO, HHO, and TSA can give fiercely competitive outcomes when compared to MA, according to the findings. The suggested SMA-PS and HHO-PS optimization search technique was proved to be better in terms of UM functions. Second, the MM feature findings confirmed SMA-PS and HHO-PS exploration potential. Third, the FD findings revealed an increased avoidance of local optima. Finally, the SMA-PS and HHO-PS convergence review study confirmed the convergence of our method for BM.

Further, the CE analyses demonstrated that the SMA-PS and HHO-PS context of improving method is highly efficient in complex, challenging search environments. In addition, the suggested SMA-PS and HHO-PS outperforms two standard HHO, SMA algorithms in a comparison examination. It's worth noting that tests on semi-real and genuine difficulties have proven that SMA-PS and HHO-PS can achieve good results not only on unrestricted but also on constrained challenges.

Furtherly from the overall outcomes for the benchmarks SMA-PS performs superior results than other optimizers. But for engineering constraints in some cases SMA-PS and HHO-PS depicts similar results. The SMA-PS and HHO-PS optimizers furtherly attempted to apply in LFR considering RES, ESD, FACTS devices, and battery electric vehicle (BEV) plugin charging and discharging.

Chapter-4

LOAD FREQUENCY REGULATION IN MULTI-AREA MULTI-SOURCE POWER SYSTEM

4.1 INTRODUCTION

In a multi-area network, load frequency regulation (LFR) in DPS network has been a popular topic, and investigators have produced numerous improvements to accomplish acquisition and supplying loads in the recent years. Following deregulation, emerging business actors such as ISOs, GENCOs, DISCOs, and TRANSCOs have entered in the dynamic electrical market. The power system becomes more complicated because of the individual contributions of various entities. Within extremely modest and distributed systems, such freshly established groups have their own obligation to preserve cohesion, safeguarding, and dependability. LFR is becoming increasingly crucial in this new electrical market context to ensure higher power dependability and protection. Furthermore, the number of DISCOs is steadily increasing to meet the growing demand for household and commercial applications. Current power systems are having difficulty regulating frequency, which is causing worry among system operators and regulators [45][11].

Because of the enormous demand in all areas, the scale of the electricity network has been increased on a regular basis (example. Industrial and agricultural). Due to these kinds of problems, there's a chance that every producing unit may collapse, resulting in a total or near-complete blackout of the electric grid. As a result, individual power source frequency management has proven challenging to sustain in the current period. In the open market, it leads to a multi-area electric power system with tie line error management approaches.

POOLCO premised exchange, bilateral exchange, and contract violation contracts are all viable ways for power transactions to take place in a DPS. Operation and planning of the system with the development of many organizations to meet the newly augmented DPS is required to provide consistency and security. As a result, by stabilizing the frequency controlling and changes the power flow via the whole system's tie line power, the LFR controls these power exchanges between surrounding control regions.

A GRC of 10 percentage per minute for said thermal power stations is used either decreasing or growing rates [23]. The normal contribution of GRC for hydro plant and gas plant in declining and growing production scenarios has been calculated to be 360 percentage per

minute and 270 percentage per minute, correspondingly [25]. Hydro, Gas, and Thermal (H- G – T) producing plants are given participation factors (PF) of 0.30, 0.10, and 0.60 respectively, in this study [46].

According to literature, the kind of controller, evolutionary optimization approaches used to improve controller settings, studying their behavior in multi-area DPS is crucial. Furthermore, there has been no attempt to apply the SMA-PS and HHO-PS algorithms for optimizing the gain values of the proportional and integral (PI) controller for two-area reformed systems with H-T-G multi-sources till now. As a result, an attempt was made to investigate LFR in multi-area DPS using a SMA-PS and HHO-PS tuned PI controller. Here, table 4.1 parameters of LFR two area DPS.

Table.4.1 parameters of LFR two area DPS

Area number and capacity	Generating units (GENCO)	Distributing company's (DISCO)
1 with 2000MW	H – T – G (3 sources)	02
2 with 1640MW	H – T – G (3 sources)	02

4.2 MATHEMATICAL FORMULATION

Two areas are considered, each containing H- G- T sources. A tie line was tied intermittently to control the abrupt variations in TLP. An optimised PI controller is utilised to control the entire DPS. PI controller has been most used controller for LFR methods, as per literature (refer chapter -2). The advantage of this regulator is that it reduces the steady-state error to zero. The transfer function model of the LFR of two region H- G – T producing sources of DPS is shown in fig 4.1.

A thermal power plant converts heat into energy. Usually, fuel is used to heat water in a massive pressure tank to create higher steam, often used to operate a steam turbine that is linked to a generator. The turbine's low-pressure output is recirculated after flowing into a steam collector.

Here, a A GRC of 10 percentage per minute for said thermal power stations is used either decreasing or growing rates. 0.60 has been the participation factor for the thermal origination plant with 10% of GRC in each area. Fig 4.2 has been the thermal unit elements and its transfer

function model. From the fig 4.2, $k_r = 0.300\ sec$ as Gain constant, $T_r = 10 sec$ as Turbine time constant and $T_{sg} = 0.08\ sec$ as Governor time constant are outstanding parameters of the thermal unit.

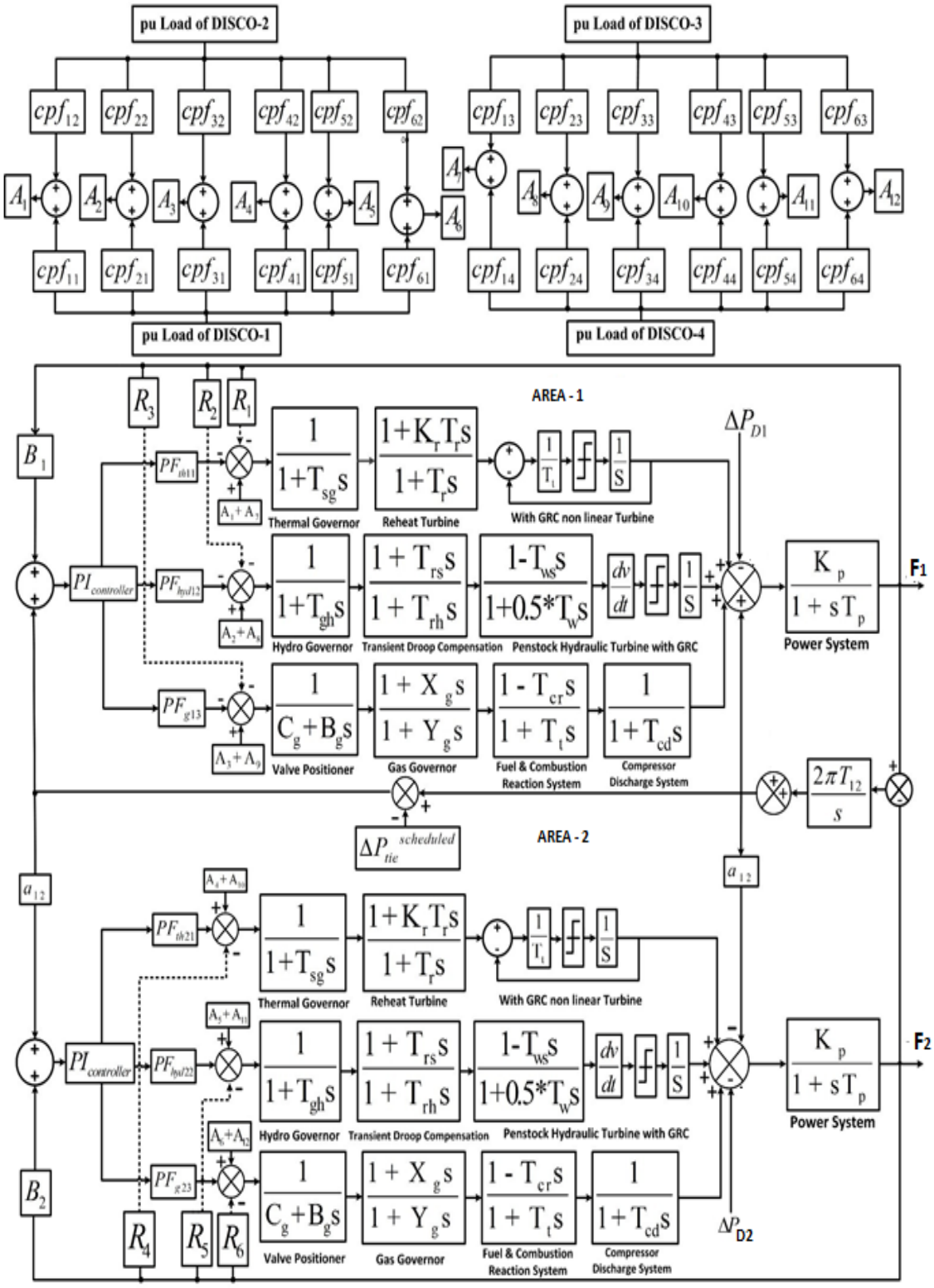

Fig.4.1 Block diagram model for LFR of two area multi source DPS.

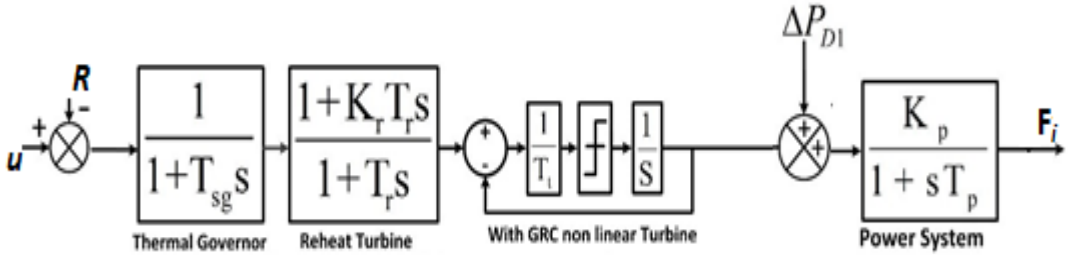

Fig.4.2 Thermal unit with GRC transfer function model

Hydroelectric plants (which originate hydroelectricity), they use a wind turbine to transmit the force of water to produce energy. Here, the participation factor for the hydro unit is 0.30 with GRC in each region. Fig 4.3 illustrates the hydro unit elements and its transfer function model. $T_{sg} = 0.20\ sec\ as$ Governor time constant, $T_{rs} = 5.00\ sec\ as$ Hydro turbine speed governor reset time, $T_{rh} = 28.75\ sec$ as Hydro turbine speed governor transient droop time constant, and $T_{ws} = 1.00$ sec as Hydro water time constant parameters of the hydro origination unit.

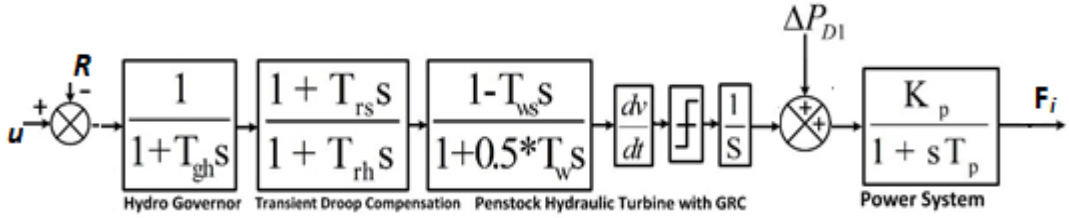

Fig.4.3 Hydro unit with GRC transfer function model

Natural gas is used to create energy at a gas-fired power station. Gas power plants provide over a quarter of the world's electricity and contribute significantly to global greenhouse gas emissions and climate change. Here, the participation factor for the hydro unit is 0.10 with GRC in each region. Fig 4.4 depicts the gas unit elements and its transfer function model. $T_{cd} = 0.20$ sec as Compressor dicharge system time, Governor servo time and droop time constants as $X_g = 0.60$ sec , $Y_g = 1.00\ sec$, $B_g = 0.050\ sec$, Cg=1.00 sec as Valve positioner time constants, $T_f = 0.23\ sec\ as$ Fuel dynamics of turbine and $T_{cr} = 0.010\ sec$ Turbine compressor discharge.

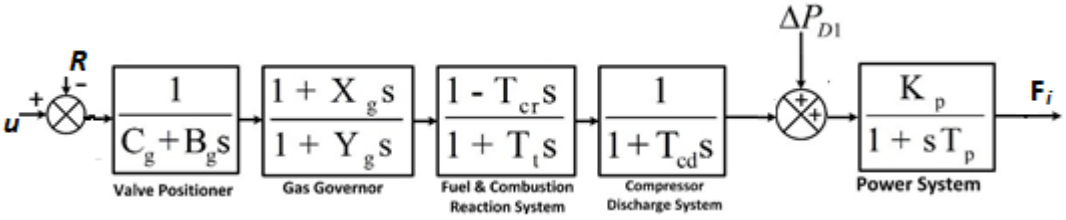

Fig.4.4 Gas unit transfer function model

Here, LFR of the two area with each region having three GENCOs (H – T – G) sources and power exchanged tie line interlinked DPS network is developed, to control the sudden changes in the tie line power (TLP). To control the entire DPS network system, an optimized PI controller is used. The benefit of this regulator is that the steady-state error is reduced to zero.

Area-1 overall generating power (from fig. 4.1) is

$$P_{POWER1} = PF_{themal1} + PF_{hydro1} + PF_{gas1} \quad 4.1$$

Area-2 overall generating power (fig. 3.1) is

$$P_{POWER2} = PF_{themal2} + PF_{hydro2} + PF_{gas2} \quad 4.2$$

Here, $PF_{themal1}$ & $PF_{themal2}$ replicates thermal, PF_{hydro1} & PF_{hydro2} replicates hydro, PF_{gas1} & PF_{gas2} replicates diesel originating units.

The total generating net amount of power is as follows

$$Total\ P_{POWER} = P_{POWER1} + P_{POWER2} \quad 4.3$$

The various GENCOs of the new hybrid system mentioned here are the resources of power generation stated above. DISCOs can contract any GENCOs for electricity needs. Under GENCOs-DISCOs, DPM (Disco Participation Matrix) assists in the envisioning of contracts.

DPM for the proposed DPS is

$$\boldsymbol{DPM} = \begin{bmatrix} \boldsymbol{cpf_{v11}} & \boldsymbol{cpf_{v12}} & \boldsymbol{cpf_{v13}} & \boldsymbol{cpf_{v14}} \\ \boldsymbol{cpf_{v21}} & \boldsymbol{cpf_{v22}} & \boldsymbol{cpf_{v23}} & \boldsymbol{cpf_{v24}} \\ \boldsymbol{cpf_{v31}} & \boldsymbol{cpf_{v32}} & \boldsymbol{cpf_{v33}} & \boldsymbol{cpf_{v34}} \\ \boldsymbol{cpf_{v41}} & \boldsymbol{cpf_{v42}} & \boldsymbol{cpf_{v43}} & \boldsymbol{cpf_{v44}} \\ \boldsymbol{cpf_{v51}} & \boldsymbol{cpf_{v52}} & \boldsymbol{cpf_{v53}} & \boldsymbol{cpf_{v54}} \\ \boldsymbol{cpf_{v61}} & \boldsymbol{cpf_{v62}} & \boldsymbol{cpf_{v63}} & \boldsymbol{cpf_{v64}} \end{bmatrix} \quad 4.4$$

cpf_{vij} depicts contract participation matrix factor

$$\sum_{i=1}^{n} cpf_{vij} = 1, \text{ here j=1,2.....k} \quad 4.5$$

k replicates the sum of DISCOs

n replicates the sum of GENCOs

The cpf-matrix measures the outcome of a fraction quantity of load approved by DISCOs, and the GENCOs involved in the transaction commit on this demand[26].

The local load in a DPS market is

$$\Delta p_{l1} + \Delta p_{l2} = \Delta p_{D1} \quad 4.6$$

$$\Delta p_{l3} + \Delta p_{l4} = \Delta p_{D2} \quad 4.7$$

Each GENCOs power generation as per contract is

$$\Delta p_{Gci} = \sum_{j=1}^{GENCO,total} cpf_{vij} * \Delta p_{lj} \quad 4.8$$

Similarly, if a DISCOs breaks the contract by requesting additional energy or exceeding contractual limits, the unrecognized contractual need is portrayed as an unagreed additional load, which is fulfilled by GENCOs in the similar region as the DISCOs[27].

Likewise, whether any DISCO violates the agreement by requiring more than predefined power or contractual limitations, then the unidentified contractual demand is expressed as an unagreed more load, and demand met by the GENCOs which belonging to the very same region as the DISCOs[27]. Unagreed power load requests are given to GENCOs based on (apfs) area participation factors.

Here, area-1 *apfs* are $PF_{\text{thermal11}}$, PF_{hydro12}, $and\ PF_{\text{gas13}}$.

And Area-2, *apfs* are considered as,$PF_{\text{thermal21}}$, PF_{hydro22}, $and\ PF_{\text{gas23}}$.

Except for the outward change of power, every GENCOs may be constructed as follows according to its *apfs* and specified contract

$$\Delta p_{Gi} = cpf_{i1} * \Delta p_{l1} + cpf_{i2} * \Delta p_{l2} + cpf_{i3} * \Delta p_{l3} + cpf_{i4} * \Delta p_{l4} + apf_i \Delta p_{Li}^{uc} \quad 4.9$$

And hence, the local unagreed electricity demand is as follows

$$\Delta p_{L1}^{uc} + \Delta p_{l1} + \Delta p_{l2} = \Delta p_{D1} \quad 4.10$$

$$\Delta p_{L2}^{uc} + \Delta p_{l3} + \Delta p_{l4} = \Delta p_{D2} \quad 4.11$$

Here, Δp_{L2}^{uc} and Δp_{L1}^{uc} were the unagreed load requisitions for area-2 and 1. The ACE (Area Control Error) [54], is the unplanned demands or shift in the assigned power that creates changes in the tie-line power flow. The frame tie-line power exchange amongst regions rates may be measured as

$$\Delta p_{tieline,12}^{allocated} = \sum_{n=1}^{3}\sum_{m=3}^{4} cpf_{nm}\Delta p_{lm} - \sum_{n=4}^{6}\sum_{m=1}^{2} cpf_{nm}\Delta p_{lm} \quad 4.12$$

Eqn (3.13) can be used to express the relevance that goes through tie-line

$$\Delta p_{tieline,12}^{real} = \frac{2\Pi T_{12}}{s}[\Delta F_1 - \Delta F_2] \quad 4.13$$

Eqn (3.14) describes the error that arises in tie-line power owing to the strict limit in DPS

$$\Delta p_{tieline,12}^{error} = \Delta p_{tieline,12}^{real} - \Delta p_{tieline,12}^{allocated} \quad 4.14$$

If an actual tie line power flow surpasses the power flow error limitations, the current flow setup quantity ($\Delta p_{tieline,12}^{error}$) is zero, and this is referred to as the constant state situation. ACE may be represented in an area described by eqn (4.15 & 4.16) as a linear combination of the power flow error in the tie line and weighted frequency variation.

$$ACE_1 = \Delta F_1 * B_1 + p_{tieline,12}^{error} \text{ and as well as,} \quad 4.15$$

$$ACE_2 = \Delta F_2 * B_2 + p_{tieline,21}^{error} \quad 4.16$$

The linear dynamics aspect of the present concept for LFR in a competing electric grid may be demonstrated using static variable differential mathematical is Eqn (4.17)

$$A = PX + QY + RZ + S\lambda \quad 4.17$$

The measures of R, Q, P and S are consistent Appropriate Matrices. [27].

The matrices for the suggested method during investigation will be shown in summary in eqns (4.18 – 4.21)

$$X = [\Delta F_1 \Delta F_2 \Delta p_{tie,12}^{real} \Delta p_{Gc1} \Delta p_{Gc2} \Delta p_{Gc3} \Delta p_{Gc4} \Delta p_{Gc5} \Delta p_{Gc6} \Delta p_{Gc1} \Delta p_{CES1} \Delta p_{CES2} \Delta p_{TCPS}]^T \quad 4.18$$

$$U_S = [U_{S1} U_{S2}]^T \quad 4.19$$

$$p = [\Delta p_{l1} + \Delta p_{l2} + \Delta p_{l3} + \Delta p_{l4}]^T \ or \ p = [\Delta p_{l1} \Delta p_{l1}]^T \quad 4.20$$

$$and \ p^{'} = [\Delta p_{l1}^{uc} \Delta p_{l2}^{uc}]^T \quad 4.21$$

4.2.1 PI CONTROLLER DESIGN

PI controllers are presently utmost commonly utilized form of regulator in innovation, despite its basic framework. A PI controller that controls speed, temperature, pressure, flow, and a variety of other industrial flow characteristics. It is almost widespread as a means of temperature control and is used in a variety of chemical and scientific processes, as well as in automation.

$$G(s) = K_p + \frac{K_i}{S} \quad 4.22$$

4.3 HYBRID MEMETIC SMA-PS SEARCH OPTIMIZATION ALGORITHM

To develop hybrid memetic Slime Mould-Pattern search (SMA-PS) algorithm for LFR of H – T – G sources two area DPS problem, the general operating variables of SMA and PS are integrated recursively. The operating variables of PS optimizer acceleration factor υ and pattern search Location x^{int} are replace with SM location of $\vec{S}$ and best possible location of each SM $\overrightarrow{S_b}$. The suggested hybrid memetic SMA-PS algorithm for the for LFR of H – T – G sources two area DPS problem is described as follow in proceedings section.

To improvise and upgradation stage of PS, the new SM location of $\overrightarrow{S_b}$ is determined by the rules of crossover and mutation strategy operation of SMA optimizer. The optimal process solution of LFR of the two area DPS is described as follow.

Step-1: Enter the LFR variable parameter data and enter the data and constants of SMA-PS optimizer i.e., $\overrightarrow{vb}$, $\overrightarrow{vc}$, $\overrightarrow{S_A}$, $\overrightarrow{S_B}$, $DF, r \ and \ wF$ and acceleration factor (ν), vector disturbance (y^o) and vector disturbance tolerance (τ) variables

To resolve and simplify the LFR of the two area DPS problem, initialize the data for each contract scenario separately as per the contraction method. The disco participation factors are

$$\text{DPM} = \begin{bmatrix} \text{cpf}_{\text{v11}} & \text{cpf}_{\text{v12}} & \text{cpf}_{\text{v13}} & \text{cpf}_{\text{v14}} \\ \text{cpf}_{\text{v21}} & \text{cpf}_{\text{v22}} & \text{cpf}_{\text{v23}} & \text{cpf}_{\text{v24}} \\ \text{cpf}_{\text{v31}} & \text{cpf}_{\text{v32}} & \text{cpf}_{\text{v33}} & \text{cpf}_{\text{v34}} \\ \text{cpf}_{\text{v41}} & \text{cpf}_{\text{v42}} & \text{cpf}_{\text{v43}} & \text{cpf}_{\text{v44}} \\ \text{cpf}_{\text{v51}} & \text{cpf}_{\text{v52}} & \text{cpf}_{\text{v53}} & \text{cpf}_{\text{v54}} \\ \text{cpf}_{\text{v61}} & \text{cpf}_{\text{v62}} & \text{cpf}_{\text{v63}} & \text{cpf}_{\text{v64}} \end{bmatrix} \text{ here, } \sum_{i=1}^{n} cpf_{vij} = 1, \text{ here j=1,2.....k}$$

k replicates the sum of DISCOs

n replicates the sum of GENCOs

Step -2: Contract methods are different as per their contraction principles along with DISCO-GENCO participation, initialize the data as per the contraction method separately in each case.

Step-3: Set-up the random search location of the using eqn (3.14 & 3.15)

Step-4: Verify each randomly generated search agents by using objective function (J), eqn (3.16) and to find the best fitness value of the J

Step-4: Evaluate the each of the randomly generated search agents by using objective function of eqn (4.16) and determine the best. worst values of fitness to J

Step-5: Upgrade the randomly generated vector rand, r, t, z variables

Step-6: Clculate each generator randomly in sequence to match the demand and upgrade the best value of fitness and upgrade the location of J

Step-7: Check the condition if $random\ value < z$ (parameter setting =0.03), the condition satisfies, upgrade the search agent location by using eqn (3.21) of limited constraint parameter settings

Step-8: Evaluate each of the randomly generated search agents by using the objective function to determine and estimate the best objective function value of fitness.

Step-9: Carry the best fitness value of SM by the pattern search operators at the termination end of the global search optimizer to search the local region of the objective function (refer algorithm-3 PSEUDO-CODE).

Step-10: Analyse and upgrade the location of the each randomly generated search agents by using the objective function to determine and estimate the best, worst of the objective function value of fitness

Step-11: Check the condition $iter = \max\_iteration$, then go to step13.

Step-12: If $iter < \max\_iteration$, increase the size of iteration by 1 and go back to step-3

Step-13: Stop the simulation and obtained optimal variable solution of the LFR of two are Area DPS issue from each location in the size of the population that generated energy with the least frequency variation.

4.4 HYBRID MEMETIC HHO-PS SEARCH OPTIMIZATION ALGORITHM

The general operators of the Harris Hawks optimizer and the Pattern search algorithm are recursively hybridised to generate the hybrid memetic Harris Hawks Optimizer-Pattern search (HHO-PS) methodology for the LFR issue. Using the Harris Hawks method, a Harris Hawks solution is constructed for the whole population (global search region), and the best solution is chosen from the global search region. This optimal best outcome is then analysed to the Pattern search algorithm's solution (inside the local search region), and the overall optimal best outcome within the whole search region is discovered (global search region and local search region). In the next part, we'll go through the suggested hybrid HHO-PS method for the LFR issue.

HHO is used in the proposed methodology to optimise a objective function 'J' of LFR of the two area DPS to minimise area frequency fluctuations and tie line error within constraint limitations. As the search advances, the parameter values can be changed. The following are the steps in the proposed Hybrid memetic HHO-PS search algorithm:

Step-1: The size of the HHO-PS varies generally from 1 to 100 (for the test system on various contract methods of POOLCO, bilateral, and Contract violation cases)

The higher and lower boundary constraints of J value set-up as 5 to -5 in LFR issue and in the HHO boundary constraints are varies as per the objective function

Step-2: Set-up the load frequency regulation parameters and hawk's vectors as many as hawks' location tracing paths using eqn (3.1)

Each participation in the LFR issue is depends on the DISCO-GENCO participation factors, the DPM matrices is defined as

$$\text{DPM} = \begin{bmatrix} \text{cpf}_{\text{v11}} & \text{cpf}_{\text{v12}} & \text{cpf}_{\text{v13}} & \text{cpf}_{\text{v14}} \\ \text{cpf}_{\text{v21}} & \text{cpf}_{\text{v22}} & \text{cpf}_{\text{v23}} & \text{cpf}_{\text{v24}} \\ \text{cpf}_{\text{v31}} & \text{cpf}_{\text{v32}} & \text{cpf}_{\text{v33}} & \text{cpf}_{\text{v34}} \\ \text{cpf}_{\text{v41}} & \text{cpf}_{\text{v42}} & \text{cpf}_{\text{v43}} & \text{cpf}_{\text{v44}} \\ \text{cpf}_{\text{v51}} & \text{cpf}_{\text{v52}} & \text{cpf}_{\text{v53}} & \text{cpf}_{\text{v54}} \\ \text{cpf}_{\text{v61}} & \text{cpf}_{\text{v62}} & \text{cpf}_{\text{v63}} & \text{cpf}_{\text{v64}} \end{bmatrix} \text{ here, } \sum_{i=1}^{n} cpf_{vij} = 1, \text{ here j=1,2.....k}$$

k replicates the sum of DISCOs

n replicates the sum of GENCOs

Step-3: Initialize and Set-up LFR data as per contraction method of participation factors and constraints.

Step-4: Set-up the initial random generated position of hawks to search the prey of LFR issue.

Step-5: Evaluate the location of the search agents and verify the each randomly generated search agents by using objective function (J), eqn (4.16) to upgrade the position for objective function by using different operating conditions of specie, eqn (3.3).

Step-6: For the exploration period of the search agent check the condition $if\,(|EP| \geq 1), then$ upgrade the location of objective function by using eqn (3.1)

Sptep-7: For the exploitation period of search agents, check $if\,(|EP| < 1), then$ upgrade the location of the search agent by using eqns (3.4, 3.6, 3.10, 3.11).

Step-8: Analyse and compute each of the randomly generated search agents by using the objective function to determine and estimate fitness of best value.

Step-9: Carry along with the objective function best fitness value of HHO by the pattern search operators at the termination end of the global search optimizer to search the local region of the objective function (refer algorithm-3 PSEUDO-CODE).

Step-10: Upgrade the location of the each randomly generated search agents by using the objective function to determine and estimate the best, worst fitness values.

Step-11: Check once the condition for search agents, $iter = \max\_iteration$, then go to step13.

Step-12: If the condition $iter < \max\_iteration$, satisfies then increase the size of iteration by 1 and go back to step-3 to 12.

Step-13: Stop the computed optimal variable solution of the LFR of DPS network issue from each search location in the size of the population generated energy with the least frequency variation values of gains.

4.5 THE OBJECTIVE FUNCTION OF DESIGNING AN OPTIMAL LFR CONTROLLER

The optimal gain variable parameters of the augmented controller with the performance index of the objective function with constrained limitations using the integral time absolute error computing method is describes in this section.

In LFR of the Of the DPS network different nature of the objective functions with time domain performance are available in the global market. The maximum allowable settling time and overshoot of the LFR controller are being optimized in the timescale using performance criteria such as ITAE Integral Time Square Error, ITAE Integral Time Absolute Error, IAE Integral Absolute Error, and ISE Integral Square Error, or a combination of mentioned error criterions[18].

$$J1: ITAE = \int_0^{tsim} t*(|\Delta F_1| + |\Delta F_2| + |\Delta P_{tie12}|)dt \qquad 4.23$$

$$J2: ITSE = \int_0^{tsim} t*((|\Delta F_1|)^2 + (|\Delta F_2|)^2 + (|\Delta P_{tie12}|)^2)dt \qquad 4.24$$

$$J3: IAE = \int_0^{tsim} (|\Delta F_1| + |\Delta F_2| + |\Delta P_{tie12}|)dt \qquad 4.25$$

$$J4: ISE = \int_0^{tsim} ((|\Delta F_1|)^2 + (|\Delta F_2|)^2 + (|\Delta P_{tie12}|)^2)dt \qquad 4.26$$

With reference to chapter – 1 literature, IATE criteria is chooses as an objective function to compute the performance index of the developed LFR of the two area G – H – T units TLP interlinked DPS network. With reference to chapter – 1 literature, IATE criteria is chooses as an objective function to compute the performance index of the to compute the performance index of the developed LFR of the two area G – H – T units TLP interlinked DPS network.

To optimize and compute the objective function, *eqn* (4.23) has been used[28] [18] [46][41].

$$J = \int_0^{t_{sim}} (|\Delta F_1| + |\Delta F_2| + |\Delta P_{tie}|) * t * dt \qquad 4.23$$

The discrete variables of the incremental frequency oscillation changes in the developed DPS network of area-1 and area-2 are represented by ΔF_1 *and* ΔF_2.

ΔP_{tie} *is been the tie line power exchange value.*

't' stands for the overall simulation time in seconds.

The ITAE index is been used to the mitigate and set to steady state for the developed DPS network using the *HHO – PS tuned PI controller* , *SMA – PS tuned PI controller*, *HHO tuned PI controller* and SMA *tuned PI controller* gains in both region, according to the following constraints:

To minimize the performance index objective function variable the parametric condition is

$$K_i^P \min \le K_i^P \max \text{ and } K_i^{\text{int}} \min \le K_i^{\text{int}} \max$$

Here, K_i^P is the proportional gain of the optimized PI controller.

K_i^{int} is the integral gain of the optimized PI controller, here '*i'* has been the area of the DPS network (for i = 1, 2.) respectively.

Each region optimal gain constraints variable limits are set to between the ranges of (-5, 5).

The objective function's performance index provides a quantifiable assessment of a system's performance. In the case of the hybrid memetic SMA-PS optimizer, the performance index is lower, indicating that the suggested system is more stable than the hybrid memetic HHO-PS optimizer, classic HHO, and classic SMA optimizer of the developed DPS network. In the developed study, these statistical analyses show that the hybrid memetic SMA-PS optimizer outperforms the hybrid memetic HHO-PS optimizer, classic HHO, and classic SMA optimizer. The controller gain settings for the developed DPS network under investigation are listed in

Table 4.2. The performance of suggested optimizers in the LFR mechanism in the developed DPS network can be examined using these parameters.

Table.4.2 Performance of HHO, SMA, HHO-PS and SMA-PS algorithms tuned PI gains and objective values

Algorithm	k_1^P	k_1^i	k_2^P	k_2^i	Objective (J) function value
HHO	-1.96770	0.51651	-1.41549	0.90495	12.04242
SMA	-2.07057	0.60055	-1.24403	1.01499	11.69459
HHO-PS	-1.54858	0.63386	-1.30379	0.62264	11.48522
SMA-PS	-1.92707	0.73406	-1.80957	0.84743	11.36849

4.6 RESULTS AND DISCUSSION

The developed LFR of the two area G – H – T originating units TLP interlinked DPS is studied and verified under DPS market scenario, was created in the Simulink environment in MATLAB 2018a. The non-linearity effect of the GRC is evaluated using a DPS network with G – H – T originating units in each area. A series operation of simulation performance has been performed in each region and to minimise TLP flow reaction with the rapid response of the frequency reaction in each region of the DPS network.

Various studies for possibly realistic power contracts in a DPS network have been done. Each DISCOs have considered a load disturbance of 0.005 percent step change, resulting in an overall fluctuation of 0.01 percent in each region. Each GENCO's involvement in LFR is entirely dependent on their *apfs*. The simulation is run in accordance with the DPM and the contracts among the DISCOs and GENCOs. Three distinct case studies were done, and the results are reported in the sections below.

4.6.1 POOLCO or Unilateral Transaction Method

Only GENCOs and DISCOs in the similar region are eligible to engage in unilateral power contracts.

Here, each GENCOs contributes to LFR of DPS premised on *apfs*, and each DISCOs have an agreement (contract) with the GENCOs in their same region. i.e., PF for the T – H- G originating units are $PF_{\text{thermal1}} = 0.6$, $PF_{\text{hydro1}} = 0.3$, and PF_{gas1}=0.1, so that $PF_{\text{thermal1}} +$

$PF_{\text{hydro1}} + PF_{\text{gas1}}$= 0.6+0.3+0.1 = 1 in area -1. And similarly, area-2 is $PF_{\text{thermal2}} + PF_{\text{hydro2}} + PF_{\text{gas2}} = 1.$

Here, as per contraction only area - 1 has a load fluctuation, with sudden load demand of DISCOs, and the demand is 0.005 pu MW.

$$\Delta p_{l1} = \Delta p_{l2} = 0.005\ pu\ MW$$

such that in area - 1 an overall load change of two DISCOs is 0.01 pu MW occurs. In other case, area – 2 has no demand of load variation is zero, so $\Delta p_{l3} = \Delta p_{l4} = 0\ pu\ MW$

here, as per eqn (4.6) and (4.7)

$$\Delta p_{D1} = \Delta p_{l1} + \Delta p_{l2} = 0.005 + 0.005 = 0.01 pu\ MW$$

$$\Delta p_{D2} = \Delta p_{l1} + \Delta p_{l2} = 0\, pu\ MW$$

In this method, distribution of power among each DISCOs and GENCOs in the studied DPS network premised on the followed DPM matrix.

$$DPM = \begin{bmatrix} 0.33330 & 0.33330 & 0 & 0 \\ 0.33330 & 0.33330 & 0 & 0 \\ 0.33330 & 0.33330 & 0 & 0 \\ 0 & 0 & 0 & 0 \\ 0 & 0 & 0 & 0 \\ 0 & 0 & 0 & 0 \end{bmatrix}$$

As mentioned in eqn. (4.8). The participated each GENCO power response in the proposed DPS network calculated as follows

Thermal (GENCO-1) in area-1 as,

$$\Delta P_{Gc1} = 0.005 * 0.3333 + 0.005 * 0.3333 + 0.00 + 0.00 = 0.003333 \text{ pu MW}$$

Likewise, gas (GENCOs-3) and hydro (GENCOs-2) in area-1 are 0.003330 pu MW in each region, respectively. For area -2, $\Delta P_{Gc4} = \Delta P_{Gc5} = \Delta P_{Gc6} = 0,$ Because, according to the established contract, DISCOs-3 and 4 in area-2 have no power demand.

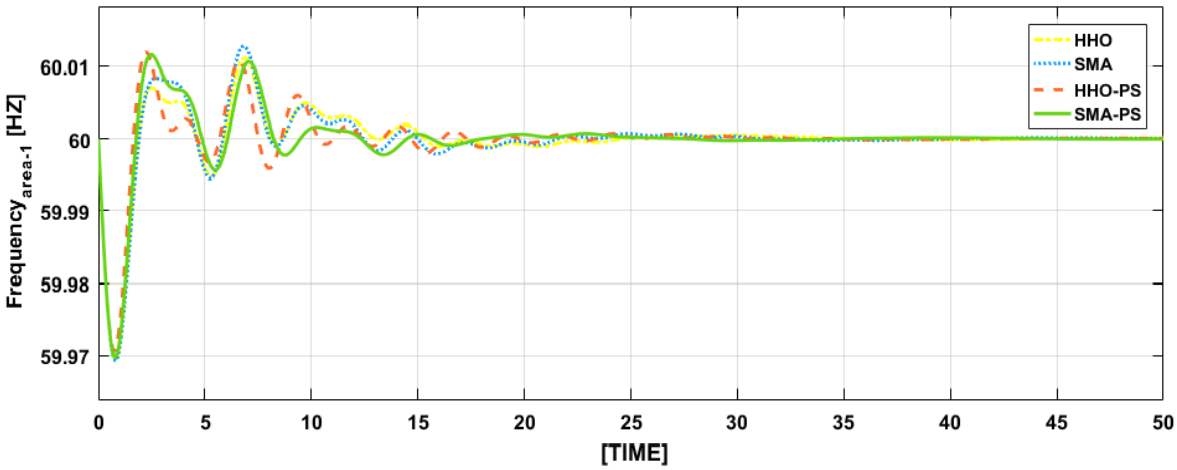

Fig.4.5 area-1 frequency reaction for LFR of the DPS network under POOLCO power exchange method having different optimized controllers.

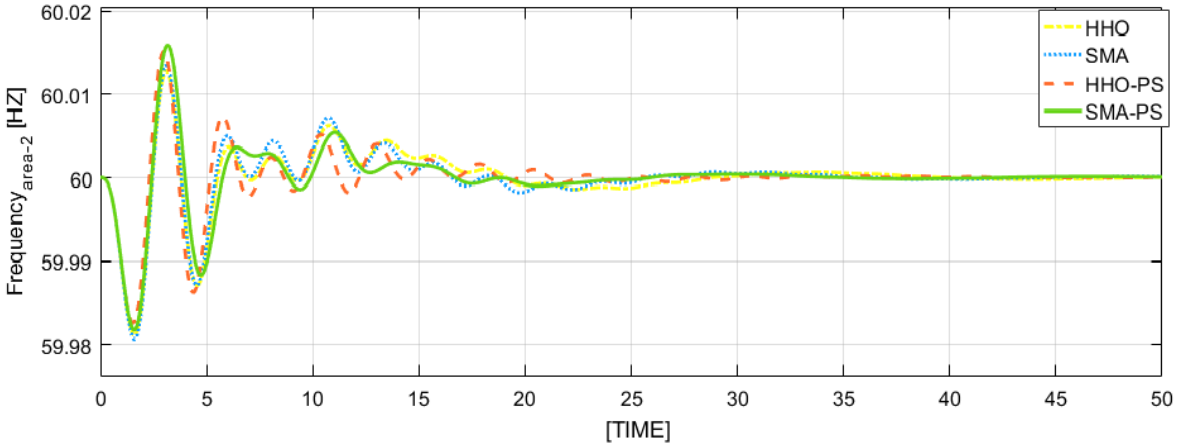

Fig.4.6 Area-2 dynamic frequency reaction for LFR of the DPS network under POOLCO power exchange method having different optimized controllers

Figures 4.5–4.10 demonstrate the performance analysis for the POOLCO premised contract in the form of frequency responses in each region, TLP exchange of actual and error responses, and GENCOs responses in each area of DPS network after a sudden load shift.

Here, fig 4.5 and 4.6 depicts the fluctuation of frequency reaction in both regions with POOLCO contraction in response to load change for the different optimization premised PI controllers. As per the comparative analysis for HHO, SMA, HHO-PS and SMA-PS optimizers, it is stated that the SMA-PS approach produces higher dynamic performance than the other optimizers.

Fig 4.8 depicts the fluctuation in tie line power in the region 1 power system for a 0.01 pu load shift. The results demonstrate that the hybrid SMA-PS approach easily dampens real tie line power flow variation after a load shift.

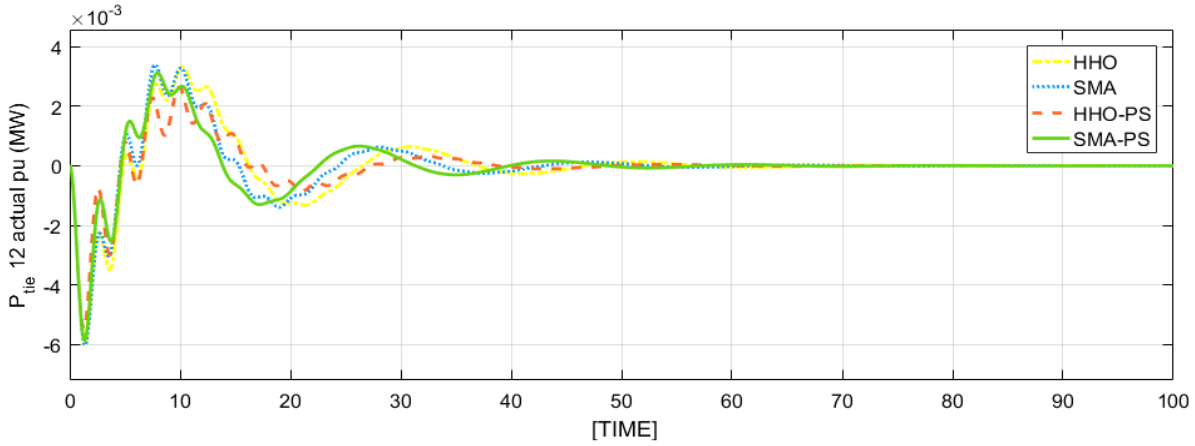

Fig.4.7 Actual TLP flow reaction under POOLCO contract

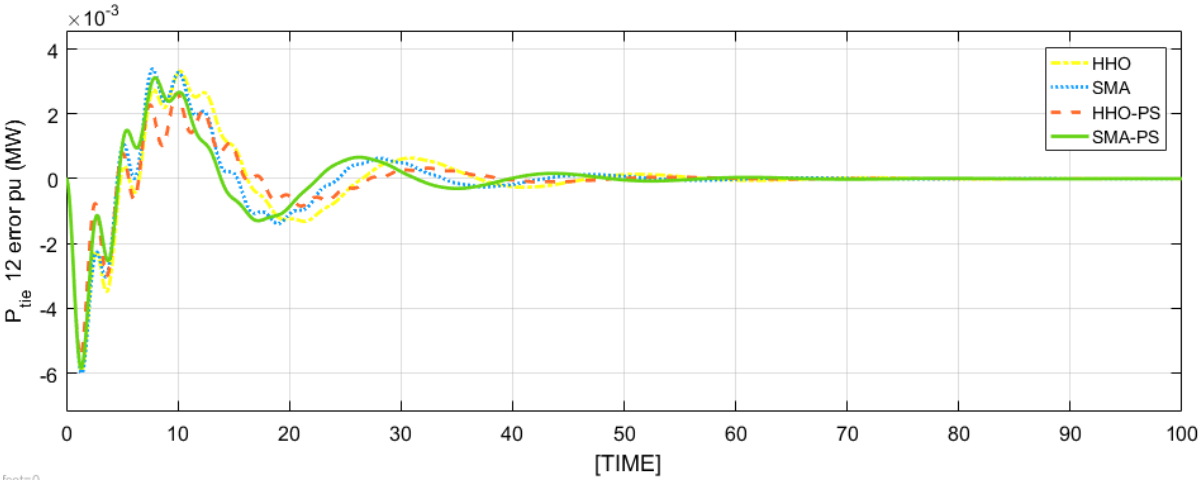

Fig.4.8 Error of the TLP flow variation under POOLCO contract

Fig 4.7 and 4.8 depicts the fluctuation in actual tieline power and tie line error in the region 1 power system for a 0.01 pu load shift. The results demonstrate that the hybrid SMA-PS approach easily dampens real TLP flow variation after a load shift.

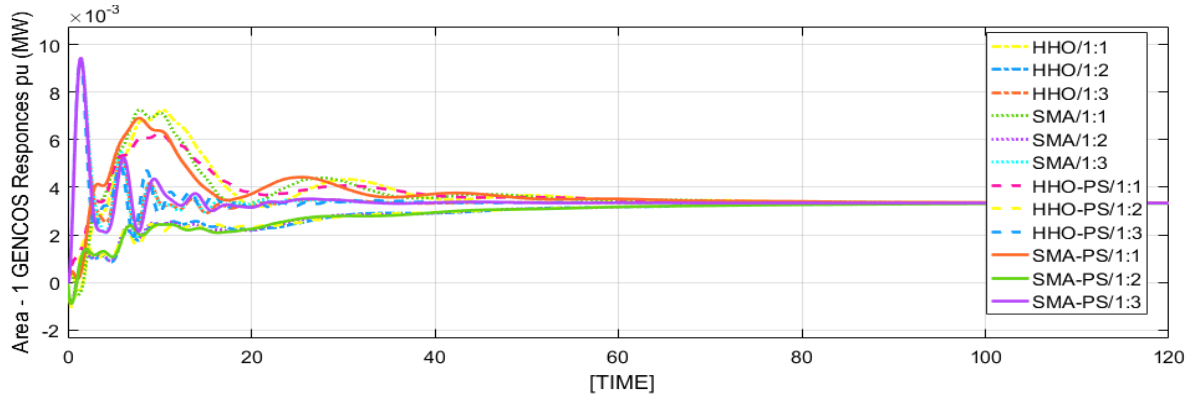

Fig.4.9 Area-1 GENCOs reaction under POOLCO transaction power exchange

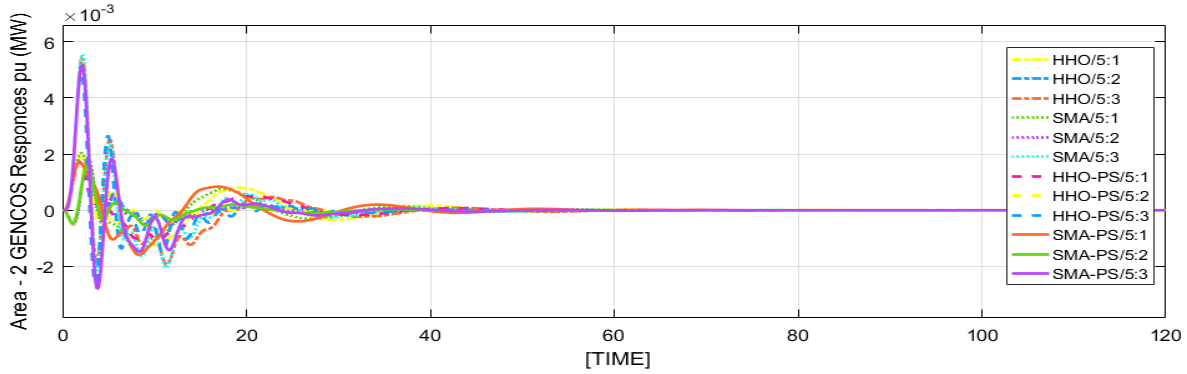

Fig.4.10 Area-2 GENCOs responses under POOLCO method.

Area 1's Disco's demand electricity to their own GENCOs., therefore, the GENCOs must meet their contractual obligations. The power generating reaction of area 1 & 2 GENCOs are shown in Figures 4.9 and 4.10, respectively. The waveforms obtained demonstrate that area1 GENCOs, i.e., GENCOs 1, 2, and 3 generate electricity premised on requirement and cpfs. The hybrid SMA-PS optimization approach improves deviation, and generators reach their steady-state stage rapidly. Figure 4.10 indicates that the DISCOs have no demand in region 2. As a result, the change in generated power by all GENCOs related to this area is zero in steady state.

The SMA-PS optimizer outperforms the other optimizers in terms of dynamic responsiveness, according to the generation response outputs of different GENCOS. It can be observed from the above data that the SMA-PS optimizer approach achieves higher dynamics performances in terms of settling time value of ΔF1, ΔF2, and ΔP_{tieine} power.

4.6.2 BILATERAL TRANSACTION METHOD

This section, depicts a situation in which a GENCOs and DISCOs conduct transactions in the any region of each, referred to as a bilateral transaction. In this situation, GENCOs and DISCOs fully adhere to the contract conditions[46]. In the developed DPS network, every GENCO and DISCO in the system under investigation forms contracts as per following DPM

$$DPM = \begin{bmatrix} 0.2 & 0.1 & 0.3 & 0 \\ 0.2 & 0.2 & 0.1 & 0.1666 \\ 0.1 & 0.3 & 0.1 & 0.1666 \\ 0.2 & 0.1 & 0.1 & 0.3336 \\ 0.2 & 0.2 & 0.2 & 0.1666 \\ 0.1 & 0.1 & 0,2 & 0.1666 \end{bmatrix}$$

Every DISCOs in its control area required as represented by the cpfs in the DPM matrix, requires 0.005 pu MW energy from the GENCOs, according to the bilateral transaction. As a result, area-1 and area-2 experience a complete load disruption of 0.01 pu MW of each. As a

result, the power consumption in each location is 0.01 pu MW, according to eqns. (4.6) and (4.7). Following a sudden load requirement, the produced power responses of each GENCOs in area 1, estimated using eqn. (4.7) as follows:

For GENCO-1 (Thermal):

$$\Delta P_{Gc1} = 0.2*0.005 + 0.1*0.005 + 0.3*0.005 + 0*0.005 = 0.0030 \text{ pu MW}$$

For GENCO-2 (Hydro):

$$\Delta P_{Gc2} = 0.2*0.005 + 0.2*0.005 + 0.1*0.005 + 0.1666*0.005 = 0.00333 \text{ pu MW}$$

For GENCO-3 (Gas):

$$\Delta P_{Gc3} = 0.1*0.005 + 0.3*0.005 + 0.1*0.005 + 0.1666*0.005 = 0.00333 \text{ pu MW}$$

In addition, for area-2 are,

$$\Delta P_{Gc4} = 0.2*0.005 + 0.1*0.005 + 0.1*0.005 + 0.3336*0.005 = 0.003668 \text{ pu MW}$$

$$\Delta P_{Gc5} = 0.2*0.005 + 0.2*0.005 + 0.2*0.005 + 0.2*0.005 = 0.003883 \text{ pu MW}$$ and

$$\Delta P_{Gc6} = 0.1*0.005 + 0.1*0.005 + 0.2*0.005 + 0.1666*0.005 = 0.00283 \text{ pu MW}$$ respectively

The DPS network performance has been evaluated with immediate variations in load demand, a bilateral contract is established among each region DISCOs and GENCOs. On the above-mentioned DPM, the agreement between different DISCOs and available GENCOs is simulated.

Figure 4.11 & 4.12 depicts the frequency deviations in both areas in a deregulated market with a sudden load change. Because of the SMA-PS methodology, the system frequency deviations were performed with reduced peak overshoot, shorter settling time, and peak rise time, the findings show improved dynamics performance. In both regions, frequency deviations are immediately dampened.

Figure 4.13 & 4.14 depicts the tie line actual and error in the DPS. Figure 4.15 & 4.16 illustrates each area generation (GENCOs -1 to GENCOs – 6) responses of DPS. From the obtained outcomes the proposed methodology SMA-PS optimizer performs superior performance than the HHO, SMA and HHO-PS optimizers.

Figures 4.11 – 4.16 demonstrate performance analysis for the bilateral premised contract in the form of frequency responses in each region, tie line power exchange of actual and error responses, and power generation responses in each area of DPS after a sudden load shift

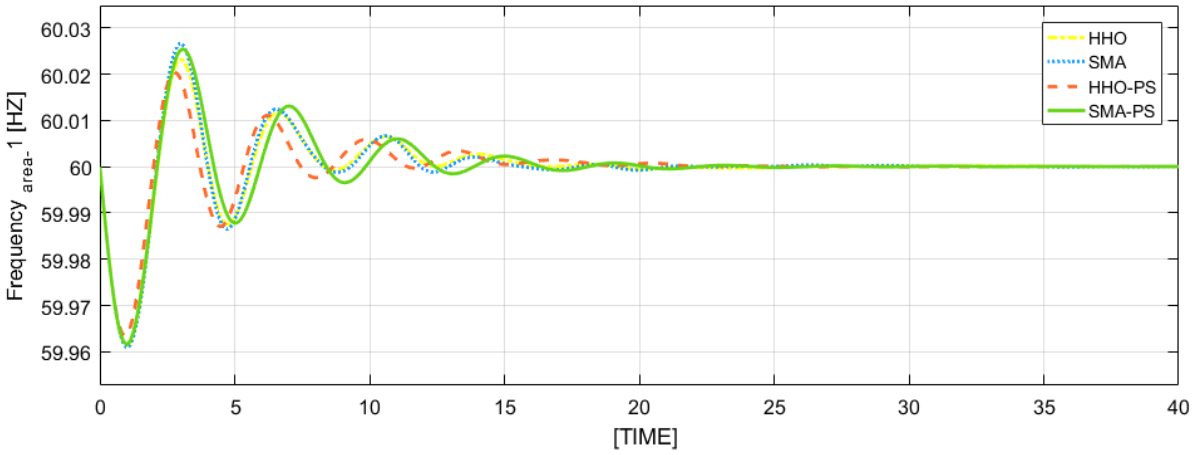

Fig.4.11 Frequency reaction under a bilateral method for area – 1

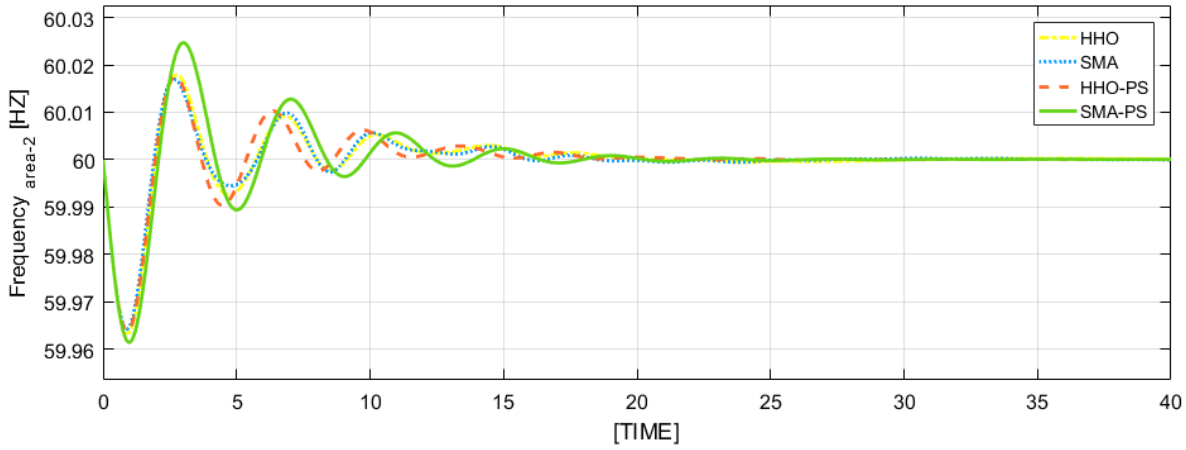

Fig.4.12 Frequency deviation responses of area - 2, under a bilateral method

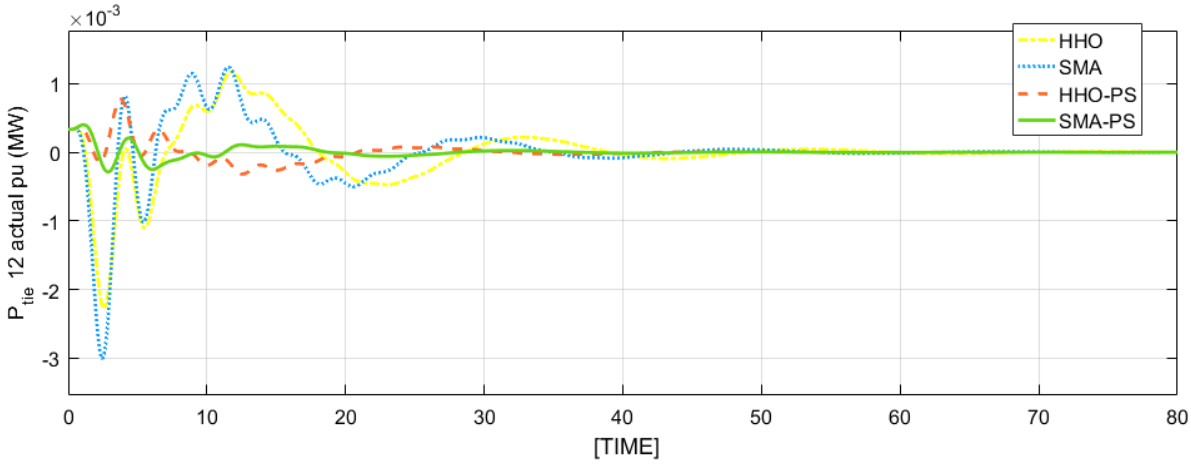

Fig.4.13 Actual TLP flow under bilateral transaction

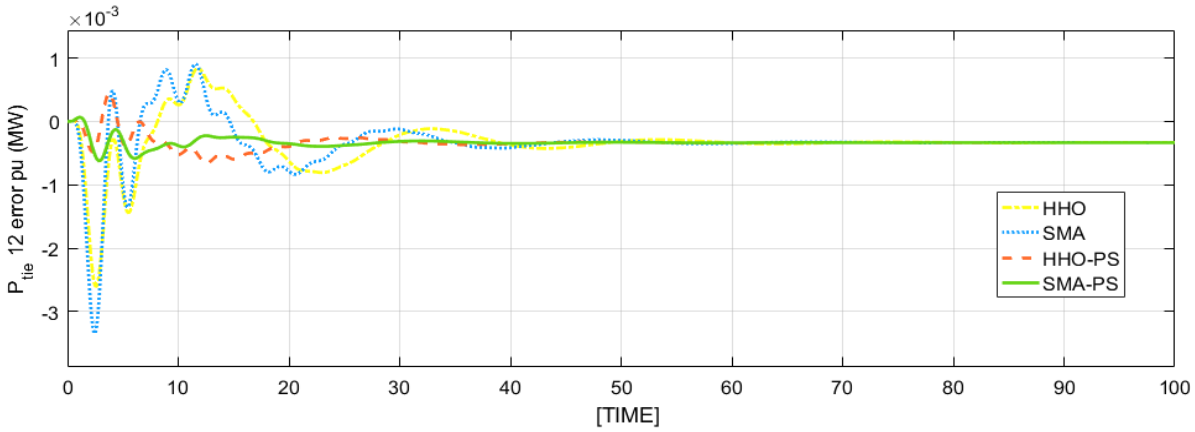

Fig.4.14 TLP flow error response, under bilateral transaction

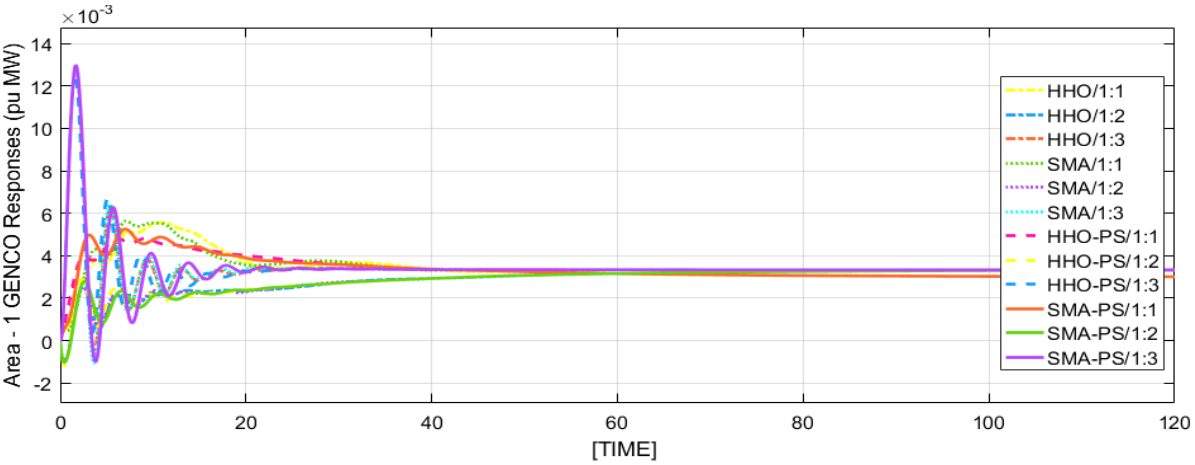

Fig.4.15 Area-1 GENCO's generation responses under bilateral premised transaction method

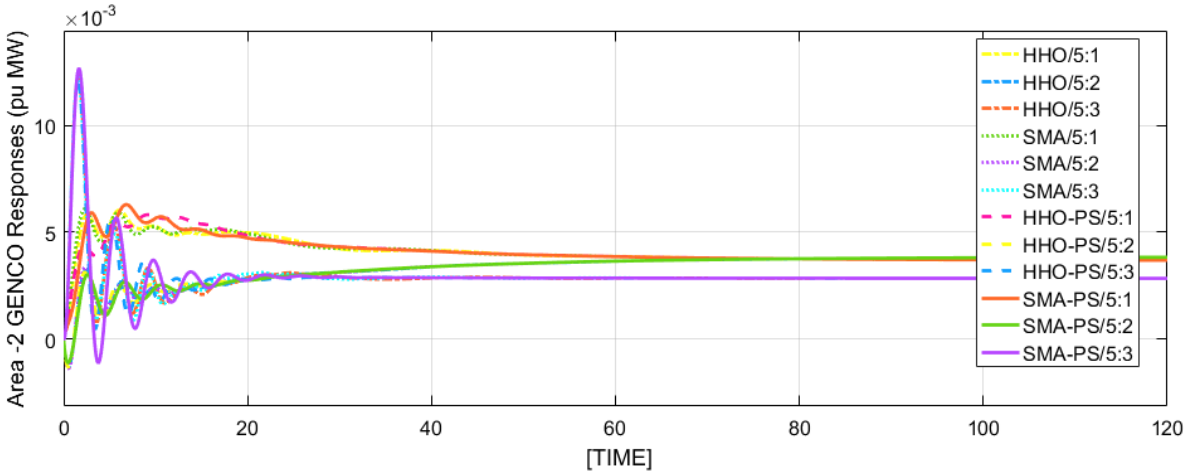

Fig.4.16 Area-2 GENCO's generation responses under bilateral premised transaction method.

4.6.3 CONTRACT VIOLATION

Here, a CV happens when a DISCOs oscillates from the predetermined arrangement by requesting more power from the GENCOs than was specified in the contract. The GENCOs operating in the any region of the DISCOs should ideally meet this uncontracted power load demand.

Consider case-B, in which DISCOs requests 0.0030 pu MW of more energy, which the GENCOs of area-1 can assume sudden as an excess load of 0.0030 pu MW after 40 seconds during simulation. Due to the DISCOs' request for more energy, the overall load requested in area-1 has increased to 0.0130 pu MW. Because the increased power demand happens solely in area-1, the power requested in area-2 remains unchanged. As a result of eqns. (4.6) and (4.7), the power requested in both regions are as follows.

$$\Delta p_{D1} = 0.005 + 0.005 + 0.003 = 0.013 \; pu \; MW$$

$$\Delta p_{D2} = 0.005 + 0.005 = 0.01 \; pu \; MW$$

By using eqn (4.5), After a sudden unexpected load demand, the produced power reaction of several GENCOs in area-1 may be computed as

For GENCO-1 (Thermal):

$$\Delta p_{Gc1} = 0.2*0.005 + 0.1*0.005 + 0.3*0.005 + 0*0.005 + 0.6*0.003 = 0.0048 \; pu \; MW$$

For GENCO-2 (Hydro):

$$\Delta p_{Gc2} = 0.2*0.005 + 0.2*0.005 + 0.1*0.005 + 0.1666*0.005 + 0.3*0.003 = 0.004233 \; pu \; MW$$

For GENCO-3 (Gas):

$$\Delta p_{Gc3} = 0.1*0.005 + 0.3*0.005 + 0.1*0.005 + 0.1666*0.005 + 0.1*0.003 = 0.003633 \; pu \; MW$$

In addition, for area-2 are,

$$\Delta p_{Gc4} = 0.2*0.005 + 0.1*0.005 + 0.1*0.005 + 0.3336*0.005 + 0.6*0.003 = 0.003668 \; pu \; MW$$

$$\Delta p_{Gc5} = 0.2*0.005 + 0.2*0.005 + 0.2*0.005 + 0.2*0.005 + 0.3*0.003 = 0.003883 \; pu \; MW$$

$\Delta p_{Gc6} = 0.1*0.005 + 0.1*0.005 + 0.2*0.005 + 0.1666*0.005 + 0.1*0.003 = 0.00283 \; pu \; MW$, respectively.

In the presence of classic HHO, classic SMA, hybrid memetic HHO-PS, and hybrid memetic SMA-PS optimally tuned PI controllers, the various dynamic reaction in terms of tie-line exchanging power, each area frequencies, and power generations are illustrating in Figs. 4.17 – 4.22.

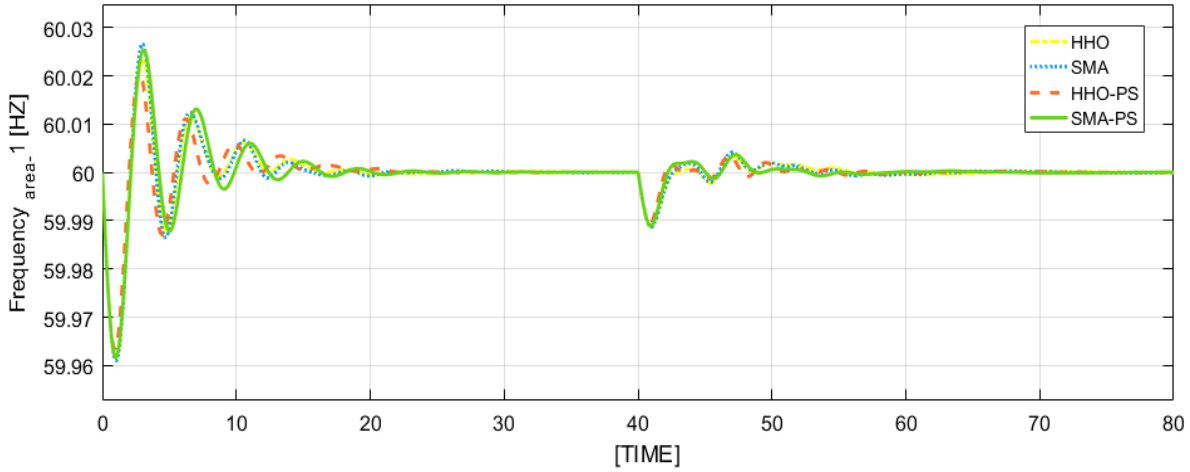

Fig.4.17 Frequency deviation responses of area - 1 for CV case

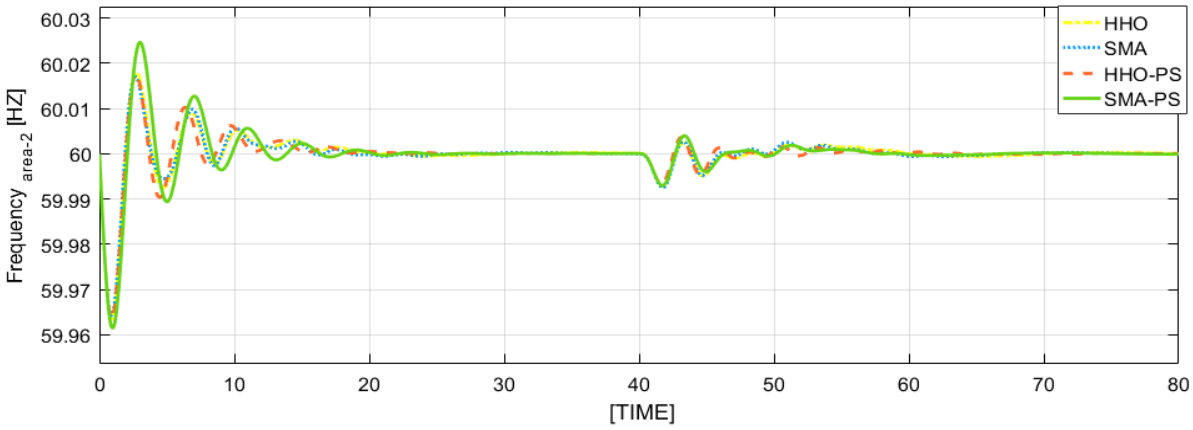

Fig.4.18 Frequency deviation responses of area 2, for CV case

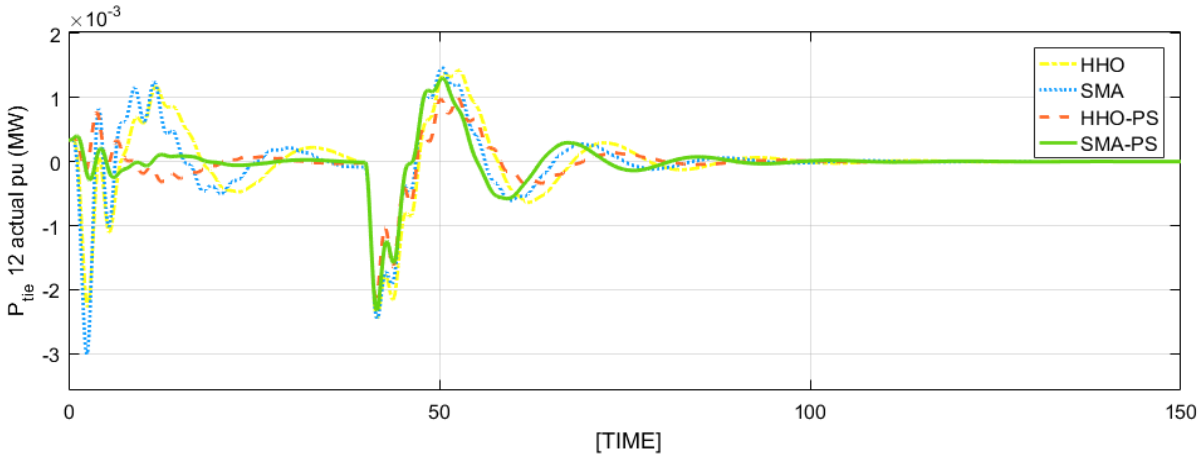

Fig.4.19 Actual TLP reaction under CV case

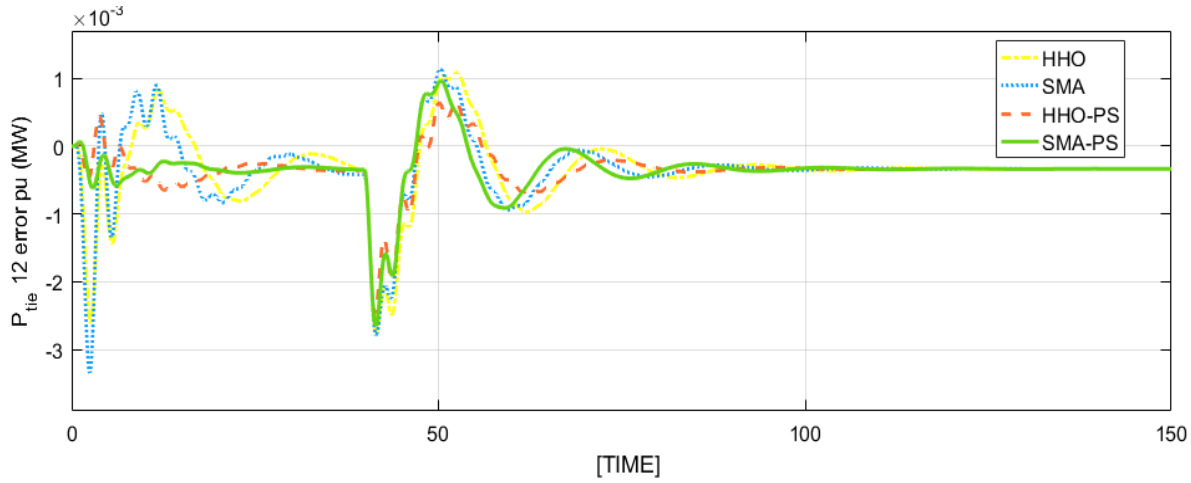

Fig.4.20 TLP error reaction under CV case

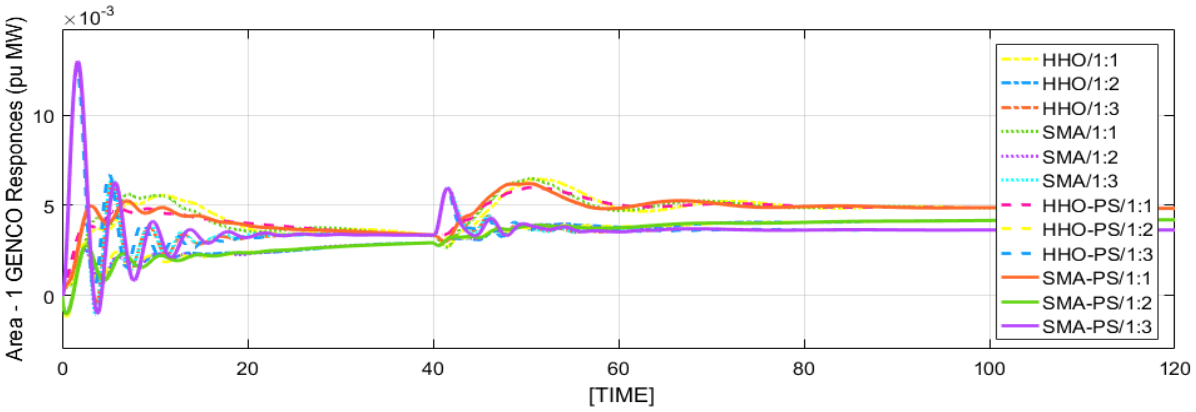

Fig.4.21 Area-1 GENCO's generation responses under contract violation method

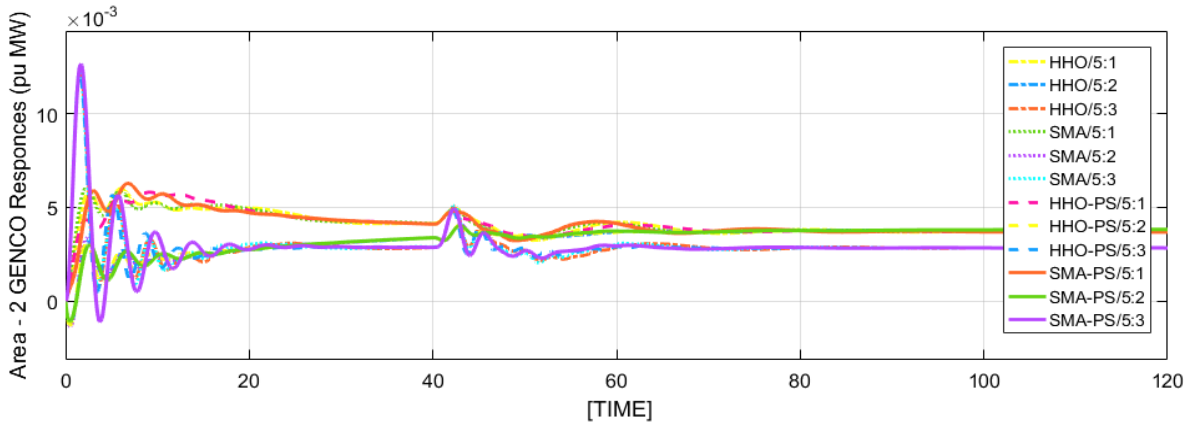

Fig.4.22 Area-2 GENCO's generation responses under contract violation method

Table.4.3 During a unilateral transaction, a comparative study of different controllers.

Parameters	HHO	SMA	HHO-PS	SMA-PS

Settling time (sec)	ΔF_1	36	34	35	30
	ΔF_2	30	30	25	20
	P - tie	40	40	30	30
Under shoot response	ΔF_1	59.9810	59.9805	59.9825	59.9820
	ΔF_2	59.9695	59.9696	59.9705	59.9700
	P - tie	-0.00595	-0.0060	-0.00550	-0.00585
Peak overshoot response	ΔF_1	60.0080	60.0090	60.0120	60.0120
	ΔF_2	60.01250	60.0130	60.0150	60.0150
	P - tie	0.0032	0.0032	0.0025	0.0025

Table.4.4 Comparative analysis of various controllers under bilateral transaction methods

Parameters		HHO	SMA	HHO-PS	SMA-PS
Settling time (sec)	ΔF_1	20	20	20	20
	ΔF_2	25	25	20	20
	P - tie	40	40	30	20
Under shoot response	ΔF_1	59.9615	59.9625	59.9640	59.9620
	ΔF_2	59.9635	59.9645	59.9635	59.9620
	P - tie	-0.0025	-0.0033	-0.0050	-0.0050
Peak overshoot response	ΔF_1	60.0230	60.0250	60.0200	60.0250
	ΔF_2	60.0180	60.0170	60.0170	60.0240
	P - tie	0	0	0	0

Table.4.5 During Contract violation, comparative analysis for different controllers

Parameters		HHO	SMA	HHO-PS	SMA-PS
Settling time (sec)	ΔF_1	66	64	62	58
	ΔF_2	60	58	56	54
	P - tie	75	75	72	65
Under shoot response	ΔF_1	59.9625	59.9610	59.6400	59.9620
	ΔF_2	59.9630	59.9640	59.9640	59.9620
	P - tie	-0.0025	-0.0030	0	0
	ΔF_1	60.0230	60.0270	60.0200	60.0250

Peak overshoot response	ΔF_2	60.025	60.0150	60.0150	60.0200
	P - tie	0	0.0005	0	0

Figures 4.5, 4.6, 4.11, 4.12, 4.17, & 4.18 shows the simulation rection in terms of frequency changes in both regions with HHO, SMA, HHO-PS, and SMA-PS tuned PI controllers under CV, bilateral, and unilateral cases scenarios in a deregulated energy market. The collected findings show that in any contract's scenarios of the deregulated energy system, the performances of all suggested controllers are satisfactory. However, as compared to a HHO, SMA, and HHO-PS based PI controller, a SMA-PS based PI controller achieves steady state faster and with low deviations in terms of undershoot, peak overshoot, and settling time.

Figures 4.7, 4.8, 4.13, 4.14, 4.19 & 4.20 show the influence of optimal tune PI controllers with various optimizers on the TLP flow reaction in DPS under CV, bilateral, and unilateral, case situations, respectively. In the unilateral contract scenario, there is no electricity demand between area-1 and area-2. As a result, the tie line's planned power is reduced to zero. The actual TLP settle at 0.0003340 pu MW in the bilateral and CV scenarios, which is the in the steady state, planned power on the tie-line as per eqn (4.5). The simulated and theoretical values of real power in the tie line between areas 1 & 2 are identical and exactly as specified in the contract. The efficacy of the hybrid memetic SMA-PS tuned PI controller outperforms the HHO, SMA, and HHO-PS based PI controllers in every contract scenario. The power flow through the tie line between the connecting locations follows the established contract's scheduled transaction. After achieving steady state, the tie line error becomes zero. The reported findings support the SMA-PS optimizer's efficacy in the intended investigation.

Figures 4.9, 4.10, 4.15, 4.16, 4.21 & 4.22 shows the power generation reaction of each GENCO in the system under contract breach, bilateral, and unilateral situations in a deregulated market, respectively.

Fig. 4.9 demonstrates that in the unilateral scenario, the area-1 GENCOs (GENCO -1, 2, & 3), generate power in accordance with demand and their cpfs. The DISCOs have no demand in area 2, as shown in Fig. 4.10. Similarly, fig. 4.15 & 4.16 depicts the power generation reaction of each GENCO, under a bilateral contract scenario. Each GENCO reacts to its predetermined transaction contract by generating the precise quantity of electricity required to meet the demands of different DISCOs. The uncontracted load demand affects the produced power response of area 1's GENCOs 1, 2, & 3. However, area 2's GENCO 4, 5, and 6 are unaffected

by the uncontracted load. As indicated in the data, the generation reactions of area-1 GENCOs to meet the surplus power demand are clearly represented in their outputs. Every generator in area-1 reacts in accordance with its apf's and soon reaches the new generation limitations to meet the DISCOs' increased power demand.

The power flow in the TLP and generation power responses of each producing unit are clearly represented in the acquired data, and they match the calculated values. During the transient situation, each GENCO respond according to its apfs, and the proposed system under investigation soon achieves steady state.

The generated power of various GENCOs also show that the system with a SMA-PS premised PI controller has a superior dynamic reaction than HHO, SMA, HHO-PS tuned PI controller, and the generators quickly reach steady-state. The system's peak overshoot and setting time are shorter, and oscillations are damped more quickly. In over and under frequency occurrences, the exchanging power to grid to alleviate the load on linked conventional generating plants and to assist stabilize LFR much faster than the present primary response.

Tables 4.3, 4.4, and 4.5 compare the proposed system's HHO, SMA, HHO-PS, and SMA-PS based PI controllers in bilateral, contract violation and unilateral transactions, respectively. The frequency response of both regions, the reaction of power generation and tie line power, rection of several generating units were examined, and various characteristics such as settling time, undershoot, and peak overshoot of different waveforms were obtained. In the suggested power system, it can be shown that the SMA-PS tuned PI controller achieves higher dynamic performance when compared to the HHO, SMA, and HHO-PS based PI controllers.

4.7 **SENSITIVITY ANALYSIS**

The research effort has gone through many sensitive analyses that are followed by a broad discrepancy of system dependant factors to support the established system, robustness, and excellence of suggested hybrid memetic SMA-PS and hybrid memetic HHO-PS optimizers premised PI controllers. The *governor* time constant (T_{sg}) and *inertia* constant H, which leads to change the load constant (T_{ps}) are regularised from nominal values in the range of ±25% . Tables 4.6, 4.8, 4.10, and 4.12 show the variation of gain parameters, whereas tables 4.7, 4.9, 4.11, and 4.13 provide the performance analysis data. The dynamic reactions displayed in Figures 4.23 to 4.34 because of changes in T_{ps} and T_{sg}

constants. The suggested hybrid memetic SMA-PS and hybrid memetic HHO-PS predicated PI controllers are hence resilient. Tables 4.6, 4.8, 4.10, and 4.12 depicts the different performance indices for the novel augmented electric system under the POOLCO premised tactic, including ITAE values and settling, peak undershoot and overshoot and responses under nominal and electric system parameter variable modification situations. The suggested optimum hybrid memetic SMA-PS optimizer premised PI controller is a resilient controller, as shown in Tables 4.7, 4.9, 4.11, and 4.13, and when either load is applied to either a change in loading situation or a change in parameters, no need to retune its settings. Figures 4.23 to 4.34 show the frequency deviations of Area-1, 2 and TLP flow reactions as a function of Tsg. The effect of changing operational loading circumstances on system responses is minor, as can be shown in Figures 4.23 to 4.34. As a result, the suggested control technique can be concluded to offer stable control across a wide range of system loads and parameter changes.

Table.4.6 Gain parameters for the proposed DPS network after changing Tsg value -25%

Tsg= - 25%	k_1^P	k_1^i	k_2^P	k_2^i	J
HHO	-1.46429	0.66254	-1.37823	0.686835	17.22383
SMA	-1.5735	0.66433	-1.51159	0.67927	12.11126
HHO-PS	-1.56102	0.598884	-1.76225	0.604654	11.92009
SMA-PS	-1.57566	0.662313	-1.48906	0.686353	10.87906

Table.4.7 Performance analysis of the proposed DPS network after changing Tsg as - 25%

Tsg= - 25%		HHO	SMA	HHO-PS	SMA-PS
Settling time (sec)	ΔF_1	31	30	29	27
	ΔF_2	35	34	32	30
	P - tie	40	52	50	45
Peak overshoot response	ΔF_1	60.012	59.972	60.011	60.011
	ΔF_2	60.0150	60.0150	60.0150	60.0150
	P - tie	0.0027	0.0027	0.0026	0.0025
Peak undershoot response	ΔF_1	59.972	59.972	59.972	59.972
	ΔF_2	59.9830	59.9830	59.9830	59.9830
	P - tie	-0.0055	-0.0055	-0.0055	-0.0055

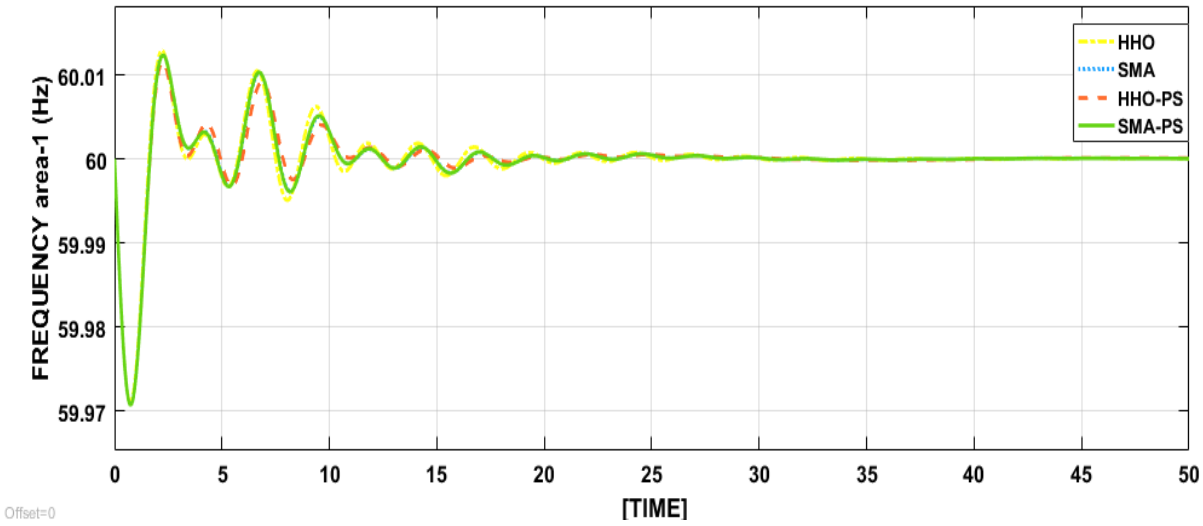

Fig.4.23 Area-1 frequency reaction of the DPS network after changing the Tsg as - 25%

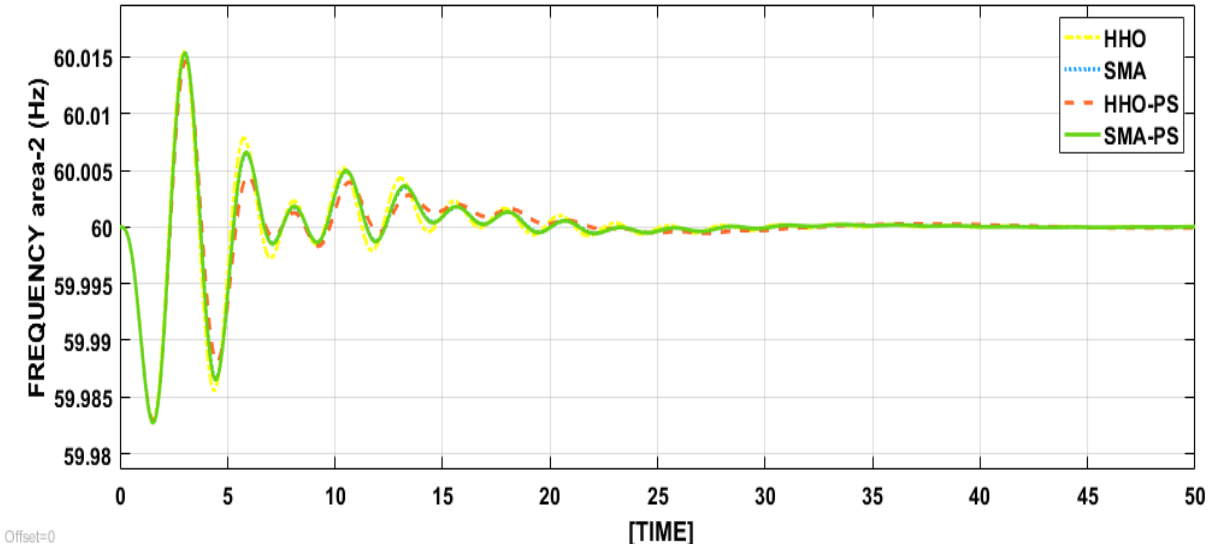

Fig.4.24 Area-2 frequency reaction of the DPS network after changing the Tsg as - 25%

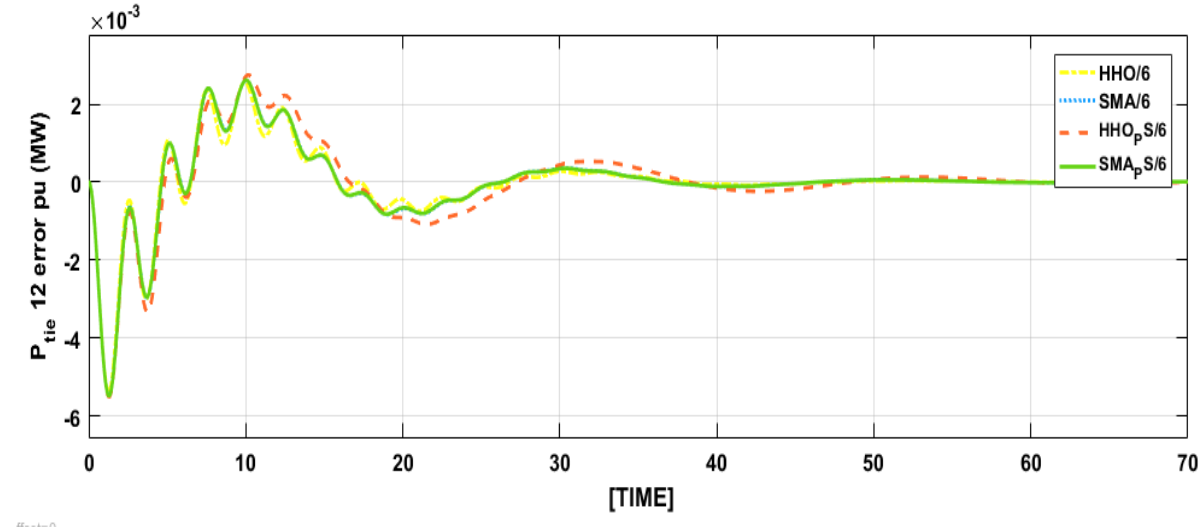

Fig.4.25 TLP flow reaction of the DPS network after changing the Tsg as - 25%

Table.4.8 Gain parameters for the proposed DPS network after changing Tsg value +25%

Tsg= + 25%	k_1^P	k_1^i	k_2^P	k_2^i	J
HHO	-1.59945	0.657991	-1.52566	0.669293	13.60888
SMA	-1.70280	0.67328	-1.64761	0.68599	11.06263
HHO-PS	-1.60788	0.658594	-1.54232	0.673494	11.02562
SMA-PS	-1.66322	0.662656	-1.58483	0.678781	11.00202

Table.4.9 Performance analysis of the proposed DPS network after changing Tsg as + 25%

Tsg= +25%		HHO	SMA	HHO-PS	SMA-PS
Settling time (sec)	ΔF_1	30.5	30.5	30	29
	ΔF_2	30	30	29.5	29
	P - tie	45	45	43	43
Peak overshoot response	ΔF_1	60.0125	60.0120	60.0119	60.0118
	ΔF_2	60.0157	60.154	60.0155	60.0150
	P - tie	0.0024	0.0024	0.0023	0.0023
Peak undershoot response	ΔF_1	59.9700	59.9700	59.9700	59.9700
	ΔF_2	59.9835	59.9835	59.9830	59.9830
	P - tie	-0.0054	-0.0054	-0.0055	-0.0055

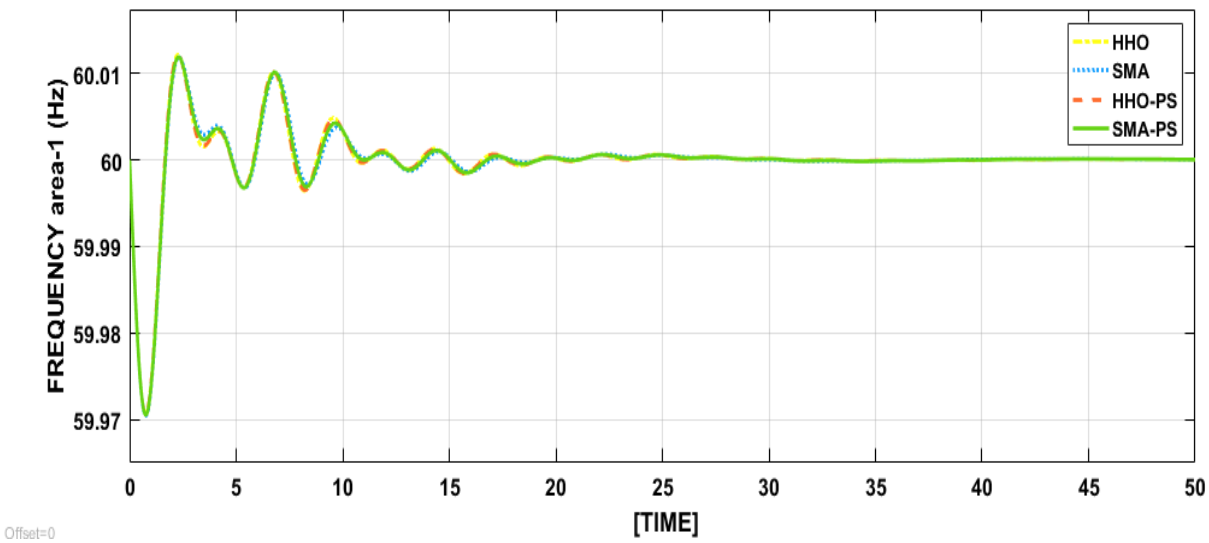

Fig.4.26 Area-1 frequency dynamic reaction of the DPS network after changing the Tsg as + 25%

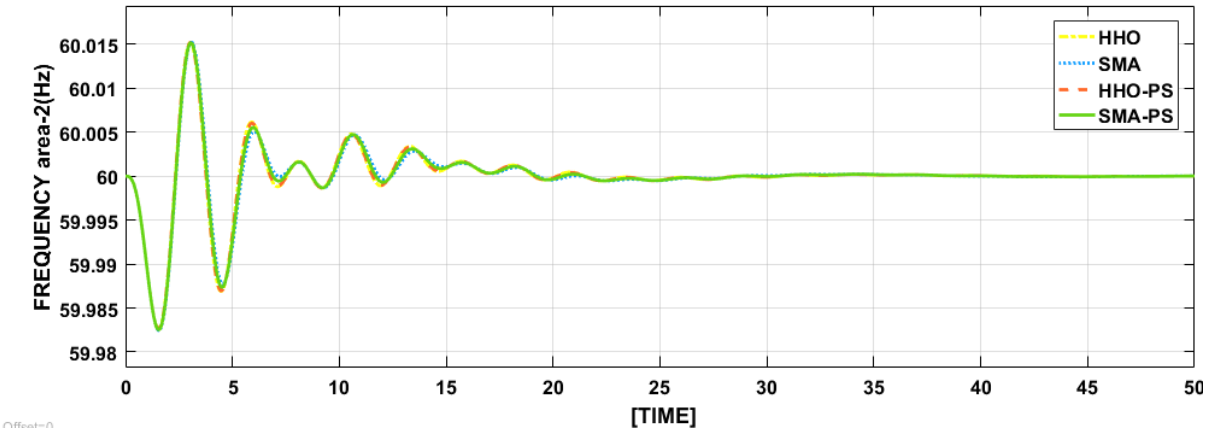

Fig.4.27 Area-1 frequency reaction of the DPS network after changing the Tsg as - 25%

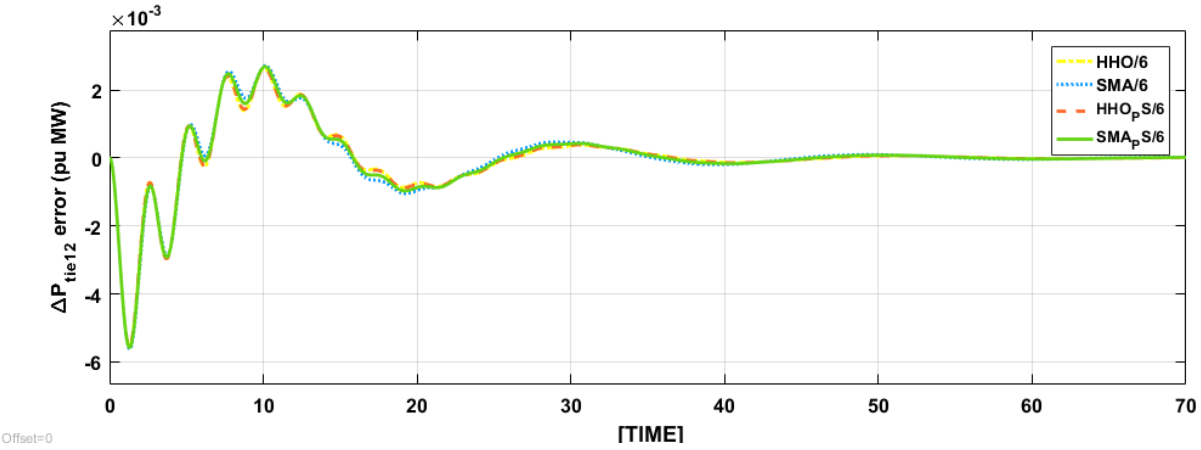

Fig.4.28 TLP flow reaction of the DPS network after changing the Tsg as -+25%

Table.4.10 Gain parameters for the proposed DPS network after changing H value +25%

H= + 25%	k_1^P	k_1^i	k_2^P	k_2^i	J
HHO	1.09607	0.84745	-1.06309	0.86617	8.803637
SMA	-0.96049	0.87519	-0.94869	0.87175	8.73169
HHO-PS	-1.09822	0.851043	-1.07436	0.86545	8.341387
SMA-PS	-1.10074	0.846275	-1.06329	0.871003	8.330392

Table.4.11 Performance analysis of the proposed DPS network after changing H as + 25%

H= +25%		HHO	SMA	HHO-PS	SMA-PS
Settling time (sec)	ΔF_1	38	38	35	35
	ΔF_2	40	39	36	35
	P - tie	38	39	36	35

Peak overshoot response	ΔF_1	60.0130	60.0135	60.0130	60.0128
	ΔF_2	60.0123	60.0125	60.0120	60.0120
	P - tie	0.0022	0.0022	0.0022	0.0022
Peak undershoot response	ΔF_1	59.9750	59.9760	59.9760	59.9760
	ΔF_2	59.9863	59.9866	59.9863	59.9863
	P - tie	-0.0048	-0.0047	-0.0048	-0.0048

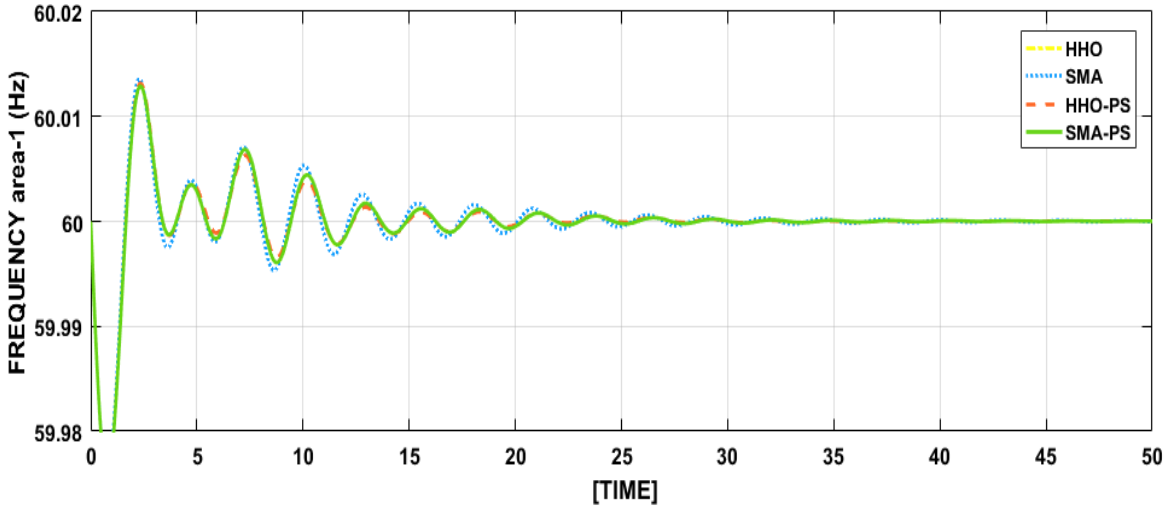

Fig.4.29 Area-1 frequency reaction of the DPS network after changing the H as + 25%

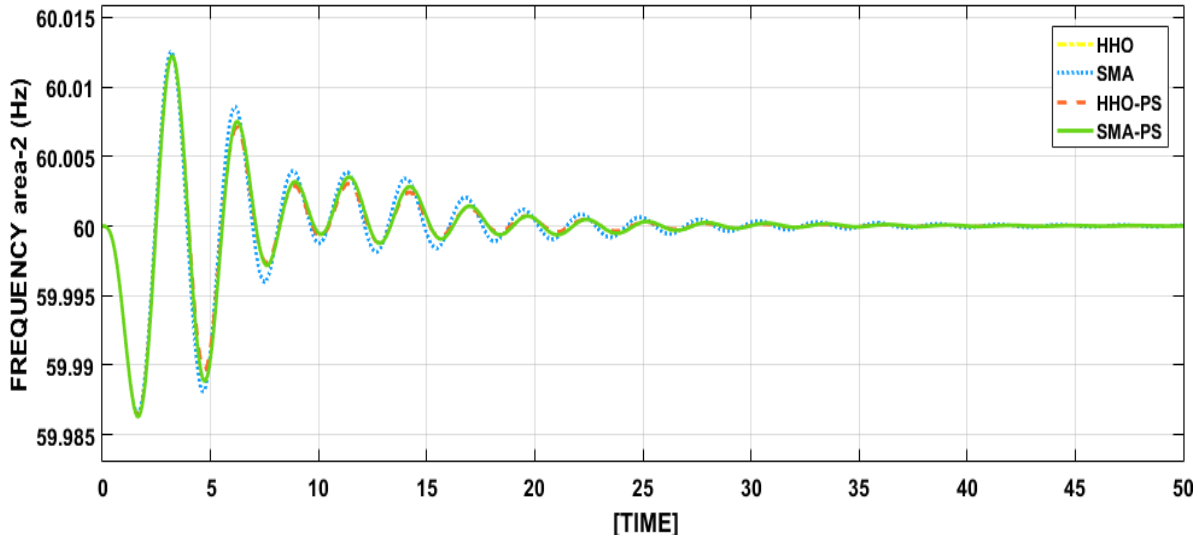

Fig.4.30 Area-1 frequency reaction of the DPS network after changing the H as + 25%

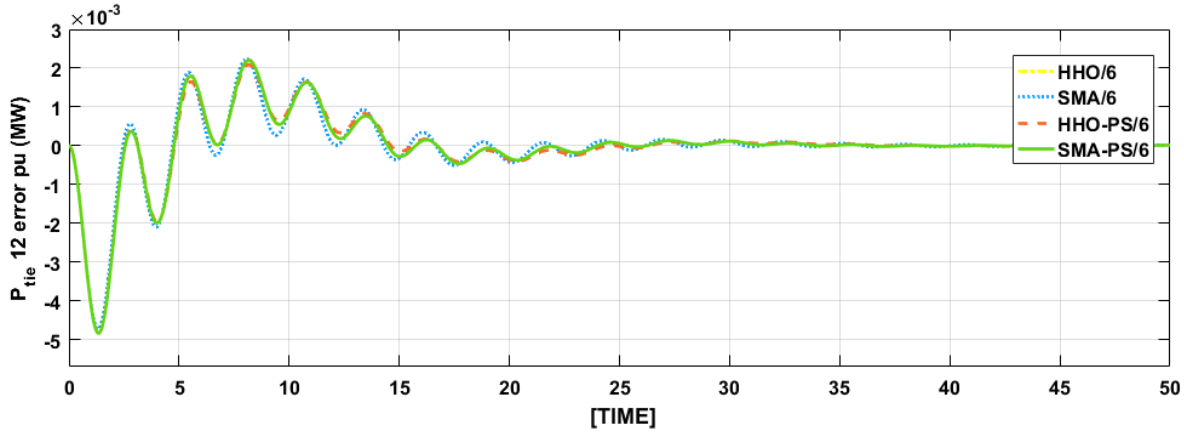

Fig.4.31 TLP response of the DPS network after changing the H as + 25%

Table.4.12 Gain parameters for the suggested DPS network after exchange H variable as – 25%

H= - 25%	k_1^P	k_1^i	k_2^P	k_2^i	J
HHO	-1.2687	2.073703	-1.92079	0.972238	21.7675
SMA	-1.71576	0.423441	-1.74871	0.908894	19.2243
HHO-PS	-1.94317	0.467887	-1.86217	0.977141	17.16425
SMA-PS	-2.08843	0.481123	-2.02558	0.986326	16.80083

Table.4.13 Performance analysis for the suggested DPS network after exchange H value as – 25%

H= -25%		HHO	SMA	HHO-PS	SMA-PS
Settling time (sec)	ΔF_1	42	30	37	38
	ΔF_2	52	48	41	40
	P - tie	57	52	45	35
Peak overshoot response	ΔF_1	60.0050	60.0051	60.0052	60.0280
	ΔF_2	60.0054	60.0054	60.0055	60.0200
	P - tie	0.0038	0.0025	0.0037	0.0036
Peak undershoot response	ΔF_1	59.9741	59.9743	59.9740	59.9760
	ΔF_2	59.9840	59.9850	59.9855	59.9800
	P - tie	-0.0060	-0.0058	-0.0058	-0.0045

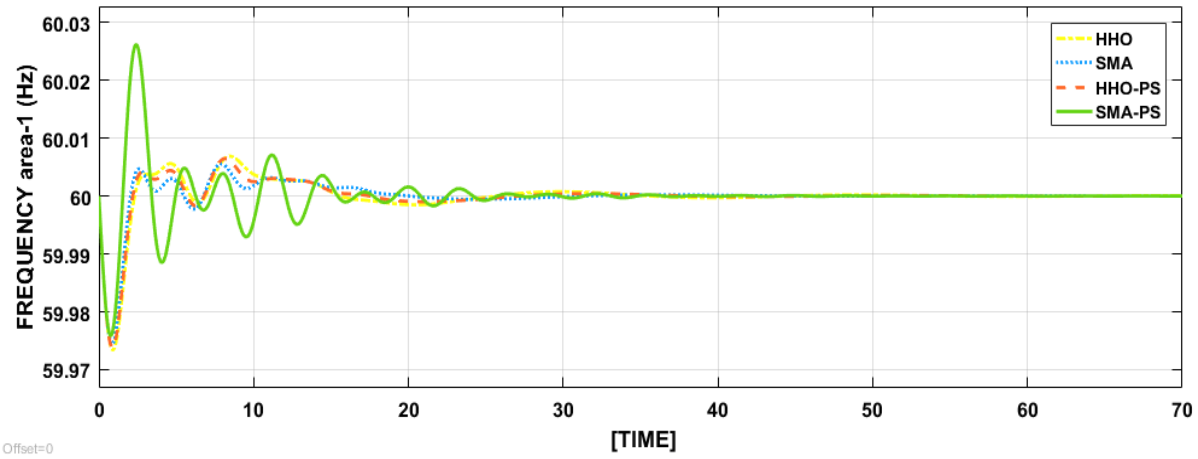

Fig.4.32 Area -1 frequency oscillation for the developed DPS network after exchange H as – 25%

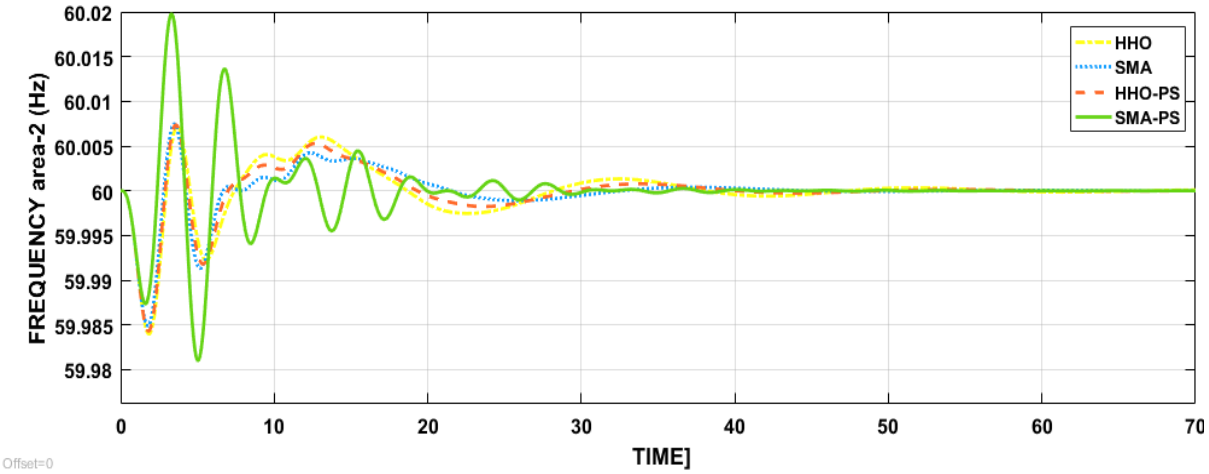

Fig.4.33 Area -2 frequency oscillation for the developed DPS network after exchange H value as – 25%

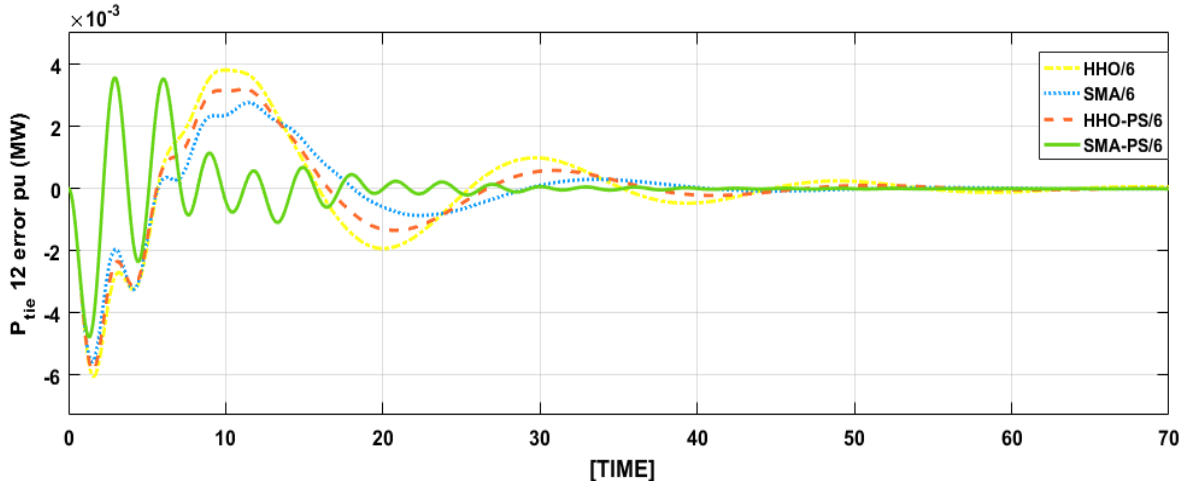

Fig.4.34 TLP response of the DPS network after changing the H as - 25%

4.8 CONCLUSION

The LFR analysis of a two-area DPS with G – H – T sources with optimally tuned PI controllers is presented in this research. In this chapter, the developed hybrid variants SMA-PS and HHO- are tested to optimise the parameters of PI controller. Under all conceivable deregulated circumstances, comparative studies of a hybrid memetic SMA-PS-tuned PI controller with HHO, SMA, and hybrid memetic HHO-PS-tuned PI controller are done. Investigations indicated that the suggested hybrid memetic SMA-PS optimised PI controller outperforms the HHO, SMA, and hybrid memetic HHO-PS optimised PI controllers in terms of system responsiveness. To validate the robust of the augmented two-area DPS with G – H – T sources, sensitivity analysis has performed with changes in T_{sg}, and H variables as $\pm 25\%$ of their nominal values, the outcomes reveal that there is notable reaction modifications in the system settling time, and also hybrid memetic SMA-PS optimised PI controller outperforms the other optimizers.

In the current study, hybrid memetic SMA-PS outperforms the renowned HHO, SMA, and hybrid memetic HHO-PS algorithms in terms of convergence performance. Every GENCO's reaction to generate power with tie-line power interchanges was verified using mathematically derived values. Every generating unit's output power response and TLP flows have been determined to match the frequency range is kept within an acceptable range (around 60 Hz) to meet the LFR requirement in the suggested system. The objective function value of LFR of deregulated two area H – T – G sources deregulated power system is 11.36849 for a hybrid memetic SMA-PS tuned PI controller.

CHAPTER - 5

IMPACT OF CES ON LOAD FREQUENCY REGULATION

5.1 INTRODUCTION

Managing the power system's safety, consistency, and stability is critical for ensuring an uninterrupted and high-quality electric power supply[39]. Power quality is measured by frequency stability in electric system network. In the electrical system, load frequency regulation (LFR) is a critical factor for originating high-quality power. The variation in system TLP and frequency from the expected values is reduced by LFR. Because of the non-minimum phase characteristics of water turbines, these oscillations can grow and potentially cause system instability, especially in hydro plants. However, some sort of energy storage or additional origination is typically sought to minimize frequency/power oscillations in the electric network.

Furthermore, an energy storage devices (ESD) for restoration of an electric network to the nominal position, has a lot of promise for supporting the LFR in DPS network by preserving power balance and maintaining grid frequency during unexpected disruptions [47]. Recently, significant progress has been achieved in the era of frequency response delivery using ESD. Flexible AC transmission systems (FACTS) premised ESD such as SMES [45][48][49], RFB [50] [51][54][52], and CES [41][46] are used to dampening unexpected load perturbations very effectively by absorbing or adding the necessary value of power into the grid, according to the literature (chapter – 2). As per literature, ESD may play a significant role in system frequency control in a considerably shorter timescale than traditional network assets, therefore satisfying the LFR criterion.

The addition of a modest capacity energy storage units, such as a CES to DPS network, as well as an effective LFR controller, can significantly improve the frequency disturbance reaction with TLP quality. LFR should be resilient to system parametric uncertainty and have strong load-demand disturbance rejection ability to maintain improved power supply quality. To achieve the necessary dynamic performance of the electric system, a sophisticated, intelligent, and durable supplemental LFR controller is required in addition to CES units.

According to previous research, the kind of controller, evolutionary optimization approaches used to improve controller settings, and ESD all have a role in the complex power system's frequency stability. The reaction of CES unit in conjunction with a TLP controller of TCPS

unit has only been investigated in the LFR of conventional systems, according to the literature review. As a result, studying their behavior in multi-area DPS is crucial. Furthermore, there has been no attempt to apply the hybrid memetic HHO-PS algorithm, and hybrid memetic SMA-PS algorithm for optimizing the gain values of the PI controller for LFR of the two area H – T – G units till now. As a result, an attempt was made to investigate LFR in two-area DPS network using a hybrid memetic HHO-PS algorithm tuned PI controller, and hybrid memetic SMA-PS algorithm tuned PI controller along with CES unit in each region and TCPS at tie line of the DPS network. Here, table 5.1 depicts the configuration parameters for the LFR of two area multi sources DPS network with CES/TCPS units. Fig 5.1 replicates the LFR of the two area H – T – G units with CES/TCPS units DPS network.

Table.5.1 LFR of DPS configuration parameters with CES/TCPS

Area number	Generating units (GENCO)	Energy storage unit (CES)	Distributing company's (DISCO)	TCPS
01	H – T – G	01	02	01
02	H – T – G	01	02	

5.2 MATHEMATICAL MODELING OF THE DEVELOPED ELECTRIC NETWORK WITH CES/TCPS UNITS

The developed LFR of the two area with three GENCOs (H – T – G) sources model was upgraded, and power frequency reaction was modified, the power exchanged CES units was added at the grid network to restore the power in each region are taken into consideration along with TLP controller of TCPS unit integrated at the tie line to control the sudden changes in the in the DPS network. An optimizing search algorithm customized PI regulating controller is utilized to govern the whole DPS network. The advantage with this regulator is that it reduces the steady-state error to zero.

Area-1 overall generating power (fig. 5.1) is

$$P_{POWER1} = PF_{themal1} + PF_{hydro1} + PF_{gas1} \pm PF_{ces1} \qquad 5.1$$

Area-2 overall originating power (refer fig 4.1) is

$$P_{POWER2} = PF_{themal2} + PF_{hydro2} + PF_{gas2} \pm PF_{ces2} \quad 5.2$$

The entire outcome of the developed DPS network calculated as

$$Total\ P_{POWER} = P_{POWER1} + P_{POWER2} \quad 5.3$$

From the developed DPS network PF power variables are $PF_{themal\_b}, PF_{hydro\_b}, PF_{gas\_b}, and\ PF_{ces\_b}$ represents the thermal, hydro, gas, and CES units. Here, b=1, and 2 replicates the area of the DPS network.

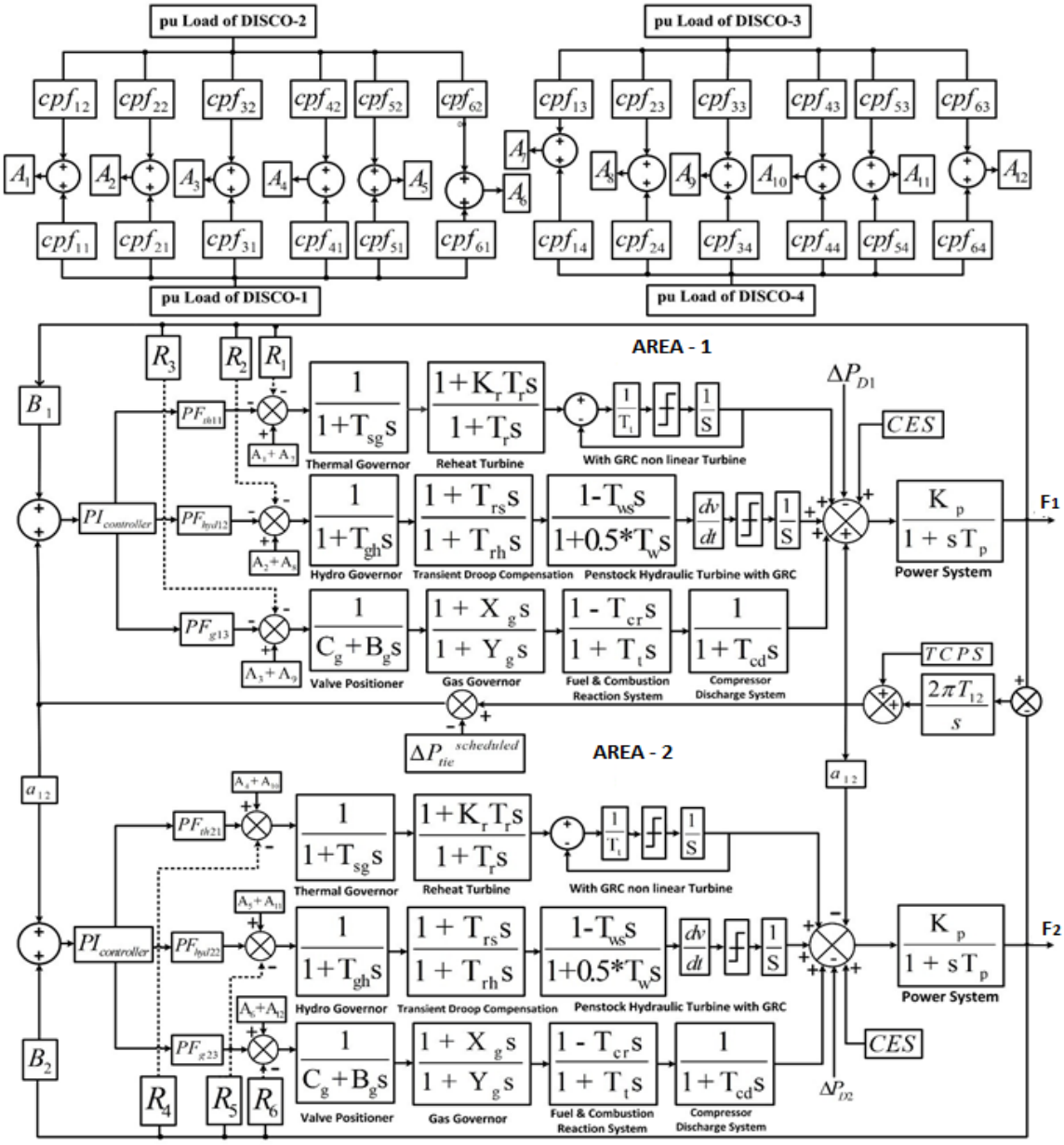

Fig.5.1 Block diagram representation of the LFR with CES/TCPS for two area multi source system.

After adding the energy restoration unit of CES device at the grid of each region of DPS network and TLP controller of TCPS device at the tie line of the DPS network, the agreement among the GENCOs – DISCOs of the DPM matrices of the cpf can interchange the energy as per contracts.

DPM of the developed network is,

$$DPM = \begin{bmatrix} cpf_{v11} & cpf_{v12} & cpf_{v13} & cpf_{v14} \\ cpf_{v21} & cpf_{v22} & cpf_{v23} & cpf_{v24} \\ cpf_{v31} & cpf_{v32} & cpf_{v33} & cpf_{v34} \\ cpf_{v41} & cpf_{v42} & cpf_{v43} & cpf_{v44} \\ cpf_{v51} & cpf_{v52} & cpf_{v53} & cpf_{v54} \\ cpf_{v61} & cpf_{v62} & cpf_{v63} & cpf_{v64} \end{bmatrix} \quad 5.4$$

cpf_{vij} depicts contract participation matrix factor

$\sum_{i=1}^{n} cpf_{vij} = 1,\ \text{here j=1,2.....k}$, 'k' replicates the sum of DISCOs and 'n' replicates the sum of GENCOs

The suggested LFR of the DPS network, after adding CES with TCPS units the energy demand is same from each region of the DPS network with the $DISCOs - GENCOs$ participation as per the LFR of the DPS network (refer to figs 4.1 and 5.1).

The power originated in the electric network as per the scheduled and unallocated power demand is calculated as

$$\Delta p_{Gi} = cpf_{i1} * \Delta p_{l1} + cpf_{i2} * \Delta p_{l2} + cpf_{i3} * \Delta p_{l3} + cpf_{i4} * \Delta p_{l4} + apf_i \Delta p_{Li}^{uc} \quad 5.5$$

Here, cpf involved in the $DISCOs - GENCOs$ contract allocated and committed energy is calculated as per the scheduled and unscheduled rapid demand of energy due to sudden oscillations in the local demand of $DISCOs - GENCOs$ units of the DPS network as follows.

$$\Delta p_{L1}^{uc} + \Delta p_{l1} + \Delta p_{l2} = \Delta p_{D1} \quad 5.6$$

$$\Delta p_{L2}^{uc} + \Delta p_{l3} + \Delta p_{l4} = \Delta p_{D2} \quad 5.7$$

From the $eqns$ 5.6 and 5.7 if the load matches the GENCOs-DISCO's participations the unscheduled load demand PF of $\Delta p_{L1}^{uc} = \Delta p_{L2}^{uc} = 0$. In other case, if demand of the

$DISCOs - GENCOs$ participations mismatch due to unexpected load disturbances or supply in the DPS network, the unexpected load demand measures with the Δp_{L1}^{uc}, and Δp_{L2}^{uc} factors.

The TLP is measures as real and allocated power demand among each region of 1 and 2. The real power of the interlinked DPS network is the frequency difference among each region of the developed network. and allocated TLP is measured using each region GENCOs power demand.

The TLP error of the DPS network is as the subtraction of the of the real TLP and allocated TLP of the DPS network is calculated with using $eqns$ (5.8 and 5.9) is as follows

$$\Delta p_{tieline,12}^{error} = \Delta p_{tieline,12}^{real} - \Delta p_{tieline,12}^{allocated} \quad 5.8$$

$$\Delta p_{tieline,12}^{error} = \frac{2\Pi T_{12}}{s}[\Delta F_1 - \Delta F_2] - \sum_{n=1}^{3}\sum_{m=3}^{4} cpf_{nm}\Delta p_{lm} - \sum_{n=4}^{6}\sum_{m=1}^{2} cpf_{nm}\Delta p_{lm} \quad 5.9$$

If in case, the real TLP flow exceeds the set-out power flow error limits in the network, the current flow setup quantity ($\Delta p_{tieline,12}^{error}$) is zero, and this state is referred to as the constant state situation.

The linear combination of the ACE is represented in $eqns$ (5.10 and 5.11) as TLP flow error in the frequency variation in each region of the DPS network.

$$ACE_1 = \Delta F_1 * B_1 + p_{tieline,12}^{error} \quad 5.10$$

$$ACE_2 = \Delta F_2 * B_2 + p_{tieline,21}^{error} \quad 5.11$$

5.2.1 CES

The CES device is ideally suited to applications requiring up to 20 MW of power [53]. The STORE project has installed ranges of 4 MW to 20 MW CES systems for La Palma power system financed by Spanish Ministry of Economy and Competitiveness' (SPAIN) [55]. References [56] and [57] investigate a modest rating conventional CES with a maximum storage capacity of 3.8 MJ for AGC application's in two-area systems. It is appropriate for use in ESS because of several key characteristics, including fastest discharge/charge rate, response time without loss of efficacy [44].

During normal operation, in capacitor plates, the CES unit store energy in terms of electrostatic, which it then releases into the grid when there is a sudden load disruption. As a result, governor and other control mechanisms begin to work to bring the system back into balance. The system stays back to its steady state configuration after stabilizing.

The mathematical and simulation model of a CES unit is shown in Figure 5.2 [40]. CES units have been included in both parts of the model to ensure improved dynamic reaction of systems and reduce oscillations.

CES has outperformed the current ESD in terms of effectiveness. Similarly main qualities, such as rapid charge and discharge rate, prevent effectiveness loss. To be acceptable for usage in an ESS, it must have a fast reaction time for large cycle numbers, a high power density, a longer useable lifecycle, and the capacity to transmit more and greater power requisitions to the grid[44].

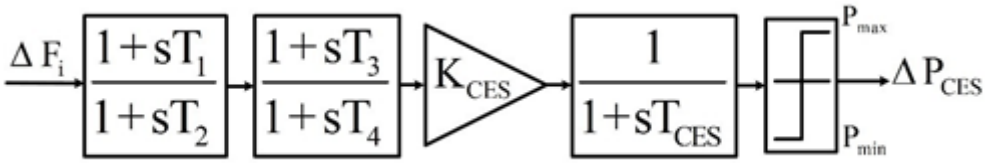

Fig.5.2 CES as a frequency stabilizer in a linearized model

Every region's frequency response output is utilized like a control input signals to the CES entity, which supplies the needed level of power in response to the frequency variation. The maximum permissible absorbed energy matches the maximum possible energy discharge at the CES's traditional limits. If the energy requirement surpasses the storage's capacity factor, it may result in discontinuous control. To test the CES' behavior under specific contract conditions, the limiter $\Delta P_{min} \leq \Delta P_{CES} \leq \Delta P_{max}$ on a system base of 2000 MVA is added to the output ΔP_{max} of the CES, as shown in Fig. 5.1. ΔP_{min} and ΔP_{max} values are -0.01 pu MW and 0.01 pu MW, respectively.

Here, ΔF_i is for the area – 1 and 2 frequency deviation. $T_4 = 0.39\ sec, T_3 = 0.0411\ sec, T_2 = 0.025\ sec$ and $T_1 = 0.280\ sec$ are the time constant variables of CES unit's two stage correction variables. Transfer function model of the CES is depict in eqn (5.12)

$\mathrm{T_{CES}} = 0.046$ sec is the time constant gain of the CES and

$\mathrm{K_{CES}} = 0.3$ is the gain constant of the CES.

$$\Delta p_{ces} = [\frac{K_{ces}}{1+sT_{ces}}][\frac{1+sT_{C1}}{1+sT_{C2}}][\frac{1+sT_{C30}}{1+sT_{C4}}]\Delta F_i(S) \quad 5.12$$

5.2.2 TCPS

TCPS is one of the most widely used FACT's regulator units in system in series with applicability by degree of compensate in realistic innovative energy systems. TCPS helps the electric grid preserve its stability and efficiency by allowing for flexible power scheduling in a variety of (changing) operational scenarios. It may be utilized to boost the power-transfer capabilities of a transmission line by dampening energy fluctuations caused by cross-area and regional vibrations. During difficult situations, the TCPS maintains the true power flow across transmission lines (tie lines), reduces greater frequency, and manages the output of the electricity system by altering the phase angle comparison. Figure 5.3 shows the schematic system's TCPS paradigm.

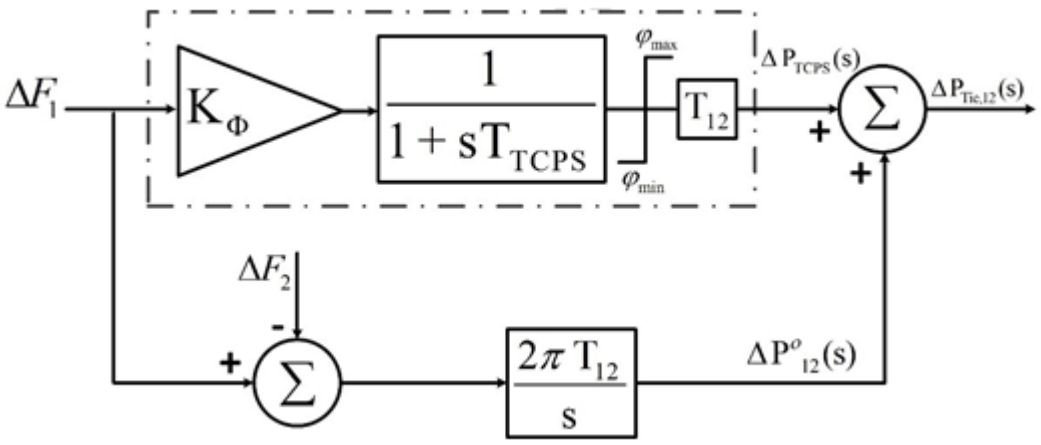

Fig.5.3 TCPS unit linearized model.

The exponentially load voltage between area-2 and 1 of the tie-line interconnection, as suggested by eqn (5.12a) is

$$\Delta p^{o}_{tieline}(s) = \frac{2\pi T^{o}_{12}}{s}(\Delta F_1(s) - \Delta F_2(s)) \quad 5.12a$$

After including a TCPS unit into the model, the real power flow interchange among area-1 and 2 is

$$\Delta p^{real}_{tieline,12} = \frac{|V_1||V_2|}{X_{12}} \sin(\delta_1 + \delta_2 - \phi) \quad 5.13$$

Here, $\delta_1^0, \delta_2^0 \; and \; \phi^0$ values from $\delta_1, \delta_2 \; and \; \phi$ original values respectively. As indicated in eqn (5.14), the voltage regulation oscillating among tie lines follows a restricted signal approximation technique.

$$\Delta p_{tieline,12}^{real} = T_{12}(\Delta\delta_1 + \Delta\delta_2) + T_{12}\Delta\phi) \quad 5.14$$

Here, $$T_{12} = \frac{|V_1||V_2|}{X_{12}}\cos(\delta_1^0 + \delta_2^0 - \phi) \quad 5.15$$

Furthermore, the angular variation may be written as,

$$\Delta\delta_1 = 2\pi\Delta F_1 dt \; and \; \Delta\delta_2 = 2\pi\Delta F_2 dt \quad 5.16$$

Using the Laplace transform of eqn (5.17) is

$$\Delta p_{tieline,12}^{real}(s) = \frac{2\pi T_{12}^o}{S}\left(\Delta F_1(s) - \Delta F_2(s)\right) + T_{12}\Delta\phi(s) \quad 4.\ 17$$

The angle of the phase shifter ($\Delta\phi$) affects the interchange of power flow in the tie-line, as shown in eqn. (5.18). The math formula that expresses the phase shifter's angle(s) is as follows:

$$\phi(s) = \Delta F_1(s)\frac{k_\phi}{1+sT_{TCPS}}\Delta Error \quad 5.18$$

Here.

frequency fluctuation in area 1 is $\Delta F_1(s)$, which one is taken as error signal depicted in (4.18). further eqn (5.19) is as

$$\Delta p_{tieline,12}^{real}(s) = \frac{2\pi T_{12}^o}{S}\left(\Delta F_1(s) - \Delta F_2(s)\right) + \Delta F_1(s)\frac{k_\phi}{1+sT_{TCPS}}T_{12} \quad 5.19$$

Here, $T_{TCPS} = 0.01\; sec,$ has been the TCPS unit time constant variable.

k_ϕ = 0.3 rad/Hz, is the TCPS unit stabilization gain

And the limitations of the ΔF_1

5.2.3 PI CONTROLLER DESIGN

As per literature done earlier (reference chapter 2), at present in the global market PI controller is the utmost commonly used form of regulator. It is simple in construction, modeling and controls the speed, temperature, pressure, flow, and a variety of other industrial flow characteristics at very ease. It is widely employed in a range of scientific and chemical processes, including in automating, as a way of temperature regulation.

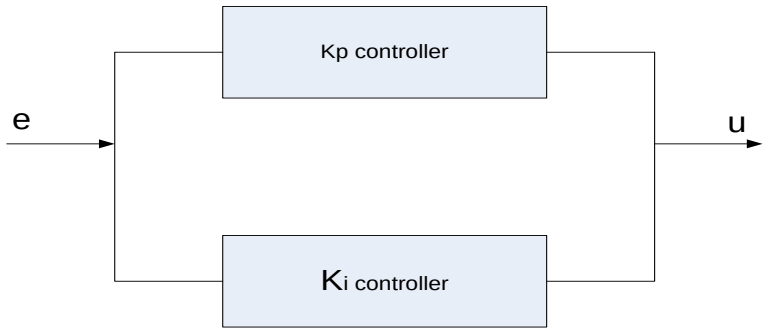

Fig.5.4 PI controller design for the suggested system

5.3 SOLUTION APPROACH

This chapter includes the integrated hybrid memetic HHO-PS and hybrid memetic SMA-PS optimization search algorithms are furtherly extended to resolve and simplify the Load frequency regulation challenge. The oscillation of frequency of variation and energy origination with restoration units have consideration to account to formulate and compute the objective function of the LFR of the DPS network with CES and TCPS units. This extended version of the objective function is appended to one scalar function using weighting coefficients. To optimize and takeover the physical and operational limits of the LFR of the DPS network with CES and TCPS units challenge, heuristics procedure is adopted.

To originate and regulate the network frequency variation for the simulated weight combinations, the procedure outlined as stepwise below.

1. initiate and generate the Δp_{Gci} of the generation combinations as mentioned in above sections

2. set-up the weight counter, i=0

3. and increment weight of the counter, *i=i+1.*

4. furtherly, select the *ith* weight combination.

5. Compute and evaluate the objective function J using eqn. (4.20) by applying suggested hybrid memetic HHO-PS and hybrid memetic SMA-PS methodologies.

6. If (iteration<max_iteration), then GOTO step 3.

7. evaluate and select the maximum and minimum values of the objectives from all the originated combination sets. Compute the best possible solution of LFR of the DPS network with FACTS units.

8. set-up the optimal solution from the above origination and restoration units.

9. Stop.

5.4 INTEGRATED HYBRID MEMETIC HARRIS HAWKS OPTIMIZER AND PATTERN SEARCH ALGORITHM

To efficiently applying the integrated hybrid memetic HHO-PS algorithm, 50 trail test runs are made for each challenge issue starting with various initial and set-up populations. Size of population 40 has been taken in overall performance of LFR of the DPS network with CES unit. The suggested methodology is performed on MATLAB 2018a software on intel Intel(R) Core (TM) i7-8550U CPU @ 1.80GHz system. The optimal procedure for the suggested hybrid memetic HHO-PS algorithm for solving LFR of the DPS network with CES unit is as follows.

Step-1: Initialize and set-up the random location of the GENCOs in the population.

Step-2: Compute the priority list of GENCO-DISCO participation factors according to the scheduled and unscheduled power allocations.

Step-3: Modify the each GENCOs status of location in the overall population to meet the GENCO-DISCO contributions.

Step-4: Adjust and evaluate the each GENCOs to match the population to reduce the frequency regulation as per ACE in eqns (5.10 and 5.11).

Step-5: After evaluating the location of the search agents, upgrade the location of the objective (J) using eqn (5.20).

Step-6: Adjust the location of the search agents using HHO-PS optimizer for population of each as per section 3.4.

Step-7: Evaluate the outcome of best fitness of HHO operators and carry them with the black box derive method of PS operators.

Step-8: Modify the random region of the search prey using the objective to estimate the best available fitness.

Step-9: Verify the generation condition if iteration = max_iteration, then go to step 10. Otherwise, increase iteration number and go back to step 1.

Step-10: Stop optimal compute variable solution

5.5 INTEGRATED HYBRID MEMETIC SLIME MOULD AND PATTERN SEARCH ALGORITHM

To verify the efficient performance of the hybrid memetic SMA-PS optimizer, the size of population considered as 40 for all runs and 50 test trail runs are made to each challenge set. The efficacy of the developed optimizer tested on Intel(R) Core (TM) i7-8550U CPU @ 1.80GHz system. The heuristics procedure of the hybrid memetic SMA-PS optimizer for the developed LFR challenge as follows.

Step-1: Initialize and set-up the random location of GENCO-DISCO participations in the population.

Step-2: Calculate the priority list of participation factors according to match the load demands.

Step-3: Modify the load disturbance of each agent to search the location in the overall population to satisfy the participation factors.

Step-4: Verify each search agent location in the population to minimize the frequency regulation.

Step-5: Analyse and evaluate the objective function within constraints.

Step-6: Originate and verify the condition of the parameter setting of the LFR, if the frequency match the system parameter limits, modify the location of search agent.

Steo-7: Verify the fitness of the GNECO-DISCO participations, by using the objective function to compute the best outcome.

Step-8: Upgrade the best optimal location of the search agent by using the black box derivative methodology operators

Step-9: Evaluate and verify the best, worst optimal outcomes for the objective function value.

Step-10: Verify the search agent location by within limits of participation factors. If the participation factors satisfy the limited constraint condition, stop the programme.

Step-11: If the generation <max_generaion size, then go to and repeat the process form step-2.

Step-12: Otherwise increase the step size of the population generation.

5.6 THE OBJECTIVE FUNCTION FOR DESIGNING AN OPTIMAL LFR CONTROLLER

The controller and objective function used in the current investigation are briefly described in this section.

The objective function is ITAE criteria.

To optimize the objective function, eqn (5.20) has been used[28].

$$J= \int_0^{t_{sim}} |\Delta F_1| + |\Delta F_2| + |\Delta P_{tie}| * t * dt \qquad 5.20$$

The discrete values of the incremental frequency change in area-1 and area-2 are represented by ΔF_1 and ΔF_2.

ΔP_{tie} is the value of the tie line exchange.

't' stands for the overall simulation time in seconds.

The ITAE index is minimized using the SMA-PS and HHO, SMA, and HHO-PS optimizers to obtain of the PI controller gains in both areas, according to the following constraints:

To minimize J,

k_i^P min $\leq$ $k_i^P \leq k_i^P max$ and k_i^{int} min $\leq$ $k_i^{int} \leq k_i^{int} max$

Here, k_i^P is the proportional gain of the optimized PI controller.

k_i^{int} is the integral gain of the optimized PI controller in 'i' th area (i = 1, 2).

In the range limit, both area gains are optimized (-5, 5).

The proposed SMA-PS optimization algorithm's flowchart, shown in Figure 2, can give information on the proposed technique's execution processes. The PI controller's optimal gain is determined by running a series of tests for 50 iterations and 50 runs for all HHO, SMA, HHO-PS and SMA-PS algorithms.

All HHO, SMA, HHO-PS and SMA-PS algorithms achieves the best optimal solutions as per their search strategy and capability. And Table 4.2 shows the PI controller's performance and optimized gain values for the proposed system using the HHO, SMA, HHO-PS, and SMA-PS algorithms.

Table.5.2 LFR with CES/TCPS by using HHO, SMA, HHO-PS and SMA-PS algorithms tuned PI controller gains and their respective objective value.

Algorithm	k_1^P	k_1^i	k_2^P	k_2^i	Objective function value
HHO	1.9831	3.7465	0.2594	3.5670	2.0622
SMA	1.8532	4.6073	0.6179	3.5739	2.0312
HHO-PS	2.0316	4.3994	0.4596	3.5219	2.0069
SMA-PS	1.8903	4.3999	0.6082	3.5341	2.0048

5.7 RESULTS AND DISCUSSIONS

This subsection focuses on the behavior of a two-area DPS with optimally tuned PI controllers in a competitive market situation. The proposed power system, which includes CES along with a TCPS unit, was created in the MATLAB (R2018a). In a deregulated context, many

evaluations have been conducted regarding possible realistic electricity contracts. In the appendix, you can find the power system parameters utilized in the simulation (A). The simulation was run with different contracts between DISCOs and GENCOs premised on DPM and a 1% step change load deviation in each location. The resonant frequency within each region is provided in respect to the regular (60 Hz) frequency, as per information in the supplement. Every generating unit's simulation response is also compared to the actual computed values in the study.

5.8 CASE STUDIES

The following are the several case studies that were done under different scenarios of a deregulated electricity market:

5.8.1 POOLCO or Unilateral Transaction Method

Here, each GENCOs can contribute to LFR based on their apfs, and each DISCOs have a contract with the same GENCOs in their same region. i.e., apfs for thermal, hydro, and gas units are $PF_{\text{thermal1}} = 0.6$, $PF_{\text{hydro1}} = 0.3$, and PF_{gas1}=0.1, so that $PF_{\text{thermal1}} + PF_{\text{hydro1}} + PF_{\text{gas1}}$= 0.6+0.3+0.1 = 1 in area-1. And similarly, area-2 is $PF_{\text{thermal2}} + PF_{\text{hydro2}} + PF_{\text{gas2}} = 1$.

Here, only area - 1 has a load fluctuation, and the load demand of the DISCOs in area - 1 has been estimated to be 0.01 pu MW each.

$$\Delta p_{l2} = \Delta p_{l1} = 0.005\ pu\ MW$$

such that in area - 1 a total load change of 0.010 pu MW occurs. Such that, area – 2 load demand is zero ($\Delta p_{l4} = \Delta p_{l3} = 0$)

here, as per eqn (5.10) and (5.11)

$$\Delta p_{D1} = \Delta p_{l2} + \Delta p_{l1} = 0.005 + 0.005 = 0.01\ pu\ MW$$

$$\Delta p_{D2} = \Delta p_{l4} + \Delta p_{l3} = 0 \text{ pu MW}$$

in this method, distribution systems between each GENCOs and DISCOs in the under-studied system based on the following DPM

$$DPM = \begin{bmatrix} 0.33330 & 0.33330 & 0 & 0 \\ 0.33330 & 0.33330 & 0 & 0 \\ 0.33330 & 0.33330 & 0 & 0 \\ 0 & 0 & 0 & 0 \\ 0 & 0 & 0 & 0 \\ 0 & 0 & 0 & 0 \end{bmatrix}$$

As per eqn (5.12). The power reaction of each GENCOs in the system can be calculated as

For GENCO-1 (Thermal) in area-1:

$$\Delta p_{Gc1} = 0.3333 * 0.005 + 0.3333 * 0.005 + 0 + 0 = \ 0.003333\ pu\ MW$$

Likewise, the power responses of GENCOs 2 & 3 in area-1 are 0.00333 pu MW each, respectively. For area -2, $\Delta p_{Gc4} = \ \Delta p_{Gc5} = \ \Delta p_{Gc6} = 0$, Because, according to the established contract, DISCOs 3 and 4 in area-2 have no power need.

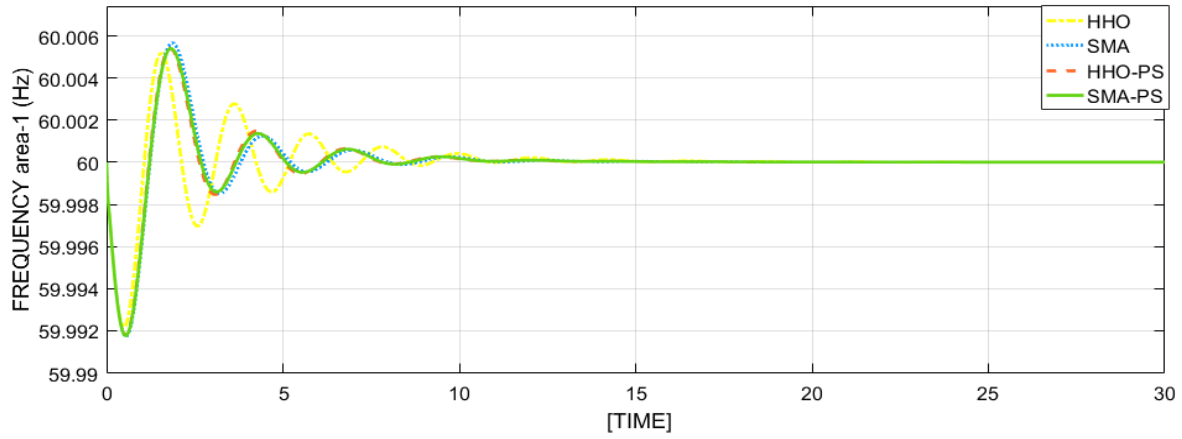

Fig.5.5 Area – 1 frequency reactions for the LFR of DPS with CES/TCPS devices

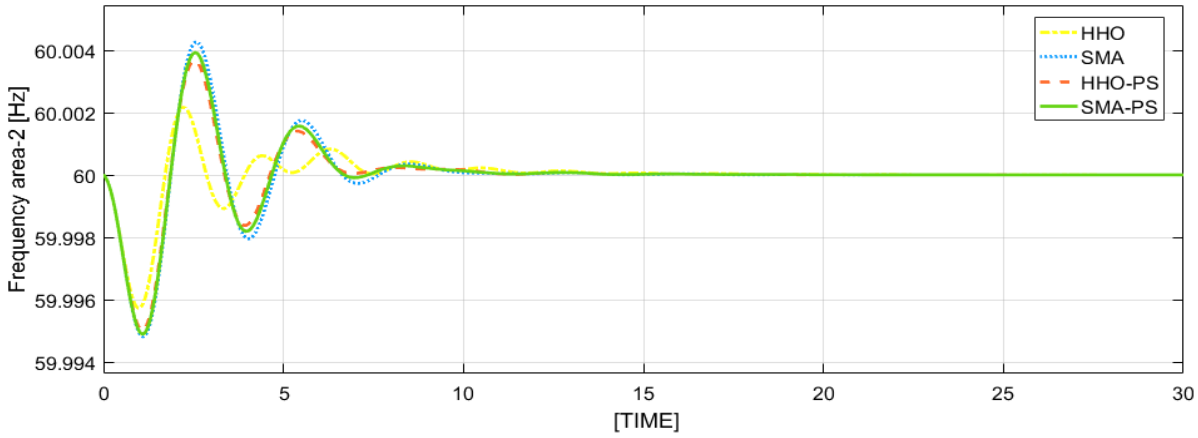

Fig.5.6 Area – 2 frequency reactions for the LFR of DPS with CES/TCPS devices

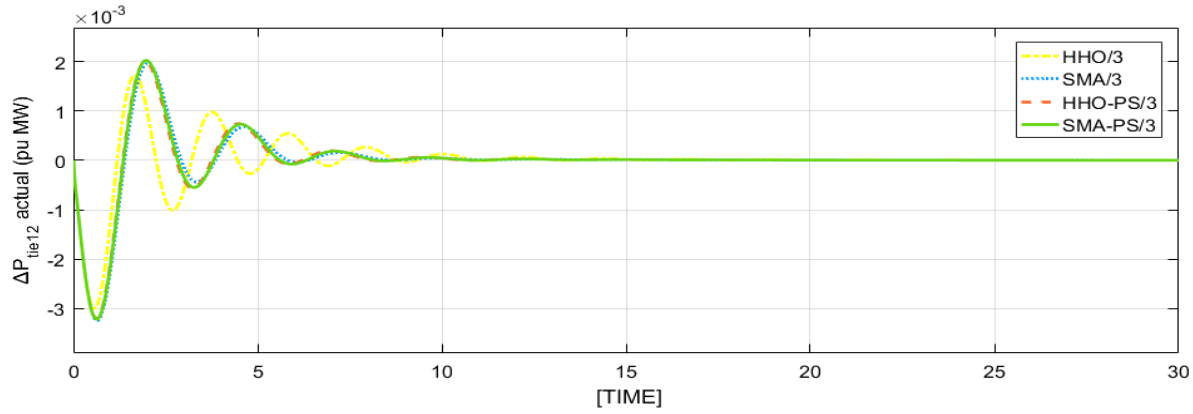

Fig.5.7 Actual TLP of the DPS network with CES units under POOLCO transaction

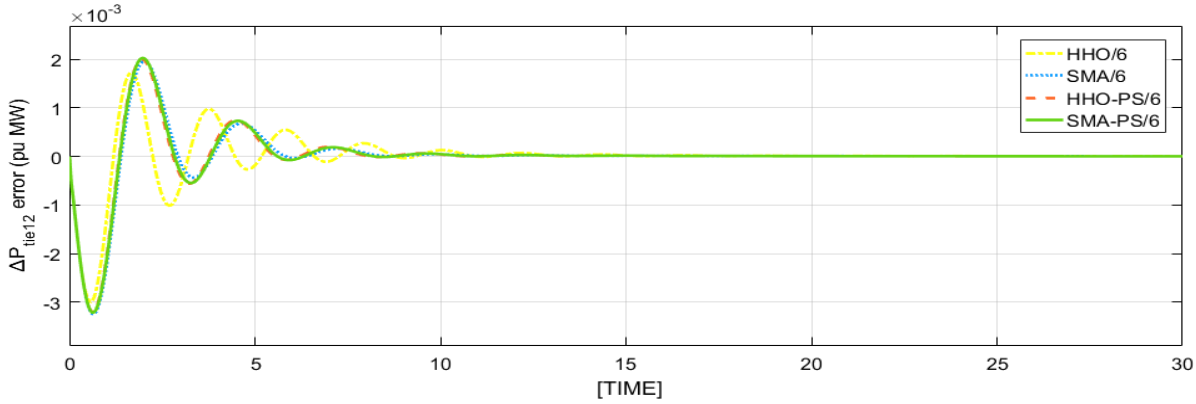

Fig.5.8 TLP error response of the DPS network with CES units under POOLCO transaction.

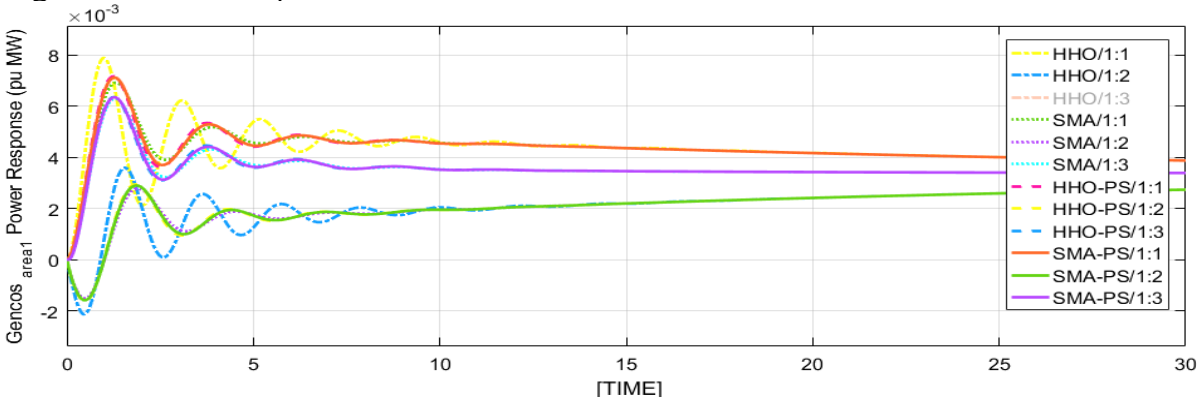

Fig.5.9 Area - 1 GENCOs power generation response of the DPS network with CES units

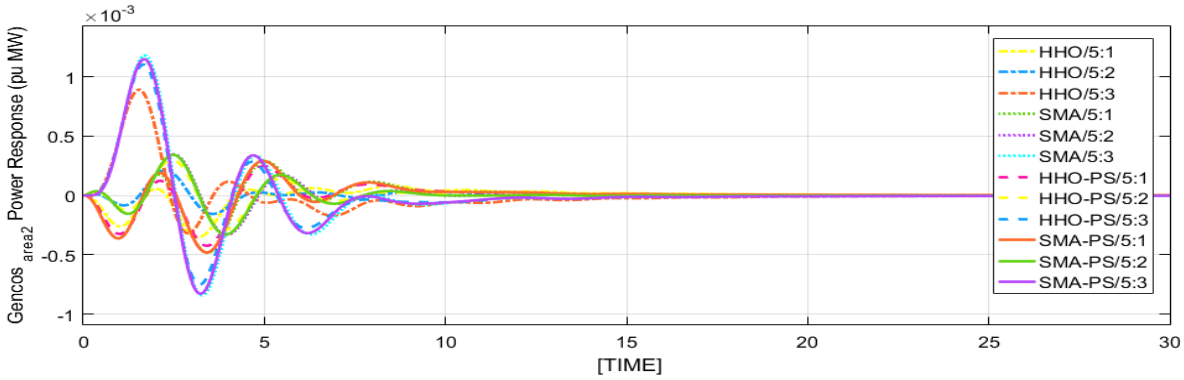

Fig.5.10 Area - 2 GENCOs power generation response of the DPS network with CES units

Figures 5.5 – 5.10 demonstrate performance analysis for the POOLCO premised contract in the form of frequency deviation, tie line reaction, and power generation response after a sudden load shift in the system.

Here, figs 5.5 & 5.6 demonstrate the fluctuation of frequencies in both regions with unilateral contraction in response to load change for the different optimization premised PI controller. As per the comparative analysis for HHO, SMA, HHO-PS and SMA-PS optimizers, it is stated that the SMA-PS approach produces higher dynamic performance.

Fig 5.7 & 5.8 depicts the fluctuation in TLP in the region 1 power system for a 0.01 pu MW load shift. The results demonstrate that the hybrid SMA-PS approach easily dampens real tie line power flow variation after a load shift.

The DISCOs of area 1 require power from their own area GENCOS, therefore the GENCOS must meet their contractual obligations. The generation responses of area 1 & 2 GENCOs are shown in Figures 5.9 & 5.10, respectively. The waveforms obtained demonstrate that area1GENCOS, i.e., GENCO1, GENCO2, and GENCO3, generate electricity based on demand and contract participation factor. The hybrid SMA-PS optimization approach improves deviation, and generators reach their steady-state stage rapidly. Figure 4.10 indicates that the DISCOs have no demand in region 2. As a result, in steady state, the change in produced power by all GENCO's corresponding to this region is zero.

The SMA-PS optimizer outperforms the other optimizers in terms of dynamic responsiveness, according to the generation response outputs of different GENCOS. It can be observed from the above data that the SMA-PS optimizer approach achieves higher dynamics performances in terms of peak rising time, peak overshoot, and settling time value of ΔF1, ΔF2, and ΔPtieine power.

5.8.2 BILATERAL Transaction Method

This section, depicts a situation in which a DISCO and a GENCO conduct transactions in any other field, referred to as a bilateral transaction. In this situation, GENCOs and DISCOs fully adhere to the contract conditions [46]. In DPS, every GENCO and DISCO in the system forms their contract as per DPM

$$DPM = \begin{bmatrix} 0.2 & 0.1 & 0.3 & 0 \\ 0.2 & 0.2 & 0.1 & 0.1666 \\ 0.1 & 0.3 & 0.1 & 0.1666 \\ 0.2 & 0.1 & 0.1 & 0.3336 \\ 0.2 & 0.2 & 0.2 & 0.1666 \\ 0.1 & 0.1 & 0,2 & 0.1666 \end{bmatrix}$$

Each DISCO control area, as indicates by the cpfs in the form of DPM matrix, requires 0.0050 pu MW energy from the GENCOs, as per bilateral mrthod. As a result, area-1 and area-2 experiences variance of 0.010 pu MW. As a result, the power consumption in each location is 0.01 pu MW, according to eqns. (5.10) and (5.11). The generation of various GENCOs in area-1 following a quick load demand may be estimated using eqn (5.12) as follows:

For GENCO-1 (Thermal):

$$\Delta p_{Gc1} = 0.2 * 0.005 + 0.1 * 0.005 + 0.3 * 0.005 + 0 * 0.005 = \ 0.0030 \ pu \ MW$$

For GENCO-2 (Hydro):

$$\Delta p_{Gc2} = 0.2 * 0.005 + 0.2 * 0.005 + 0.1 * 0.005 + 0.1666 * 0.005 = \ 0.00333 \ pu \ MW$$

For GENCO-3 (Gas):

$$\Delta p_{Gc3} = 0.1 * 0.005 + 0.3 * 0.005 + 0.1 * 0.005 + 0.1666 * 0.005 = \ 0.00333 \ pu \ MW$$

In addition, for area-2 are,

$$\Delta p_{Gc4} = 0.2 * 0.005 + 0.1 * 0.005 + 0.1 * 0.005 + 0.3336 * 0.005 = \ 0.003668 \ pu \ MW$$

$$\Delta p_{Gc5} = 0.2 * 0.005 + 0.2 * 0.005 + 0.2 * 0.005 + 0.2 * 0.005 = \ 0.003833 \ pu \ MW$$

$\Delta p_{Gc6} = 0.1 * 0.005 + 0.1 * 0.005 + 0.2 * 0.005 + 0.1666 * 0.005 = \ 0.00283 \ pu \ MW$, respectively.

The system performance has been evaluated in a bilateral contract with instantaneous changes in load demand between several GENCOs and DISCOs. On the above-mentioned DPM, the agreement between different DISCO and available GENCOs is simulated.

Figure 5.11 & 5.12 depicts the frequency deviations in both areas in a DPS with a sudden load change. Because of the SMA-PS methodology, the system frequency deviations were performed with reduced peak overshoot, shorter settling time, and peak rise time, the findings

show improved dynamics performance. In both regions, frequency deviations are immediately dampened.

Figure 5.13 & 5.14 depicts the actual and error of the tie line power in the developed power system. Figure 5.15 & 5.16 illustrates each area generation (GENCO -1 to GENCO – 6) performance of the system. From the obtained outcomes the proposed methodology SMA-PS optimizer performs superior performance than the HHO, SMA and HHO-PS optimizers.

Figures 5.11 – 5.16 depicts the simulated reaction of the proposed system under a bilateral contract in terms of each area frequency oscillation, tie line power exchanges, and generation response at rapid load shift.

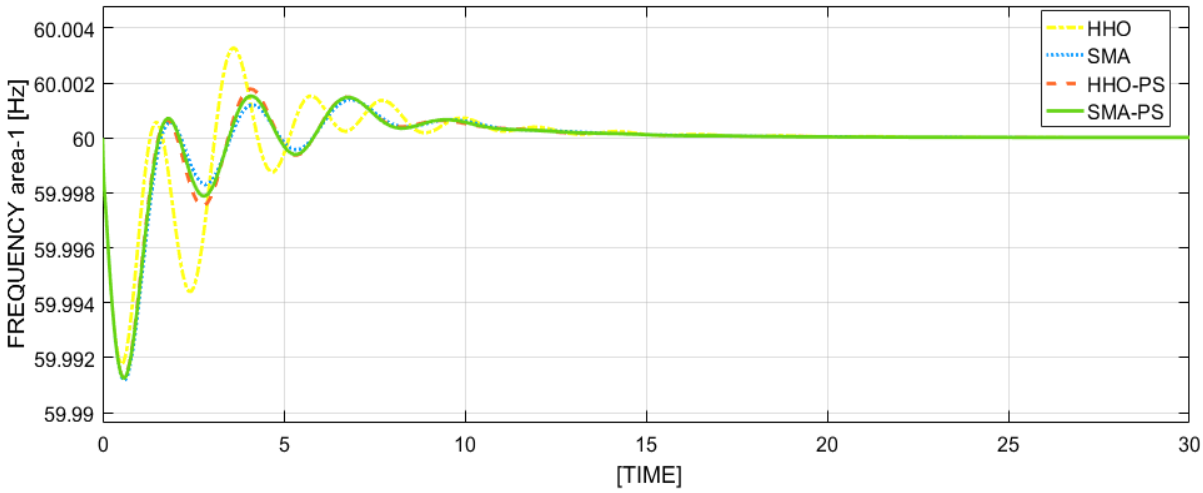

Fig.5.11 Area – 1 frequency response (bilateral method) for LFR of DPS with CES devices

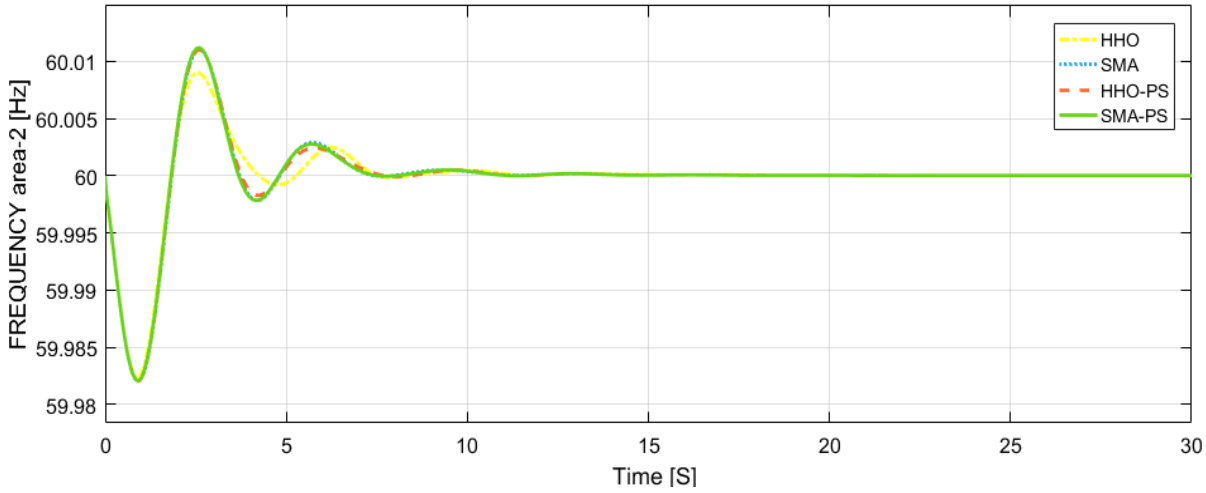

Fig.5.12 Area – 2 frequency response (bilateral method) for LFR of DPS with CES devices

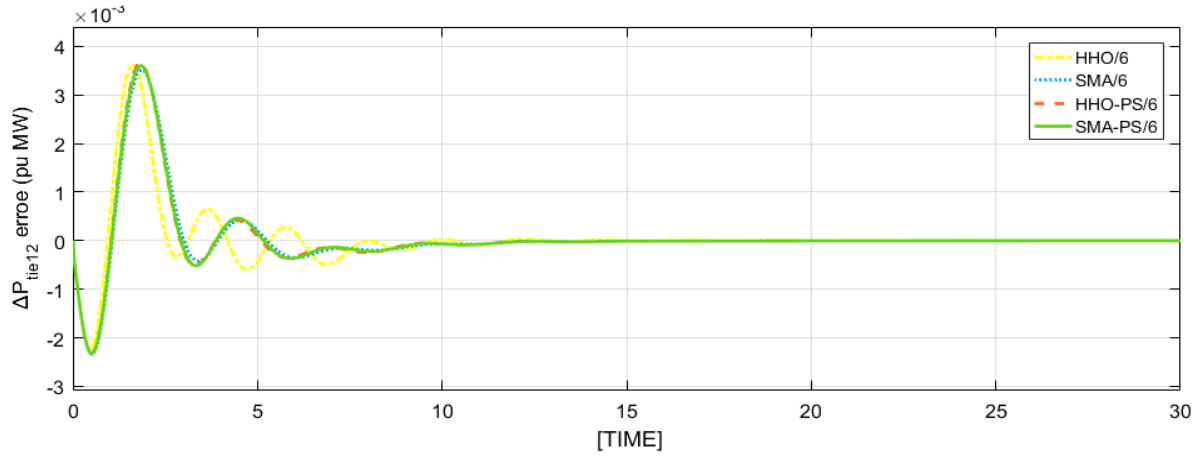

Fig.5.13 Actual TLP reaction for the LFR of the DPS network with CES unit (bilateral case)

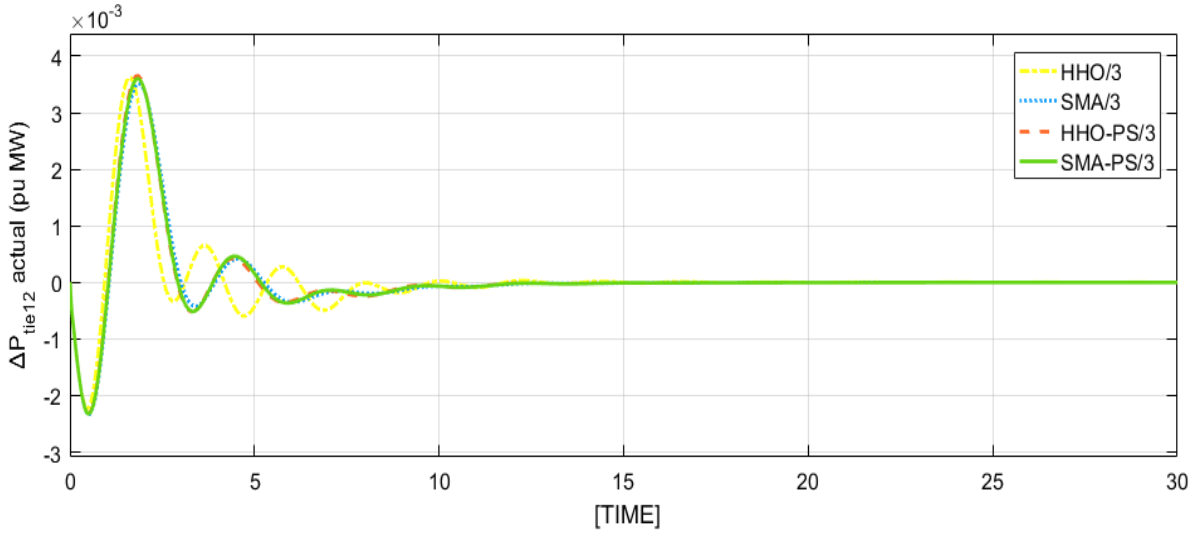

Fig.5.14 TLP error reaction for the LFR of the DPS with CES unit (bilateral method)

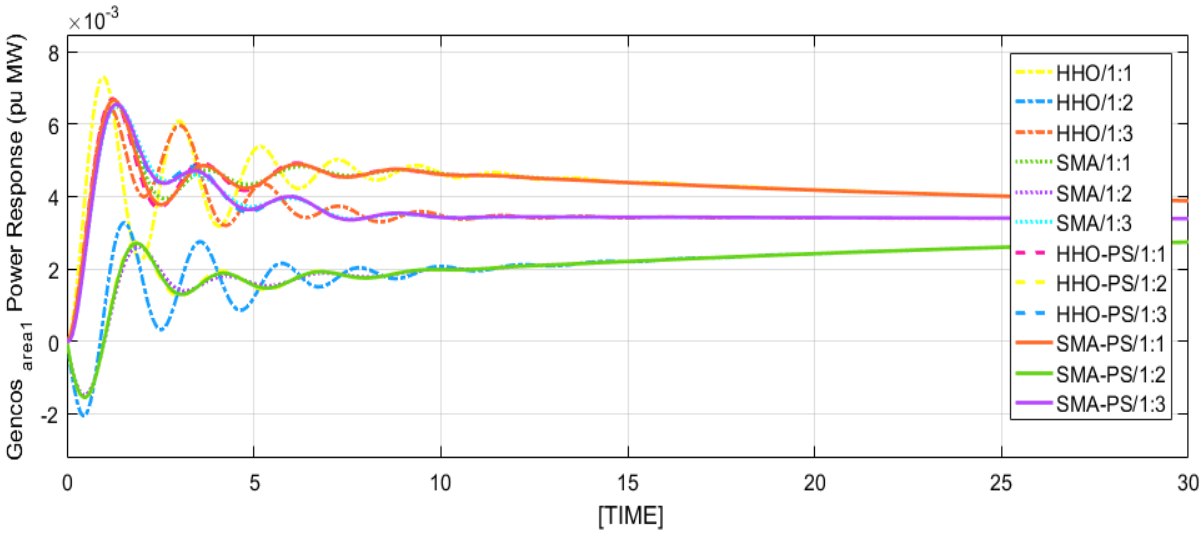

Fig.5.15 Area - 1 GENCOs response for the proposed system (bilateral transaction method)

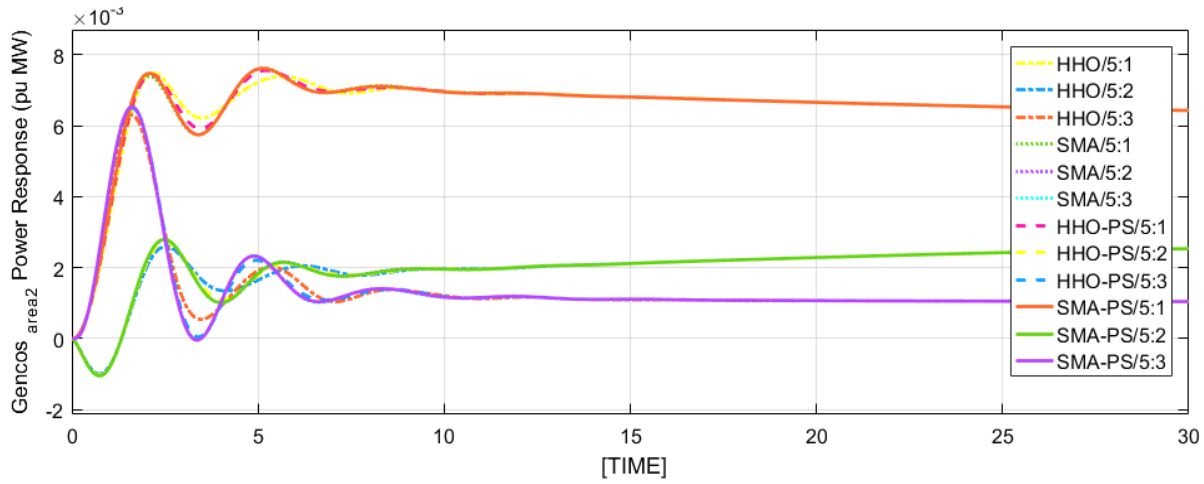

Fig.5.16 Area - 2 GENCOs response for the proposed system (bilateral transaction method)

5.8.3 CONTRACT Violation

Here, a contract breach happens when a DISCO oscillates from the predetermined arrangement by requesting more power from the GENCO's than was specified in the contract. The GENCO's operating in the same region as the DISCO should ideally meet this uncontracted power load demand.

Consider case-B, in which DISCO requests 0.0030 pu MW of more energy, which the GENCOs of area-1 can assume as an excess load of 0.0030 pu MW after 25 seconds during simulation. Due to the DISCOs' request for more energy, the overall load demand at area-1 has increased to 0.0130 pu MW. Because the increased power demand happens solely in area-1, the power demand in area-2 remains unchanged. As a result of eqns. (5.14) and (5.15), the power demands in both regions are as follows.

$$\Delta p_{D1} = 0.005 + 0.005 + 0.003 = 0.013 \ pu\ MW$$

$$\Delta p_{D2} = 0.005 + 0.005 = 0.01 \text{ pu MW}$$

By using eqn (5.13), After a sudden unagreed load demand, the generation of several GENCOs in area-1 may be computed as

For GENCO-1 (Thermal):

$$\Delta p_{Gc1} = 0.2 * 0.005 + 0.1 * 0.005 + 0.3 * 0.005 + 0 * 0.005 + 0.6 * 0.003$$
$$= 0.0048\ pu\ MW$$

For GENCO-2 (Hydro):

$$\Delta p_{Gc2} = 0.2 * 0.005 + 0.2 * 0.005 + 0.1 * 0.005 + 0.1666 * 0.005 + 0.3 * 0.003$$
$$= 0.004233\ pu\ MW$$

For GENCO-3 (Gas):

$$\Delta p_{Gc3} = 0.1 * 0.005 + 0.3 * 0.005 + 0.1 * 0.005 + 0.1666 * 0.005 + 0.1 * 0.003$$
$$= 0.003633\ pu\ MW$$

In addition, for area-2 are,

$$\Delta p_{Gc4} = 0.2 * 0.005 + 0.1 * 0.005 + 0.1 * 0.005 + 0.3336 * 0.005 + 0.6 * 0.003$$
$$= 0.003668\ pu\ MW$$

$$\Delta p_{Gc5} = 0.2 * 0.005 + 0.2 * 0.005 + 0.2 * 0.005 + 0.2 * 0.005 + 0.3 * 0.003$$
$$= 0.003833\ pu\ MW$$

$\Delta p_{Gc6} = 0.1 * 0.005 + 0.1 * 0.005 + 0.2 * 0.005 + 0.1666 * 0.005 + 0.1 * 0.003 =$ $0.00283\ pu\ MW$ respectively.

In the presence of HHO, SMA, HHO-PS, and SMA-PS optimally tuned PI controllers, the various dynamic reaction in terms of TLP, each region frequencies, and power generation are illustrated in Figs. 5.17 – 5.22.

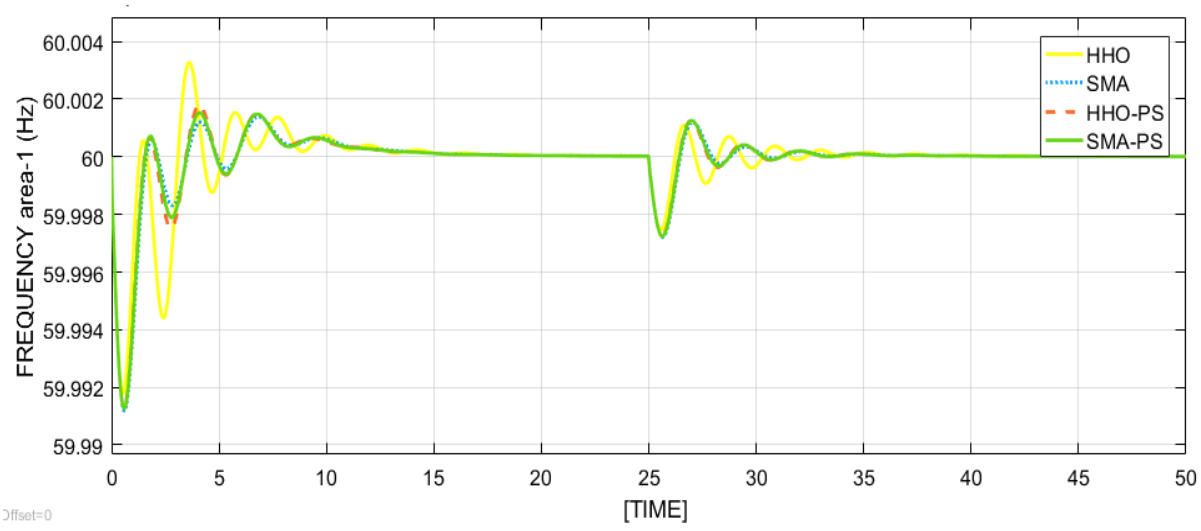

Fig.5.17 Area – 1 frequency oscillation reaction under CV case for the proposed network with CES

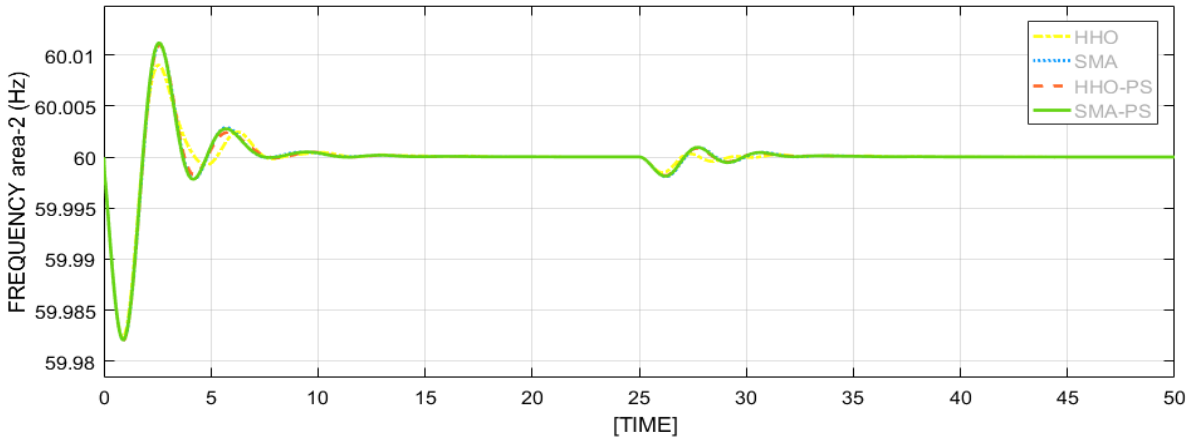

Fig.5.18 Area – 2 frequency oscillation reaction under CV case for the proposed network with CES

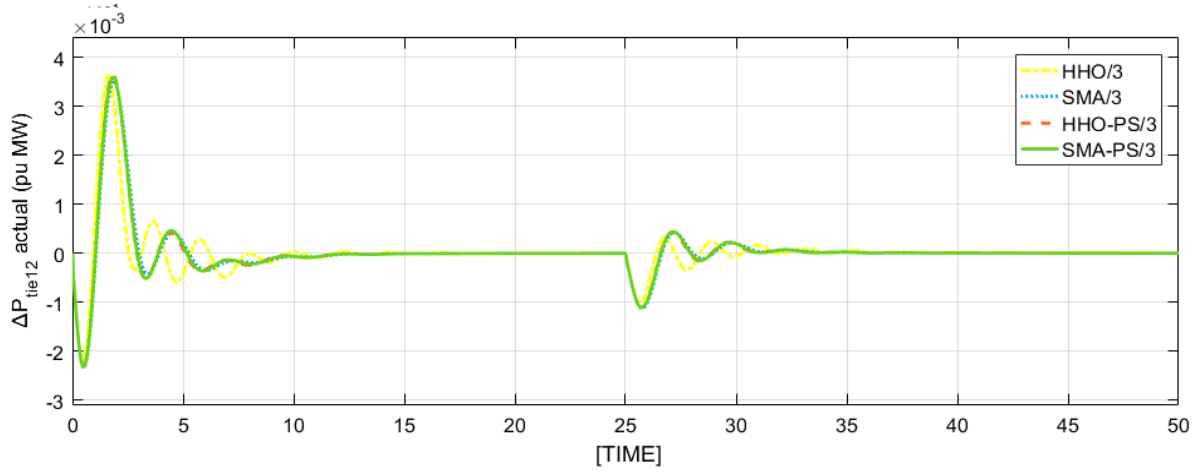

Fig.5.19 TLP flow actual reaction under CV case for the developed network with CES

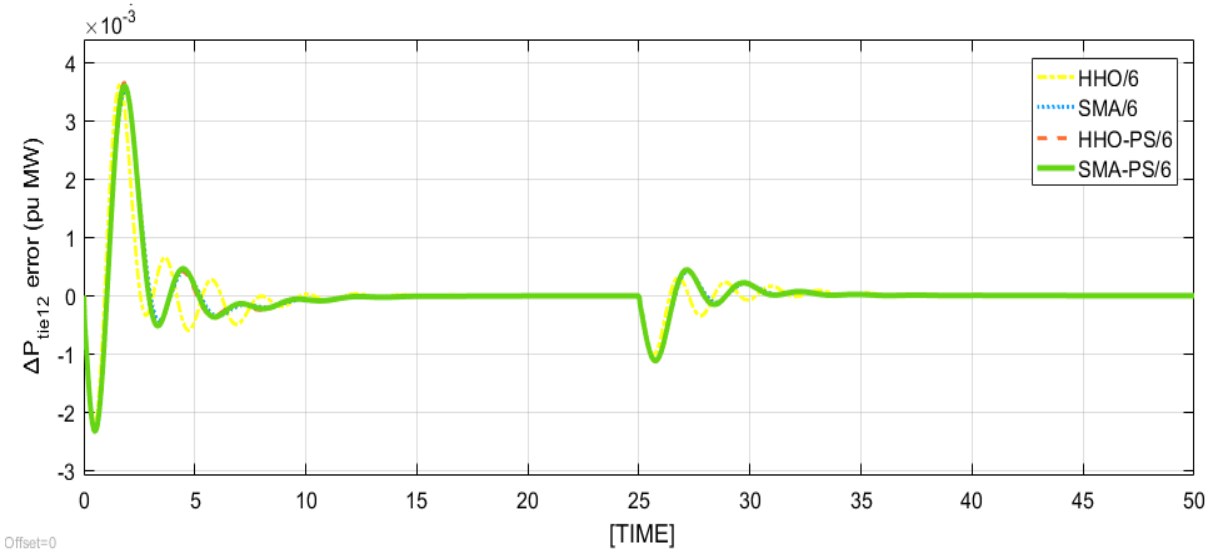

Fig.5.20 TLP flow error reaction under CV case for the developed network with CES

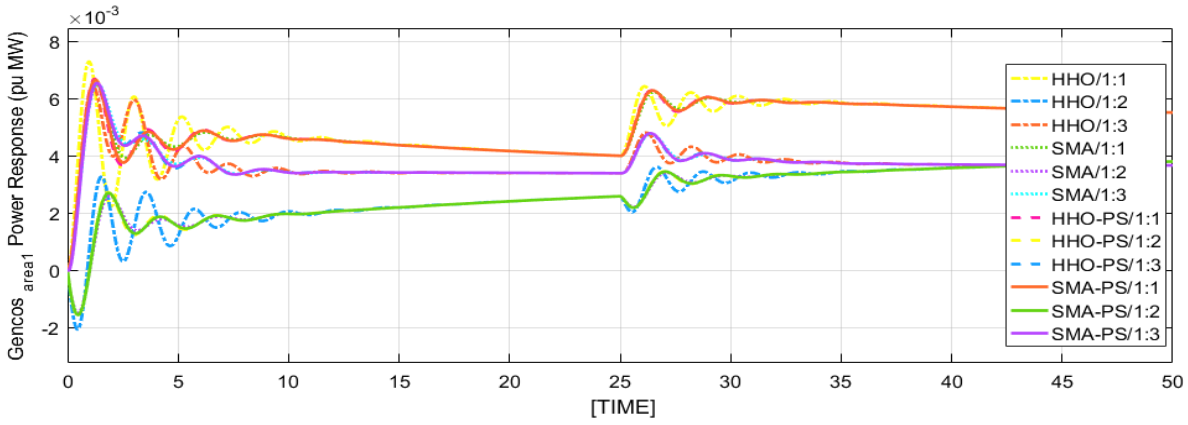

Fig.5.21 Area -1 GENCOs (1 to 3) reaction under CV case for the suggested system with CES

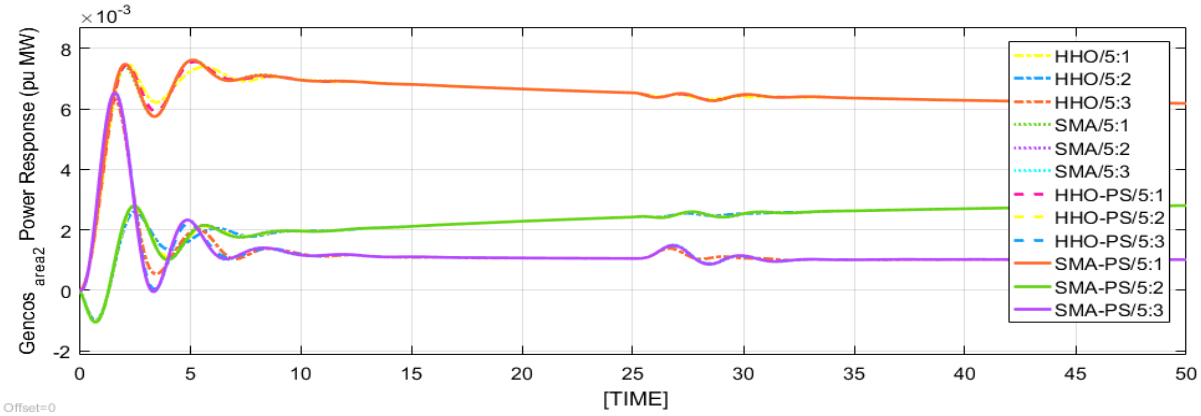

Fig.5.22 Area- 2 GENCOs (4 to 6) reaction under CV case for the suggested system with CES

Table.5.3 Unilateral transaction method with CES/TCPS, comparative analysis for different controllers.

Parameters		HHO	SMA	HHO-PS	SMA-PS
Settling time (sec)	ΔF_1	18	15	12	12
	ΔF_2	11	10	9	9
	P - tie	14	10.5	10	10
Peak overshoot response	ΔF_1	60.00020	60.00400	60.00400	60.00400
	ΔF_2	60.00070	60.00025	60.00020	60.00020

	P - tie	0.00150	0.00200	0.00200	0.00200
Under shoot response	ΔF_1	59.99985	59.99995	59.99990	59.99990
	ΔF_2	59.99600	59.99500	59.99500	59.99500
	P - tie	-0.00300	-0.00320	-0.00320	-0.00320

Table.5.4 Under Bilateral transaction method with CES/TCPS, comparative analysis for different controllers

Parameters		HHO	SMA	HHO-PS	SMA-PS
Settling time (sec)	ΔF_1	10	10	10	10
	ΔF_2	10	8	10	7
	P - tie	15	11	15	10
Under shoot response	ΔF_1	59.9920	59.9920	59.9980	59.9920
	ΔF_2	59.9830	59.9830	59.9850	59.9830
	P - tie	-0.0025	-0.0025	-0.0010	-0.0020
Peak overshoot response	ΔF_1	60.0020	60.0001	60.0001	60.0001
	ΔF_2	60.0090	60.0090	60.0110	60.0110
	P - tie	0.0030	0.0030	0.0020	0.0030

Table.5.5 Contract violation method with CES/TCPS, comparative analysis for different controllers

Parameters		HHO	SMA	HHO-PS	SMA-PS
Settling time (sec)	ΔF_1	32	31	30	30
	ΔF_2	30	29	29	29
	P - tie	33	31	31	31
Peak overshoot response	ΔF_1	60.006	60.006	60.007	60.007
	ΔF_2	60.0090	60.0110	60.0110	60.010
	P - tie	0.0035	0.0035	0.0035	0.0035
Undershoot response	ΔF_1	59.9920	59.9910	59.9910	59.9910
	ΔF_2	59.9820	59.9820	59.9820	59.9820
	P - tie	-0.0020	-0.0020	-0.0020	-0.0020

Figures 5.5 & 5.6, 5.11 & 5.12, and 5.17 & 5.18 shows in terms of frequency oscillation in each region with optimally tuned PI controllers including CES/TCPS units in a deregulated electricity market under contract violation, unilateral, and bilateral contract cases, respectively. The collected findings indicate that HHO, SMA, and HHO-PS based PI controller's performances are adequate in deregulated system. However, when compared to HHO, SMA, and HHO-PS based PI controllers, a SMA-PS tuned PI controller rapidly achieves the stabilization with reduced oscillation in terms of undershoot, overshoot, and settling time. In addition, the CES exchanges its stored power to the system and improves the system's dynamic efficacy by quickly resolving oscillation and overshoot caused by unexpected load fluctuations. Furthermore, when compared to the HHO, SMA, and HHO-PS based PI controllers with CES,

the SMA-PS tuned PI controller with CES immediately dampens the oscillations in both regions and offered superior dynamics.

Figures 5.7 & 5.8, 5.13 & 5.14, and 5.19 & 5.20 shows optimally regulating PI controllers with TCPS on TLP flow response under bilateral, contract breach and unilateral energy exchange scenarios in a system, respectively. In the unilateral contract scenario, there is no electricity demand between area-1 & 2. As a result, the tie line's planned power is reduced to zero. The actual tie-line power stabilized to 0.0003340 pu MW in the bilateral and contract breach scenarios. The simulated and theoretical of real power in the tie line between areas 1 and 2 are identical and exactly as specified in the contract. Each tactic in the DPS network, the performance evaluation of the SMA-PS premised PI regulating controller outranks the HHO, SMA premised PI regulating controller with a TCPS unit, as shown in the data. and HHO-PS premised PI regulating controller achieves results that are comparable to SMA-PS.

Figures 5.9 & 5.10, 5.15 & 5.16, and 5.21 & 5.22 shows the power generation of each GENCO in the system for various contract strategies.

The simulated response shown in Fig. 5.9 demonstrates that in the unilateral scenario, the area-1 GENCOs, i.e., GENCO-1, 2 & 3 generate power in accordance with demand and their cpfs. The DISCOs have no demand in area 2, as seen in Fig. 5.10. As a result, at the steady state, the change in produced power by all GENCOs w r to region is zero. Similarly, Fig. 5.13 & 5.14 shows the generation of power of each GENCO in the proposed system under a bilateral. Each GENCO reacts to its predetermined transaction contract by generating the precise quantity of electricity required to meet the demands of multiple DISCOs. Figure 5.21 & 5.22 depicts the dynamical reactions of power generation by various GENCOs in all control regions under the contact violation situation. The uncontracted load demand affects the produced power response of area-1's GENCO-1, 2, &3. However, area-2's GENCO-4, 5, &6 are unaffected by the uncontracted load. As indicated in the data, the generation reactions of area-1 GENCOs to meet the surplus power demand are clearly represented in their outputs. Every generator in area-1 reacts in accordance with its apfs and soon reaches the new generation limitations to meet the DISCOs' increased power demand.

The power of tie-line and generation reaction of each generating unit matches the corresponding scheduled values, as shown in the findings. During the transient situation, each

GENCO responds according to its apfs and rapidly achieves the stability in the system under consideration.

The system with a SMA-PS tuned PI controller with CES has greater performance than the system without it, according to the generation findings. The CES unit in the system reduces the deviation, and the generators soon reach their stability (refer chapter - 4).

Tables 5.3, 5.4, and 5.5 compare the HHO, SMA, HHO-PS, and SMA-PS optimized controllers with CES along with TCPS in the system for contract violation unilateral, and bilateral transactions, respectively. The oscillation of each region, the reaction power of tie line, and different generating units were examined, and various characteristics such as overshoot, settling time and undershoot of different reactions were obtained. In the proposed power system, it can be shown that the SMA-PS optimized controller with a CES achieves higher dynamic performance when compared to the HHO, SMA, and HHO-PS optimized controller.

5.9 SENSITIVITY ANALYSIS

Demonstrate the robust excellence of the suggested hybrid memetic SMA-PS and hybrid memetic HHO-PS premised PI regulating controllers, the study underwent many sensitive analyses, which included a broad variance of created DPS network system with CES unit and FACTS controller with due consideration of Bilateral transaction exchange tactic. In this regard the T_{sg} time costant of governor and inertia constant (H), which leads to change in load constant T_{ps} are governed at a rate of ±25% of their notional value The parameter variation in the developed electric DPS network with CES units in each region optimized gain parameters is followed through tables 5.6, 5.8, 5.10, and 5.12. And performance analysis values are depicted in tables 5.7, 5.9, 5.11, and 5.13. Its dynamical reactions represented in Figures 5.23 to 5.34 represent simple overlaps with others due to variation in T_{sg} and H . This concludes proposed hybrid memetic SMA-PS and hybrid memetic HHO-PS premised PI controller is robust in nature. For analysis, proposed hybrid memetic SMA-PS algorithm technique optimized PI controller is considered for its superiority

Table.5.6 Performance gain parameters for the proposed system with CES after changing the Tsg = -25%

Tsg= - 25%	k_1^P	k_1^i	k_2^P	k_2^i	J

HHO	2.918739	5	-0.44374	4.041155	1.459036
SMA	3.35741	5	-0.27002	4.234447	1.407993
HHO-PS	1.843782	5.203625	-0.44205	4.459747	1.401006
SMA-PS	2.805965	5	-0.45028	4.134179	1.400056

Table.5.7 Performance of the proposed system with CES after changing the Tps = -25%

Tsg= - 25%		HHO	SMA	HHO-PS	SMA-PS
Settling time (sec)	ΔF_1	12.5	13	12	12
	ΔF_2	14.5	14.5	14	12
	P - tie	14	14	13	13
Peak overshoot response	ΔF_1	60.0060	60.0060	60.0060	60.0060
	ΔF_2	60.0035	60.0025	60.0025	60.0035
	P - tie	0.0025	0.0020	0.0020	0.0020
Peak undershoot response	ΔF_1	59.9922	59.9920	59.9920	59.9920
	ΔF_2	59.9953	59.9957	59.9957	59.9954
	P - tie	-0.003	-0.003	-0.003	-0.003

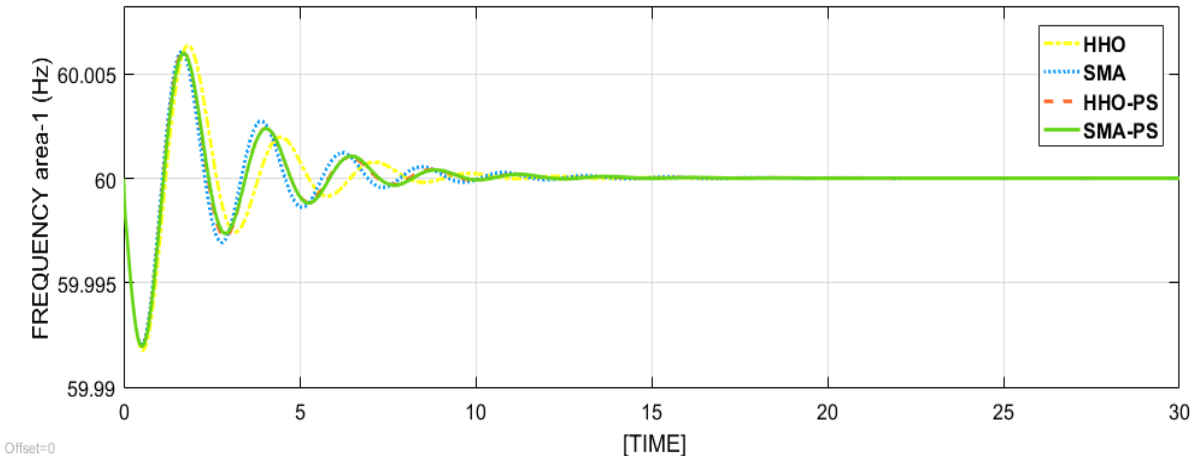

Fig.5.23 Area-1 frequency oscillation reaction for the suggested network with CES unit after changing turbine governor value -25%

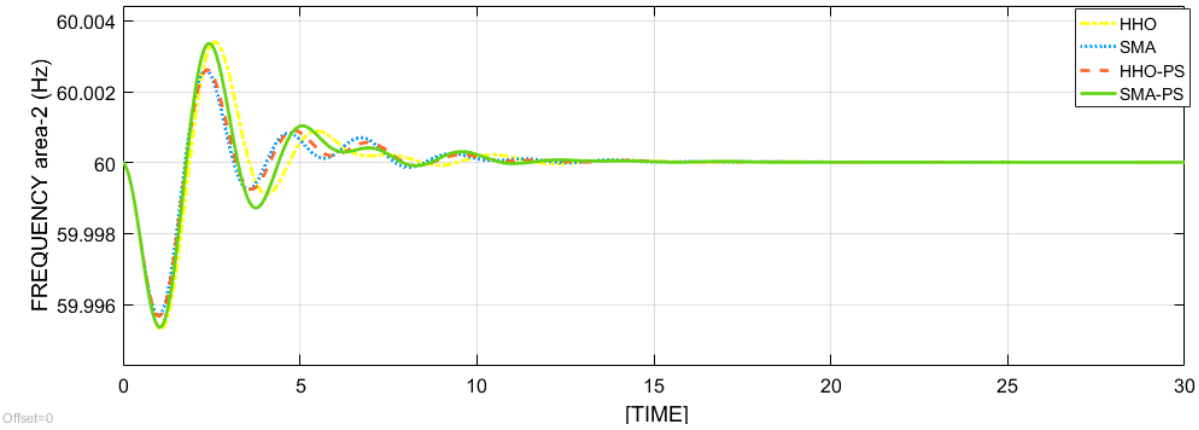

Fig.5.24 Area-2 frequency oscillation reaction for the suggested network with CES unit after changing turbine governor value -25%

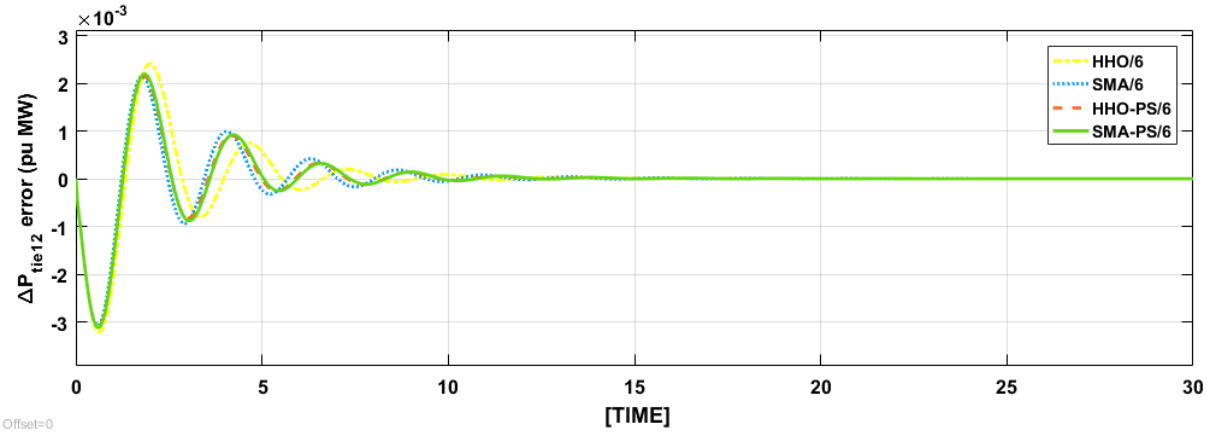

Fig.5.25 TLP dynamic reaction for the suggested network with CES unit after changing turbine governor value -25%

Table.5.8 Gain parameters for the developed network with CES unit after changing turbine governor value +25%

Tsg= +25%	k_1^P	k_1^i	k_2^P	k_2^i	J
HHO	2.68799	4.578462	0.089153	3.892493	1.578992
SMA	3.251577	4.977514	-0.0595	3.671359	1.556757
HHO-PS	2.613118	5.158389	-0.19427	3.687272	1.555025
SMA-PS-PS	2.972555	5	-0.00662	3.694892	1.553432

Table.5.9 Performance of the proposed system with CES after changing the Tsg = +25%

Tsg= + 25%		HHO	SMA	HHO-PS	SMA-PS
Settling time (sec)	ΔF_1	15	14	13	13
	ΔF_2	14.5	14.5	13	13
	P - tie	14.5	14	14	13

Peak overshoot response	ΔF_1	60.0055	60.0055	60.0060	60.0057
	ΔF_2	60.0025	60.0028	60.0028	60.0027
	P - tie	0.0022	0.0020	0.0022	0.0022
Peak undershoot response	ΔF_1	59.9900	59.9900	59.9900	59.9900
	ΔF_2	59.9960	59.9956	59.9960	59.9958
	P - tie	-0.0030	-0.0030	-0.0030	-0.0028

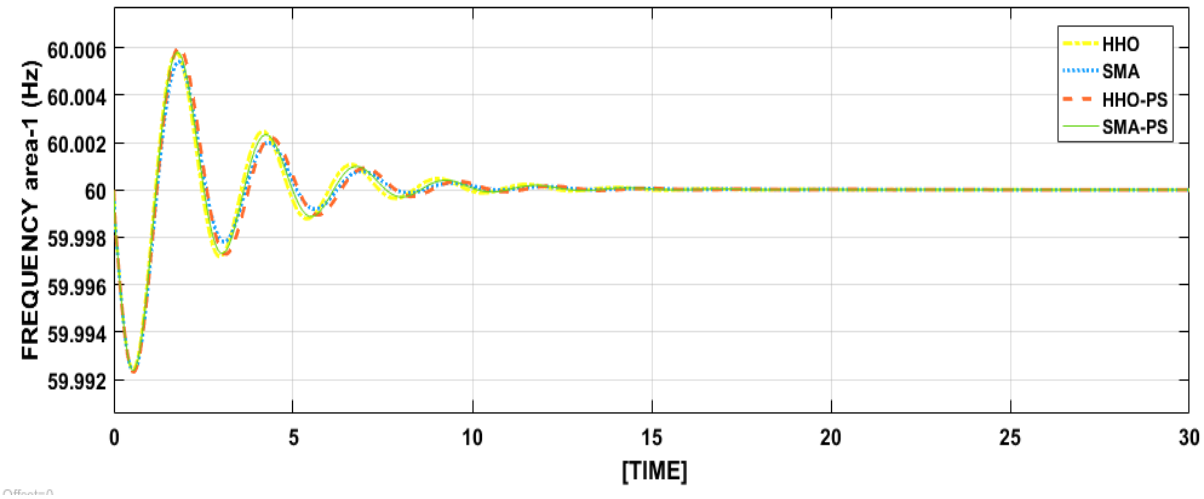

Fig.5.26 Area-1 frequency oscillation reaction for the suggested network with CES unit after changing turbine governor value +25%

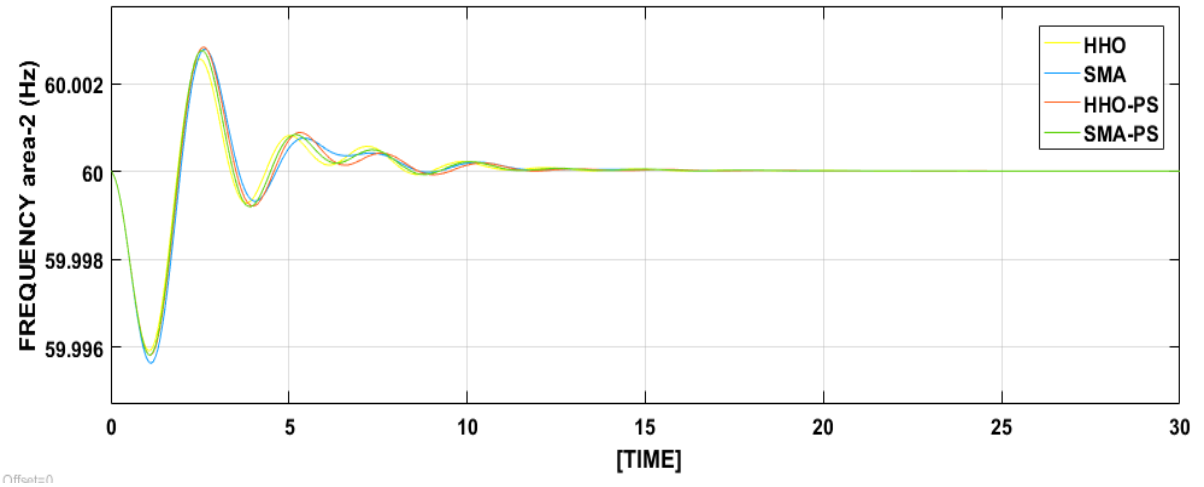

Fig.5.27 area-2 Frequency oscillation reaction for the suggested network with CES unit after changing turbine governor value +25%

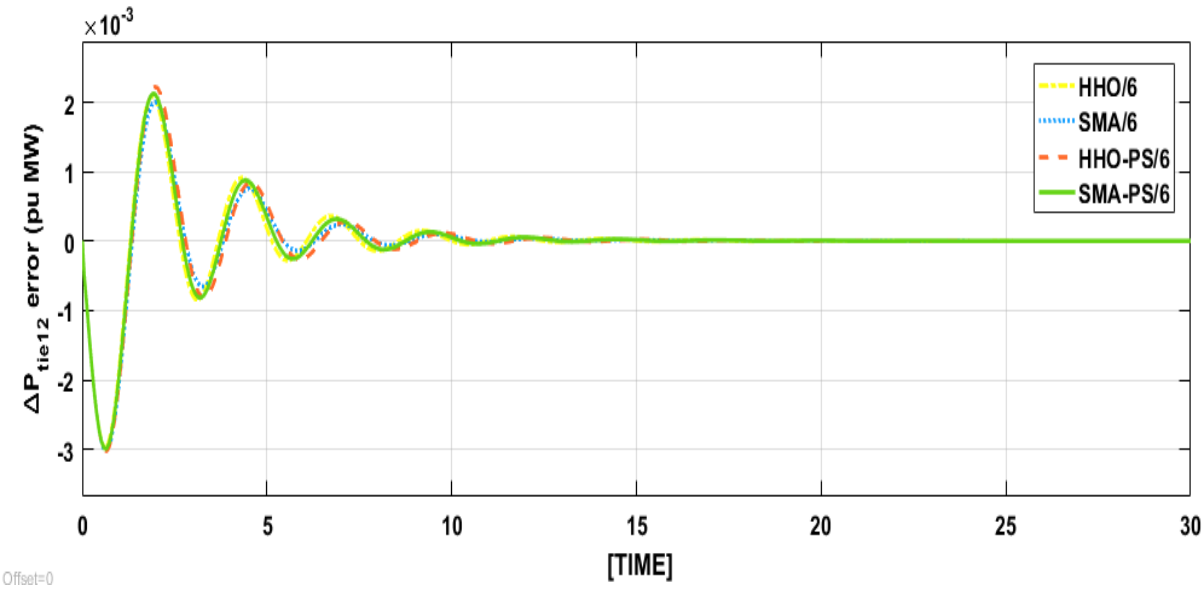

Fig.5.28 TLP dynamic reaction for the suggested network with CES unit after changing turbine governor value +25%

Table.5.10 Gain parameters for the developed network with CES unit after changing inertia constant (H) +25%

H= + 25%	k_1^P	k_1^i	k_2^P	k_2^i	J
HHO	2.66371	5	0.039768	3.783783	1.53805
SMA	2.732005	5	-0.37609	3.770522	1.512788
HHO-PS	2.743813	5	-0.36158	3.763203	1.512578
SMA-PS	2.917207	5.501336	-1.24586	3.908527	1.510339

Table.5.11 Performance of the proposed system with CES after changing the changing inertia constant (H) = +25%

H= + 25%		HHO	SMA	HHO-PS	SMA-PS
Settling time (sec)	ΔF_1	12.5	12.5	12	12
	ΔF_2	11.6	11.7	11	11
	P - tie	13.2	13.2	13.1	13
Peak overshoot response	ΔF_1	60.006	60.006	60.006	60.007
	ΔF_2	60.003	60.003	60.003	60.002
	P - tie	0.0025	0.0025	0.0025	0.0026
Peak undershoot response	ΔF_1	59.9920	59.9920	59.9920	59.9922
	ΔF_2	59.9960	59.9960	59.9955	59.9960
	P - tie	-0.0032	-0.0032	-0.0032	-0.0031

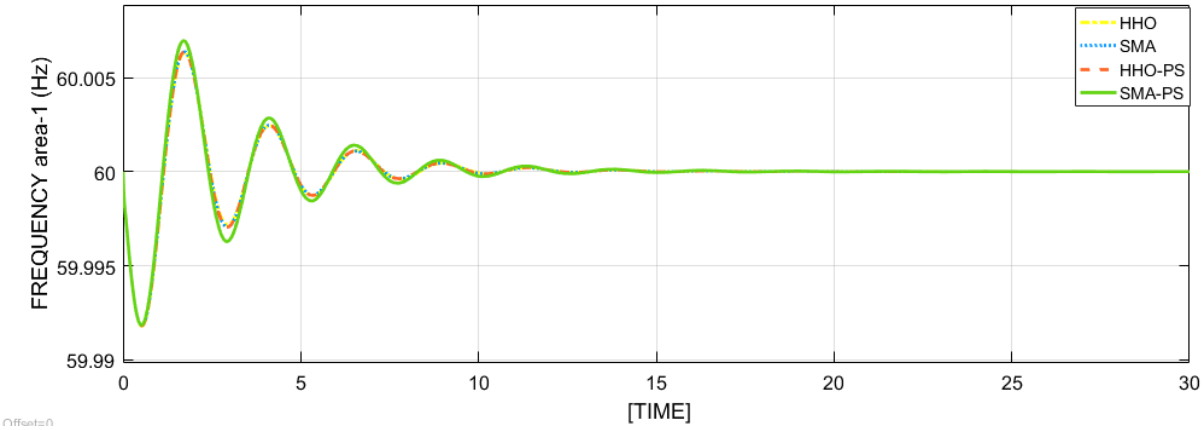

Fig.5.29 Area-1 frequency oscillation reaction for the suggested network with CES unit after changing inertia constant value +25%

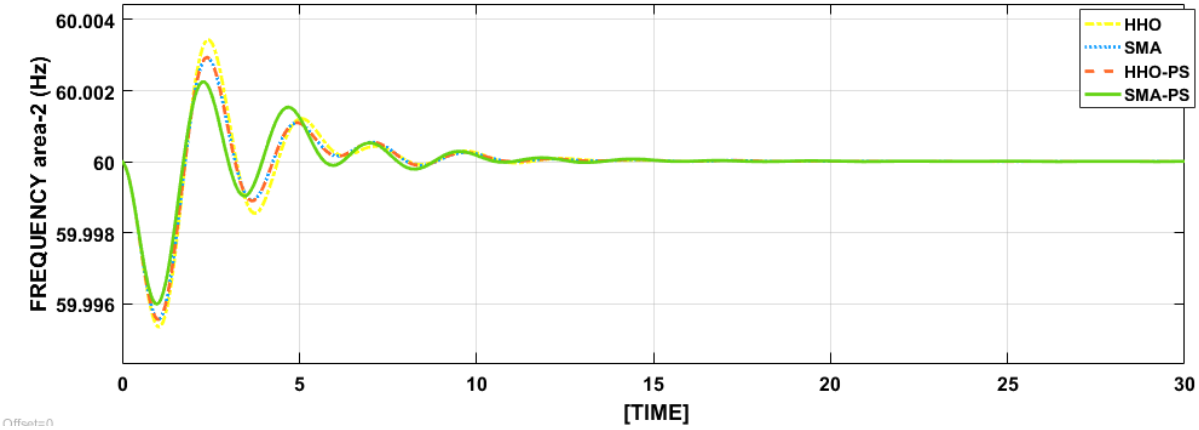

Fig.5.30 Area-2 frequency oscillation reaction for the suggested network with CES unit after changing inertia constant value +25%

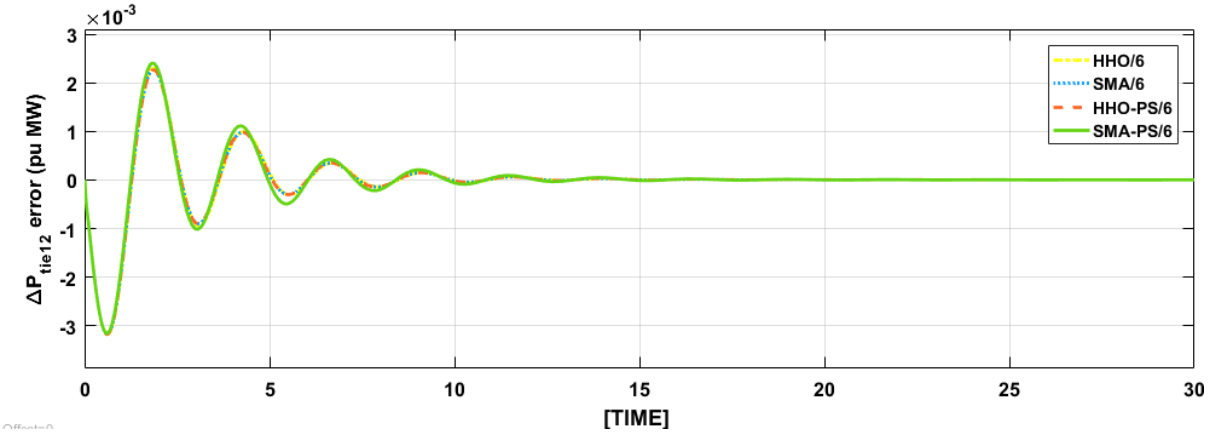

Fig.5.31 TLP dynamic reaction for the suggested network with CES unit after changing inertia constant value +25%

Table.5.12 Gain values of the proposed network with CES after exchange value H value as – 25%

H= - 25%	k_1^P	k_1^i	k_2^P	k_2^i	J
HHO	3.054633	7.058199	-0.68933	3.688118	1.458161
SMA	3.236389	5	0.121455	4.006412	1.456035
HHO-PS	3.438995	5	0.125031	4.046053	1.452782
SMA-PS	3.270124	5	-0.09006	3.963272	1.451902

Table.5.13 Performance of the proposed system with CES and EVs after changing the H = - 25%

H= - 25%		HHO	SMA	HHO-PS	SMA-PS
Settling time (sec)	ΔF_1	18	14	14	14
	ΔF_2	16	12.5	12	12
	P - tie	17	12.5	12	11
Peak overshoot response	ΔF_1	60.007	60.0060	60.0060	60.0055
	ΔF_2	60.0035	60.0030	60.0030	60.0025
	P - tie	0.0027	0.0020	0.0020	0.0020
Peak undershoot response	ΔF_1	59.9925	59.9925	59.9925	59.9925
	ΔF_2	59.9960	59.9955	59.9955	59.9955
	P - tie	-0.0030	-0.0030	-0.0029	-0.0029

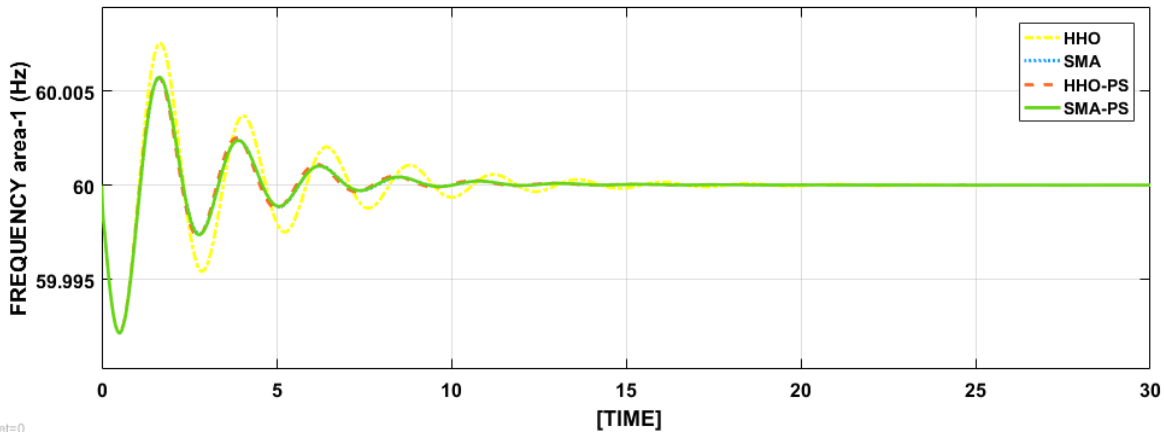

Fig.5.32 Area-1 frequency oscillation reaction for the suggested network with CES unit after changing inertia constant value -25%

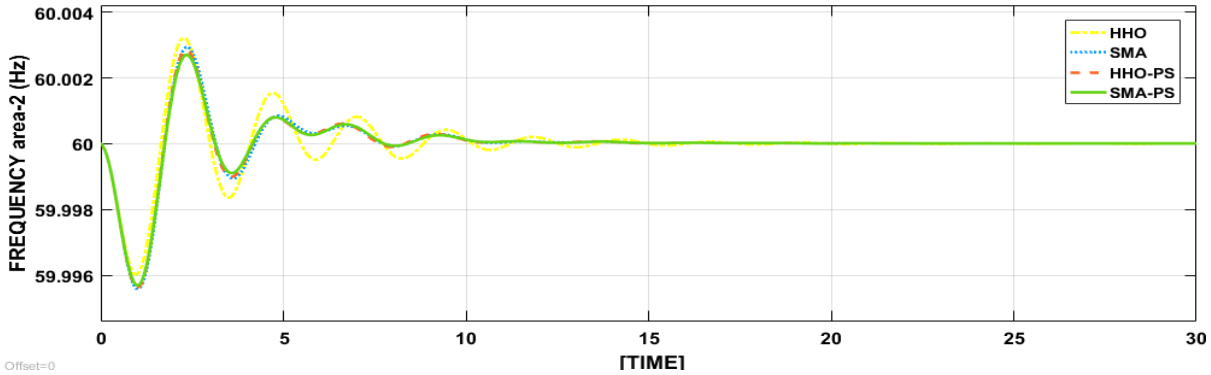

Fig.5.33 Area-2 frequency oscillation reaction for the suggested network with CES unit after changing inertia constant value -25%

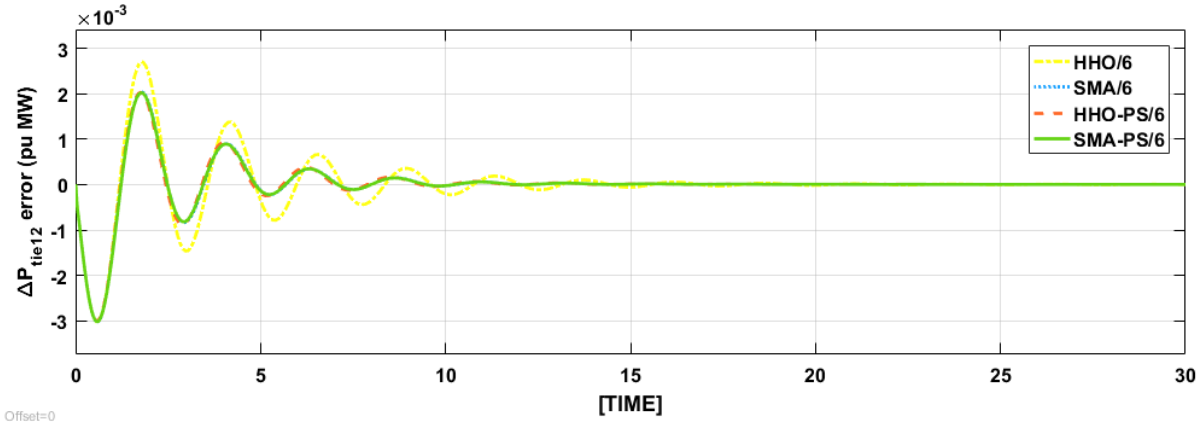

Fig.5.34 TLP dynamic reaction for the suggested network with CES unit after changing inertia constant value -25%

5.10 CONCLUSION

In the presence of CES and TCPS units, the LFR of DPS network analysis optimally tuned PI controllers was examined. In this chapter, the developed hybrid variants SMA-PS and HHO- are tested to optimise the parameters of PI controller. Under all conceivable unregulated situations, comparative studies of a hybrid memetic SMA-PS tuned PI controller and an HHO, SMA, and hybrid memetic HHO-PS optimized controller with CES/TCPS units are undertaken. Investigations indicated that the suggested hybrid memetic SMA-PS optimized PI controller outperforms the HHO, SMA, and hybrid memetic HHO-PS optimized PI controllers in terms of system responsiveness. In the current study, hybrid memetic SMA-PS outperforms the common HHO, SMA, and hybrid memetic HHO-PS algorithms in terms of statistical performance as well as improved optimum transient performance. Every GENCO's simulated reaction to power generation and tie-line exchanges was verified. Every generating unit's output power response performs within an acceptable range (around 60 Hz) to meet the LFR.

In addition, to prove the efficacy of the DPS network with CES units, sensitivity analysis is done under different variable parameter changes of $inertia$ constant H and T_{sg} changes as $\pm 25\%$ their nominal system predetermined values with POOLCO exchange tactic. The outcomes reveal that hybrid memetic SMA-PS premised PI regulator optimized two area H – T – G origin sources DPS network with CES performs robust manner without changing the notable in terms of settling time, under shoot response and overshoot reactions in the electric DPS network with CES. And the sensitivity analysis comparative studies of a hybrid memetic SMA-PS tuned PI controller with HHO, SMA, and hybrid memetic HHO-PS optimized controllers performed, and the analysis reveals that hybrid memetic SMA-PS premised PI regulator has best efficacious outcomes among other optimizers.

Chapter – 6

IMPACT OF EVs AND RES ON LOAD FREQUENCY REGULATION

6.1 INTRODUCTION

LFR is a vital area of study that aims to maintain tie-line and frequency exchange within set out limits. There are several electricity generating resources, often known as conventional generators, such as hydro, thermal and gas. The researchers are concerned about several key concerns, including the depletion of fossil fuels and the environmental risks associated with their usage. These factors compel investigators to focus increasingly on the use of alternative, environmentally friendly RES such as ocean thermal, solar (PV cell), and wind energy. Many dispersed generating sources, such as aqua electrolysers and battery energy storage sources (BESS), are also available and may be used to load requisition. Electric vehicles (EVs) are increasingly seen as a type of BESS which can stores energy of charge in a battery and link to the regular power grid to fulfill increased demand [68].

Engineers working on power systems strive to find balance among energy generation and consumption to ensure continuous frequency and tie-line power exchange across interconnected locations of LFR [29]. Many other types of systems are considered, such as H-T-G and others. Many academics have recently developed and proposed the notion of a multi-source power system in LFR.

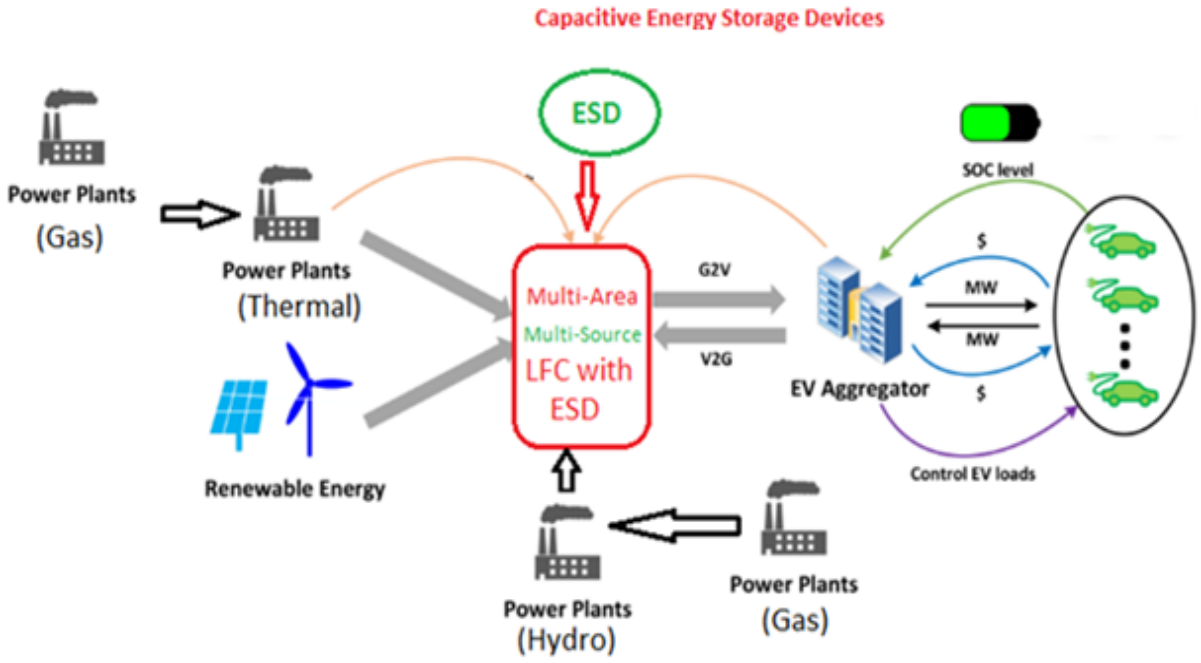

Fig.6.1 LFR of proposed DPS with EV

Furthermore, concern for the environment, the researchers' focus is turning toward greater integration of RES into the DPS for electric power generation. Solar power is one such source of energy. EVs have been used for LFC in an electrical network, as evidenced by several recent publications [69][70][63][62]. Here, table 6.1 depicts configuration parameters for the developed model. And fig 6.1 shows the block diagram of the developed model.

Table.6.1 Configuration parameters for proposed model EVs/PV

AREAs	GENCOs	DISCOs	CES	TCPS	EV	PV
1	Hydro(H), Thermal(T), and gas(G)	2	1	1	200	1
2	Hydro(H), Thermal(T), and gas(G)	2	1		300	1

6.2 MATHEMATICAL MODELING WITH RES/EV

Here, two area with three GENCOs (H-T-G) originating source with power exchanged CES in each region is considered. A FACTS controller unit of TCPS is integrated at the tie line, to maintain control over the TLP fluctuations. An optimized PI control strategy is utilised to regulate the significant power network. The Control scheme is most utilised LFC techniques. This regulator has the advantage of reducing steady-state error to zero.

Area-1 overall generating power (fig. 6.1) is

$$P_{POWER1} = PF_{themal1} + PF_{hydro1} + PF_{gas1} \pm PF_{ces1} + PF_{EV1} \quad 6.1$$

Area-2 overall generating power (fig. 6.1) is

$$P_{POWER2} = PF_{themal2} + PF_{hydro2} + PF_{gas2} \pm PF_{ces2} + PF_{EV2} \quad 6.2$$

Here, PF_{thermal1} & PF_{thermal2} replicates thermal, PF_{hydro1} & PF_{hydro2} replicates hydro, PF_{diesel1} & PF_{diesel2} replicates diesel power generating resources and PF_{ces1} & PF_{ces1} replicates exchanged CES banks.

The total generating net amount of power is as follows

$$Total\ POWER\ =\ POWER1\ +\ POWER2 \qquad 6.3$$

6.2.1 Electric Vehicle

BEVs (battery electric vehicles) might offer combined storage capacity and power revert to the system in any of multiple electrical energy markets, a notion known as vehicle-to-grid power or V2G power. Since, (EVs) electric vehicles run on energy, a high market penetration of EVs is anticipated to increase power consumption. Power companies must contend with the possibility that such surplus supply would result in an increase in peak load, allowing them to return more power to the system. Furthermore, EVs remain stationary for more than 90% of the time; when not in use, they may serve as large-scale distributed batteries, providing power storage and auxiliary services to the energy grid.

Frequency deviations rise because of the RESs' intermittency. EVs link to the electric grid and provide a frequency management method while they are idle [71][69]. The following (fig 6.2) is a model of an EV fleet that includes a battery charger, primary frequency control, and LFC:

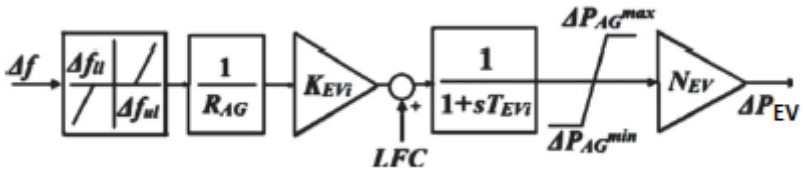

Fig.6.2 EVs/BEV aggregate model structure

Each EV is equipped with a dead band function with droop characteristics, as EVs may get disconnected from the grid, resulting in an undesirable frequency response. The upper limit (f_{UL}) and lower limit (f_{LL}) of the dead band are 10 and -10 mHZ, correspondingly.

The value of the aggregate model droop coefficient (R_{AG}) is 2.4Hz/p.u.MW in conventional units. $K_{EVi}$and T_{EVi} are the EV gain and battery time constant, respectively, in Figure 6.2. The value of $K_{EVi}$is determined by the EV's state of charge (SOC). The incremental generation change of EV is known as ΔP_{EVi}. ΔP_{AG}^{max} is the maximum and ΔP_{AG}^{min} is the minimum power outputs of electric vehicle fleets, respectively, and may be computed as [67]

$$\Delta P_{AG}^{\max} = +[\frac{1}{N_{EV}} * \Delta P_{EVi}] \qquad 6.4$$

$$\Delta P_{AG}^{\min} = -[\frac{1}{N_{EV}} * \Delta P_{EVi}] \qquad 6.5$$

N_{EV} stands for the number of electric cars that are linked. In the scenario, a total of 200 EVs have been discharged in area – 1 & 2 is 300 EVs, respectively, are evaluated. The control system is designed using the ITAE. The test system's transfer function model and the block diagram model is shown in figs 6.6 and 6.1 (main block diagram). The charging and discharging capacity of an EV is regarded within ± 5 kW for study, however it can reach 50 kW or even more during quick start.

The value of K_{EVi} changes with the battery's (li-ion) SOC level, which indicates EVs' involvement in LFR while connected to the grid. As an example, Fig. 6.3 depicts the involvement of EVs in discharge mode, i.e., idle mode operation. Until EV's SOC is less than SOC2, K_{EV} is always equal to 1. EV fleets do not completely engage in LFR between SOC1 and SOC2. Fig 6.4 depicts the K_{EVi} VS State of charge.

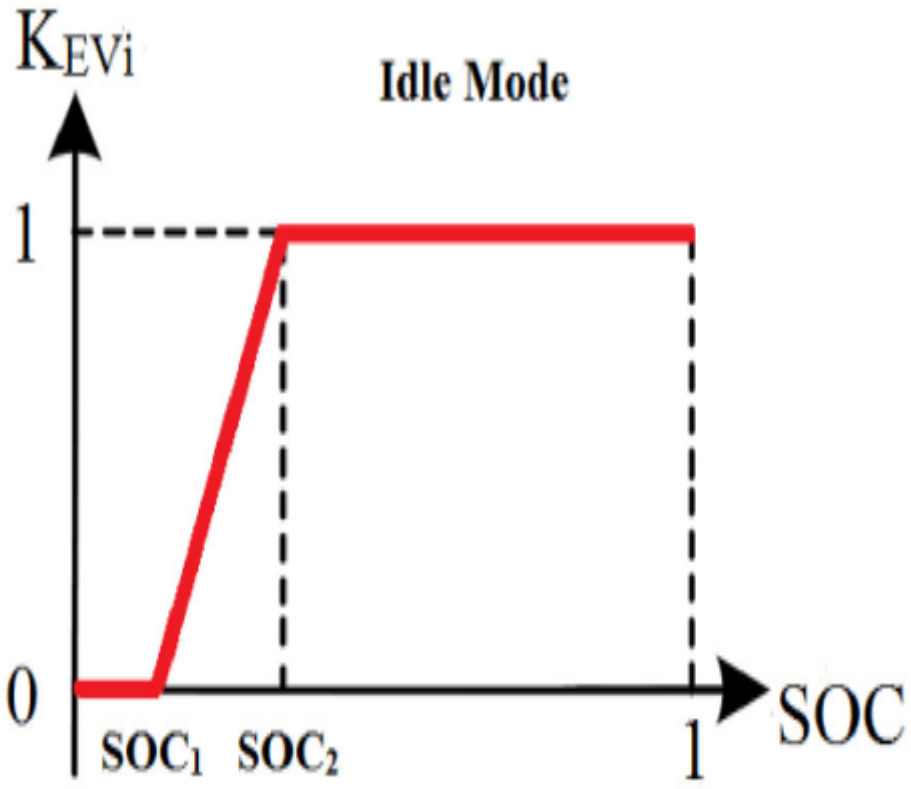

Fig.6.3 K_{EVi} vs SOC for idle mode condition

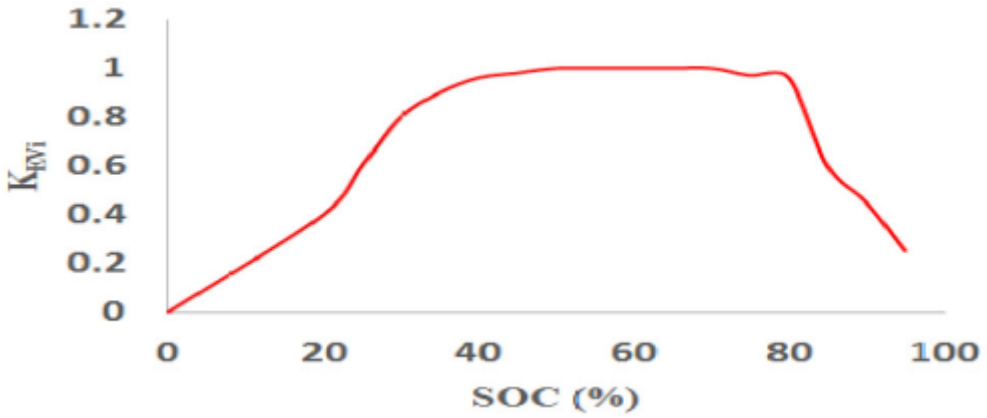

Fig.6.4 K_{EVi} vs SOC

The numerical data for our simulation is obtained from[70], where K_{EVi} =1 between 50 and 70 percent SOC. K_{EVi} ranges from 0 to 1, depending on whether you're below 50 percent or beyond 70 percent. The value of K_{EVi}in relation to SOC is shown in Figure 6.4.

Here, N_{EV} denotes the number of EVs that are connected. EV's transfer function model is as follows:

$$G_{EV} = \frac{K_{EV}}{1+sT_{EV}} \qquad 6.6$$

6.2.2 PV cell model

To create the needed electricity, a PV array is made up of series and parallel linked PV cells. ϕ (Solar insolation) is utilised as a PV array input. the power supplied by a PV array is[58] :

$$P_{PV} = \eta S\phi\{1-0.005(T_a+25)\} \qquad 6.7$$

Here, S is the size of the PV array in (m^2), ϕ is the solar insolation in (kw/m^2), and T_a is the ambient temperature in (°C) corresponds to conversion efficiency with a range of 9 to 12 percent (^{0}C). η and S are both constants. The PV array's output power is determined by and T_a. The PV power generating simplified transfer function is as follows:

$$G_{PV} = \frac{K_{PV}}{1 + sT_{PV}} \quad 6.8$$

PV's gain and time constant are denoted by K_{PV} and T_{PV}, respectively.

The various GENCOs of the new hybrid system mentioned here are the resources of power generation stated above. DISCOs can contract any GENCOs for electricity needs. Under GENCOs-DISCOs, DPM (Disco Participation Matrix) assists in the envisioning of contracts.

DPM for the proposed DPS is

$$DPM = \begin{bmatrix} cpf_{v11} & cpf_{v12} & cpf_{v13} & cpf_{v14} \\ cpf_{v21} & cpf_{v22} & cpf_{v23} & cpf_{v24} \\ cpf_{v31} & cpf_{v32} & cpf_{v33} & cpf_{v34} \\ cpf_{v41} & cpf_{v42} & cpf_{v43} & cpf_{v44} \\ cpf_{v51} & cpf_{v52} & cpf_{v53} & cpf_{v54} \\ cpf_{v61} & cpf_{v62} & cpf_{v63} & cpf_{v64} \end{bmatrix} \quad 6.9$$

cpf_{vij} depicts contract participation matrix factor

$\sum_{i=1}^{n} cpf_{vij} = 1$, here j=1,2……k

k replicates the sum of DISCOs

n replicates the sum of GENCOs

with reference to section 4.2, the local load demand of each region is calculating as,

$$\Delta p_{l2} + \Delta p_{l1} = \Delta p_{D1} \quad 6.10$$

$$\Delta p_{l4} + \Delta p_{l3} = \Delta p_{D2} \quad 6.11$$

Each GENCOs power generation as per contract is

$$\Delta p_{Gci} = \sum_{j=1}^{GENCO_{total}} cpf_{vij} * \Delta p_{lj} \quad 6.12$$

And hence, the local unagreed electricity (refer section 4.2) demand is as follows

$$\Delta p_{L1}^{uc} + \Delta p_{l2} + \Delta p_{l1} = \Delta p_{D1} \quad 6.13$$

$$\Delta p_{L2}^{uc} + \Delta p_{l4} + \Delta p_{l3} = \Delta p_{D2} \quad 6.14$$

Here, Δp_{L2}^{uc} and Δp_{L1}^{uc} were the unagreed load requisitions for area-2 and 1. The ACE (Area Control Error) [54], is the unplanned demands or shift in the assigned power that creates changes in the tie-line power flow. The frame tie-line power exchange amongst regions rates may be measured as

$$\Delta p_{tieline,12}^{allocated} = \sum_{n=1}^{3} \sum_{m=3}^{4} \text{cp} f_{nm}\ \Delta p_{lm} - \sum_{n=4}^{6} \sum_{m=1}^{2} \text{cp} f_{nm}\ \Delta p_{lm} \quad 6.15$$

Eqn (6.15) can be used to express the relevance that goes through tie-line

$$\Delta p_{tieline,12}^{real} = \frac{2\pi T_{12}}{s}(\Delta F_1 - \Delta F_2) \quad 6.16$$

Eqn (6.17) describes the error that arises in tie-line power owing to the strict limit in DPS

$$\Delta p_{tieline,12}^{error} = \Delta p_{tie,12}^{real} - \Delta p_{tieline,12}^{allocated} \quad 6.17$$

If an actual tie line power flow surpasses the power flow error limitations, the current flow setup quantity ($\Delta p_{tieline,12}^{error}$) is zero, and this is referred to as the constant state situation. ACE may be represented in an area described by Eqn (6.18) as a linear combination of the power flow error in the tie line and weighted frequency variation.

$ACE_1 = \Delta F_1 * B_1 + \Delta p_{tieline,12}^{error}$ and as well as, $ACE_2 = \Delta F_2 * B_2 + \Delta p_{tieline,21}^{error}$ 6.18

6.2.3 CES

The CES device is ideally suited to applications requiring up to 20 MW of power [53]. The STORE project has installed ranges of 4 MW to 20 MW CES systems for La Palma power system financed by Spanish Ministry of Economy and Competitiveness' (SPAIN) [55]. References [56] and [57] investigate a modest rating conventional CES with a maximum storage capacity of 3.8 MJ for AGC application's in two-area systems. It is appropriate for use in ESS because of several key characteristics, including fastest discharge/charge rate, response time without loss of efficacy [44].

During normal operation, in capacitor plates, the CES unit store energy in terms of electrostatic, which it then releases into the grid when there is a sudden load disruption. As a result, governor and other control mechanisms begin to work to bring the system back into balance. The system stays back to its steady state configuration after stabilizing.

CES units have been included in both parts of the model to ensure improved dynamic reaction of systems and reduce oscillations [40].

CES has outperformed the current ESD in terms of effectiveness. Similarly main qualities, such as rapid charge and discharge rate, prevent effectiveness loss. To be acceptable for usage in an ESS, it must have a fast reaction time for large cycle numbers, a high power density, a longer useable lifecycle, and the capacity to transmit more and greater power requisitions to the grid [44].

$$\Delta p_{ces} = \left[\frac{k_{ces}}{1+sT_{ces}}\right] + \left[\frac{1+sT_{c1}}{1+sT_{c2}}\right] + \left[\frac{1+sT_{c3}}{1+sT_{c4}}\right]\Delta F_i(s) \qquad 6.19$$

6.2.4 TCPS

TCPS is one of the most widely used FACT's regulator units in system in series with applicability by degree of compensate in realistic innovative energy systems. TCPS helps the electric grid preserve its stability and efficiency by allowing for flexible power scheduling in a variety of (changing) operational scenarios. It may be utilized to boost the power-transfer capabilities of a transmission line by dampening energy fluctuations caused by cross-area and regional vibrations [17]. During difficult situations, the TCPS maintains the true power flow across transmission lines (tie lines), reduces greater frequency, and manages the output of the electricity system by altering the phase angle comparison.

The exponentially load voltage between area-2 and 1 of the tie-line interconnection, as suggested by eqn (6.20) is

$$\Delta p^{o}_{tieline}(s) = \frac{2\pi T^{o}_{12}}{S}(\Delta F_1(s) - \Delta F_2(s)) \qquad 6.20$$

After including a TCPS unit into the model, the real power flow interchange among area-1 and 2 is

$$\Delta p^{real}_{tieline,12} = \frac{|V_1||V_2|}{X_{12}}\sin(\delta_1 + \delta_2 - \phi) \qquad 6.21$$

Here, $\delta_1^0, \delta_2^0 \; and \; \phi^0$ values from $\delta_1, \delta_2 \; and \; \phi$ original values respectively. As indicated in eqn (6.22), the voltage regulation oscillating among tie lines follows a restricted signal approximation technique.

$$\Delta p_{tieline,12}^{real} = T_{12}(\Delta\delta_1 + \Delta\delta_2) + T_{12}\Delta\phi) \quad 6.22$$

Here, $$T_{12} = \frac{|V_1||V_2|}{X_{12}}\cos(\delta_1^0 + \delta_2^0 - \phi) \quad 6.23$$

Furthermore, the angular variation may be written as,

$$\Delta\delta_1 = 2\pi\Delta F_1 dt \; and \; \Delta\delta_2 = 2\pi\Delta F_2 dt \quad 6.24$$

Using the Laplace transform of eqn (5.22) is

$$\Delta p_{tieline,12}^{real}(s) = \frac{2\pi T_{12}^o}{S}\left(\Delta F_1(s) - \Delta F_2(s)\right) + T_{12}\Delta\phi(s) \quad 6.25$$

The angle of the phase shifter ($\Delta\phi$) affects the interchange of TLP flow, as shown in eqn. (6.26). The math formula that expresses the phase shifter's angle(s) is as follows:

$$\phi(s) = \Delta F_1(s)\frac{k_\phi}{1+sT_{TCPS}}\Delta Error \quad 6.26$$

Here.

frequency fluctuation in area 1 is $\Delta F_1(s)$, which one is taken as error signal depicted in (5.18). further eqn (6.25) is as

$$\Delta p_{tieline,12}^{real}(s) = \frac{2\pi T_{12}^o}{S}\left(\Delta F_1(s) - \Delta F_2(s)\right) + \Delta F_1(s)\frac{k_\phi}{1+sT_{TCPS}}T_{12} \quad 6.27$$

6.2.5 PI CONTROLLER DESIGN

The combination of the proportional with the integral optimal control for the augmented LFR of DPS network with CES and EV is designed and shows in fig 6.5. PI optimal regulator useful to regulate the higher complexity challenges in DPS (refer chapter -2 literature).

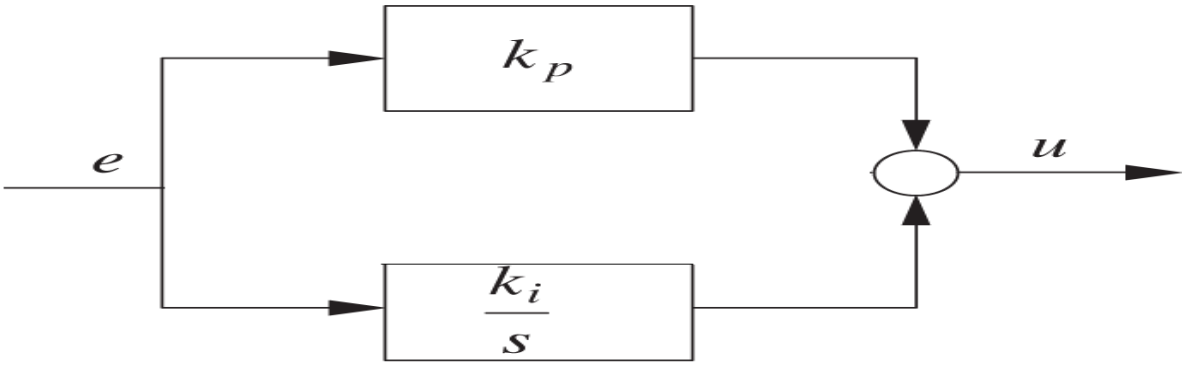

Fig.6.5 PI controller design

$$G(s) = k_p + \frac{k_i}{s}$$

6.3 HYBRID MEMETIC SLIME MOULD ALGORITHM INTEGRATED WITH THE PATERN SEARCH METHOD

To verify the optimal performance of Integrated SMA-PS algorithm, for every issue collection, 50 testing attempts were created, with each run beginning with a distinct baseline population. In all trials, a populace of 40 was used for a two-area DPS network with CES and EV unit test equipment. The proposed method is evaluated on MATLAB version 2018a on intel Intel(R) Core (TM) i7-8550U CPU @ 1.80GHz system. The suggested hybrid memetic HHO-PS algorithm optimal process for solving the LFR of the DPS network with CES and EV is as follows.

Step-1: Read the originating units characteristics, profile for the load demand of two area network with CES and EV units.

Step-2: Use hybrid memetic SMA-PS optimization method to optimize the LFR of the DPS network with CES and EV units.

Step-3: set-up the LFR network power generators to match load demand with frequency regulation constraints.

Step-4: verify each generator performance with the participation factors overall frequency and evaluate the objective function.

Stwp-5: compute all the generators position as their respected contract with GENCO-DISCO participation.

. Step-6: upgrade the power generators outcome with reducing the frequency regulation of each area frequency.

Step-7: analyse the best fitness of the random search generator by using the objective function.

Step-8: the analysed best outcome of the objective function is carried at the termination end of the global searcher is carried out with the local search PS optimizer.

Step-9: upgrade the position of the objective function by using the local searcher

Step-10: evaluate the best, worst available fitness with the objective function by using eqn (3.22).

Step-11: check size of iteration condition to reach the objective function, if the maximum iteration obtained then go to step-13.

Step-12: otherwise, rise the size of iteration by 1, then repeat from step 3.

Step-13: stop the entire optimal process and evaluate the solution of LFR of the DPS network.

6.4 THE OBJECTIVE FUNCTION FOR DESIGNING AN OPTIMAL LFR CONTROLLER WITH RES/EV

The controller and objective function used in the current investigation are briefly described in this section. The ITAE criteria are used as the objective function in this study to optimize the objective function, which can be written as[28]:

$$J= \int_0^{t_{sim}} |\Delta F_1| + |\Delta F_2| + |\Delta P_{tie}| * t * dt \qquad 6.28$$

The discrete value of incremental oscillation deviation in area- 1 & 2 are represented by ΔF_1 and ΔF_2.

ΔP_{tie} is the value of the tie line exchange.

't' stands for the overall simulation time in seconds.

The ITAE index is minimized using the SMA-PS and HHO, SMA, and HHO-PS algorithms to optimize the parameters of the PI controllers in both areas, according to the following constraints:

To minimize J,

$$k_i^P \min \leq k_i^P \leq k_i^P \max \text{ and } k_i^{int} \min \leq k_i^{int} \leq k_i^{int} \max$$

Here, k_i^{int} is the integral gain of the PI controller and k_i^P is the proportional gain of the PI controller for the 'i' th area (i = 1, 2). In the range limit, both area gains are optimized (-5, 5).

6.5 IMPLEMENTATION OF PROPOSED ALGORITHM

Here, HHO, SMA, HHO-PS and SMA-PS algorithms programs were written in a MATLAB (in.mfile). In the optimization algorithm, the objective function is derived in the form of Eqn. (5.28). In the current research, the initialization parameters were taken for the HHO, SMA, HHO-PS and SMA-PS were given as population size of N = 40, dimension size is as 4. Simulations to run the HHO, SMA, HHO-PS and SMA-PS algorithms examined on 1.80 GHz, 8 GB, Intel Core i7, 64-bit processor, Windows-10 machine in version of MATLAB-(R2018a).

The PI controller's optimal gain is determined by running a series of tests for 50 iterations and 50 runs for all HHO, SMA, HHO-PS and SMA-PS algorithms.

Table 6.2 shows the PI controller's performance and optimized gain values for the proposed system using the HHO, SMA, HHO-PS, and SMA-PS algorithms. And fig. 6.6 illustrates the overall LFR transfer function model of the two area H-T-G sources with CES and EV hybrid deregulated power system model.

Table.6.2 Optimized controller gain values for the LFR of the suggested system with RES/EV.

Algorithm	k_1^P	k_1^i	k_2^P	k_2^i	Objective function value
HHO	-4.9951	-5	-5	-5	0.004273025
SMA	-5	-5	-5	-4.9469	0.004269933
HHO-PS	-5	-5	-5	-1.2469	0.004258932
SMA-PS	-5	-5	-5	-0.9017	0.004219357

6.6 RESULTS AND DISCUSSIONS

The proposed power system, which is made up of various power generation sources and is being studied in a competitive market scenario, was created in the Simulink environment in MATLAB 2018a. The non-linearity effect of GDB and GRC is evaluated using a realistic model of a power system with various generating units such as H-T-G in each area. And later, proposed model was integrated with CES/TCPS (FACTS devices) for energy storing and to

stabilize tie line power frequency. A series simulation has been performed in both the areas and to minimise tie-line power flow.

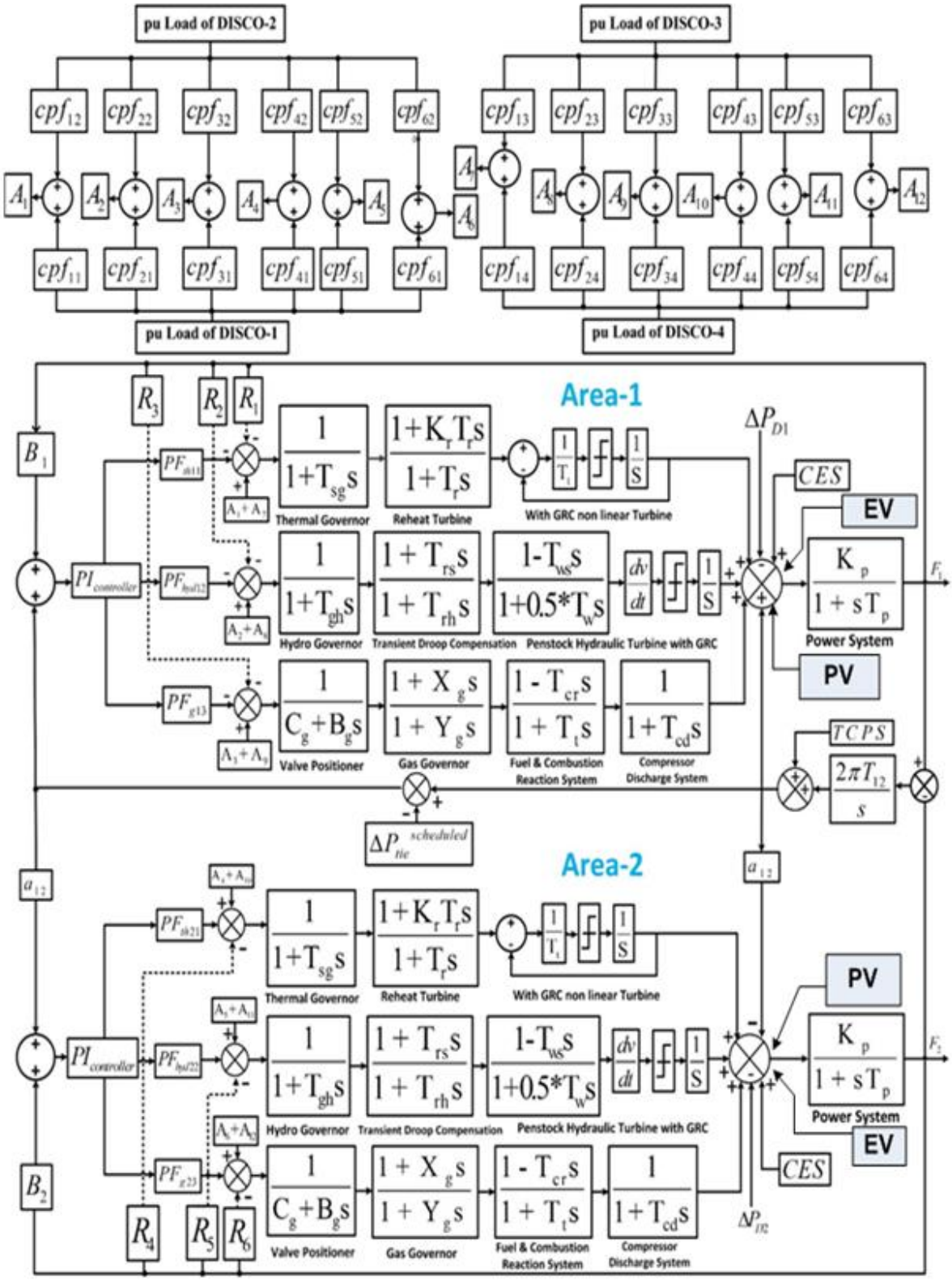

Fig.6.6 Proposed transfer function model with CES/TCPS and integrating RES as PV/EV sources

In addition, the developed deregulated power system was interconnected with PV/EV (EV/BEV) for reducing power system tie line power frequency complexity with pollution less and friendly environment nature. Here, the power demand in demand in each contract method similar with and without PV/EV. But due to add in PV/EV the deregulated power system frequency disturbance has been reduced extraordinarily. HHO, SMA, HHO-PS, and SMA-PS optimizers tuned PI controller is applied for the application of PV/EV for deregulated two area H-T-G sources deregulated power system with integrating CES/TCPS units. Fig 5.8 depicts the developed transfer function model with CES/TCPS and integrating RES as PV/EV sources.

Various studies for possibly realistic power contracts in a deregulated economy have been done. Each DISCO has a load demand of 0.005 pu MW. The simulation is run in accordance with the DPM and the contract between the GENCOs and DISCOs. Three distinct case studies were done, and the results are reported in the sections below.

6.6.1 POOLCO or UNILATEAL TRANSACTION METHOD

In this scenario, each GENCO can contribute to LFR based on their apfs, and each DISCO has a contract with the same GENCOs in their same region. i.e., apfs for thermal, hydro, and gas units are $PF_{\text{thermal1}} = 0.6$, $PF_{\text{hydro1}} = 0.3$, and PF_{gas1}=0.1, so that $PF_{\text{thermal1}} + PF_{\text{hydro1}} + PF_{\text{gas1}}$= 0.6+0.3+0.1 = 1 in area -1. And similarly, area-2 is $PF_{\text{thermal2}} + PF_{\text{hydro2}} + PF_{\text{gas2}} = 1$.

Here, only area - 1 has a load fluctuation, and the load demand of the DISCOs in area - 1 has been estimated to be 0.005 pu MW each.

$$\Delta p_{l2} = \Delta p_{l1} = 0.005\ pu\ MW$$

such that in area - 1 a total load change of 0.01 pu MW occurs. Such that, area – 2 load demand is zero ($\Delta p_{l4} = \Delta p_{l3} = 0$)

here, as per eqn (6.11) and (6.12)

$$\Delta p_{D1} = \Delta p_{l2} + \Delta p_{l1} = 0.005 + 0.005 = 0.01\ pu\ MW$$

$$\Delta p_{D2} = \Delta p_{l4} + \Delta p_{l3} = 0 \text{ pu MW}$$

in this method, distribution systems between each GENCO and DISCO in the system with a DPM matrix is

$$DPM = \begin{bmatrix} 0.33330 & 0.33330 & 0 & 0 \\ 0.33330 & 0.33330 & 0 & 0 \\ 0.33330 & 0.33330 & 0 & 0 \\ 0 & 0 & 0 & 0 \\ 0 & 0 & 0 & 0 \\ 0 & 0 & 0 & 0 \end{bmatrix}$$

As per eqn. (6.13). The power generation of GENCO in the suggested system is

For GENCO-1 (Thermal) in area-1:

$$\Delta p_{Gc1} = 0.3333 * 0.005 + 0.3333 * 0.005 + 0 + 0 = \ 0.003333\ pu\ MW$$

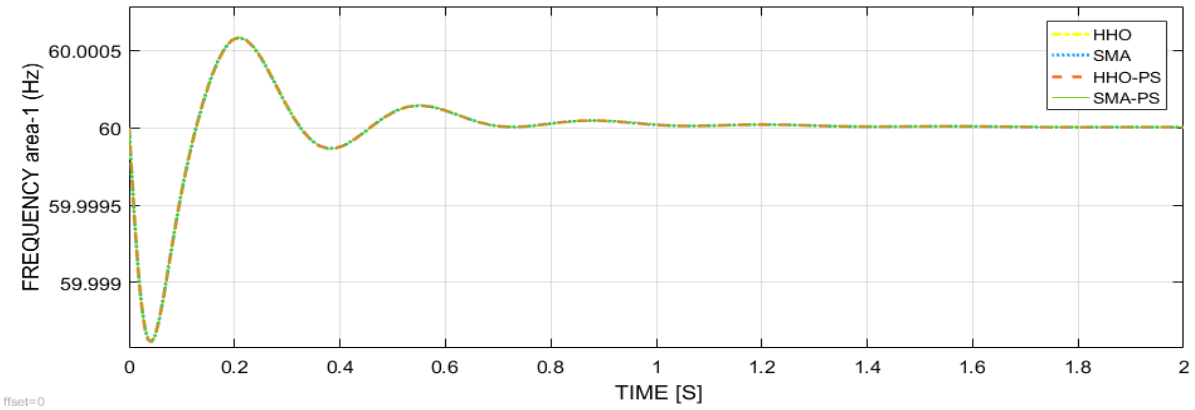

Fig.6.7 Area -1 frequencies responses of the developed deregulated system after adding PV/EV elements (POOLCO method)

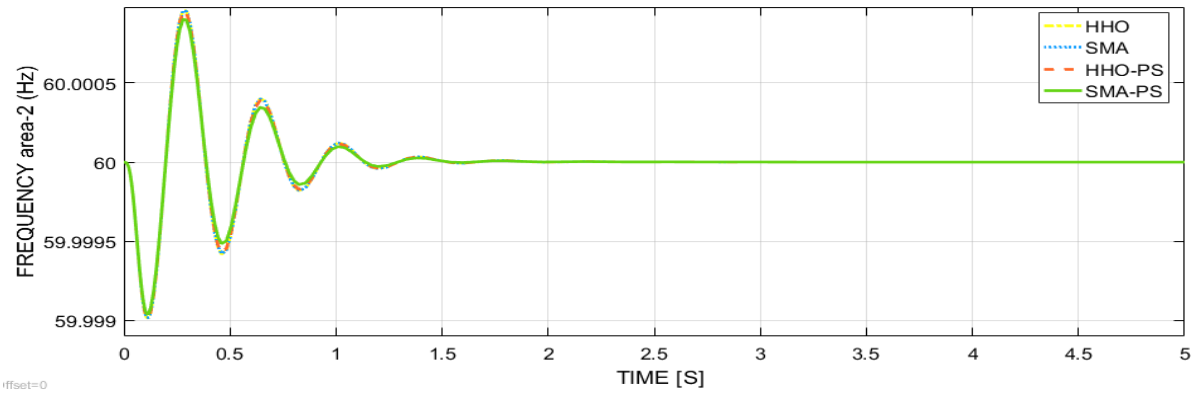

Fig.6.8 Area -1 frequencies responses of the developed deregulated system after adding PV/EV elements (POOLCO method)

Likewise, the power responses of GENCO-2 & 3 in area-1 are 0.00333 pu MW each, respectively. For area -2, $\Delta p_{Gc4} = \Delta p_{Gc5} = \Delta p_{Gc6} = 0$, Because, according to the established contract, DISCOs 3 and 4 in area-2 have no power need.

We can observe from following figures and analysis the frequency deviation decreased extraordinarily after integrating with PV/EV sources as power generating and storage sources.

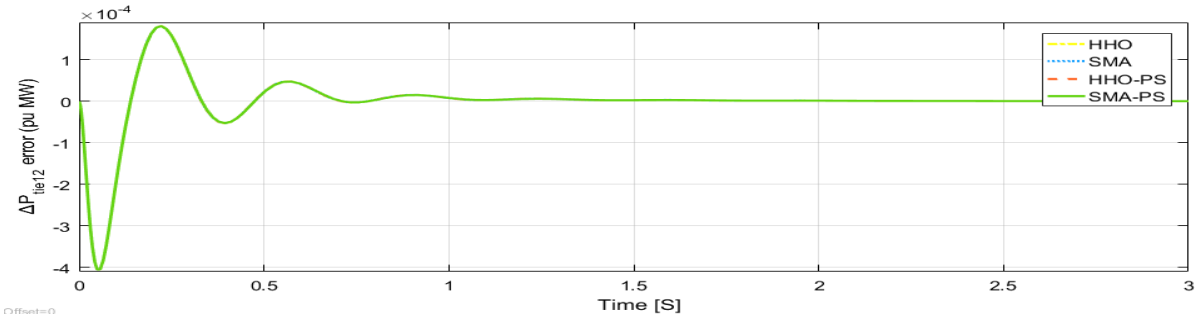

Fig.6.9 Responses of the various optimizers based TLP actual flow after addition of PV/EV (POOLCO method)

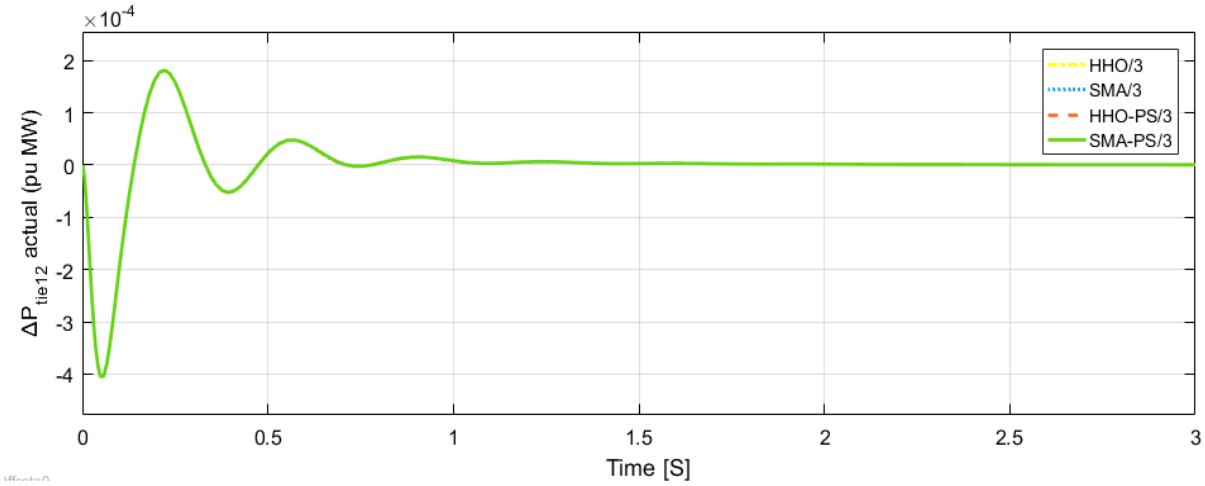

Fig.6.10 Responses of the various optimizers based TLP error flow after addition of PV/EV (POOLCO method)

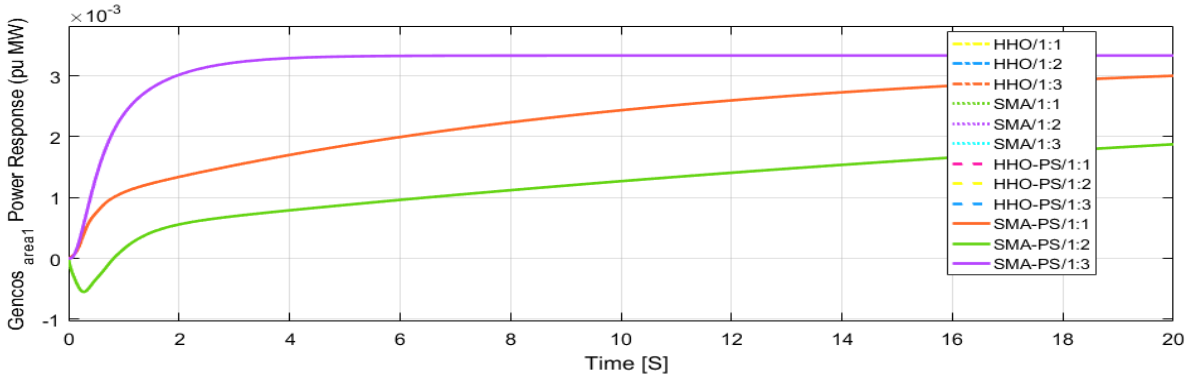

Fig.6.11 Power generating responses of area-1 for different optimized controller with PV/EV sources (POOLCO method)

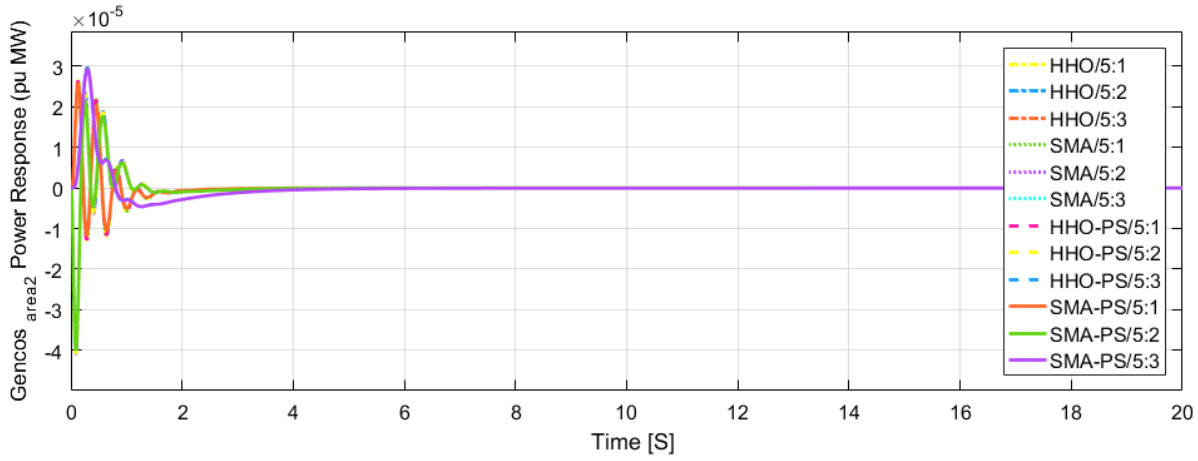

Fig.6.12 Power generating responses of area-2 for different optimized controller with PV/EV sources (POOLCO method)

Figures (6.7 to 6.12) demonstrate performance analysis for the POOLCO premised contract in the form of frequency deviation, tie - line error, and power generation after a sudden load shift in the proposed system.

Here, figs 6.9 & 6.10 demonstrate the fluctuation of frequencies in both regions with unilateral contraction in response to load change for the different optimization premised PI controller with the addition of PV/EV elements. As per the comparative analysis for HHO, SMA, HHO-PS and SMA-PS optimizers, it is stated that the SMA-PS approach produces area-2 (ΔF2) less peak overshoot value as compared to other optimizers.

Figures 6.11 & 6.12 depicts the fluctuation in tie line power in the region 1 power system for a 0.01 pu load shift. The results demonstrate that the SMA, HHO, hybrid SMA-PS hybrid HHO-PS approaches easily dampens real tie line power flow variation after a load shift.

The DISCOs of area 1 require power from their own area GENCOS, therefore the GENCOS must meet their contractual obligations. The generation responses of area 1 and area 2 GENCOs are shown in Fig 6.11 & 6.12, respectively. The waveforms obtained demonstrate that area1GENCOS, i.e., GENCO1, GENCO2, and GENCO3, generate electricity based on demand and contract participation factor. As a result, in steady state, the change in produced power by all GENCO's corresponding to this region is zero.

The SMA-PS optimizer equally performs with the other optimizers in terms of dynamic responsiveness, according to the generation response outputs of different GENCOS. It can be

observed from the above data that the SMA-PS optimizer approach achieves higher dynamics performances in terms of peak overshoot, value of ΔF2 for area – 2 frequency response.

6.6.2 BILATERAL TRANSACTION METHOD

This section, depicts a situation in which a DISCO and a GENCO conduct transactions in any other field, referred to as a bilateral transaction. In this situation, GENCOs and DISCOs fully adhere to the contract conditions [46]. In a deregulated market scenario, every GENCO and DISCO in the system under investigation as per DPM is

$$DPM = \begin{bmatrix} 0.2 & 0.1 & 0.3 & 0 \\ 0.2 & 0.2 & 0.1 & 0.1666 \\ 0.1 & 0.3 & 0.1 & 0.1666 \\ 0.2 & 0.1 & 0.1 & 0.3336 \\ 0.2 & 0.2 & 0.2 & 0.1666 \\ 0.1 & 0.1 & 0,2 & 0.1666 \end{bmatrix}$$

Each DISCO in control area, by the cpfs in the DPM matrix, requires 0.005 pu MW from the GENCOs, according to the bilateral transaction. As a result, area-1 and area-2 experience a total load disturbance of 0.010 pu MW. As a result, the power consumption in each location is 0.01 pu MW, according to eqns. (6.11) and (6.12). the power generation at area -1 as per Eqn. (6.13) as follows

For GENCO-1 (Thermal):

$$\Delta p_{Gc1} = 0.2 * 0.005 + 0.1 * 0.005 + 0.3 * 0.005 + 0 * 0.005 = \ 0.0030 \ pu \ MW$$

For GENCO-2 (Hydro):

$$\Delta p_{Gc2} = 0.2 * 0.005 + 0.2 * 0.005 + 0.1 * 0.005 + 0.1666 * 0.005 = \ 0.00333 \ pu \ MW$$

For GENCO-3 (Gas):

$$\Delta p_{Gc3} = 0.1 * 0.005 + 0.3 * 0.005 + 0.1 * 0.005 + 0.1666 * 0.005 = \ 0.00333 \ pu \ MW$$

In addition, for area-2 are,

$$\Delta p_{Gc4} = 0.2 * 0.005 + 0.1 * 0.005 + 0.1 * 0.005 + 0.3336 * 0.005 = \ 0.003668 \ pu \ MW$$

$$\Delta p_{Gc5} = 0.2 * 0.005 + 0.2 * 0.005 + 0.2 * 0.005 + 0.2 * 0.005 = \ 0.003833 \ pu \ MW$$

$\Delta p_{Gc6} = 0.1 * 0.005 + 0.1 * 0.005 + 0.2 * 0.005 + 0.1666 * 0.005 = \ 0.00283\ pu\ MW$, respectively.

The system performance has been evaluated in a bilateral contract with instantaneous changes in load demand between several GENCOs and DISCOs. On the above-mentioned DPM, the agreement between different DISCO and available GENCOs is simulated.

Figure 6.12 (a & b) depicts the frequency deviations in both areas in a deregulated market with a sudden load change. Because of the SMA-PS methodology, the system frequency deviations were performed with reduced peak overshoot, shorter settling time, and peak rise time, the findings show improved dynamics performance. In both regions, frequency deviations are immediately dampened.

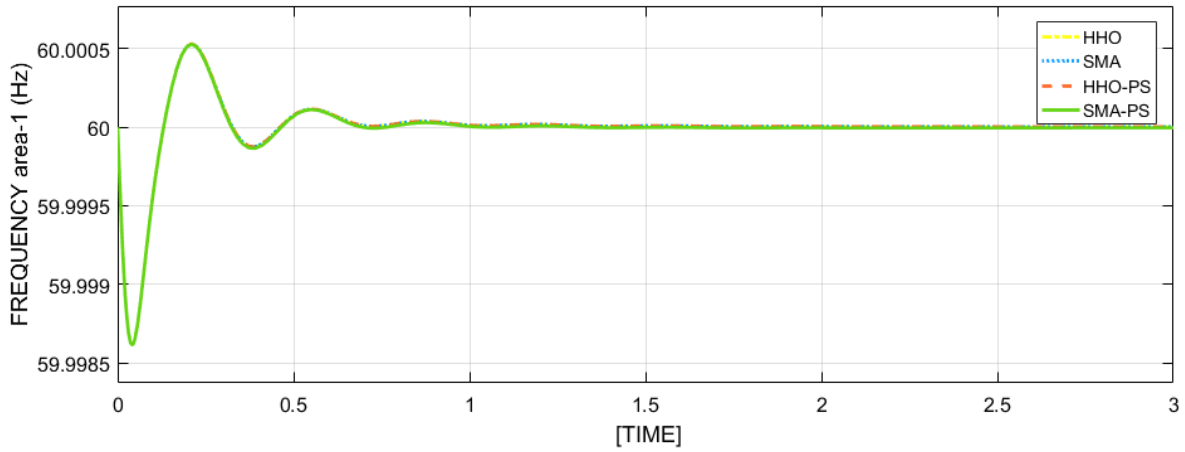

Fig.6.13 Area -1 Frequencies Responses Of The Proposed LFR Electrical System With Adding PV/EV elements (BILATERAL method)

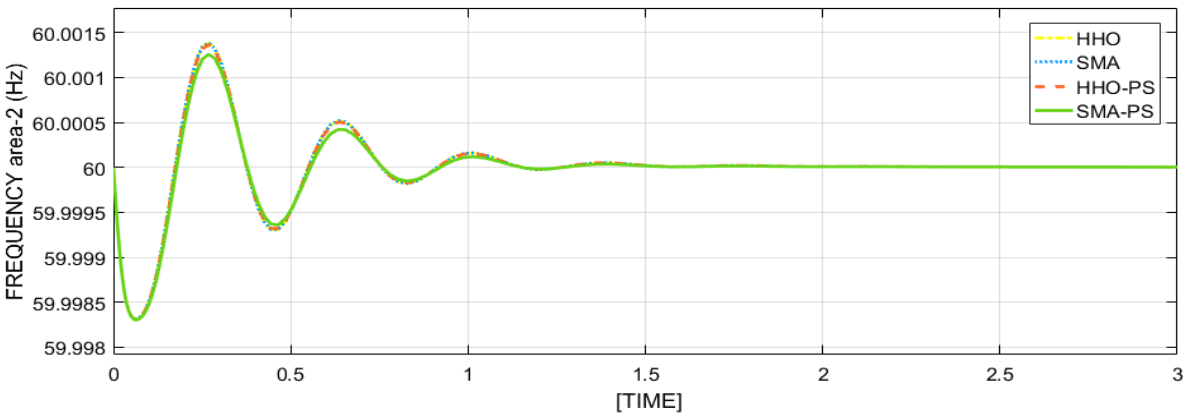

Fig.6.14 Area -1 frequencies responses of the proposed LFR electrical system with adding PV/EV elements (BILATERAL method)

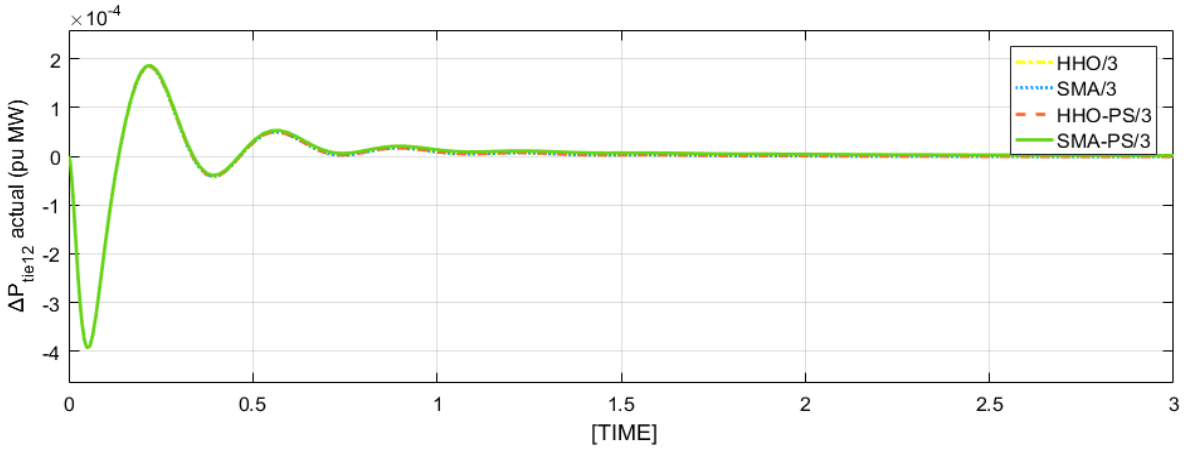

Fig.6.15 Actual TLP response after adding PV/EV model (BILATERAL method)

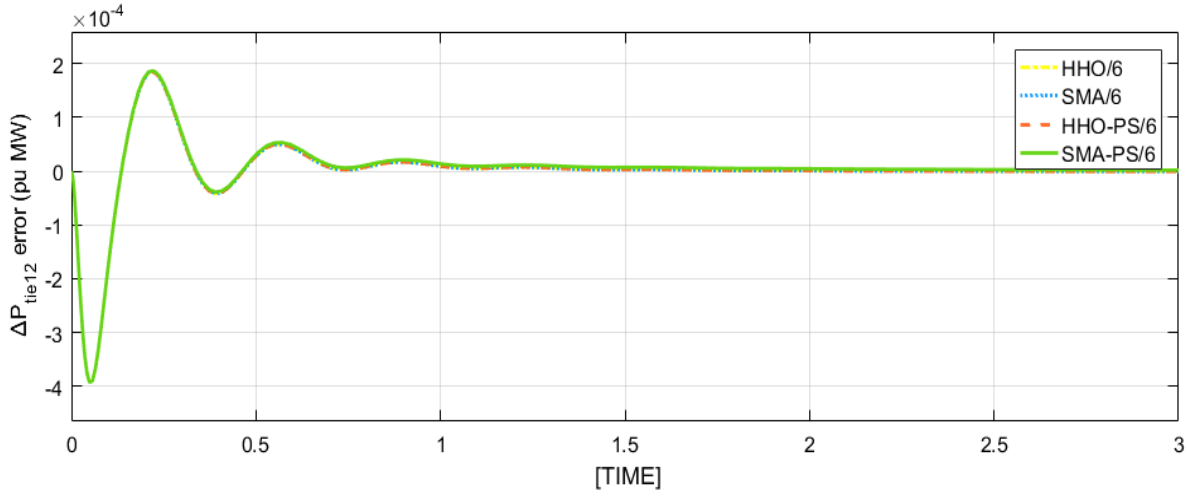

Fig.6.16 TLP error response after adding PV/EV model (BILATERAL method)

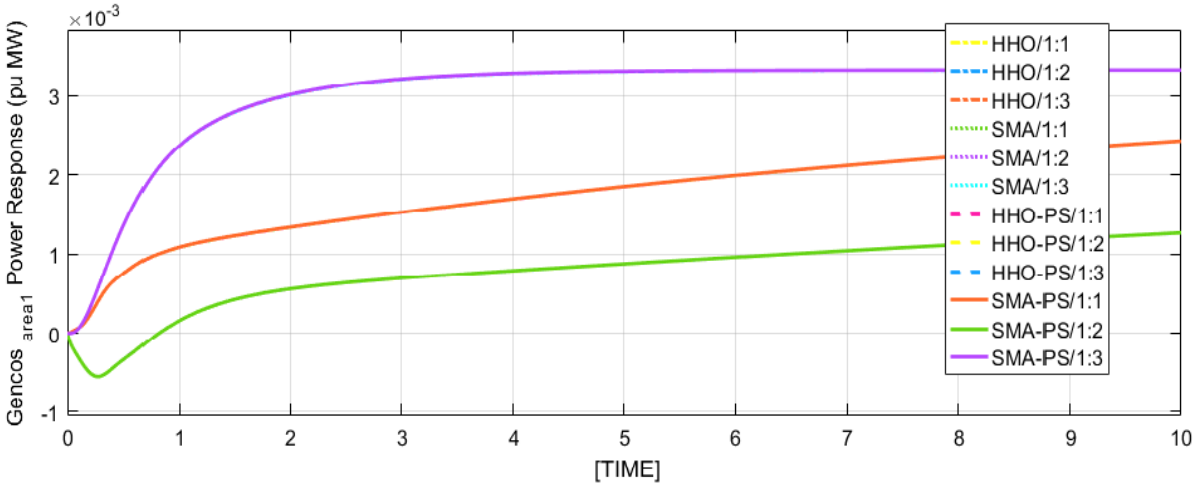

Fig.6.17 Power generation of the each GENCO responses for area -1 deregulated system with integrating PV/EV sources (BILATERAL method)

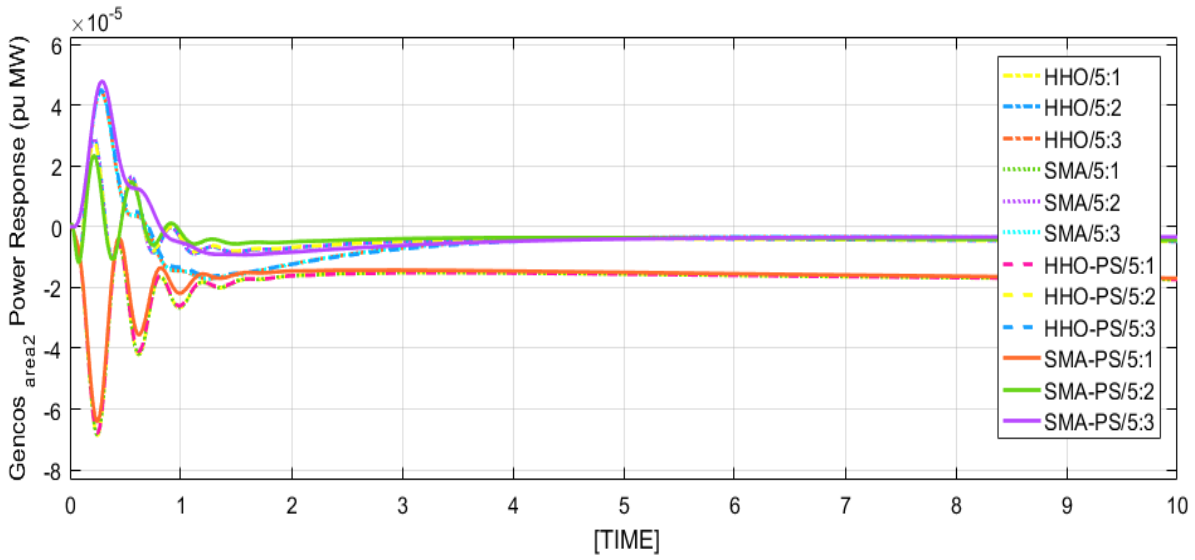

Fig.6.18 Power generation of the each GENCO responses for area -2 deregulated system with integrating PV/EV sources (BILATERAL method)

Figure 6.13 & 6.14 depicts the actual & error of the TLP in the developed power system. Figure 6.17 & 6.18 illustrates each area generation (GENCO -1 to GENCO – 6) performance of the system. From the obtained outcomes the proposed methodology SMA-PS optimizer performs superior performance than the HHO, SMA and HHO-PS optimizers in terms of peak overshot in area -2 frequency response.

Figures 6.13 to 6.18 depicts the simulated reaction of the proposed system under a bilateral contract in terms of oscillation changes in both areas, tie-line power reaction, and the different power generation units following a rapid load shift.

6.6.3 CONTRACT VIOLATION

Here, a contract violation happens when a DISCO deviates from the predetermined arrangement by requesting more power from the GENCOs than was specified in the contract. The GENCOs operating in the same region as the DISCO should ideally meet this uncontracted power load demand.

Consider case-B, in which DISCO requests 0.0030 pu MW of more energy, which the GENCOs of area-1 can assume as an excess load of 0.0030 pu MW after 7 seconds during simulation. Due to the DISCOs' request for more energy, the overall load demand in area-1 has increased to 0.0130 pu MW. Because the increased power demand happens solely in area-1, and area-2 remains unchanged. As a result of eqns. (6.15) and (6.16) the power demands in both regions are as follows.

$$\Delta p_{D1} = 0.005 + 0.005 + 0.003 = 0.013 \ pu\ MW$$

$$\Delta p_{D2} = 0.005 + 0.005 = 0.01 \text{ pu MW}$$

By using eqn (6.14), After a sudden unagreed load requirement, the generation response of several GENCOs in area-1 may be computed as

For GENCO-1 (Thermal):

$$\Delta p_{Gc1} = 0.2 * 0.005 + 0.1 * 0.005 + 0.3 * 0.005 + 0 * 0.005 + 0.6 * 0.003 = 0.0048\ pu\ MW$$

For GENCO-2 (Hydro):

$$\Delta p_{Gc2} = 0.2 * 0.005 + 0.2 * 0.005 + 0.1 * 0.005 + 0.1666 * 0.005 + 0.3 * 0.003 = 0.004233\ pu\ MW$$

For GENCO-3 (Gas):

$$\Delta p_{Gc3} = 0.1 * 0.005 + 0.3 * 0.005 + 0.1 * 0.005 + 0.1666 * 0.005 + 0.1 * 0.003 = 0.003633\ pu\ MW$$

In addition, for area-2 are,

$$\Delta p_{Gc4} = 0.2 * 0.005 + 0.1 * 0.005 + 0.1 * 0.005 + 0.3336 * 0.005 + 0.6 * 0.003 = 0.003668\ pu\ MW$$

$$\Delta p_{Gc5} = 0.2 * 0.005 + 0.2 * 0.005 + 0.2 * 0.005 + 0.2 * 0.005 + 0.3 * 0.003 = 0.003833\ pu\ MW$$

$\Delta p_{Gc6} = 0.1 * 0.005 + 0.1 * 0.005 + 0.2 * 0.005 + 0.1666 * 0.005 + 0.1 * 0.003 = 0.00283\ pu\ MW$ respectively.

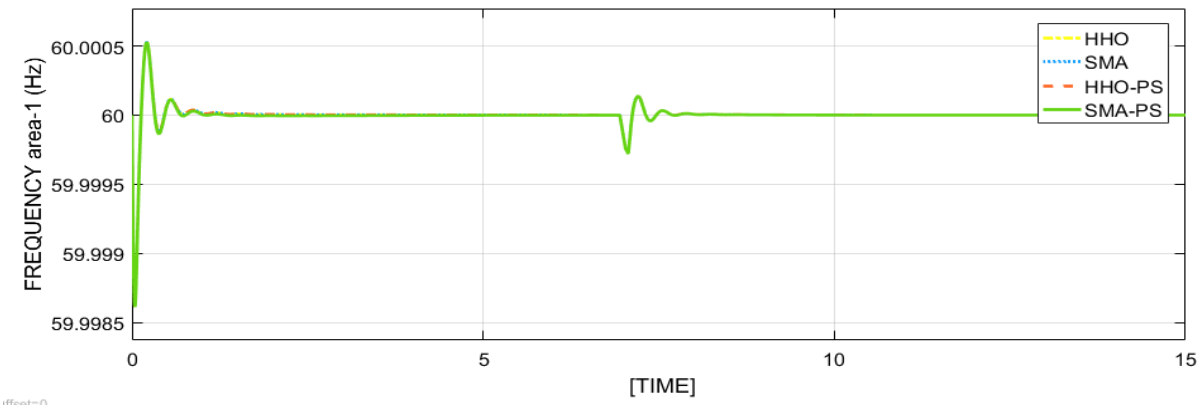

Fig.6.19 Area-1 frequency responses with addition of PV/EV sources (CV method)

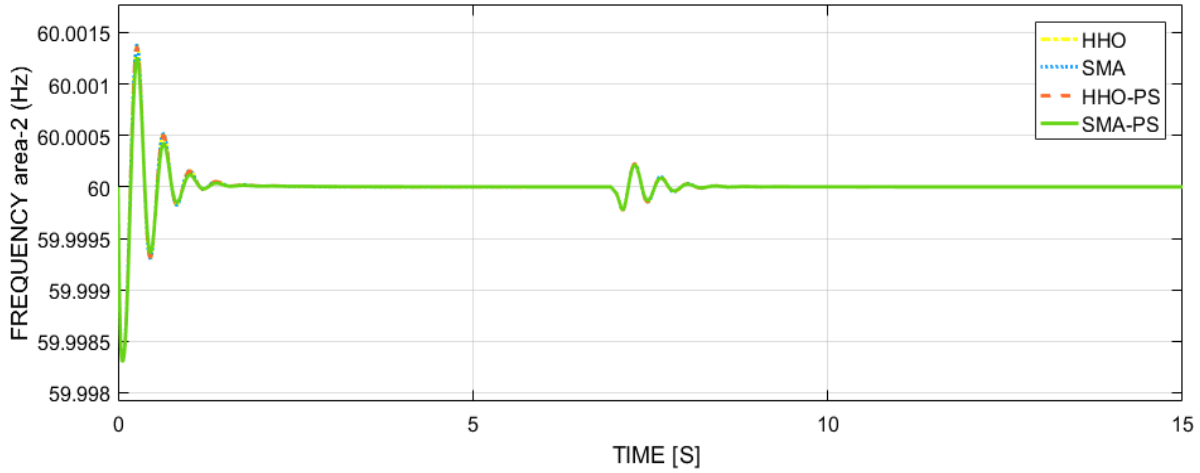

Fig.6.20 Area-2 frequency responses with addition of PV/EV sources (CV method)

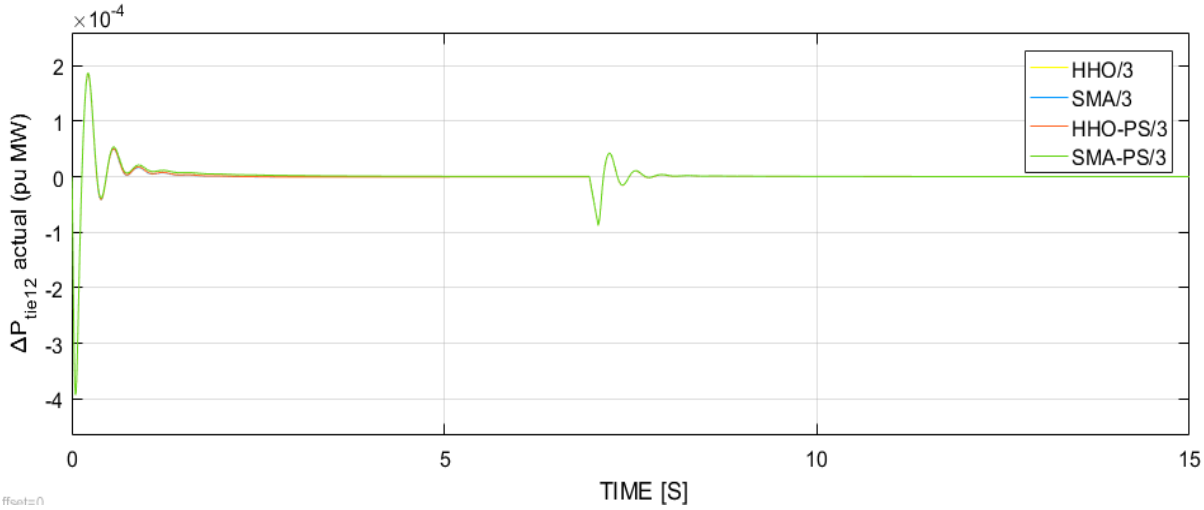

Fig.6.21 TLP actual power response of the system with PV/EV sources (CV method)

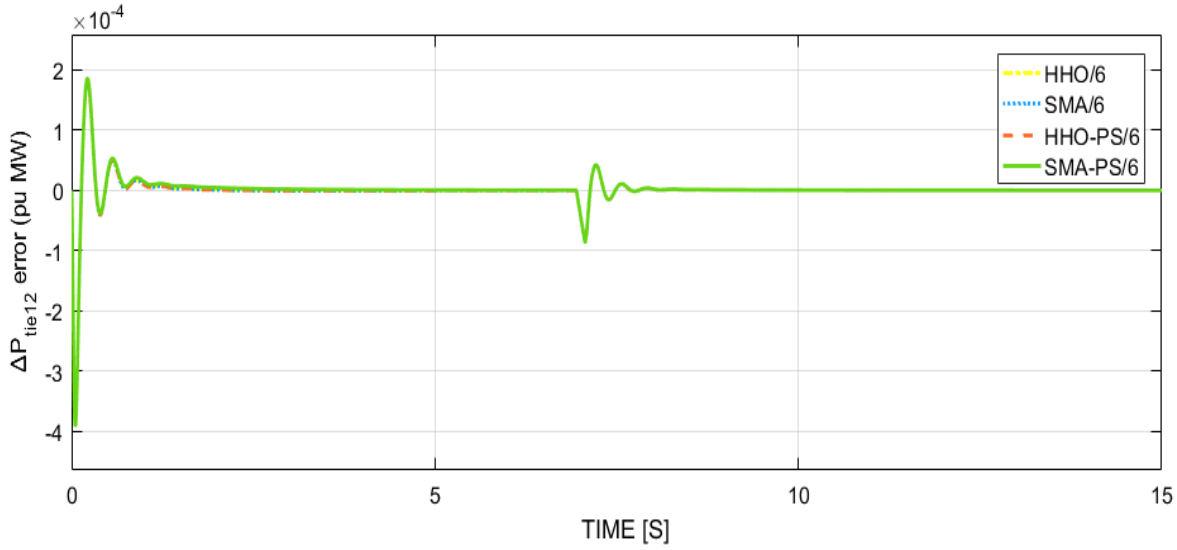

Fig.6.22 TLP error power response of the system with PV/EV sources (CV method)

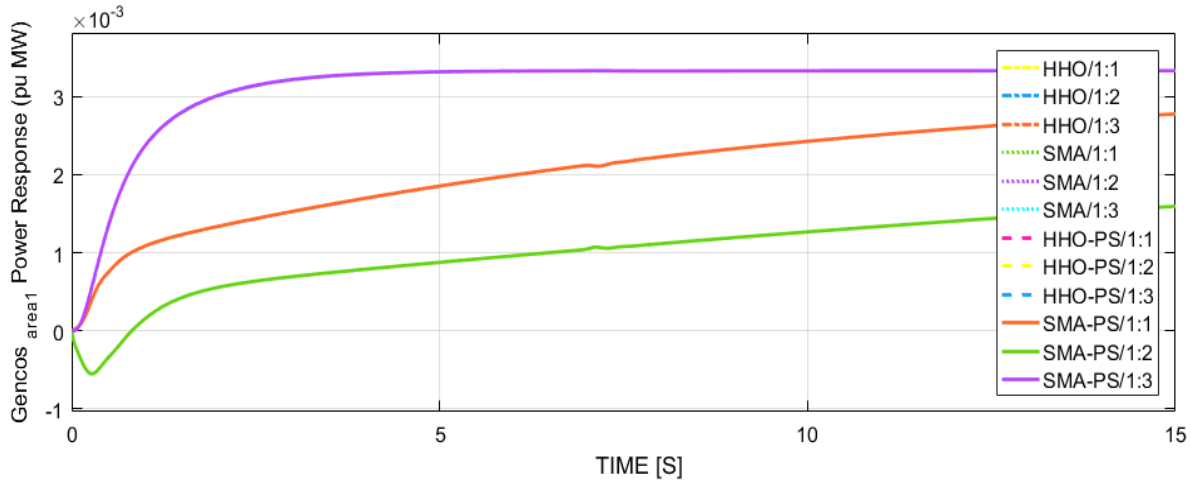

Fig.6.23 Area- 1 power generation responses with PV/EV sources (CV method)

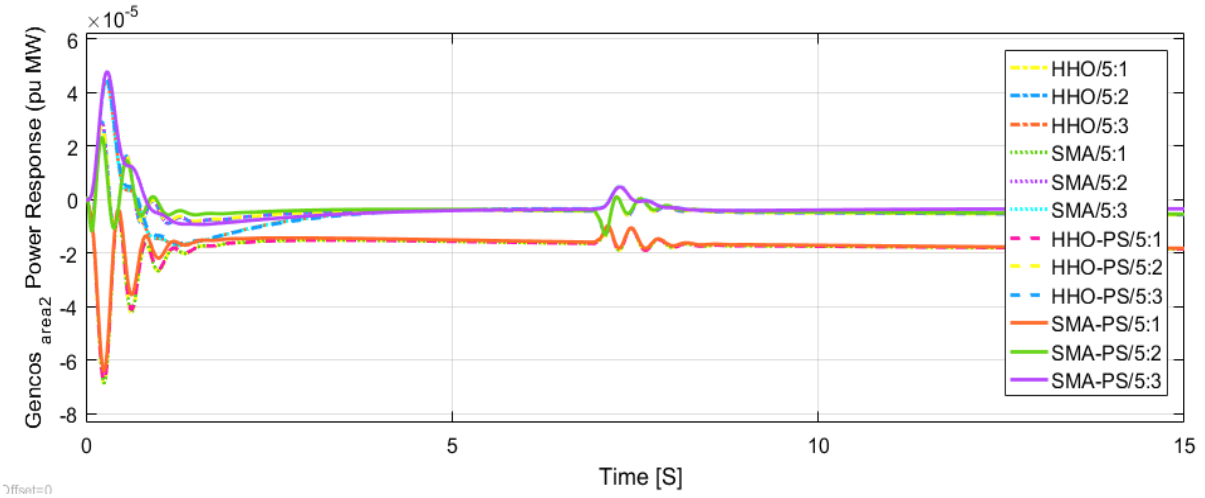

Fig 6.24 Area- 2 power generation responses with PV/EV sources (CV method)

In the presence of HHO, SMA, HHO-PS, and SMA-PS optimally tuned PI controllers, the various dynamic reaction in terms of frequencies, tie-line power, and power generation are illustrating in Figs. 6.19 – 6.24.

Table.6.3 During the POOLCO transaction case, a comparative study of several controllers for suggested DPS with RES/EV

Parameters		HHO	SMA	HHO-PS	SMA-PS
Settling time (sec)	ΔF_1	1	1	1	1
	ΔF_2	1.5	1.5	1.5	1.5

	P - tie	1.5	1.5	1.5	1.5
Under shoot response (Frequency HZ)	ΔF_1	59.99857	59.99857	59.99857	59.99857
	ΔF_2	59.9990	59.9990	59.9990	59.9988
	P - tie	-0.00041	-0.00041	-0.00041	-0.00041
Peak overshoot response (Frequency HZ)	ΔF_1	60.00078	60.00078	60.00078	60.00078
	ΔF_2	60.00098	60.00098	60.00098	60.00090
	P - tie	0.00019	0.00019	0.00019	0.00019

Table.6.4 During the bilateral case, a comparative study of several controllers for suggested DPS with RES/EV

Parameters		HHO	SMA	HHO-PS	SMA-PS
Settling time (sec)	ΔF_1	1	1	1	1
	ΔF_2	1.5	1.5	1.5	1.5
	P - tie	1.2	1.2	1.2	1.2
Under shoot response (Frequency HZ)	ΔF_1	59.99859	59.99859	59.99859	59.99859
	ΔF_2	59.99850	59.99850	59.99850	59.99850
	P - tie	-0.00039	-0.00039	-0.00039	-0.00039
	ΔF_1	60.00054	60.00054	60.00054	60.00054

Peak overshoot response (Frequency HZ)	ΔF_2	60.00138	60.00138	60.00136	60.00125
	P - tie	0.00019	0.00019	0.00019	0.00019

Table.6.5 During the contract violation case, a comparative study of several controllers for suggested DPS with RES/EV

Parameters		HHO	SMA	HHO-PS	SMA-PS
Settling time (sec)	ΔF_1	7.8	7.8	7.8	7.8
	ΔF_2	8	8	8	8
	P - tie	7.6	7.6	7.6	7.6
Under shoot response (Frequency HZ)	ΔF_1	59.99858	59.99858	59.99858	59.99858
	ΔF_2	59.99830	59.99830	59.99830	59.99830
	P - tie	-0.000088	-0.000088	-0.000088	-0.000088
Peak overshoot response (Frequency HZ)	ΔF_1	60.00055	60.00055	60.00055	60.00055
	ΔF_2	60.00140	60.00140	60.00140	60.00125
	P - tie	0.000043	0.000043	0.000043	0.000043

Figures 6.7, 6.8, 6.13, 6.14, 6.19, & 6.20 show the responses of suggested system with PV/EV elements in a deregulated electricity market under bilateral, contract violation and unilateral cases, respectively. The collected findings indicate that HHO, SMA, and HHO-PS based PI controllers outperforms every contract scenario. However, when compared to HHO, SMA, and

HHO-PS based PI controllers, all the controllers quickly achieve the steady state with reduced oscillation in terms of settling time and undershoot. In case of peak overshoot, when compared to HHO, SMA, and HHO-PS based PI controllers, SMA-PS tuned PI controller performs greater efficacy results for area -2 frequency response. In addition, the EV/PV unit transfers/stores its generated/observed energy to the grid and improves the system's dynamic response by quickly resolving oscillation and overshoot caused by unexpected load fluctuations. Furthermore, when compared to the HHO, SMA, and HHO-PS, and SMA-PS based PI controller-based PI controllers with PV/EV units, immediately dampens the frequency changes in both regions and offered superior dynamics.

Figures 6.9, 6.10, 6.15, 6.16, 6.21 & 6.22 show the influence of optimally tuned PI controllers on TLP reaction under contract breach, unilateral and bilateral contract scenarios in a system, respectively. In the unilateral contract scenario, there is no electricity demand between area-1 & 2. As a result, the tie line's planned power is reduced to zero. The actual tie-line power settles to 0.0003340 pu MW in the bilateral and contract breach scenarios, which is the planned power on the tie-line in the steady state. The theoretical and simulated values of real power flow in the tie line between areas 1 and 2 are identical and exactly as specified in the contract. In every contract scenario in the deregulated energy market, the performance of the SMA-PS based PI controller outperforms the HHO, SMA based PI controller with PV/EV unit in terms of peak overshoot in area -2 frequency response as shown in the data. and HHO-PS, HHO, and SMA based PI controller achieves results that are comparable to SMA-PS. The electricity flow through the tie line between the connecting locations follows the established contract's scheduled transaction. After achieving steady state, the tie line error becomes zero. By regulating the grid oscillations, the EV/PV unit achieves improved dynamic performance in the system. The acquired findings support the PV/EV unit's efficacy in the planned investigation. The objective value for LFR of deregulated electric system with and without CES/TCPS units is 11.41406 and 2.0069. further after adding PV/EV in the LFR system the performance index objective value is 0.0018 for the SMA-PS optimizer.

Figures 6.11, 6.12, 6.17, 6.18, 6.23 & 6.24 shows generation responses of all possible contract cases. The simulated response shown in Fig. 6.23 demonstrates that in the unilateral scenario, the area-1 GENCO 1, 2, & 3, generate power in accordance with demand and their cpf. The DISCOs have no demand in area 2, as seen in Fig. 6.24. As a result, at the steady state, the change in produced power by all GENCOs corresponding to this region is zero. Similarly, Fig.

6.17, & 6.18 shows the power output response of each GENCO in the proposed system under a bilateral contract scenario. Each GENCO reacts to its predetermined transaction contract by generating the precise quantity of electricity required to meet the demands of multiple DISCOs. Figure 6.23 & 6.24 depicts the dynamical reactions of power generation by various GENCOs in all control regions under the contact violation situation. The uncontracted load demand affects the produced power response of area-1's GENCO 1, 2, & 3. However, area-2's GENCO-4, 5, & 6 are unaffected by the uncontracted load. As indicated in the data, the generation reactions of area-1 GENCOs to meet the surplus power demand are clearly represented in their outputs. Every generator in area-1 reacts in accordance with its area participation factor and soon reaches the new generation limitations to meet the DISCOs' increased power demand.

The system with a SMA-PS optimized controller with RES and EV has a superior dynamic reaction than the system without it. the action of the EV unit in the system reduces the deviation, and the generators soon reach their stability (refer chapter - 3). After including the EV unit, the system's setup time and peak overshoot are reduced, and oscillations are damped more rapidly. In over and under frequency occurrences, the EV unit swaps power with the grid to lessen the load on connecting conventional generating plants and to assist sustain the frequency response much faster than the present primary reaction.

Tables 6.3 – 6.5 illustrates the LFR of proposed deregulated power system with integration of RES and Electrical vehicle to the grid in each area comparative analysis of SMA-PS tuned PI controller with HHO, SMA, and SMA-PS tuned PI controller under contract violation, POOLCO, and bilateral transaction methods. The analysis reveals that the proposed system dampens its frequency oscillations after integrating RES/EV in grid system effectively. The SMA-PS tuned PI controller outperforms the other methods.

6.7 **SENSITIVITY ANALYSIS**

To prove effectiveness of the developed electric network with CES and EVs, quality and robustness of the proposed hybrid memetic SMA-PS and hybrid memetic HHO-PS premised PI controllers, this investigation work has been subjected to a variety of sensitive analyses, as well as a wide range of system-dependent factors. In this regard, T_{sg} time constant of governor and H inertia constant (*which leads change the load constant* T_{ps}) are regulated and varied from their nominal values in the range of ±25%. To verify the robustness, POOLCO exchange tactic is taken to consideration for analysis of the DPS network

with CES and EV units. Due to variation the T_{sg} and H parameters in the developed DPS network with CES and EV, the gain parameters are varying and the those are tabulated in Tables 6.6, 6.8, 6.10, and 6.12. later, the performance analysis of the proposed network with CES and EV are depicted in tables 6.7, 6.9, 6.11, and 6.13. The performance analysis of the network with dynamic reactions were depicted in Fig. 6.25 to 6.36 due to variation in T_{sg} and H and 'load' are simple overlap with each other. The analysis report concludes proposed hybrid memetic SMA-PS and hybrid memetic HHO-PS premised PI controller is robust than classic SMA and HHO in nature. The performance indexes such as ITAE values, $T_{setting\ \text{time}}$ $P_{overshoot}$ *and* $P_{undershoot}$, Tables 6.6, 6.8, 6.10, and 6.12 illustrates standard and parametric variability instances for the network underneath the POOLCO exchanged tactic. The suggested optimum hybrid memetic SMA-PS optimizer controller is a resilient controller, as shown in Tables 6.7, 6.9, 6.11, and 6.13, so there is no need to retune its metrics whenever the network is subjected to either fluctuation in loading circumstance or modification in network parametric. Figures 6.25 to 6.26 illustrate the switching frequency of Area-1, Area-2, and TLP flow reactions as a function of T_{sg}. The effect of changing operational loading circumstances on the network responses is minor, as shown in Figures 6.25 to 6.36. As a result, the suggested control technique can be concluded to offer stable control across a wide range of network loads and parametric changes.

Table.6.6 Performance gain values with the proposed system with CES and EVs after changing the Tsg = -25%

Tsg=-25%	k_1^P	k_1^i	k_2^P	k_2^i	J
HHO	-2.835528958	-3.356847447	-5	-5	0.008228
SMA	-2.812526149	-3.429407874	-5	-5	0.008221
HHO-PS	-2.807733095	-3.446784582	-5	-5	0.008221
SMA-PS	2.984694435	-3.589271743	-5	-5	0.007093

Table.6.7 Performance of the proposed system with CES and EVs after changing the Tsg = -25%

Tsg = - 25%		HHO	SMA	HHO-PS	SMA-PS
Settling time (sec)	ΔF_1	2.6	2.6	2.5	2
	ΔF_2	2.1	2.1	2	1.8

	P - tie	2.8	2.8	2.6	2.4
Under shoot response	ΔF_1	60.00107	60.00108	60.00108	60.00102
	ΔF_2	60.0015	60.0015	60.0015	60.0015
	P - tie	0.0003	0.0003	0.0003	0.0003
Peak overshoot response	ΔF_1	59.99842	59.99842	59.99842	59.99843
	ΔF_2	59.9986	59.9986	59.9986	59.9986
	P - tie	-0.00048	-0.00048	-0.00048	-0.00047

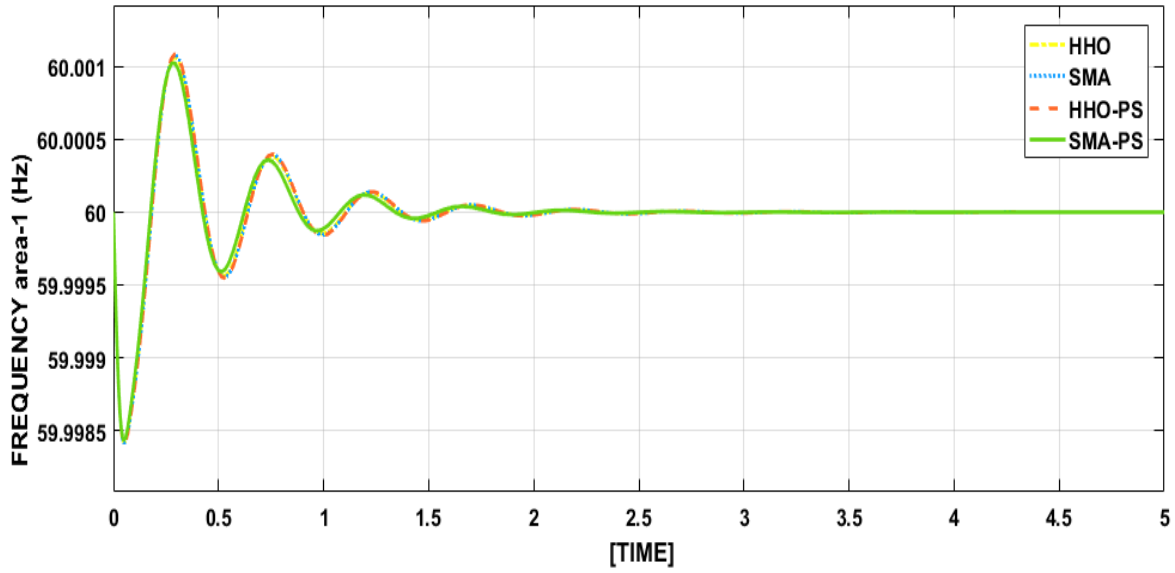

Fig.6.25 Proposed system area- 1 frequency reaction after changing the Tsg = - 25%

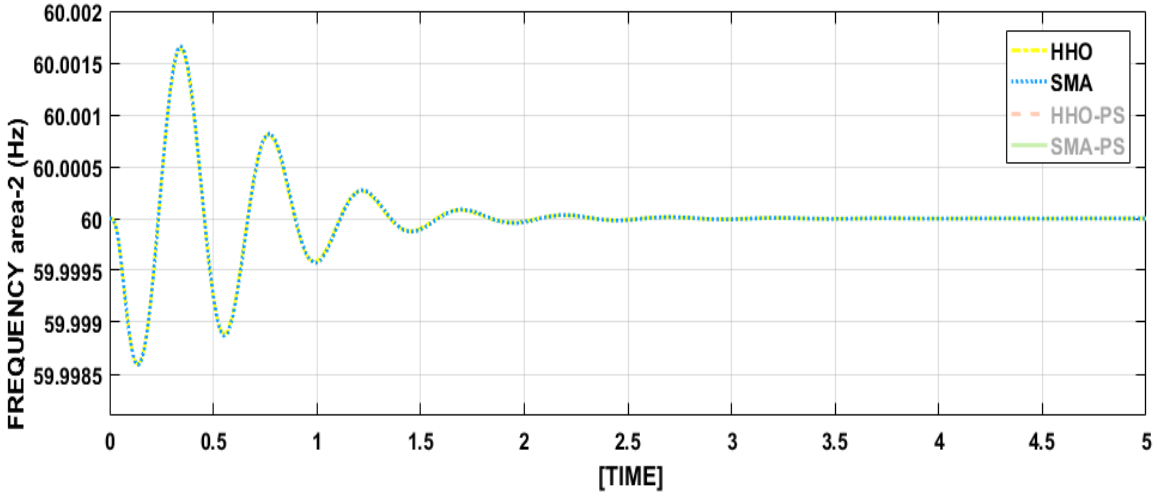

Fig.6.26 Proposed system area- 1 frequency reaction after changing the Tsg = - 25%

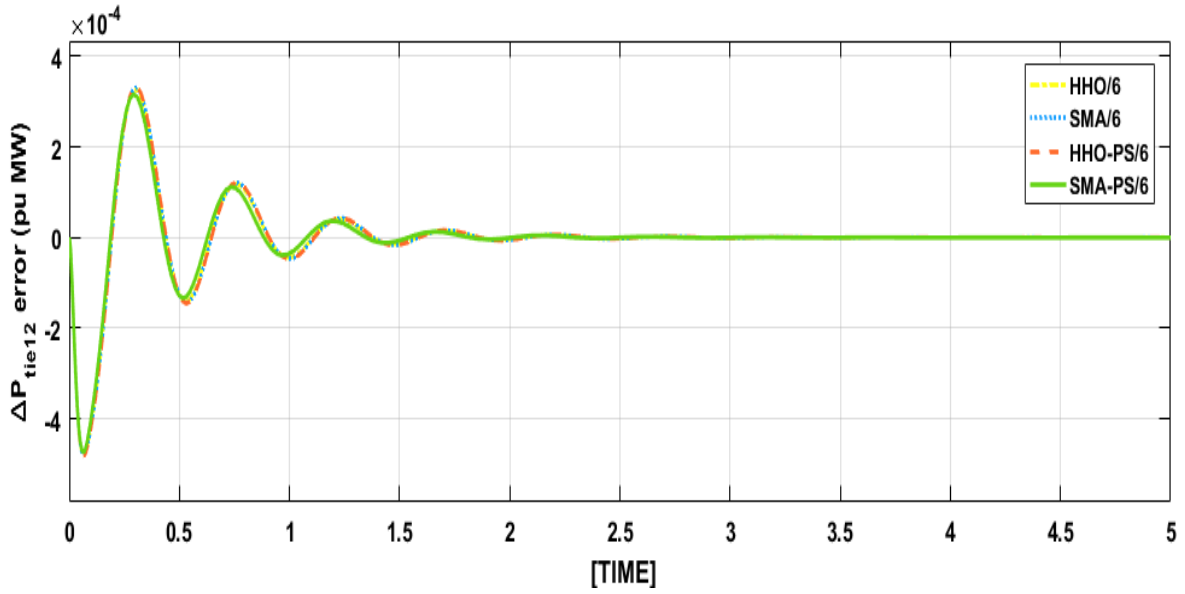

Fig.6.27 Proposed system TLP flow reaction after changing the Tsg = - 25%

Table.6.8 Performance gain values with the proposed system with CES and EVs after changing the Tsg = +25%

Tsg= + 25%	k_1^P	k_1^i	k_2^P	k_2^i	J
HHO	-2.89802	-3.94025	-4.99927	-4.99934	0.008334
SMA	-2.83182	-3.26025	-5	-5	0.008245
HHO-PS	-2.82306	-3.19495	-5	-5	0.008235
SMA-PS	-4.7917	-3.53575	-12.1295	-9.11896	0.006118

Table.6.9 Performance of the proposed system with CES and EVs after changing the Tsg = +25%

Tsg = + 25%		HHO	SMA	HHO-PS	SMA-PS
Settling time (sec)	ΔF_1	2	2	1.8	1.2
	ΔF_2	2.2	2.2	2	1
	P - tie	1.8	1.8	1.7	1.3
Under shoot response	ΔF_1	60.001	60.001	60.001	60.0005
	ΔF_2	60.0016	60.0016	60.0016	60.0007
	P - tie	0.0032	0.0032	0.0032	0.0018
Peak overshoot response	ΔF_1	59.9985	59.9985	59.9985	59.9988
	ΔF_2	59.9985	59.9985	59.9985	59.9988
	P - tie	-0.0048	-0.0048	-0.0048	-0.0004

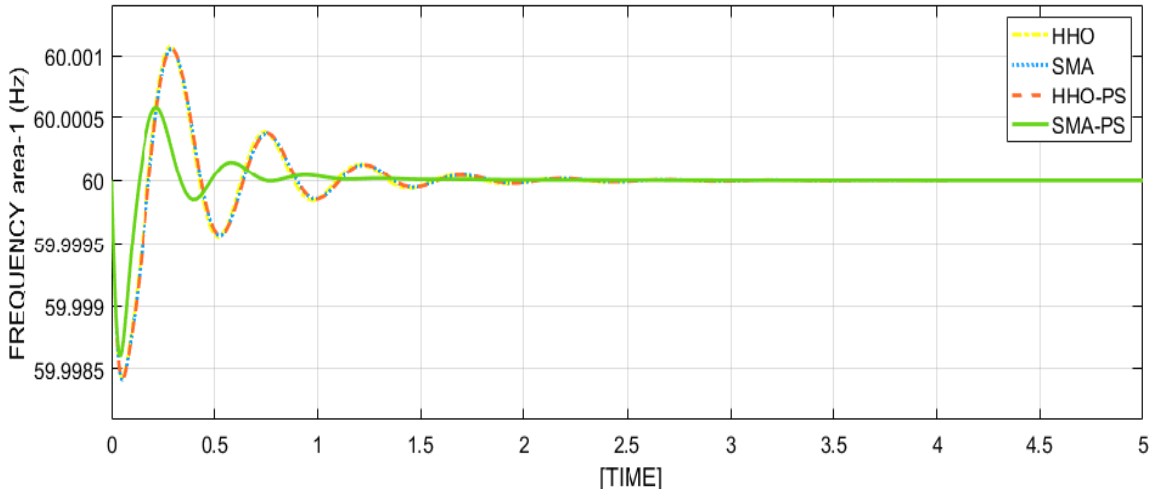

Fig.6.28 Proposed system area- 1 frequency reaction after changing the Tsg = + 25%

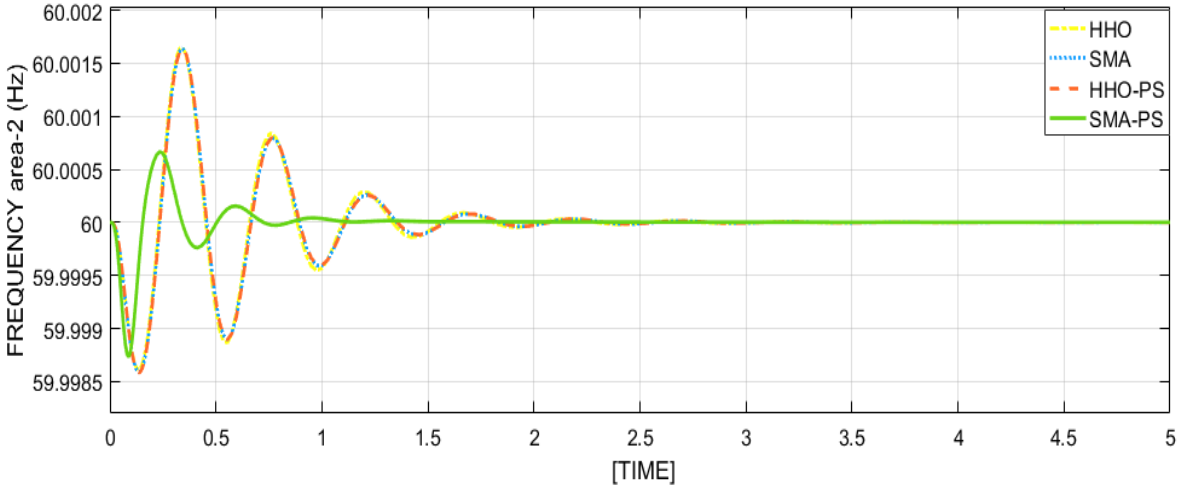

Fig.6.29 Proposed system area- 2 frequency reaction after changing the Tsg = + 25%

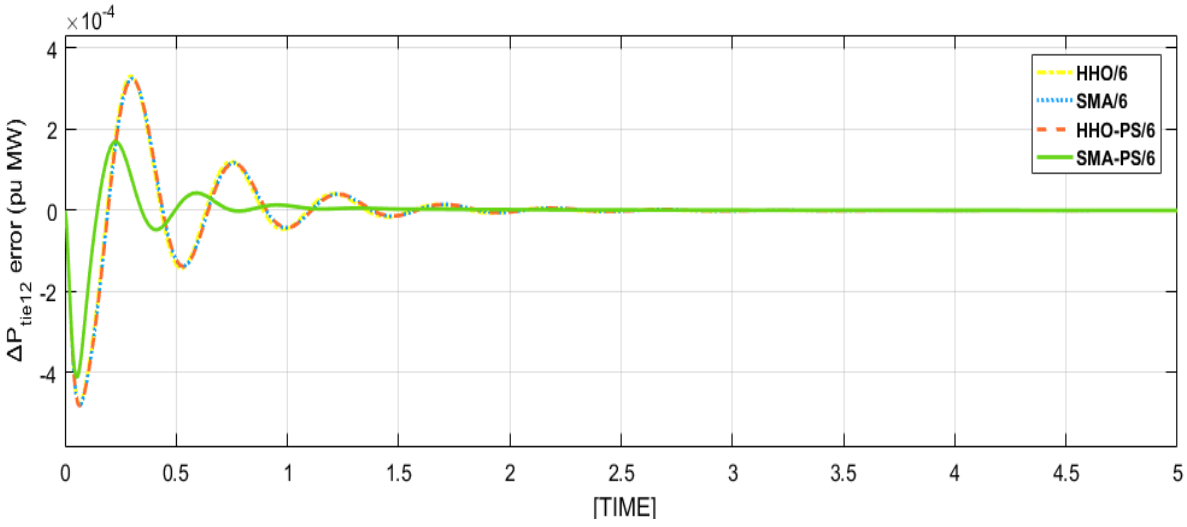

Fig.6.30 Proposed system TLP flow reaction after changing the Tsg = + 25%

Table.6.10 Performance gain values with the proposed system with CES and EVs after changing the H = +25%

H= + 25%	k_1^P	k_1^i	k_2^P	k_2^i	J
HHO	-5	-3.28004	-3.19099	-2.52866	0.013416
SMA	-2.95749	-2.80443	-5	-4.79916	0.011999
HHO-PS	-2.88002	-2.55558	-5	-5	0.011888
SMA-PS	-2.95749	-2.80443	-5	-4.79916	0.008507

Table 6.11 performance of the proposed system with CES and EVs after changing the H = +25%

H= + 25%		HHO	SMA	HHO-PS	SMA-PS
Settling time (sec)	ΔF_1	2.2	2.1	2	1.2
	ΔF_2	2.4	2.4	2.3	1.3
	P - tie	2.4	2.4	2.3	1.3
Under shoot response	ΔF_1	60.0012	60.0012	60.001	60.0006
	ΔF_2	60.0017	60.0017	60.0016	60.0007
	P - tie	0.0032	0.0032	0.0031	0.0002
Peak overshoot response	ΔF_1	59.9984	59.9984	59.9984	59.9985
	ΔF_2	59.9986	59.9986	59.9986	59.9988
	P - tie	-0.0005	-0.0005	-0.00048	-0.0004

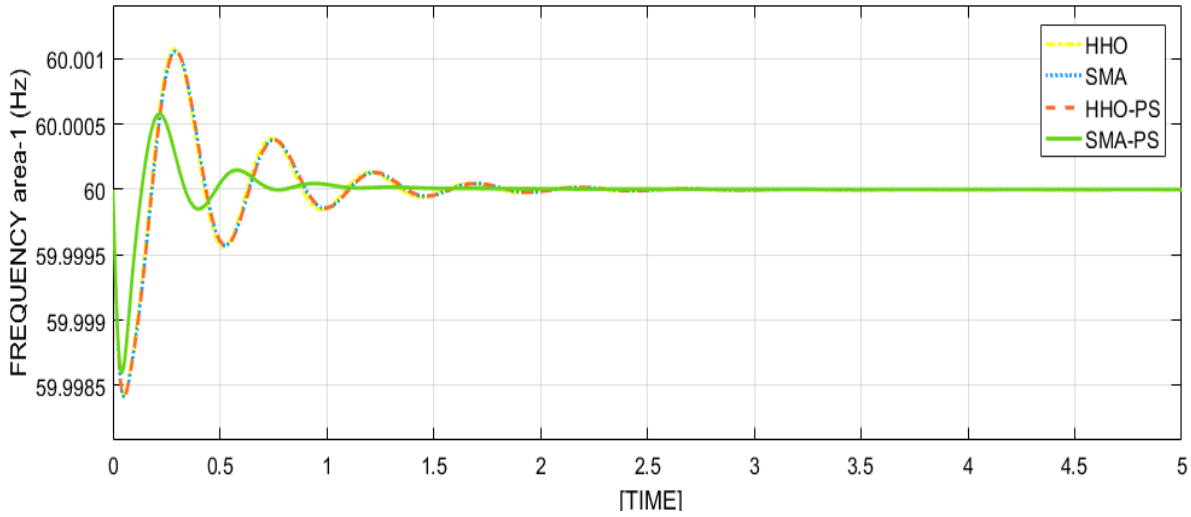

Fig.6.31 Proposed system area- 1 frequency reaction after changing the H = + 25%

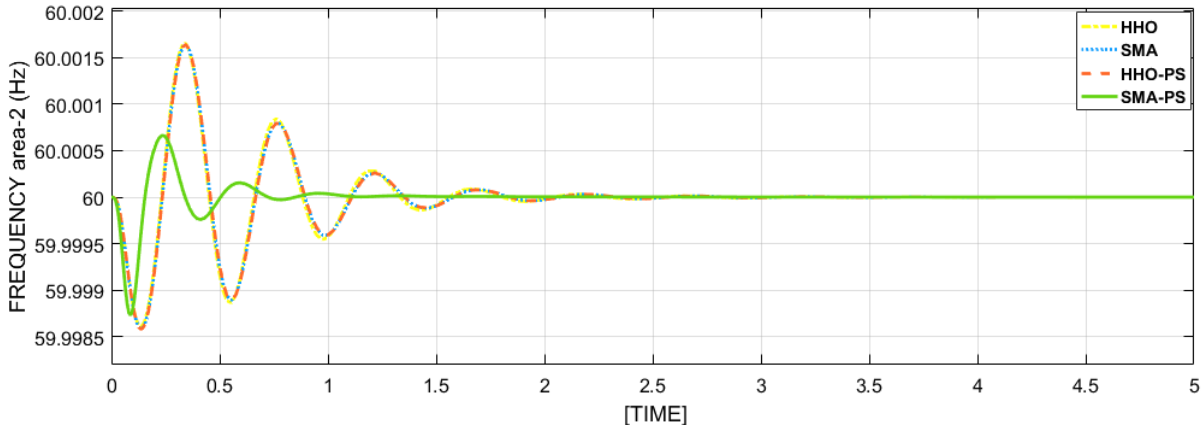

Fig.6.32 Proposed system area- 2 frequency reaction after changing the H = + 25%

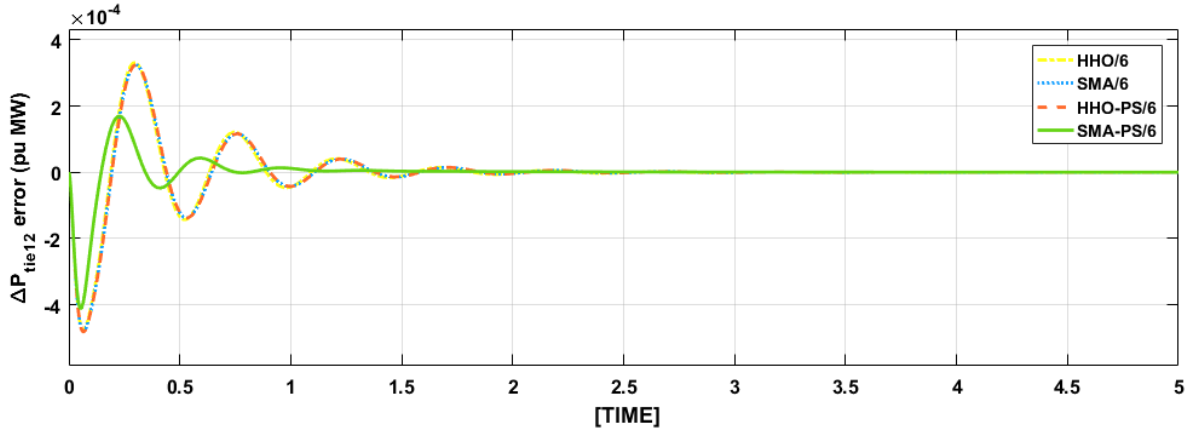

Fig.6.33 Proposed system TLP flow reaction after changing the H = + 25

Table.6.12 Performance gain values with the proposed system with CES and EVs after changing the H= -25%

H= - 25%	k_1^P	k_1^i	k_2^P	k_2^i	J
HHO	-5	-5	-3.06202	-5	0.005955
SMA	-2.74816	-5	-5	-5	0.005532
HHO-PS	-2.75133	-5	-5	-4.99817	0.005524
SMA-PS	-3.97553	-4.89238	-8.53073	-9.58541	0.004373

Table.6.13 Performance of the proposed system with CES and EVs after changing the H = - 25%

H= - 25%		HHO	SMA	HHO-PS	SMA-PS
Settling time	ΔF_1	1.8	1.8	1.1	1.2

(sec)	ΔF_2	2	2	1.8	1.3
	P - tie	1.9	1.8	1.1	1.2
Under shoot response	ΔF_1	60.0012	60.0012	60.0007	60.0005
	ΔF_2	60.0015	60.0015	60.0008	60.0008
	P - tie	0.0037	0.0037	0.0019	0.0002
Peak overshoot response	ΔF_1	59.9985	59.9985	59.9983	59.9984
	ΔF_2	59.9983	59.9987	59.9983	59.9987
	P - tie	-0.0048	-0.0048	-0.0042	-0.0043

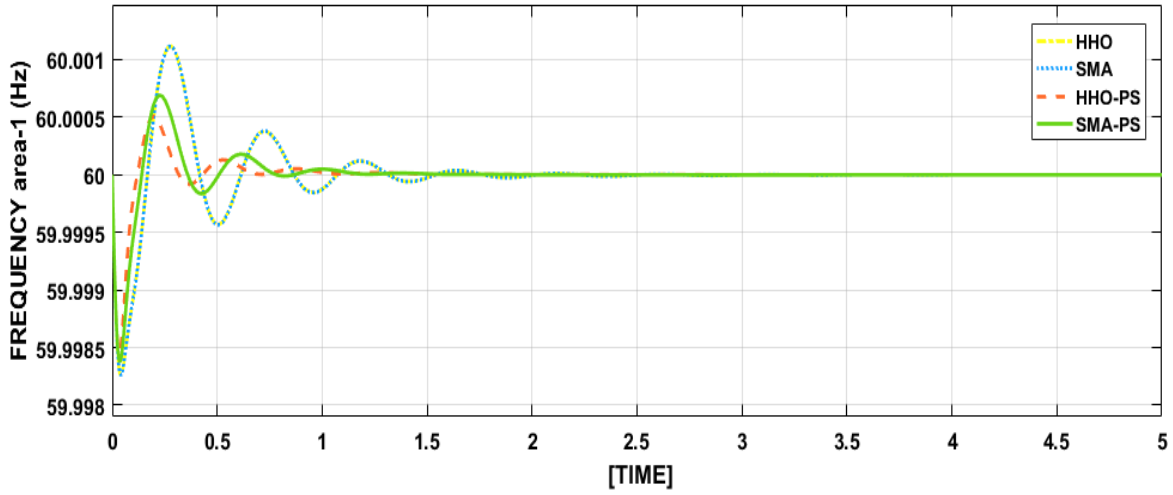

Fig.6.34 Proposed system area- 1 frequency reaction after changing the H = - 25%

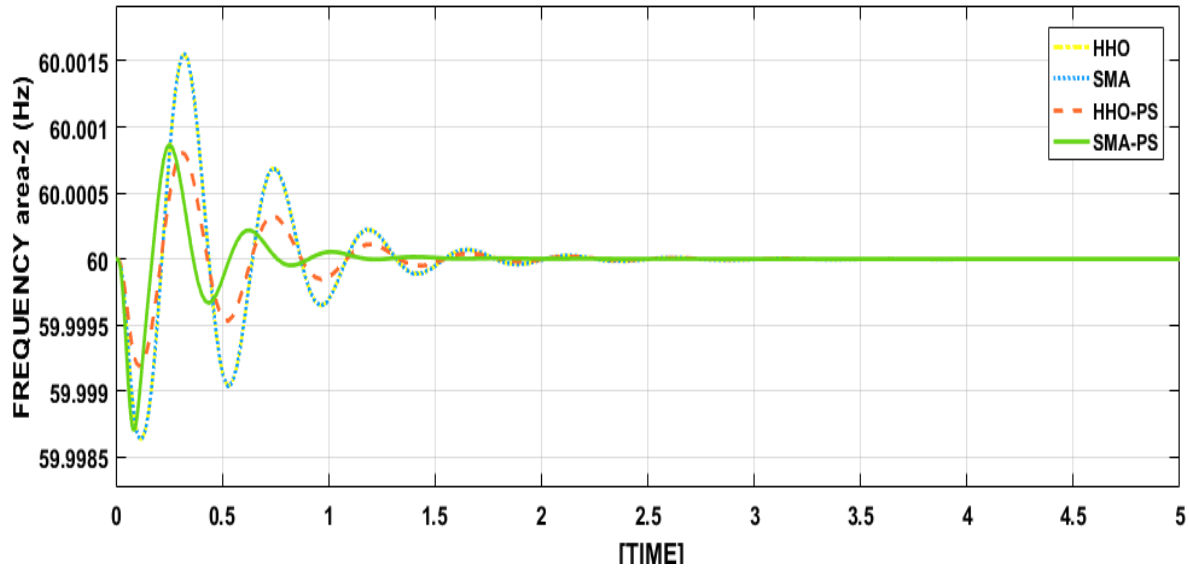

Fig.6.35 Proposed system area- 2 frequency reaction after changing the H = - 25%

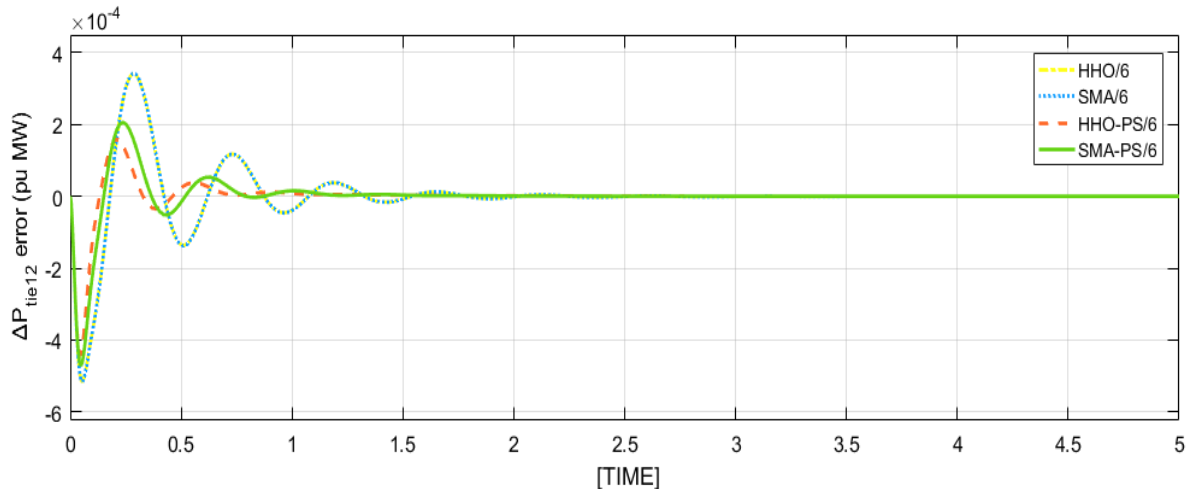

Fig.6.36 Proposed system TLP flow reaction after changing the H = - 25%

6.8 CONCLUSION

Electric vehicles (EVs) have the potential to significantly expand in popularity soon, posing new difficulties and possibilities for power systems. EVs may provide a variety of power system auxiliary services. The capacity to store energy and the ability of EVs' fast-switching converters to give immediate active power management are two appealing qualities that enable EVs to provide a variety of auxiliary services, such as primary frequency control (PFC) for LFR. Concurrently, EVs must be operated and managed within certain parameters, which restricts EV grid assistance. This study offers a novel EV model based on a participation factor, which allows for the integration of many EV fleet features. An aggregate model of EVs is presented for LFR analysis of the suggested system of optimally tuned PI controllers to decrease computational complexity. Earlier the proposed system was integrated with CES/TCPS for frequency oscillation damping, in addition to that EV/PV was added to the grid in each area of the system.

Under all possible situations, comparative studies along with sensitivity analysis of ‘Tsg’ and ‘H’ changing ± 25% of variables, the hybrid memetic SMA-PS tuned PI controller and an HHO, SMA, and hybrid memetic HHO-PS tuned PI controller with PV/EV units are undertaken. Investigations indicated that the suggested hybrid memetic SMA-PS optimized PI controller outperforms the HHO, SMA, and hybrid memetic HHO-PS optimized PI controllers in terms of peak overshoot for the area -2 frequency response. Remain other cases the HHO, SMA, hybrid memetic HHO-PS and hybrid memetic SMA-PS tuned PI controller equally performs with the PV/EV elements.

CHAPTER – 7

CONCLUSION AND FUTURE SCOPE

7.1 INTRODUCTION

This chapter ensures the significant and essential findings of the research performed in this thesis, thus a detailed findings on some recommendations for the future works. The listed below are the original significant findings.

7.2 SIGNIFICANT CONTRIBUTION

The current study contribution is premised on an optimal tuned controller solution to resolve the LFR of the two-area tie line interlinked challenge of DPS, additionally, with integrating CES/TCPS as a power exchange unit, and later stage PV/EV are integrated as an energy originating sources to mitigate the settling time and time complexity of the system while meeting the power balance among GENCOs – DISCO's contributions constraints. Hybrid memetic HHO-PS and SMA-PS optimizers are suggested and successfully developed to resolve the LFR of the two-area tie line interlinked challenge of DPS at several contracts.

Electricity is essential to social development of countries. Due to the rise in energy consumption, current situation in power sector is necessary to balance the rise in energy requisition of load with rise in energy origination. To provide continuous energy supply to the DISCOs, the energy origination requires more attention. As a result, the energy origination forms of traditional origination methodologies, and RES are gaining popularity as a solution to power balance among rise in energy requisition of load with origination. Due to the sudden power faults between GENCOs – DISCOs, LFR may lead to mismatch the energy load demand and origination of the electricity network, it can harm entire network or may lead to damage the equipment of the electricity network. To simplify the LFR of the electricity network, additional energy origination and exchange units are needed to interlink through grid connection. Due to using cumbersome equipment for several energy origination units, the grid may lead to complexity challenge as energy generation. And furtherly, to mitigate the complexity of the grid system, tie line interlinked deregulated power system (DPS) is introduced as a solution. And here, after addition of multi areas through tie interlink, the size of the DPS has increased. Due to the increase in the size of DPS network, network complexity may arise. For simplifying the network complexity and deduce the settling time, a powerful optimal control augmentation in LFR of the DPS network is needful.

For stable operation and mitigating DPS time complexity, an energy restoration and tie line control units are introduced in this research. In the current DPS market all the existing power origination systems are mostly non-RES like, thermal, coal, gas etc. due to the large number of non-RES origination units', nature also effects. Due to the environmental friendliness RES sources needful to mitigate the time complexity of tie line error, frequency fluctuation and origination in a developed DPS network. Here, PV is introduced as RES, the intermittency of PV source causes arises the technical issues in the DPS network, and to address the arising challenges EV are introduced with batteries on the wheels of the EV. Due to the EV nature of the energy origination and restoration bank capability, the application of EV introducing in LFR of the DPS network is emerging. Here, RES with EV is introduced furtherly to the existing DPS network.

LFR of two area tie line interlinked H – T – G sources DPS network has designed. To achieve the power balance among and minimize the time complexity of DPS, energy restoration and tie line control units are introduced in the DPS network, energy restoration and tie line control as CES/TCPS units and furtherly the developed DPS network extended with integration of PV/EV units.

The objective of this research report is to investigate the new methodologies to establishing, extending, and defining optimum LFR strategies in multi-source two area tie line interlinked DPS network with power exchange units and energy origination units while taking consideration several physical and network limits. Heuristics search methodologies are introducing as a solution to the challenge. HHO And SMA is exploited to boost the capability and global performance of the PS optimizer. This research has made the following notable contributions:

1. LFR having a non-convex, mixed integer, and non-linear challenge. To balance the origination amount of energy and load demand in LFR of the DPS network, and to resolve and simplify the network complexity of the LFR of multi area tie line interlinked DPS network, a powerful optimal tuned controller is required. To tune the controller an optimizer is needful, such as novel developed search optimizers are taken to consideration. The recent developed and existing search optimizers are useful for the global optimal challenging issues and those are having the time complexity and those optimizers are still having local optima with exploration trapping challenges. Due to that a power and simplified hybrid memetic optimizer with the integration of global and local search optimal methods are suggested to resolve the LFR of the multi area tie line

interlinked DPS problem as per literature done. A hybrid memetic HHO-PS, and SMA-PS optimizers are developed and suggested to resolve the LFR of the multi area tie line interlinked DPS network complexity.

2. The suggested optimizers, hybrid memetic HHO-PS, and SMA-PS optimizers are developed with the general operators of the HHO, and SMA each optimizer are combined with operators of the PS optimizer search operators respectively. To test and prove the efficacy of the suggested optimizers, twenty-three classic BM and nine classic CE problems are taken to consideration. The classic BM functions are categorized into three types, those are UM, MM, and FD BM functions with computational limits. The suggested hybrid memetic optimizers are performed 500 generations and thirty trail runs for each BM and CE issues. The statistical outcomes of the suggested hybrid memetic search optimizers are evaluated with the existing recently augmented optimizers. The statistical and convergence curves analysis for the BM and CE problems reveals that the suggested HHO-PS and SMA-PS optimizers performs greater efficacy outcomes than existing search optimizers. And from the outcomes, in some cases for the BM and CE issues, the suggested hybrid memetic optimizers perform competitive and equal results each. But the overall outcomes reveal that hybrid memetic SMA-PS optimizer performs greater results over hybrid memetic HHO-PS optimizer. Due to the huge number of fitness assessments performance, the hybrid memetic HHO-PS optimizer lacks computing efficiency.
3. A LFR of the two-area tie line interlinked H – T – G sources DPS has been formulated to mitigate the settling complexity time of the tie line, frequency fluctuations and originating sources subject to technical and network limits while satisfying the GENCOs and DISCOs contracts. LFR having a non-convex, mixed integer, and non-linear challenge and resolved by applying heuristics search procedure such as hybrid memetic HHO-PS and SMA-PS optimizers tuned controllers. These optimizers have been developed to obtain the optimum tune PI controller for operating and improving the performance of the LFR of two-area tie line interlinked H – T – G sources DPS and to balance the energy origination and distribution of the DPS network with considering technical and network limits. To obtain the hybrid memetic SMA-PS optimizer, the general operators of the SMA each optimizer are combined with operators of the PS operator respectively. Heuristics search methodology is applied to tackle the several technical and network limits of the LFR of two-area tie line interlinked H – T – G sources DPS. This search method, by using hybrid memetic SMA-PS optimizer tuned PI

controller are successfully developed to tackle the POOLCO, Bilateral, Contract violation contract methods.

4. The outcomes of the hybrid memetic HHO-PS and SMA-PS optimizers tuned PI controllers for the developed LFR of the DPS model is analyzed, with the other classic HHO, and SMA optimizers tuned PI controllers. The analysis reveals that hybrid memetic HHO-PS and SMA-PS optimizers tuned PI controllers performs greater efficacy results over classic HHO and SMA optimizers tuned PI controller. The overall settling time of the tie line, frequency fluctuations and originating sources subject to technical and network limits in hybrid memetic SMA-PS optimizer tuned PI controller is better than the hybrid memetic HHO-PS optimizer.

- Two area T – G – H sources LFR of the DPS electric network dynamic performance reaction under POOLCO exchange tactic was noted underneath for the proposed hybrid HHO-PS and hybrid SMA-PS optimizers premised PI regulator.
    - *Settling time reaction:* The result obtained by hybrid SMA-PS optimizer premised PI regulator settling time performance for region – 1, region – 2, and TLP flow error was 30 sec, 20 sec, and 30 sec respectively. Likewise, hybrid HHO-PS optimizer premised PI regulator settling time performance for region – 1, region – 2, and TLP flow error was 35 sec, 25 sec, and 35 sec. While comparing the outcomes for POOLCO exchange transaction, hybrid SMA-PS premised PI regulator dampens quicker oscillation reaction than the hybrid HHO-PS premised PI regulator.
    - *Peak undershoot reaction:* The result obtained by hybrid SMA-PS optimizer premised PI regulator, peak undershoot performance for region – 1, region – 2, and TLP flow error was 59.9820 HZ sec, 59.9700 HZ sec, and – 0.00585 HZ respectively. Likewise, hybrid HHO-PS optimizer premised PI regulator peak undershoot performance for region – 1, region – 2, and TLP flow error was 59.9825 HZ, 59.9705 HZ, and – 0.00550 HZ. While comparing the outcomes for POOLCO exchange transaction, hybrid SMA-PS premised PI regulator had better performance for area – 1 and area – 2 undershoot reaction than the hybrid HHO-PS premised PI regulator. And for TLP flow error reaction, hybrid HHO-PS regulator had better undershoot reaction performance than hybrid SMA-PS regulator.
    - *Peak overshoot reaction:* The result obtained by hybrid SMA-PS optimizer premised PI regulator, peak overshoot performance for region – 1, region – 2,

and TLP flow error was 60.0120 HZ sec, 60.0150 HZ sec, and 0.0025 HZ respectively. Likewise, hybrid HHO-PS optimizer premised PI regulator peak overshoot performance also produces similar outcomes.

- Two area T – G – H sources LFR of the DPS electric network dynamic performance reaction under Bilateral exchange tactic was noted underneath for the developed hybrid HHO-PS and hybrid SMA-PS optimizers premised PI regulator.
    - *Settling time reaction:* The result obtained by hybrid SMA-PS optimizer premised PI regulator settling time performance for region – 1, region – 2, and TLP flow error was 30 sec, 20 sec, and 20 sec respectively. Likewise, hybrid HHO-PS optimizer premised PI regulator settling time performance for region – 1, region – 2, and TLP flow error was 20 sec, 20 sec, and 30 sec. While comparing the outcomes for Bilateral exchange transaction, hybrid SMA-PS premised PI regulator, area – 1 and area – 2 oscillation reaction was similar with the hybrid HHO-PS premised PI regulator. TLP flow error reaction, hybrid SMA-PS regulator had better settle time performance reaction than the hybrid HHO-PS regulator.
    - *Peak undershoot reaction:* The result obtained by hybrid SMA-PS optimizer premised PI regulator, peak undershoot performance for region – 1, region – 2, and TLP flow error was 59.5960 HZ sec, 59.5960 HZ sec, and – 0.0050 HZ respectively. Likewise, hybrid HHO-PS optimizer premised PI regulator peak undershoot performance for region – 1, region – 2, and TLP flow error was 59.9640 HZ, 59.9635 HZ, and – 0.0050 HZ. While comparing the outcomes for Bilateral exchange transaction, hybrid SMA-PS premised PI regulator had better undershoot performance for area – 1 and area – 2 than the hybrid HHO-PS premised PI regulator. And for TLP flow error reaction, hybrid HHO-PS regulator and hybrid SMA-PS regulator performs similar undershoot reaction performances.
    - *Peak overshoot reaction:* The result obtained by hybrid SMA-PS optimizer premised PI regulator, peak overshoot performance for region – 1, region – 2, and TLP flow error was 60.0250 HZ sec, 60.0240 HZ sec, and 0 HZ respectively. Likewise, hybrid HHO-PS optimizer premised PI regulator peak overshoot performance for region – 1, region – 2, and TLP flow error was 60.0250 HZ, 60.0170 HZ, 0 HZ. While comparing the outcomes for Bilateral exchange

transaction, hybrid HHO-PS premised PI regulator had better overshoot performance than the hybrid HHO-PS premised PI regulator.

- Two area T – G – H sources LFR of the DPS electric network performance reaction under CV exchange tactic was noted underneath for the proposed hybrid HHO-PS and hybrid SMA-PS optimizers premised PI regulator.

  - *Settling time reaction:* The result obtained by hybrid SMA-PS optimizer premised PI regulator settling time performance for region – 1, region – 2, and TLP flow error was 58 sec, 54 sec, and 65 sec respectively. Likewise, hybrid HHO-PS optimizer premised PI regulator settling time performance for region – 1, region – 2, and TLP flow error was 62 sec, 56 sec, and 72 sec. While comparing the outcomes for CV exchange transaction, hybrid SMA-PS premised PI regulator validates greater efficacy outcomes than hybrid HHO-PS premised PI regulator.
  - *Peak undershoot reaction:* The result obtained by hybrid SMA-PS optimizer premised PI regulator Peak undershoot reaction for region – 1, region – 2, and TLP flow error was 59.9620 HZ, 59.9620 HZ, and 0 HZ respectively. Likewise, hybrid HHO-PS optimizer premised PI regulator Peak undershoot reaction for region – 1, region – 2, and TLP flow error was 59.6400 HZ, 59.9640 HZ, and 0 HZ. While comparing the outcomes for CV exchange transaction, hybrid SMA-PS premised PI regulator validates region – 1 had greater efficacy outcomes than hybrid HHO-PS premised PI regulator. For region – 2 hybrid HHO-PS premised PI regulator validates greater efficacy outcomes than hybrid SMA-PS premised PI regulator. In case of TLP flow error, both are showing similar results to each other.
  - *Peak overshoot reaction:* The result obtained by hybrid SMA-PS optimizer premised PI regulator Peak overshoot reaction for region – 1, region – 2, and TLP flow error was 60.0250 HZ, 60.0200 HZ, and 0 HZ respectively. Likewise, hybrid HHO-PS optimizer premised PI regulator settling time performance for region – 1, region – 2, and TLP flow error was 60.0200 HZ, 60.0150 HZ, and 0 HZ. While comparing the outcomes for CV exchange transaction, hybrid HHO-PS premised PI regulator validates greater efficacy than hybrid SMA-PS premised PI regulator.

- To validate the robustness of developed LFR of DPS Two area T – G – H sources electric network, sensitivity analysis was carried out by using POOLCO exchange with ±25% variation of *governor* time constant (T_{sg}) *and inertia* constant H, which leads to change the load constant (T_{ps}). After variation, the system reaction was

noted underneath for the developed hybrid HHO-PS and hybrid SMA-PS optimizers premised PI regulator.

- *settling time,* peak overshoot, peak undershoot *reactions after changing* T_{sg} *as* -25%:

The settling response of region – 1, region – 2 and TLP error for novel hybrid SMA-PS optimizer premised PI regulator was 27 sec, 30 sec, and 45 sec, and hybrid HHO-PS optimizer premised PI regulator settling time performance for region – 1, region – 2, and TLP flow error was 29 sec, 32 sec, and 50 sec. While comparing the outcomes of hybrid SMA-PS premised PI regulator dampens quicker oscillation reaction than the hybrid HHO-PS premised PI regulator. The peak overshoot reaction of novel hybrid SMA-PS and hybrid HHO-PS optimizers premised PI regulator were similar for region – 1, region – 2, and TLP flow error performances as 60.0110 HZ, 60.0150 HZ, 0.0025 HZ respectively. The peak overshoot reaction of novel hybrid SMA-PS and hybrid HHO-PS optimizers premised PI regulator were similar outcome for region – 1, region – 2, and TLP flow error performances as 59.972 HZ, 59.9830 HZ, -0.0055 HZ respectively.

- *settling time,* peak overshoot, peak undershoot *reactions after changing* T_{sg} *as* +25%:

The settling time complexity `response of region – 1, region – 2 and TLP error for novel hybrid SMA-PS optimizer premised PI regulator was 29 sec, 29 sec, and 43 sec, and hybrid HHO-PS optimizer premised PI regulator settling time performance for region – 1, region – 2, and TLP flow error was 30 sec, 29.5 sec, and 43 sec. While comparing the outcomes of hybrid SMA-PS premised PI regulator dampens quicker oscillation reaction than the hybrid HHO-PS premised PI regulator for region – 1, and region – 2. hybrid SMA-PS and hybrid HHO-PS optimizer premised PI regulator were performed similar outcomes for TLP error. Peak overshoot reaction for region – 1, region – 2 and TLP error for novel hybrid SMA-PS optimizer premised PI regulator was 60.0118 HZ, 60.0150 HZ, and 0.0023 HZ. For hybrid HHO-PS premised PI regulator reaction was 60.0119 HZ, 60.0155 HZ, and 0.0023 HZ respectively. The outcomes reveals that the SMA-PS regulator performs efficient over HHO-PS regulator for region – 1 and region – 2 and for TLP error reaction both the suggested optimizers perform similar outcomes. The peak undershoot reaction both the suggested optimizers performs similar for region – 1, region – 2 and TLP error as 59.9700 HZ, 59.9830 HZ and -0.0055 HZ respectively.

- *settling time,* peak overshoot, peak undershoot *reactions after changing* H *as* +25%:

The settling time complexity response of region – 1, region – 2 and TLP error for novel hybrid SMA-PS optimizer premised PI regulator was 35 sec, 35 sec, and 35 sec, and for the hybrid HHO-PS regulator was 35 sec, 36 sec, and 36 sec respectively. The obtained results depict that for region – 2 and TLP error hybrid SMA-PS regulator has greater efficacy than other and for region – 1, both suggested optimizers perform equal. The peak overshoot reaction of region – 1, region – 2 and TLP error for hybrid SMA-PS regulator was 60.0128 HZ, 60.0120 HZ, and 0.0022 HZ, and for the hybrid HHO-PS regulator was 60.0130 HZ, 60.0120 HZ, and 0.0022 HZ respectively. Peak overshoot reaction of region – 1, the hybrid HHO-PS regulator performs greater efficacy outcomes over other and for region – 2 and TLP error reaction, both the suggested optimizers perform similar outcomes. The peak undershoots reaction of region – 1, region – 2 and TLP error for hybrid SMA-PS regulator and hybrid HHO-PS optimizers premised PI regulator performs similar outcomes as 59.9760 HZ, 59.9863 HZ, and -0.0048 HZ respectively to each other.

- *settling time,* peak overshoot, peak undershoot *reactions after changing* H *as* -25%:

The settling time complexity response of region – 1, region – 2 and TLP error for novel hybrid SMA-PS optimizer premised PI regulator was 38 sec, 40 sec, and 35 sec, and for the hybrid HHO-PS regulator was 37 sec, 41 sec, and 45 sec respectively. The obtained results depict that for region – 1, region – 2 and TLP error reaction for the hybrid SMA-PS regulator has greater efficacy than hybrid HHO-PS regulator. Peak overshoot reaction for region – 1, region – 2 and TLP error for novel hybrid SMA-PS optimizer premised PI regulator was 60.0280 HZ, 60.0200 HZ, and 0.0036 HZ. For hybrid HHO-PS premised PI regulator reaction was 60.0052 HZ, 60.0055 HZ, and 0.0037 HZ respectively. The obtained results for the peak overshoot reaction depict that region – 1, and region – 2 for the hybrid HHO-PS regulator has greater efficacy than hybrid SMA-PS regulator. And TLP error for the hybrid SMA-PS regulator has greater efficacy than hybrid HHO-PS regulator. Peak undershoot reaction for region – 1, region – 2 and TLP error for novel hybrid SMA-PS optimizer premised PI regulator was 59.9760 HZ, 59.9800 HZ, and -0.0045 HZ. For hybrid HHO-PS premised PI regulator reaction was 59.9740 HZ, 59.9855 HZ, and -0.0058 HZ respectively. The obtained results for

the peak undershoot reaction depict that region – 1, region – 2, and TLP error for the hybrid SMA-PS regulator has greater efficacy than hybrid HHO-PS regulator.

5. The objective of the power balance among interlinked two area via tie line interlinked in LFR of the DPS is extended with power exchange units at each area of the grid and tie line of the DPS network. Considering CES as both energy storing and discharging for power balance and reduce time complexity of the LFR of the DPS network. Additionally, a TCPS controller is attached at tie line of interlinked LFR of the DPS network to reduce the inter area power deviations. Hence, CES stores the exceeding energy in grid system of interlinked tie line of each area and during unexpected load disruption, it discharges it banked energy into the grid. TCPS controller is utilized to dampening the transmission line power deviations from each area oscillations among tie line interlinked LFR of the two area H – T – G originating sources DPS network.
6. The outcomes reveals that the LFR of the two area H – T – G originating sources interlinked tie line of the DPS network, after integrating CES/TCPS units, the tie line power, frequency fluctuations and originating sources time complexity is gradually mitigated in terms of settling, peak overshoot and under shoot time complexity. From comparative analysis, hybrid memetic HHO-PS and SMA-PS optimizers tuned PI controllers for the LFR of the DPS model with integrating CES/TCPS units depicts superior results over the classic HHO and SMA optimizers tuned PI controllers. Overall, time complexity of the DPS is reduced, subject to technical and network limits by using hybrid memetic SMA-PS optimizer tuned PI controller performs greater efficacy over hybrid memetic HHO-PS optimizer tuned PI controller.

- Two area T – G – H sources LFR of the DPS electric network with CES/TCPS dynamic performance reaction under POOLCO exchange tactic was noted underneath for the proposed hybrid HHO-PS and hybrid SMA-PS optimizers premised PI regulator.

  - *Settling time reaction:* for region – 1, region – 2, and TLP error reactions for the hybrid SMA-PS and hybrid HHO-PS optimizers premised PI regulator performs similar outcomes as 12 sec, 9 sec, and 10 sec respective to each other.
  - *Peak overshoot:* for region – 1, region – 2, and TLP error reactions for the hybrid SMA-PS and hybrid HHO-PS optimizers premised PI regulator performs similar outcomes as 60.00400 HZ, 60.00020 HZ, and 0.00200 HZ respective to each other.
  - *Peak undershoot:* for region – 1, region – 2, and TLP error reactions for the hybrid SMA-PS and hybrid HHO-PS optimizers premised PI regulator performs

similar outcomes as 59.99990 HZ, 59.99500 HZ, and -0.00320HZ respective to each other.

- Two area T – G – H sources LFR of the DPS electric network with CES/TCPS dynamic performance reaction under Bilateral exchange tactic was noted underneath for the suggested hybrid HHO-PS and hybrid SMA-PS optimizers premised PI regulator.
    - *Settling time reaction:* For region – 1, region – 2, and TLP error reactions for the hybrid SMA-PS regulator performs as 10 sec 7 sec, and 10 sec and hybrid SMA-PS regulator performs as 10 sec 10 sec, and 15 sec respectively. While comparing the outcomes for region – 1, both the suggested optimizers perform similar outcomes. Region – 2, and TLP error reactions, hybrid SMA-PS regulator performs greater efficacy than HHO-PS regulator.
    - *Peak undershoot:* For region – 1, region – 2, and TLP error reactions for the hybrid SMA-PS regulator performs as 59.9920 HZ, 59.9830 HZ, and -0.0020 HZ and for hybrid HHO-PS regulator performs as 59.9980 HZ, 59.9850 HZ, and -0.0010 HZ respectively. The analysis reveals that, for region – 1, and region – 2 the hybrid HHO-PS regulator performs greater outcomes than hybrid SMA-PS regulator and for TLP error, hybrid SMA-PS regulator performs greater outcomes than hybrid HHO-PS regulator.
    - *Peak overshoot:* For region – 1, region – 2, and TLP error reactions for the hybrid SMA-PS regulator performs as 60.0001 HZ, 60.0110 HZ, and 0.0030 HZ and for hybrid HHO-PS regulator performs as 60.0001HZ, 60.0110 HZ, and 0.0020 HZ respectively. The outcomes reveals that the suggested optimizers perform similar for region – 1, and region – 2, for TLP error HHO-PS regulator performs greater efficacy than SMA-PS regulator.
- Two area T – G – H sources LFR of the DPS electric network with CES/TCPS dynamic performance reaction under CV exchange tactic was noted underneath for the suggested hybrid HHO-PS and hybrid SMA-PS optimizers premised PI regulator.
    - *Settling time reaction:* For region – 1, region – 2, and TLP error reactions, both suggested optimizers of hybrid SMA-PS and HHO-PS performs similar outcomes for hybrid SMA-PS regulator performs as 30 sec 29 sec, and 31 sec.
    - *Peak overshoot:* For region – 1, region – 2, and TLP error reactions, both suggested optimizers of hybrid SMA-PS and HHO-PS performs similar outcomes for hybrid SMA-PS regulator performs as 60.007 HZ, 60.0110 HZ, and 0.0035 HZ.

➢ *Peak undershoot:* For region – 1, region – 2, and TLP error reactions, both suggested optimizers of hybrid SMA-PS and HHO-PS performs similar outcomes for hybrid SMA-PS regulator performs as 59.9910 HZ, 59.9820 HZ, and -0.0020 HZ.

- To validate the robustness of developed LFR of DPS Two area T – G – H sources electric network with CES/TCPS units, sensitivity analysis was carried out by using Bilateral exchange with ±25% variation of *governor* time constant (T_{sg}) *and inertia* constant H , which leads to change the load constant (T_{ps}). After variation, the system reaction was noted underneath for the developed hybrid HHO-PS and hybrid SMA-PS optimizers premised PI regulator.

  ➢ *settling time,* peak overshoot, peak undershoot *reactions after changing* T_{sg} *as* -25%:

  The settling time response of region – 1, region – 2 and TLP error for hybrid SMA-PS optimizer premised PI regulator was 12 sec, 12 sec, and 13 sec, and likewise, hybrid HHO-PS regulator had 12 sec, 14 sec, and 13 sec. The analysis reveals that for region – 1, both suggested optimizers perform similar outcomes with respect to each other and for region -2, and TLP error reaction, hybrid SMA-PS regulator dampens quicker oscillation reaction than the hybrid HHO-PS regulator. The peak overshoot response of region – 1, region – 2 and TLP error for hybrid SMA-PS optimizer premised PI regulator was 60.0060 HZ, 60.0035 HZ, 0.0020 HZ respectively and likewise, hybrid HHO-PS regulator had 60.0060 HZ, 60.0025 HZ, 0.0020 HZ. The outcome of peak overshoot reveals that, for region – 1 and TLP error reactions SMA – PS regulator had greater efficacy outcomes than HHO – PS regulator, and for region – 2 HHO – PS regulator had greater efficacy outcomes than SMA – PS regulator. The peak undershoots response of region – 1, region – 2 and TLP error for hybrid SMA-PS optimizer premised PI regulator was 59.9920 HZ, 59.9954 HZ, -0.003 HZ respectively and likewise, hybrid HHO-PS regulator had 59.9954 HZ, 59.9957 HZ, and -0.003 HZ. The outcome of peak undershoot reveals that, for region – 1 and TLP error reactions SMA – PS regulator had greater efficacy outcomes than HHO – PS regulator, and for region – 2 HHO – PS regulator had greater efficacy outcomes than SMA – PS regulator.

  ➢ *settling time,* peak overshoot, peak undershoot *reactions after changing* T_{sg} *as* +25%:

The settling time response of region – 1, region – 2 and TLP error for hybrid SMA-PS optimizer premised PI regulator was 13 sec, 13 sec, and 13 sec, and likewise, hybrid HHO-PS regulator had 13 sec, 13 sec, and 14 sec. The analysis reveals that for region – 1 and region – 2, both suggested optimizers perform similar outcomes with respect to each other and for TLP error reaction, hybrid SMA-PS premised regulator dampens quicker oscillation reaction than hybrid HHO-PS premised regulator. The peak overshoot response of region – 1, region – 2 and TLP error for hybrid SMA-PS optimizer premised PI regulator was 60.0057 HZ, 60.0027 HZ, and 0.0022 HZ, and likewise, hybrid HHO-PS regulator had 60.0060 HZ, 60.0028 HZ, and 0.0022 HZ. The outcome of peak overshoot reveals that, for region – 1 and region – 2 reactions SMA – PS regulator had greater efficacy outcomes than HHO – PS regulator, and for TLP error, both suggested optimizers perform similar outcomes. The peak undershoots response of region – 1, region – 2 and TLP error for hybrid SMA-PS optimizer premised PI regulator was 59.9900 HZ, 59.9958 HZ, and -0.0028 HZ, and likewise, hybrid HHO-PS regulator had 59.9900 HZ, 59.9960 HZ, and -0.0028 HZ. The outcome of peak undershoot reveals that, for region – 1 both suggested optimizers perform similar outcomes. and region – 2 and TLP error reactions HHO – PS regulator had greater efficacy outcomes than SMA – PS regulator.

- *settling time,* peak overshoot, peak undershoot *reactions after changing* H *as* +25%:

The settling time response of region – 1, region – 2 and TLP error for hybrid SMA-PS optimizer premised PI regulator was 12 sec, 11 sec, and 13 sec, and likewise, hybrid HHO-PS regulator had 12 sec, 11 sec, and 13.1 sec. The analysis reveals that for region – 1 and region – 2, both suggested optimizers perform similar outcomes with respect to each other and for TLP error reaction, hybrid SMA-PS premised regulator dampens quicker oscillation reaction than hybrid HHO-PS premised regulator. The peak overshoot response of region – 1, region – 2 and TLP error for hybrid SMA-PS optimizer premised PI regulator was 60.007 HZ, 60.002 HZ, and 0.0026 HZ, and likewise, hybrid HHO-PS regulator had 60.0060 HZ, 60.003 HZ, and 0.0025 HZ. The outcome of peak overshoot reveals that, for region – 1 and TLP error reactions HHO – PS regulator had greater efficacy outcomes than SMA – PS regulator, and for region – 2, hybrid SMA-PS premised regulator better reaction than hybrid HHO-PS premised regulator. The peak undershoots

response of region – 1, region – 2 and TLP error for hybrid SMA-PS optimizer premised PI regulator was 59.9922 HZ, 59.9960 HZ, and -0.0031 HZ, and likewise, hybrid HHO-PS regulator 59.9920 HZ, 59.9955 HZ, and -0.0032 HZ. The outcome of peak undershoot reveals that, for region – 1 and region - 2 reactions of SMA – PS regulator had greater efficacy outcomes than HHO – PS regulator, and for TLP error, hybrid HHO-PS premised regulator better reaction than hybrid SMA-PS premised regulator.

- *settling time*, peak overshoot, peak undershoot *reactions after changing* H *as* -25%:

The settling time response of region – 1, region – 2 and TLP error for hybrid SMA-PS optimizer premised PI regulator was 14 sec, 12 sec, and 11 sec, and likewise, hybrid HHO-PS regulator had 14 sec, 12 sec, and 12 sec. The analysis reveals both the suggested optimizers perform similar outcomes for region – 1 and region – 2 and for TLP error, SMA-PS premised regulator had better reaction than hybrid HHO-PS premised regulator. The peak overshoot response of region – 1, region – 2 and TLP error for hybrid SMA-PS optimizer premised PI regulator was 60.0055 HZ, 60.0025 HZ, and 0.0020 HZ, and likewise, hybrid HHO-PS regulator had 60.0060 HZ, 60.0030 HZ, and 0.0020 HZ. The outcome of peak overshoot reveals that, for region – 1 and region - 2 reactions of SMA – PS regulator had greater efficacy outcomes than HHO – PS regulator, and for TLP error, both suggested optimizers perform similar outcomes. The peak undershoots response of region – 1, region – 2 and TLP error, both suggested optimizers perform similar outcomes as 59.9925 HZ, 59.9955 HZ, and -0.0029 HZ.

7. After adding power exchange CES/TCPS units in suggested model, the possible reduction of time complexity with integrating RES sources possible to boost the performance the performance of the DPS. LFR of the two area DPS network furtherly extended with power origination and exchange units at each area of the grid with origination source PV as RES and additionally, EV is integrated as power exchange unit. After integrating PV/EV, each area fluctuation used as input signal of the PV/EV units. Here, EV having two input signals for exchanging of power in LFR of the DPS network. LFR controller is used as another input signal of the EV.
8. From the simulation outcomes of hybrid memetic HHO-PS and SMA-PS optimizers tuned PI controllers for the LFR of the two-area H – T – G originating sources interlinked tie line of the DPS network with integrating CES/TCPS units and further extension of

PV/EV units, it is observed that settling time complexity is resolved, energy origination sources at each area GENCOs depicts best optimal results. With due consideration in tie line error, it is found that suggested methodology mitigates its time complexity of the suggested DPS network. And the settling time of the frequency fluctuation at area of the LFR of the two-area H – T – G originating sources interlinked tie line of the DPS network achieve best optimal value. The suggested, hybrid memetic SMA-PS optimizer tuned PI controller gives better results than, hybrid memetic HHO-PS optimizer tuned PI controller.

- Two area T – G – H sources LFR of the DPS electric network with CES and EV/BEVs dynamic performance reaction under POOLCO exchange tactic was noted underneath for the suggested hybrid HHO-PS and hybrid SMA-PS optimizers premised PI regulator.
    - *Settling time reaction:* For region – 1, region – 2, and TLP error reactions, both suggested optimizers of hybrid SMA-PS and HHO-PS optimizers perform similar outcomes as 1 sec 1.5 sec, and 1.5 sec.
    - *Peak overshoot:* For region – 1, region – 2, and TLP error reactions, both suggested optimizers of hybrid SMA-PS and HHO-PS performs similar outcomes as 60.00078 HZ, 60.00090 HZ, and 0.00019 HZ.
    - *Peak undershoot:* For region – 1, and TLP error reactions, both suggested optimizers of hybrid SMA-PS and hybrid HHO-PS performs similar outcomes as 59.99857 HZ, and -0.00041 HZ. For region – 2, hybrid SMA-PS and hybrid HHO-PS optimizers performs as 59.9988HZ and 59.9990HZ, analysis reveals that SMA-PS regulator outperforms other.

- Two area T – G – H sources LFR of the DPS electric network with CES and EV/BEVs dynamic performance reaction under Bilateral exchange tactic was noted underneath for the suggested hybrid HHO-PS and hybrid SMA-PS optimizers premised PI regulator.
    - *Settling time reaction:* For region – 1, region – 2, and TLP error reactions, both suggested optimizers of hybrid SMA-PS and HHO-PS performs similar outcomes for hybrid SMA-PS regulator performs as 1 sec 1.5 sec, and 1.2 sec.
    - *Peak overshoot:* For region – 1, and TLP error reactions, both suggested optimizers of hybrid SMA-PS and HHO-PS performs similar outcomes for hybrid SMA-PS regulator performs as 60.00054 HZ, and 0.00019 HZ. And for region – 2,

SMA-PS and HHO-PS optimizers performs as 60.00125 HZ and 60.00136 HZ, analysis reveals that SMA-PS regulator outperforms other.

➢ *Peak undershoot:* For region – 1, region – 2 and TLP error reactions, both suggested optimizers of hybrid SMA-PS and HHO-PS performs similar outcomes for hybrid SMA-PS regulator performs as 59.99859HZ, 59.99850 HZ and -0.00039 HZ.

- Two area T – G – H sources LFR of the DPS electric network with CES and EV/BEVs dynamic performance reaction under CV exchange tactic was noted underneath for the suggested hybrid HHO-PS and hybrid SMA-PS optimizers premised PI regulator.

  ➢ *Settling time reaction:* For region – 1, region – 2, and TLP error reactions, both suggested optimizers of hybrid SMA-PS and HHO-PS performs similar outcomes for hybrid SMA-PS regulator performs as 7.8 sec 8 sec, and 7.6 sec.

  ➢ *Peak overshoot:* For region – 1, and TLP error reactions, both suggested optimizers of hybrid SMA-PS and HHO-PS performs similar outcomes for hybrid SMA-PS regulator performs as 60.00055 HZ, and 0.000043 HZ. And for region – 2, SMA-PS and HHO-PS optimizers performs as 60.00125 HZ and 60.00140 HZ, analysis reveals that SMA-PS regulator outperforms other.

  ➢ *Peak undershoot:* For region – 1, region – 2 and TLP error reactions, both suggested optimizers of hybrid SMA-PS and HHO-PS performs similar outcomes for hybrid SMA-PS regulator performs as 59.99858 HZ, 59.99830 HZ and -0.000088 HZ.

- To validate the robustness of developed LFR of DPS Two area T – G – H sources electric network with CES with EV/BEV, sensitivity analysis was carried out by using Bilateral exchange with $\pm 25\%$ variation of *governor* time constant (T_{sg}) *and inertia* constant H , which leads to change the load constant (T_{ps}). After variation, the system reaction was noted underneath for the developed hybrid HHO-PS and hybrid SMA-PS optimizers premised PI regulator.

  ➢ *settling time,* peak overshoot, peak undershoot *reactions after changing* T_{sg} *as* -25%:

  The settling time response of region – 1, region – 2 and TLP error for hybrid SMA-PS optimizer premised PI regulator was 2 sec, 1.8 sec, and 2.4 sec, and likewise, hybrid HHO-PS regulator had 2.5 sec, 2 sec, and 2.6 sec. The analysis reveals that of region – 1, region -2, and TLP error reactions, hybrid SMA-PS regulator

dampens quicker oscillation reaction than the hybrid HHO-PS regulator. The peak overshoot of region – 1, region – 2 and TLP error for hybrid SMA-PS optimizer premised PI regulator was 60.00102 HZ, 60.0015 HZ, and 0.0003 HZ, and likewise, hybrid HHO-PS regulator had 60.00108 HZ, 60.0015 HZ, and 0.0003 HZ. The analysis reveals that for region – 1, SMA-PS optimizer outperforms other. And for region – 2 and TLP error, both the suggested optimizers perform similar outcomes. The peak undershoots of region – 1, region – 2 and TLP error for hybrid SMA-PS optimizer premised PI regulator was 59.99843 HZ, 59.9986 HZ, and -0.00047 HZ, and likewise, hybrid HHO-PS regulator had 59.99842 HZ, 59.9986 HZ, and -0.00048 HZ. The analysis reveals that for region – 1, SMA-PS optimizer outperforms other and for region – 2, both the suggested optimizers perform similar outcomes. And TLP error, HHO-PS optimizer outperforms other.

- *settling time,* peak overshoot, peak undershoot *reactions after changing* T_{sg} *as* +25%:

The settling time response of region – 1, region – 2 and TLP error for hybrid SMA-PS optimizer premised PI regulator was 1.2 sec, 1 sec, and 1.3 sec, and likewise, hybrid HHO-PS regulator had 1.8 sec, 2 sec, and 1.7 sec. Analysis reveals that for settling time, hybrid SMA-PS optimizer outperforms other. The peak overshoot of region – 1, region – 2 and TLP error for hybrid SMA-PS optimizer premised PI regulator was 60.0005 HZ, 60.0007 HZ, and 0.0018 HZ, and likewise, hybrid HHO-PS regulator had 60.0010 HZ, 60.0016 HZ, and 0.0032 HZ. For region – 1, and region – 2, analysis reveals that for peak overshoot, hybrid HHO-PS optimizer outperforms other. And peak overshoot of TLP error, SMA-PS optimizer outperforms other. The peak undershoot reaction for suggested optimizers performs similar outcomes for region – 1, region – 2 and TLP error as 59.9985 HZ, 59.9985 HZ, and -0.0048 HZ respectively.

- *settling time,* peak overshoot, peak undershoot *reactions after changing* H *as* +25%:

The settling time response of region – 1, region – 2 and TLP error for hybrid SMA-PS optimizer premised PI regulator was 1.2 sec, 1.3 sec, and 1.3 sec, and likewise, hybrid HHO-PS regulator had 2 sec, 2.3 sec, and 2.3 sec. The outcomes reveal that for settling time reaction, hybrid SMA-PS optimizer outperforms other. The peak overshoot of region – 1, region – 2 and TLP error for hybrid SMA-PS optimizer premised PI regulator was 60.0006 HZ, 60.0007 HZ, and 0.0002 HZ, and likewise, hybrid HHO-PS regulator had 60.0010 HZ, 60.0016 HZ, and 0.0031 HZ. The peak

overshoot outcomes reveal that the suggested hybrid SMA-PS optimizer outperforms other. The peak undershoots of region – 1, region – 2 and TLP error for hybrid SMA-PS optimizer premised PI regulator was 59.9985 HZ, 59.9988 HZ, and -0.0004 HZ, and likewise, hybrid HHO-PS regulator had 59.9984 HZ, 59.9984 HZ, and -0.00048 HZ. The peak undershoots outcomes reveal that the suggested hybrid SMA-PS optimizer outperforms other in all the scenarios.

- *settling time,* peak overshoot, peak undershoot *reactions after changing* H *as* -25%:

The settling time response of region – 1, region – 2 and TLP error for hybrid SMA-PS optimizer premised PI regulator was 1.2 sec, 1.3 sec, and 1.2 sec, and likewise, hybrid HHO-PS regulator had 1.1 sec, 1.8 sec, and 1.1 sec. Analysis validated that of region – 1 and TLP error reactions, hybrid HHO-PS optimizer had greater efficacy results and for region – 2 reaction, hybrid SMA-PS optimizer had greater efficacy results. The peak overshoots of region – 1, region – 2 and TLP error for hybrid SMA-PS optimizer premised PI regulator was 60.0005 HZ, 60.0008 HZ, and 0.0002 HZ, and likewise, hybrid HHO-PS regulator had 60.0007 HZ, 60.0008 HZ, and 0.00019 HZ. The peak overshoots outcomes reveal that for region – 1 and TLP error the suggested hybrid SMA-PS optimizer outperforms other. And for region – 2, the suggested hybrid HHO-PS optimizer had greater efficacy outcome. The peak undershoots of region – 1, region – 2 and TLP error for hybrid SMA-PS optimizer premised PI regulator was 59.9984 HZ, 59.9987 HZ, and -0.0042 HZ, and likewise, hybrid HHO-PS regulator had 59.9983 HZ, 59.9983 HZ, and -0.0043HZ and analysis validates that in all scenarios, the suggested hybrid SMA-PS optimizer outperforms the other hybrid HHO-PS optimizer.

9. Comparative simulation findings depict the suggested hybrid memetic optimizers have prospective to optimize two-area LFR of the H – T – G sources tie line interlinked DPS with physical and network limits. It has been observed that the hybrid memetic SMA-PS optimizer tuned PI controller is much better than the hybrid memetic HHO-PS optimizer, classic HHO, and SMA optimizers tuned PI controller undertaken for comparison in the thesis. From the simulation findings, suggested hybrid memetic SMA-PS optimizer tuned PI controller has capability to determine the satisfactory and balanced LFR in acceptable computational time. Also, it has been found that suggested hybrid memetic SMA-PS optimizer tuned PI controller yield better feasible solutions in comparison to hybrid memetic HHO-PS optimizer tuned PI controller.

10. Results can be summarized as

- The hybrid memetic SMA-PS optimizer is promising. It has capability to obtain near global and local, optima for the Load frequency regulation optimization search problems.
- The functioning of the hybrid memetic HHO-PS optimizer is superior to the classic HHO, and SMA optimizers, and other variants of the HHO optimizer.
- For higher dimensions, hybrid memetic SMA-PS and HHO-PS optimizers accelerates SMA and HHO individually in general.
- Benchmarks and constrained engineering problem set depict that hybrid memetic SMA-PS and HHO-PS optimizers performs greater efficacious than the other existing MA. Hybrid memetic SMA-PS optimizer is highly competitive than the hybrid memetic HHO-PS optimizer and classic HHO and SMA optimizers for similar testing functions.
- hybrid memetic HHO-PS optimizer balances the exploitation and exploration due to poor possible solutions are capable to get knowledge from excellent ones. Similarly, excellent possible solution ones protected from destroying during search process. as a result, hybrid memetic HHO-PS optimizer is superior to the classic HHO optimizer for the UM, MM, and FD benchmarks.
- The results obtained for the developed two area LFR of the DPS electric network with and without CES, CES with EVs and RES to stabilize the developed network and mitigate settling time and frequency oscillation by applying the proposed hybrid HHO-PS and hybrid SMA-PS optimizers premised PI regulator. The factors listed underneath shows which optimizer is superior and the developed LFR of DPS electric network performance under various conditions.
- Two area T – G – H sources LFR of the DPS electric network dynamic performance with POOLCO exchange tactic was noted underneath for the suggested optimizers.

    - The result obtained by hybrid SMA-PS optimizer premised PI regulator settling time reaction for region – 1, region – 2, and TLP flow error was 30 sec, 20 sec, and 30 sec respectively. hybrid SMA-PS premised PI regulator dampens quicker oscillation reaction than other.
    - The result obtained by hybrid SMA-PS optimizer premised PI regulator peak undershoot reaction for region – 1, region – 2, and TLP flow error was 59.9820 HZ sec, 59.9700 HZ, and – 0.00585 HZ respectively. hybrid SMA-PS premised PI regulator had better performance for region – 1, and region – 2. And TLP error, HHO-PS had the greater efficacy result.

- The Peak overshoot reaction of both suggested optimizers shown similar outcomes for region – 1, region – 2, and TLP flow error as 60.0120 HZ sec, 60.0150 HZ sec, and 0.0025 HZ respectively.

- Two area T – G – H sources LFR of the DPS electric network under Bilateral exchange tactic performance was noted underneath for both suggested optimizers.
  - *Settling time reaction* for region – 1, and region – 2, both suggested optimizers perform similar outcomes as 30 sec, 20 sec, respectively. For TLP flow error reaction, hybrid SMA-PS regulator perform as 20 sec was the better efficacy than other.
  - *Peak undershoot reaction for* region – 1, and region – 2, hybrid SMA-PS optimizer premised PI regulator performs greater efficacy result than other as 59.5960 HZ, 59.5960 HZ respectively and for TLP flow error reaction, both suggested optimizers performs similar as – 0.0050 HZ.
  - *Peak overshoot reaction* of hybrid SMA-PS optimizer performs better than other for region – 2, and as 60.0250 HZ, 60.0170 HZ, 0 HZ respectively. And for region – 1, and TLP flow error response, both the suggested optimizers perform similar as 60.0250 HZ, and 0 HZ respectively.
- Two area T – G – H sources LFR of the DPS electric network under CV exchange tactic performance was noted underneath for both suggested optimizers.
  - Settling time performance of suggested hybrid SMA-PS premised PI regulator validates greater efficacy outcomes than other for region – 1, region – 2, and TLP flow error as 58 sec, 54 sec, and 65 sec respectively.
  - Peak undershoot reaction for region – 1, hybrid SMA-PS premised PI regulator validates greater efficacy outcomes than other as 59.9620 HZ. And for region – 2, and TLP flow error hybrid HHO-PS premised PI regulator validates greater efficacy outcomes than other as 59.9620 HZ, and 0 HZ respectively.
  - Peak overshoot reaction of suggested hybrid HHO-PS premised PI regulator validates greater efficacy outcomes than other for region – 1, region – 2, and TLP flow error as 60.0200 HZ, 60.0150 HZ, and 0 HZ respectively.
- Later, to improvise the efficacy of the developed two area T – G – H sources LFR of the DPS electric network upgraded with CES/TCPS units. The dynamic reaction under POOLCO exchange tactic was noted underneath for suggested optimizers.

- Settling time reaction for region – 1, region – 2, and TLP error reactions for both suggested optimizers perform similar outcomes as 12 sec, 9 sec, and 10 sec respective to each other.
- Peak overshoot for region – 1, region – 2, and TLP error reactions for both suggested optimizers perform similar outcomes as 60.00400 HZ, 60.00020 HZ, and 0.00200 HZ respective to each other.
- Peak undershoot for region – 1, region – 2, and TLP error reactions both suggested optimizers perform similar outcomes as 59.99990 HZ, 59.99500 HZ, and -0.00320HZ respective to each other.

- Two area T – G – H sources LFR of the DPS electric network with CES/TCPS dynamic reaction under Bilateral exchange tactic was noted underneath for the suggested optimizers.
  - Settling time reaction outcomes of region – 1, both the suggested optimizers perform similar outcomes as 10 sec. Region – 2, and TLP error reactions, hybrid SMA-PS regulator performs greater efficacy than HHO-PS regulator as 7 sec, and 10 sec.
  - Peak undershoot reaction for region – 1 and region – 2, suggested hybrid HHO-PS regulator performs better than other as 59.9980 HZ, and 59.9850 HZ respectively. and for TLP error, hybrid SMA-PS regulator performs greater outcomes than other as -0.0020 HZ respectively.
  - Both suggested optimizers similar outcomes under Peak overshoot reaction for region – 1, region – 2, and TLP error reaction as 60.0001 HZ, 60.0110 HZ, and 0.0030 HZ respectively.
- Two area T – G – H sources LFR of the DPS electric network with CES/TCPS dynamic performance reaction under CV exchange tactic was noted underneath for the suggested hybrid HHO-PS and hybrid SMA-PS optimizers premised PI regulator.
  - *Settling time reaction:* For region – 1, region – 2, and TLP error reactions, both suggested optimizers of hybrid SMA-PS and HHO-PS performs similar outcomes for hybrid SMA-PS regulator performs as 30 sec 29 sec, and 31 sec.
  - *Peak overshoot:* For region – 1, region – 2, and TLP error reactions, both suggested optimizers of hybrid SMA-PS and HHO-PS performs similar outcomes for hybrid SMA-PS regulator performs as 60.007 HZ, 60.0110 HZ, and 0.0035 HZ.

- *Peak undershoot:* For region – 1, region – 2, and TLP error reactions, both suggested optimizers of hybrid SMA-PS and HHO-PS performs similar outcomes for hybrid SMA-PS regulator performs as 59.9910 HZ, 59.9820 HZ, and -0.0020 HZ.

- Two area T – G – H sources LFR of the DPS electric network with CES and EV/BEVs reaction under POOLCO exchange tactic was noted underneath for the suggested optimizers.
  - *Settling time reaction:* For region – 1, region – 2, and TLP error reactions, both suggested optimizers of hybrid SMA-PS and HHO-PS performs similar outcomes for hybrid SMA-PS regulator performs as 1 sec 1.5 sec, and 1.5 sec.
  - *Peak overshoot:* For region – 1, region – 2, and TLP error reactions, both suggested optimizers of hybrid SMA-PS and HHO-PS performs similar outcomes for hybrid SMA-PS regulator performs as 60.00078 HZ, 60.00090 HZ, and 0.00019 HZ.
  - *Peak undershoot:* For region – 1, and TLP error reactions, both suggested optimizers of hybrid SMA-PS and HHO-PS performs similar outcomes for hybrid SMA-PS regulator performs as 59.99857 HZ, and -0.00041 HZ. For region – 2, SMA-PS and HHO-PS optimizers performs as 59.9988HZ and 59.9990HZ, analysis reveals that SMA-PS regulator outperforms other.

- Two area T – G – H sources LFR of the DPS electric network with CES and EV/BEVs reaction under Bilateral exchange tactic was noted underneath for the suggested optimizers.
  - *Settling time reaction f*or region – 1, region – 2, and TLP error reactions, both suggested optimizers perform similar outcomes as 1 sec 1.5 sec, and 1.2 sec respectively.
  - *Peak overshoot reaction* analysis reveals that SMA-PS regulator outperforms other for region – 1, and TLP error reactions as 60.00054 HZ, and 0.00019 HZ. And for region – 2, both suggested optimizers perform similar outcomes as 60.00136 HZ
  - *Peak undershoot:* For region – 1, region – 2 and TLP error reactions, both suggested optimizers perform similar outcomes as 59.99859HZ, 59.99850 HZ and -0.00039 HZ.

- Two area T – G – H sources LFR of the DPS electric network with CES with EV/BEVs performance under CV exchange tactic was noted underneath for the suggested optimizers
    - ➢ Settling time reaction for region – 1, region – 2, and TLP error reactions, both suggested optimizers perform similar outcomes as 7.8 sec 8 sec, and 7.6 sec.
    - ➢ Peak overshoot for region – 1, and TLP error reactions, both suggested performs similar outcomes as 60.00055 HZ, and 0.000043 HZ. And for region – 2, hybrid SMA-PS optimizer perform better outcome as 60.00125 HZ.
    - ➢ Peak undershoot for region – 1, region – 2 and TLP error reactions, both suggested optimizers performs similar outcomes as 59.99858 HZ, 59.99830 HZ and -0.000088 HZ.

Overall analysis of hybrid SMA-PS premised PI regulator was significantly better than hybrid HHO-PS premised PI regulator. Outcomes of both suggested optimizers validated for the developed two area G – H – T sources LFR of the DPS network without and with CES, CES with EVs under various power exchange tactics and to judge the robustness of the DPS electric network, sensitivity analysis was performed under variation of ±25% *governor* time constant (T_{sg}) *and inertia* constant H parameters.

7.3 FUTURE SCOPE SUGGESTIONS

The following are directions for future research:

- Load frequency regulation may be added with economic load dispatch as an objective combine function of load frequency control model.
- Commitment of generating units may also be considered in the overall objective function.
- The load frequency control problem can be used with DFIG for energy restoration instead of CES units.
- The futuristics research studies may include the combined operations of non-conventional and conventional energy resources along with hydrogen fuel cell based electric vehicles.
- In future, the proposed system may be tested with various energy storage systems and FACTS control units.

- Novel emerging search optimizers like, Reptile search algorithm, Artificial hummingbird algorithm, Red fox optimization algorithm etc. can be tried to see it is quicker for the both off line and on line implementations. A much suitable combination of swarm and moderate methodologies might be a best alternative.

REFERENCES

[1] R. Kumar and V. K. Sharma, "Automatic generation controller for multi area multisource regulated power system using grasshopper optimization algorithm with fuzzy predictive PID controller," *Int. J. Numer. Model. Electron. Networks, Devices Fields*, vol. 34, no. 1, pp. 1–27, 2021, doi: 10.1002/jnm.2802.

[2] Y. Arya, P. Dahiya, E. Çelik, G. Sharma, H. Gözde, and I. Nasiruddin, "AGC performance amelioration in multi-area interconnected thermal and thermal-hydro-gas power systems using a novel controller," *Eng. Sci. Technol. an Int. J.*, vol. 24, no. 2, pp. 384–396, Apr. 2021, doi: 10.1016/j.jestch.2020.08.015.

[3] N. Hakimuddin, I. Nasiruddin, and T. S. Bhatti, "Generation-based automatic generation control with multisources power system using bacterial foraging algorithm," *Eng. Reports*, vol. 2, no. 8, pp. 1–17, 2020, doi: 10.1002/eng2.12191.

[4] K. S. Rajesh, S. S. Dash, and R. Rajagopal, "Hybrid improved firefly-pattern search optimized fuzzy aided PID controller for automatic generation control of power systems with multi-type generations," *Swarm Evol. Comput.*, vol. 44, no. November 2017, pp. 200–211, 2019, doi: 10.1016/j.swevo.2018.03.005.

[5] S. Prakash and S. K. Sinha, "Automatic Load Frequency Control of Six Areas' Hybrid Multi-Generation Power Systems Using Neuro-Fuzzy Intelligent Controller," *IETE J. Res.*, vol. 64, no. 4, pp. 471–481, 2018, doi: 10.1080/03772063.2017.1361869.

[6] A. Ghasemi-Marzbali, "Multi-area multi-source automatic generation control in deregulated power system," *Energy*, vol. 201, p. 117667, 2020, doi: 10.1016/j.energy.2020.117667.

[7] U. . Rout, R. . Salin, and S. Pauda, "Gravitational Search Algorithm Based Automatic Generation Control for Interconnected Power System," *Int. Conf. Circuits Power Comput. Technol.*, vol. 12, no. 3, pp. 558 – 563, 2003.

[8] P. K. Hota and B. Mohanty, "Automatic generation control of multi source power generation under deregulated environment," *Int. J. Electr. Power Energy Syst.*, vol. 75, pp. 205–214, 2016, doi: 10.1016/j.ijepes.2015.09.003.

[9] S. V, P. G, K. M, and P. S, "HYBRID GREY WOLF OPTIMIZATION-PATTERN SEARCH (hGWO-PS) OPTIMIZED 2DOF-PID CONTROLLERS FOR LOAD FREQUENCY CONTROL (LFC) IN INTERCONNECTED THERMAL POWER PLANTS," *ICTACT J. Soft Comput.*, vol. 06, no. 03, pp. 1244–1256, 2016, doi: 10.21917/ijsc.2016.0172.

[10] V. Soni, G. Parmar, and A. Sikander, "Hygwo-Ps Tuned Fopid for Agc of Three Area Interconnected Hydro-Thermal Power System," *Lect. Notes Electr. Eng.*, vol. 664, pp. 697–711, 2020, doi: 10.1007/978-981-15-5089-8_68.

[11] G. T. Chandra Sekhar, R. K. Sahu, A. K. Baliarsingh, and S. Panda, "Load frequency control of power system under deregulated environment using optimal firefly algorithm," *Int. J. Electr. Power Energy Syst.*, vol. 74, pp. 195–211, 2016, doi: 10.1016/j.ijepes.2015.07.025.

[12] D. K. Gupta, A. V. Jha, B. Appasani, A. Srinivasulu, N. Bizon, and P. Thounthong,

"Load frequency control using hybrid intelligent optimization technique for multi-source power systems," *Energies*, vol. 14, no. 6, 2021, doi: 10.3390/en14061581.

[13] D. K. Gupta *et al.*, "Hybrid Gravitational – Firefly Algorithm-Based Load Frequency Control for Hydrothermal Two-Area System," pp. 1–15, 2021.

[14] C. Pradhan and C. N. Bhende, "Online load frequency control in wind integrated power systems using modified Jaya optimization," *Eng. Appl. Artif. Intell.*, vol. 77, no. October 2018, pp. 212–228, 2019, doi: 10.1016/j.engappai.2018.10.003.

[15] A. Delassi, S. Arif, and L. Mokrani, "Load frequency control problem in interconnected power systems using robust fractional PIλD controller," *Ain Shams Eng. J.*, vol. 9, no. 1, pp. 77–88, 2018, doi: 10.1016/j.asej.2015.10.004.

[16] V. P. Singh, N. Kishor, and P. Samuel, "Distributed Multi-Agent System-Based Load Frequency Control for Multi-Area Power System in Smart Grid," *IEEE Trans. Ind. Electron.*, vol. 64, no. 6, pp. 5151–5160, 2017, doi: 10.1109/TIE.2017.2668983.

[17] P. N. Topno and S. Chanana, "Load frequency control of a two-area multi-source power system using a tilt integral derivative controller," *JVC/Journal Vib. Control*, vol. 24, no. 1, pp. 110–125, 2018, doi: 10.1177/1077546316634562.

[18] N. E. Y. Kouba, M. Menaa, M. Hasni, and M. Boudour, "A new optimal load frequency control based on hybrid genetic algorithm and particle swarm optimization," *Int. J. Electr. Eng. Informatics*, vol. 9, no. 3, pp. 418–440, 2017, doi: 10.15676/ijeei.2017.9.3.1.

[19] S. J. Safi, S. S. Tezcan, I. Eke, and Z. Farhad, "Gravitational search algorithm (GSA) based PID controller design for two area multi-source power system load frequency control (LFC)," *Gazi Univ. J. Sci.*, vol. 31, no. 1, pp. 139–153, 2018.

[20] B. S R and N. M S, "Load Frequency Control of Two-area Interconnected Power System Using Optimal Controller, PID Controller and Fuzzy Logic Controller," *Helix*, vol. 10, no. 3, pp. 30–35, 2020, doi: 10.29042/2020-10-3-30-35.

[21] D. Sambariya and V. Nath, "Load Frequency Control Using Fuzzy Logic Based Controller for Multi-area Power System," *Br. J. Math. Comput. Sci.*, vol. 13, no. 5, pp. 1–19, 2016, doi: 10.9734/bjmcs/2016/22899.

[22] S. Kamel, A. H. A. Elkasem, A. Korashy, and M. H. Ahmed, "Sine cosine algorithm for load frequency control design of two area interconnected power system with DFIG based wind turbine," *Proc. Int. Conf. Comput. Control. Electr. Electron. Eng. 2019, ICCCEEE 2019*, no. September 2019, 2019, doi: 10.1109/ICCCEEE46830.2019.9071208.

[23] K. Zare, M. T. Hagh, and J. Morsali, "Effective oscillation damping of an interconnected multi-source power system with automatic generation control and TCSC," *Int. J. Electr. Power Energy Syst.*, vol. 65, pp. 220–230, 2015, doi: 10.1016/j.ijepes.2014.10.009.

[24] Z. Farooq, A. Rahman, S. M. Suhail Hussain, and T. S. Ustun, "Power Generation Control of Renewable Energy Based Hybrid Deregulated Power System," *Energies*, vol. 15, no. 2, pp. 1–19, 2022, doi: 10.3390/en15020517.

[25] J. Morsali, K. Zare, and M. Tarafdar Hagh, "Performance comparison of TCSC with TCPS and SSSC controllers in AGC of realistic interconnected multi-source power system," *Ain Shams Eng. J.*, vol. 7, no. 1, pp. 143–158, 2016, doi:

10.1016/j.asej.2015.11.012.

[26] V. Donde, M. A. Pai, and I. A. Hiskens, "Simulation and optimization in an AGC system after deregulation," *IEEE Trans. Power Syst.*, vol. 16, no. 3, pp. 481–489, 2001, doi: 10.1109/59.932285.

[27] R. J. Abraham, D. Das, and A. Patra, "AGC System after Deregulation Considering TCPS in Series with the Tie-Line," vol. 16, no. 3, pp. 281–295, 2015, doi: 10.1515/ijeeps-2013-0165.

[28] R. K. Sahu, T. S. Gorripotu, and S. Panda, "Automatic generation control of multi-area power systems with diverse energy sources using Teaching Learning Based Optimization algorithm," *Eng. Sci. Technol. an Int. J.*, vol. 19, no. 1, pp. 113–134, 2016, doi: 10.1016/j.jestch.2015.07.011.

[29] K. Prabha, "[Prabha Kundur] Power System Stability and Control." p. 1176, 1994.

[30] A. Dokht Shakibjoo, M. Moradzadeh, S. Z. Moussavi, A. Mohammadzadeh, and L. Vandevelde, "Load frequency control for multi-area power systems: A new type-2 fuzzy approach based on Levenberg–Marquardt algorithm," *ISA Trans.*, vol. 121, no. xxxx, pp. 40–52, 2022, doi: 10.1016/j.isatra.2021.03.044.

[31] M. A. Sobhy, A. Y. Abdelaziz, H. M. Hasanien, and M. Ezzat, "Marine predators algorithm for load frequency control of modern interconnected power systems including renewable energy sources and energy storage units," *Ain Shams Eng. J.*, no. xxxx, 2021, doi: 10.1016/j.asej.2021.04.031.

[32] L. V. S. Kumar, D. V. N. Ananth, Y. V. P. Kumar, D. J. Pradeep, and C. P. Reddy, "Use of Super Conductor Magnetic Energy Storage System and FACTS Devices for Two-Area Load Frequency Control Having Synchronous Generators and DFIG Wind Generators."

[33] J. Mudi, "Frequency Stabilization of Solar Thermal-Photovoltaic Hybrid Renewable Power Generation Using Energy Storage Devices," *Iran. J. Sci. Technol. Trans. Electr. Eng.*, vol. 0123456789, 2020, doi: 10.1007/s40998-020-00374-w.

[34] P. Sanki, "Automatic Generation Control in Restructured Power System with Capacitive Energy Storage and Communication Delay Based Cascaded Controller," pp. 18–19, 2020.

[35] V. Vijayan, "Model-predictive control-based hybrid optimized load frequency control of multi-area power systems," no. December 2019, pp. 1521–1537, 2021, doi: 10.1049/gtd2.12119.

[36] K. Kalpana, M. M. T. Ansari, and C. Author, "FRACTIONAL ORDER FUZZY PID BASED PITCH CONTROLLER FOR ISOLATED HYBRID POWER SYSTEM WITH CES UNIT," vol. 11, no. 10, pp. 10–19, 2020, doi: 10.34218/IJEET.11.10.2020.002.

[37] K. Peddakapu, M. R. Mohamed, M. H. Sulaiman, P. Srinivasarao, A. S. Veerendra, and P. K. Leung, "Performance analysis of distributed power flow controller with ultra-capacitor for regulating the frequency deviations in restructured power system," *J. Energy Storage*, vol. 31, no. April, p. 101676, 2020, doi: 10.1016/j.est.2020.101676.

[38] A. Dutta and S. Prakash, "Load frequency control of multi-area hybrid power system integrated with renewable energy sources utilizing FACTS & energy storage system,"

Environ. Prog. Sustain. Energy, vol. 39, no. 2, pp. 1–13, 2020, doi: 10.1002/ep.13329.

[39] Y. Arya, "AGC of PV-thermal and hydro-thermal power systems using CES and a new multi-stage FPIDF-(1+PI) controller," *Renew. Energy*, vol. 134, pp. 796–806, 2019, doi: 10.1016/j.renene.2018.11.071.

[40] M. Ponnusamy, B. Banakara, S. S. Dash, and M. Veerasamy, "Design of integral controller for Load Frequency Control of Static Synchronous Series Compensator and Capacitive Energy Source based multi area system consisting of diverse sources of generation employing Imperialistic Competition Algorithm," *Int. J. Electr. Power Energy Syst.*, vol. 73, pp. 863–871, 2015, doi: 10.1016/j.ijepes.2015.06.019.

[41] S. Dhundhara and Y. P. Verma, "Capacitive energy storage with optimized controller for frequency regulation in realistic multisource deregulated power system," *Energy*, vol. 147, pp. 1108–1128, Mar. 2018, doi: 10.1016/j.energy.2018.01.076.

[42] R. K. Khadanga and A. Kumar, "Analysis of PID controller for the load frequency control of static synchronous series compensator and capacitive energy storage source-based multi-area multi-source interconnected power system with HVDC link," *Int. J. Bio-Inspired Comput.*, vol. 13, no. 2, pp. 131–139, 2019, doi: 10.1504/IJBIC.2019.098413.

[43] P. Bhatt, R. Roy, and S. P. Ghoshal, "GA/particle swarm intelligence based optimization of two specific varieties of controller devices applied to two-area multi-units automatic generation control," *Int. J. Electr. Power Energy Syst.*, vol. 32, no. 4, pp. 299–310, 2010, doi: 10.1016/j.ijepes.2009.09.004.

[44] T. Mahto and V. Mukherjee, "A novel scaling factor based fuzzy logic controller for frequency control of an isolated hybrid power system," *Energy*, vol. 130, pp. 339–350, 2017, doi: 10.1016/j.energy.2017.04.155.

[45] A. Pappachen and A. Peer Fathima, "Load frequency control in deregulated power system integrated with SMES-TCPS combination using ANFIS controller," *Int. J. Electr. Power Energy Syst.*, vol. 82, pp. 519–534, 2016, doi: 10.1016/j.ijepes.2016.04.032.

[46] S. Dhundhara and Y. P. Verma, "Evaluation of CES and DFIG unit in AGC of realistic multisource deregulated power system," *Int. Trans. Electr. Energy Syst.*, vol. 27, no. 5, pp. 1–14, 2017, doi: 10.1002/etep.2304.

[47] M. Aneke and M. Wang, "Energy storage technologies and real life applications – A state of the art review," *Appl. Energy*, vol. 179, pp. 350–377, 2016, doi: 10.1016/j.apenergy.2016.06.097.

[48] M. Farhadi Kangarlu and M. R. Alizadeh Pahlavani, "Cascaded multilevel converter based superconducting magnetic energy storage system for frequency control," *Energy*, vol. 70, pp. 504–513, 2014, doi: 10.1016/j.energy.2014.04.025.

[49] S. Chaine and M. Tripathy, "Design of an optimal SMES for automatic generation control of two-area thermal power system using Cuckoo search algorithm," *J. Electr. Syst. Inf. Technol.*, vol. 2, no. 1, pp. 1–13, 2015, doi: 10.1016/j.jesit.2015.03.001.

[50] R. K. Selvaraju and G. Somaskandan, "Impact of energy storage units on load frequency control of deregulated power systems," *Energy*, vol. 97, pp. 214–228, 2016, doi: 10.1016/j.energy.2015.12.121.

[51] I. A. Chidambaram and B. Paramasivam, “Optimized load-frequency simulation in restructured power system with Redox Flow Batteries and Interline Power Flow Controller,” *Int. J. Electr. Power Energy Syst.*, vol. 50, no. 1, pp. 9–24, 2013, doi: 10.1016/j.ijepes.2013.02.004.

[52] Y. Arya, “AGC performance enrichment of multi-source hydrothermal gas power systems using new optimized FOFPID controller and redox flow batteries,” *Energy*, vol. 127, pp. 704–715, 2017, doi: 10.1016/j.energy.2017.03.129.

[53] J. Jensen, *Energy storage*. 1980.

[54] R. Shankar, K. Chatterjee, and R. Bhushan, “Impact of energy storage system on load frequency control for diverse sources of interconnected power system in deregulated power environment,” *Int. J. Electr. Power Energy Syst.*, vol. 79, pp. 11–26, 2016, doi: 10.1016/j.ijepes.2015.12.029.

[55] I. Egido *et al.*, “Energy storage systems for frequency stability enhancement in small-isolated power systems,” *Renew. Energy Power Qual. J.*, vol. 1, no. 13, pp. 820–825, 2015, doi: 10.24084/repqj13.002.

[56] S. C. Tripathy, R. Balasubramanian, and P. S. Chandramohanan, “Small rating capacitive energy storage for dynamic performance improvement of automatic generation control,” *IEE Proc. C Gener. Transm. Distrib.*, vol. 138, no. 1, pp. 103–111, 1991, doi: 10.1049/ip-c.1991.0013.

[57] S. C. Tripathy and I. P. Mishra, “Dynamic performance of wind-diesel power system with capacitive energy storage,” *Energy Convers. Manag.*, vol. 37, no. 12, pp. 1787–1798, 1996, doi: 10.1016/0196-8904(96)00026-X.

[58] D. C. Das, A. K. Roy, and N. Sinha, “GA based frequency controller for solar thermal-diesel-wind hybrid energy generation/energy storage system,” *Int. J. Electr. Power Energy Syst.*, vol. 43, no. 1, pp. 262–279, 2012, doi: 10.1016/j.ijepes.2012.05.025.

[59] P. K. Pathak, A. K. Yadav, A. Shastri, and P. A. Alvi, “BWOA assisted PIDF-(1+I) controller for intelligent load frequency management of standalone micro-grid,” *ISA Trans.*, no. June, 2022, doi: 10.1016/j.isatra.2022.06.010.

[60] B. Dekaraja, L. C. Saikia, and N. R. Babu, “Redox Flow Battery Support for Combined ALFC-AVR Control of Multiarea Thermal System Incorporating Renewable Energy Sources,” no. February, pp. 97–110, 2022, doi: 10.1007/978-981-16-6893-7_10.

[61] S. K. Ramoji and L. C. Saikia, “ Utilization of Electric Vehicles in combined voltage-frequency control of multi-area thermal-CCGT system using 2DOFTID controller ,” *Energy Storage*, no. February, pp. 1–20, 2021, doi: 10.1002/est2.234.

[62] E. M. Ahmed, E. A. Mohamed, A. Elmelegi, M. Aly, and O. Elbaksawi, “Optimum Modified Fractional Order Controller for Future Electric Vehicles and Renewable Energy-based Interconnected Power Systems,” *IEEE Access*, vol. 9, pp. 1–1, 2021, doi: 10.1109/access.2021.3058521.

[63] A. Oshnoei, R. Khezri, S. M. Muyeen, S. Oshnoei, and F. Blaabjerg, “Automatic Generation Control Incorporating Electric Vehicles,” *Electr. Power Components Syst.*, vol. 47, no. 8, pp. 678–690, 2019, doi: 10.1080/15325008.2019.1579270.

[64] P. Gaur, D. Bhowmik, and N. Soren, “Utilisation of plug-in electric vehicles for frequency regulation of multi-area thermal interconnected power system,” *IET Energy*

Syst. Integr., vol. 1, no. 2, pp. 88–96, 2019, doi: 10.1049/iet-esi.2018.0028.

[65] A. Oshnoei, M. T. Hagh, R. Khezri, and B. Mohammadi-Ivatloo, "Application of IPSO and fuzzy logic methods in electrical vehicles for efficient frequency control of multi-area power systems," *2017 25th Iran. Conf. Electr. Eng. ICEE 2017*, no. May, pp. 1349–1354, 2017, doi: 10.1109/IranianCEE.2017.7985251.

[66] H. Abubakr, T. H. Mohamed, M. M. Hussein, J. M. Guerrero, and G. Agundis-Tinajero, "Adaptive frequency regulation strategy in multi-area microgrids including renewable energy and electric vehicles supported by virtual inertia," *Int. J. Electr. Power Energy Syst.*, vol. 129, no. January, p. 106814, 2021, doi: 10.1016/j.ijepes.2021.106814.

[67] A. Dutta and S. Prakash, "Utilizing Electric Vehicles and Renewable Energy Sources for Load Frequency Control in Deregulated Power System Using Emotional Controller," *IETE J. Res.*, vol. 0, no. 0, pp. 1–12, 2019, doi: 10.1080/03772063.2019.1654936.

[68] P. Gaur, N. Soren, and D. Bhowmik, "Secondary frequency regulation of multi-area interconnected hybrid power system with electric vehicle," *Int. J. Electr. Eng. Informatics*, vol. 10, no. 4, pp. 738–752, 2018, doi: 10.15676/ijeei.2018.10.4.8.

[69] W. Kempton and J. Tomić, "Vehicle-to-grid power implementation: From stabilizing the grid to supporting large-scale renewable energy," *J. Power Sources*, vol. 144, no. 1, pp. 280–294, 2005, doi: 10.1016/j.jpowsour.2004.12.022.

[70] L. Ramírez Elizondo, P. Bauer, S. Izadkhast, P. Frías, and P. Garcia Gonzalez, "Evaluation of Aggregate Models of Plug-in Electric Vehicles for Primary Frequency Control," *Int. J. Automot. Technol. Manag.*, vol. 18, no. 3, p. 1, 2018, doi: 10.1504/ijatm.2018.10013218.

[71] J. Tomić and W. Kempton, "Using fleets of electric-drive vehicles for grid support," *J. Power Sources*, vol. 168, no. 2, pp. 459–468, 2007, doi: 10.1016/j.jpowsour.2007.03.010.

[72] A. Anand, P. Aryan, N. Kumari, and G. L. Raja, "Type-2 fuzzy-based branched controller tuned using arithmetic optimizer for load frequency control," *Energy Sources, Part A Recover. Util. Environ. Eff.*, vol. 44, no. 2, pp. 4575–4596, 2022, doi: 10.1080/15567036.2022.2078444.

[73] D. Khamari, R. K. Sahu, and S. Panda, "Adaptive differential evolution based PDF plus (1+PI) controller for frequency regulation of the distributed power generation system with electric vehicle," *Int. J. Ambient Energy*, vol. 43, no. 1, pp. 3040–3054, 2022, doi: 10.1080/01430750.2020.1783357.

[74] A. B. Krishna, S. Saxena, V. K. Kamboj, and C. Verma, "A memetic metaheuristics search algorithm for load frequency regulation in multi area power system," *2020 Int. Conf. Decis. Aid Sci. Appl. DASA 2020*, pp. 163–167, 2020, doi: 10.1109/DASA51403.2020.9317189.

[75] X. Yang and L. Press, *Nature-Inspired Metaheuristic Algorithms Second Edition*. .

[76] S. Li, H. Chen, M. Wang, A. A. Heidari, and S. Mirjalili, "Slime mould algorithm: A new method for stochastic optimization," *Futur. Gener. Comput. Syst.*, vol. 111, pp. 300–323, Oct. 2020, doi: 10.1016/j.future.2020.03.055.

[77] Y. Liu and R. Li, "PSA : A Photon Search Algorithm," vol. 16, no. 2, pp. 478–493, 2020.

[78] R. Storn and K. Price, “Differential Evolution - A Simple and Efficient Heuristic for Global Optimization over Continuous Spaces,” *J. Glob. Optim.*, 1997, doi: 10.1023/A:1008202821328.

[79] S. Kaur, L. K. Awasthi, A. L. Sangal, and G. Dhiman, “Tunicate Swarm Algorithm: A new bio-inspired based metaheuristic paradigm for global optimization,” *Eng. Appl. Artif. Intell.*, vol. 90, no. September, p. 103541, 2020, doi: 10.1016/j.engappai.2020.103541.

[80] S. Mirjalili, S. M. Mirjalili, and A. Lewis, “Grey Wolf Optimizer,” *Adv. Eng. Softw.*, vol. 69, pp. 46–61, 2014, doi: 10.1016/j.advengsoft.2013.12.007.

[81] S. Mirjalili, “SCA: A Sine Cosine Algorithm for solving optimization problems,” *Knowledge-Based Syst.*, vol. 96, pp. 120–133, 2016, doi: 10.1016/j.knosys.2015.12.022.

[82] E. Rashedi, H. Nezamabadi-pour, and S. Saryazdi, “GSA: A Gravitational Search Algorithm,” *Inf. Sci. (Ny).*, vol. 179, no. 13, pp. 2232–2248, 2009, doi: 10.1016/j.ins.2009.03.004.

[83] Q. Askari, I. Younas, and M. Saeed, “Political Optimizer: A novel socio-inspired meta-heuristic for global optimization,” *Knowledge-Based Syst.*, 2020, doi: 10.1016/j.knosys.2020.105709.

[84] D. Karaboga and B. Basturk, “A powerful and efficient algorithm for numerical function optimization: Artificial bee colony (ABC) algorithm,” *J. Glob. Optim.*, 2007, doi: 10.1007/s10898-007-9149-x.

[85] A. A. Heidari, S. Mirjalili, H. Faris, I. Aljarah, M. Mafarja, and H. Chen, “Harris hawks optimHization : Algorithm and applications,” no. March, 2019, doi: 10.1016/j.future.2019.02.028.

[86] J. J. Q. Yu and V. O. K. Li, “A social spider algorithm for global optimization,” *Appl. Soft Comput. J.*, 2015, doi: 10.1016/j.asoc.2015.02.014.

[87] G. Dhiman, M. Garg, A. Nagar, V. Kumar, and M. Dehghani, “A novel algorithm for global optimization: Rat Swarm Optimizer,” *J. Ambient Intell. Humaniz. Comput.*, no. 0123456789, 2020, doi: 10.1007/s12652-020-02580-0.

[88] T. Rahkar Farshi, “Battle royale optimization algorithm,” *Neural Comput. Appl.*, vol. 4, 2020, doi: 10.1007/s00521-020-05004-4.

[89] A. Tabari and A. Ahmad, “A new optimization method: Electro-Search algorithm,” *Comput. Chem. Eng.*, vol. 103, pp. 1–11, 2017, doi: 10.1016/j.compchemeng.2017.01.046.

[90] M. D. Li, H. Zhao, X. W. Weng, and T. Han, “A novel nature-inspired algorithm for optimization: Virus colony search,” *Adv. Eng. Softw.*, vol. 92, pp. 65–88, 2016, doi: 10.1016/j.advengsoft.2015.11.004.

[91] M. H. Qais, H. M. Hasanien, and S. Alghuwainem, “Transient search optimization: a new meta-heuristic optimization algorithm,” *Appl. Intell.*, 2020, doi: 10.1007/s10489-020-01727-y.

[92] S. Mirjalili, S. M. Mirjalili, and A. Hatamlou, “Multi-Verse Optimizer: a nature-inspired algorithm for global optimization,” *Neural Comput. Appl.*, vol. 27, no. 2, pp. 495–513, 2016, doi: 10.1007/s00521-015-1870-7.

[93] A. Kaveh and S. Talatahari, “A novel heuristic optimization method: Charged system search,” *Acta Mech.*, 2010, doi: 10.1007/s00707-009-0270-4.

[94] M. M. Fouad, A. I. El-Desouky, R. Al-Hajj, and E. S. M. El-Kenawy, “Dynamic Group-Based Cooperative Optimization Algorithm,” *IEEE Access*, vol. 8, pp. 148378–148403, 2020, doi: 10.1109/ACCESS.2020.3015892.

[95] A. Kaveh, M. Khanzadi, and M. Rastegar Moghaddam, “Billiards-inspired optimization algorithm; a new meta-heuristic method,” *Structures*, vol. 27, no. July, pp. 1722–1739, 2020, doi: 10.1016/j.istruc.2020.07.058.

[96] H. Abedinpourshotorban, S. Mariyam Shamsuddin, Z. Beheshti, and D. N. A. Jawawi, “Electromagnetic field optimization: A physics-inspired metaheuristic optimization algorithm,” *Swarm Evol. Comput.*, vol. 26, 2016, doi: 10.1016/j.swevo.2015.07.002.

[97] R. V. Rao, V. J. Savsani, and D. P. Vakharia, “Teaching-Learning-Based Optimization: An optimization method for continuous non-linear large scale problems,” *Inf. Sci. (Ny).*, vol. 183, no. 1, pp. 1–15, 2012, doi: 10.1016/j.ins.2011.08.006.

[98] E. H. Houssein, M. R. Saad, F. A. Hashim, H. Shaban, and M. Hassaballah, “Lévy flight distribution: A new metaheuristic algorithm for solving engineering optimization problems,” *Eng. Appl. Artif. Intell.*, vol. 94, no. April, 2020, doi: 10.1016/j.engappai.2020.103731.

[99] I. Ahmadianfar, O. Bozorg-Haddad, and X. Chu, “Gradient-based optimizer: A new metaheuristic optimization algorithm,” *Inf. Sci. (Ny).*, vol. 540, pp. 131–159, 2020, doi: 10.1016/j.ins.2020.06.037.

[100] Fred Glover, “Tabu Search - Part I,” *Orsa J. Comput.*, vol. 1, no. 3, pp. 190–206, 1989.

[101] X. Yao, Y. Liu, and G. Lin, “Evolutionary Programming Made Faster,” vol. 3, no. 2, pp. 82–102, 1999.

[102] S. Mirjalili, “Moth-flame optimization algorithm: A novel nature-inspired heuristic paradigm,” *Knowledge-Based Syst.*, vol. 89, no. July, pp. 228–249, 2015, doi: 10.1016/j.knosys.2015.07.006.

[103] Z. W. Geem, J. H. Kim, and G. V. Loganathan, “A New Heuristic Optimization Algorithm: Harmony Search,” *Simulation*, vol. 76, no. 2, pp. 60–68, 2001, doi: 10.1177/003754970107600201.

[104] S. He, Q. H. Wu, and J. R. Saunders, “Group search optimizer: An optimization algorithm inspired by animal searching behavior,” *IEEE Trans. Evol. Comput.*, 2009, doi: 10.1109/TEVC.2009.2011992.

[105] J. H. Holland, “Genetic algorithms,” *Sci. Am.*, vol. 267, no. 1, pp. 66–72, 1992, doi: 10.1038/scientificamerican0792-66.

[106] W. T. Pan, “A new Fruit Fly Optimization Algorithm: Taking the financial distress model as an example,” *Knowledge-Based Syst.*, vol. 26, pp. 69–74, 2012, doi: 10.1016/j.knosys.2011.07.001.

[107] J. Kennedy and R. Eberhart, “Particle swarm optimization,” 1995.

[108] A. H. Gandomi, “Interior search algorithm (ISA): A novel approach for global optimization,” *ISA Trans.*, vol. 53, no. 4, pp. 1168–1183, 2014, doi:

10.1016/j.isatra.2014.03.018.

[109] D. Simon, “Biogeography-based optimization,” *IEEE Trans. Evol. Comput.*, vol. 12, no. 6, pp. 702–713, 2008, doi: 10.1109/TEVC.2008.919004.

[110] X. Li, J. Zhang, and M. Yin, “Animal migration optimization: An optimization algorithm inspired by animal migration behavior,” *Neural Comput. Appl.*, vol. 24, no. 7–8, pp. 1867–1877, 2014, doi: 10.1007/s00521-013-1433-8.

[111] R. A. Formato, “Central force optimization: A new metaheuristic with applications in applied electromagnetics,” *Prog. Electromagn. Res.*, 2007, doi: 10.2528/PIER07082403.

[112] M. S. Kiran, “TSA: Tree-seed algorithm for continuous optimization,” *Expert Syst. Appl.*, 2015, doi: 10.1016/j.eswa.2015.04.055.

[113] H. Salimi, “Stochastic Fractal Search: A powerful metaheuristic algorithm,” *Knowledge-Based Syst.*, vol. 75, pp. 1–18, 2015, doi: 10.1016/j.knosys.2014.07.025.

[114] F. L. Howard, “ the Life History of Physarum Polycephalum ,” *Am. J. Bot.*, vol. 18, no. 2, pp. 116–133, 1931, doi: 10.1002/j.1537-2197.1931.tb09577.x.

[115] S. Mirjalili and A. Lewis, “The Whale Optimization Algorithm,” *Adv. Eng. Softw.*, vol. 95, pp. 51–67, 2016, doi: 10.1016/j.advengsoft.2016.01.008.

[116] A. Kaveh and A. Dadras Eslamlou, “Water strider algorithm: A new metaheuristic and applications,” *Structures*, vol. 25, no. March, pp. 520–541, 2020, doi: 10.1016/j.istruc.2020.03.033.

[117] S. Saremi, S. Mirjalili, and A. Lewis, “Grasshopper Optimisation Algorithm: Theory and application,” *Adv. Eng. Softw.*, 2017, doi: 10.1016/j.advengsoft.2017.01.004.

[118] S. Mirjalili, A. H. Gandomi, S. Z. Mirjalili, S. Saremi, H. Faris, and S. M. Mirjalili, “Salp Swarm Algorithm: A bio-inspired optimizer for engineering design problems,” *Adv. Eng. Softw.*, 2017, doi: 10.1016/j.advengsoft.2017.07.002.

[119] H. Eskandar, A. Sadollah, A. Bahreininejad, and M. Hamdi, “Water cycle algorithm - A novel metaheuristic optimization method for solving constrained engineering optimization problems,” *Comput. Struct.*, vol. 110–111, pp. 151–166, 2012, doi: 10.1016/j.compstruc.2012.07.010.

[120] A. H. Gandomi and X. S. Yang, “Benchmark problems in structural optimization,” *Stud. Comput. Intell.*, 2011, doi: 10.1007/978-3-642-20859-1_12.

[121] E. Mezura-Montes and C. A. Coello Coello, “Useful infeasible solutions in engineering optimization with evolutionary algorithms,” 2005, doi: 10.1007/11579427_66.

[122] F. A. Hashim, E. H. Houssein, M. S. Mabrouk, W. Al-Atabany, and S. Mirjalili, “Henry gas solubility optimization: A novel physics-based algorithm,” *Futur. Gener. Comput. Syst.*, vol. 101, pp. 646–667, 2019, doi: 10.1016/j.future.2019.07.015.

[123] G. Dhiman and V. Kumar, “Spotted hyena optimizer: A novel bio-inspired based metaheuristic technique for engineering applications,” *Adv. Eng. Softw.*, vol. 114, pp. 48–70, 2017, doi: 10.1016/j.advengsoft.2017.05.014.

[124] L. C. Cagnina, S. C. Esquivel, and C. A. C. Coello, “Solving engineering optimization problems with the simple constrained particle swarm optimizer,” *Bioinspired Optim.*

Methods their Appl. - Proc. 3rd Int. Conf. Bioinspired Optim. Methods their Appl. BIOMA 2008, no. May 2014, pp. 107–120, 2008.

[125] M. Dorigo, M. Birattari, and T. Stutzle, "Ant colony optimization," *IEEE Comput. Intell. Mag.*, vol. 1, no. 4, pp. 28–39, 2006, doi: 10.1109/MCI.2006.329691.

[126] S. Virmani, E. Adrian, … K. I.-I. T. on, and undefined 1989, "Implementation of a Lagrangian relaxation based unit commitment problem," *ieeexplore.ieee.org*.

[127] A. I. Cohen and M. Yoshimura, "A Branch-and-Bound Algorithm for Unit Commitment," *IEEE Trans. Power Appar. Syst.*, vol. 102, no. 2, pp. 444–451, 1983.

[128] A. Sadollah, A. Bahreininejad, H. Eskandar, and M. Hamdi, "Mine blast algorithm: A new population based algorithm for solving constrained engineering optimization problems," *Appl. Soft Comput. J.*, vol. 13, no. 5, pp. 2592–2612, 2013, doi: 10.1016/j.asoc.2012.11.026.

[129] T. Le-Duc, Q. H. Nguyen, and H. Nguyen-Xuan, "Balancing composite motion optimization," *Inf. Sci. (Ny).*, vol. 520, pp. 250–270, May 2020, doi: 10.1016/j.ins.2020.02.013.

[130] P. Savsani and V. Savsani, "Passing vehicle search (PVS): A novel metaheuristic algorithm," *Appl. Math. Model.*, vol. 40, no. 5–6, pp. 3951–3978, 2016, doi: 10.1016/j.apm.2015.10.040.

[131] E. Cuevas and A. Echavarría, "An optimization algorithm inspired by the States of Matter that improves the balance between exploration and exploitation," 2013, doi: 10.1007/s10489-013-0458-0.

[132] M. Y. Cheng and D. Prayogo, "Symbiotic Organisms Search: A new metaheuristic optimization algorithm," *Comput. Struct.*, 2014, doi: 10.1016/j.compstruc.2014.03.007.

[133] S. K., "The method of moving asymptotes - a new method for structural optimization," *Int. J. Numer. Methods Eng.*, vol. 24, no. October 1985, pp. 359–373, 1987.

[134] A. H. Gandomi, X. S. Yang, and A. H. Alavi, "Cuckoo search algorithm: A metaheuristic approach to solve structural optimization problems," *Eng. Comput.*, vol. 29, no. 1, pp. 17–35, 2013, doi: 10.1007/s00366-011-0241-y.

[135] V. K. Kamboj, A. Bhadoria, and N. Gupta, "A Novel Hybrid GWO-PS Algorithm for Standard Benchmark Optimization Problems," *Ina. Lett.*, vol. 3, no. 4, pp. 217–241, Dec. 2018, doi: 10.1007/s41403-018-0051-2.

[136] V. K. Kamboj, "A novel hybrid PSO – GWO approach for unit commitment problem," *Neural Comput. Appl.*, 2015, doi: 10.1007/s00521-015-1962-4.

[137] N. Singh and S. B. Singh, "A novel hybrid GWO-SCA approach for optimization problems," *Eng. Sci. Technol. an Int. J.*, vol. 20, no. 6, pp. 1586–1601, Dec. 2017, doi: 10.1016/j.jestch.2017.11.001.

[138] Z. Gao, J. Zhao, and S. Li, "The hybridized slime mould and particle swarm optimization algorithms," *2020 IEEE 3rd Int. Conf. Autom. Electron. Electr. Eng. AUTEEE 2020*, pp. 304–308, 2020, doi: 10.1109/AUTEEE50969.2020.9315694.

[139] H. Liu, Z. Cai, and Y. Wang, "Hybridizing particle swarm optimization with differential evolution for constrained numerical and engineering optimization," *Appl. Soft Comput.*

J., 2010, doi: 10.1016/j.asoc.2009.08.031.

[140] G. Dhiman, *ESA: a hybrid bio-inspired metaheuristic optimization approach for engineering problems*, no. September. Springer London, 2019.

[141] D. Dhawale and V. K. Kamboj, "hHHO-IGWO: A New Hybrid Harris Hawks Optimizer for Solving Global Optimization Problems," in *2020 International Conference on Computation, Automation and Knowledge Management (ICCAKM)*, Jan. 2020, pp. 52–57, doi: 10.1109/ICCAKM46823.2020.9051509.

[142] F. Wahid and R. Ghazali, "Hybrid of firefly algorithm and pattern search for solving optimization problems," *Evol. Intell.*, vol. 12, no. 1, p. 0, 2019, doi: 10.1007/s12065-018-0165-1.

[143] Z. Gao, J. Zhao, Y. Yang, and X. Tian, "The hybrid grey wolf optimization-slime mould algorithm," 2020, doi: 10.1088/1742-6596/1617/1/012034.

[144] S. N. Chegini, A. Bagheri, and F. Najafi, "PSOSCALF: A new hybrid PSO based on Sine Cosine Algorithm and Levy flight for solving optimization problems," *Appl. Soft Comput. J.*, vol. 73, pp. 697–726, 2018, doi: 10.1016/j.asoc.2018.09.019.

[145] M. Abdel-Basset, V. Chang, and R. Mohamed, "HSMA_WOA: A hybrid novel Slime mould algorithm with whale optimization algorithm for tackling the image segmentation problem of chest X-ray images," *Appl. Soft Comput. J.*, vol. 95, p. 106642, 2020, doi: 10.1016/j.asoc.2020.106642.

[146] Z. Xu *et al.*, "Orthogonally-designed adapted grasshopper optimization: A comprehensive analysis," *Expert Syst. Appl.*, vol. 150, p. 113282, 2020, doi: https://doi.org/10.1016/j.eswa.2020.113282.

[147] D. A. Muhammed, S. A. M. Saeed, and T. A. Rashid, "Improved Fitness-Dependent Optimizer Algorithm," *IEEE Access*, vol. 8, pp. 19074–19088, 2020, doi: 10.1109/ACCESS.2020.2968064.

[148] X. Chen, H. Tianfield, and K. Li, "Self-adaptive differential artificial bee colony algorithm for global optimization problems," *Swarm Evol. Comput.*, vol. 45, pp. 70–91, 2019, doi: https://doi.org/10.1016/j.swevo.2019.01.003.

[149] S. [Mostafa Bozorgi] and S. Yazdani, "IWOA: An improved whale optimization algorithm for optimization problems," *J. Comput. Des. Eng.*, vol. 6, no. 3, pp. 243–259, 2019, doi: https://doi.org/10.1016/j.jcde.2019.02.002.

[150] B. Xiao, R. Wang, Y. Xu, J. Wang, W. Song, and Y. Deng, "Simplified Salp Swarm Algorithm," in *2019 IEEE International Conference on Artificial Intelligence and Computer Applications (ICAICA)*, Mar. 2019, pp. 226–230, doi: 10.1109/ICAICA.2019.8873515.

[151] W. Zhao, L. Wang, and Z. Zhang, "Artificial ecosystem-based optimization: a novel nature-inspired meta-heuristic algorithm," *Neural Comput. Appl.*, 2019, doi: 10.1007/s00521-019-04452-x.

[152] M. Shahrouzi and A. Salehi, "IMPERIALIST COMPETITIVE LEARNER-BASED OPTIMIZATION: A HYBRID METHOD TO SOLVE ENGINEERING PROBLEMS," *Int. J. Optim. Civ. Eng.*, vol. 10, no. 1, 2020.

[153] A. Yimit, K. Iigura, and Y. Hagihara, "Refined selfish herd optimizer for global

optimization problems," *Expert Syst. Appl.*, vol. 139, p. 112838, 2020, doi: https://doi.org/10.1016/j.eswa.2019.112838.

[154] N. Banerjee and S. Mukhopadhyay, "HC-PSOGWO: Hybrid Crossover Oriented PSO and GWO based Co-Evolution for Global optimization," in *2019 IEEE Region 10 Symposium (TENSYMP)*, Jun. 2019, pp. 162–167, doi: 10.1109/TENSYMP46218.2019.8971231.

[155] H. Chen, M. Wang, and X. Zhao, "A multi-strategy enhanced sine cosine algorithm for global optimization and constrained practical engineering problems," *Appl. Math. Comput.*, vol. 369, p. 124872, 2020, doi: https://doi.org/10.1016/j.amc.2019.124872.

[156] A. Seyyedabbasi and F. Kiani, "I-GWO and Ex-GWO: improved algorithms of the Grey Wolf Optimizer to solve global optimization problems," *Eng. Comput.*, no. 0123456789, 2019, doi: 10.1007/s00366-019-00837-7.

[157] G. G. Tejani, S. Kumar, and A. H. Gandomi, "Multi-objective heat transfer search algorithm for truss optimization," *Eng. Comput.*, 2019, doi: 10.1007/s00366-019-00846-6.

[158] A. Bala Krishna, S. Saxena, and V. K. Kamboj, *hSMA-PS: a novel memetic approach for numerical and engineering design challenges*, no. 0123456789. Springer London, 2021.

[159] A. B. Krishna, S. Saxena, and V. K. Kamboj, "A novel statistical approach to numerical and multidisciplinary design optimization problems using pattern search inspired Harris hawks optimizer," *Neural Comput. Appl.*, 2021, doi: 10.1007/s00521-020-05475-5.

[160] A. Kaveh and M. Ilchi Ghazaan, "Enhanced colliding bodies optimization for design problems with continuous and discrete variables," *Adv. Eng. Softw.*, vol. 77, pp. 66–75, 2014, doi: 10.1016/j.advengsoft.2014.08.003.

[161] A. Wunnava, M. Kumar Naik, R. Panda, B. Jena, and A. Abraham, "A differential evolutionary adaptive Harris hawks optimization for two dimensional practical Masi entropy-based multilevel image thresholding," *J. King Saud Univ. - Comput. Inf. Sci.*, no. xxxx, 2020, doi: 10.1016/j.jksuci.2020.05.001.

[162] V. K. Kamboj, A. Nandi, A. Bhadoria, and S. Sehgal, "An intensify Harris Hawks optimizer for numerical and engineering optimization problems," *Appl. Soft Comput. J.*, vol. 89, p. 106018, 2020, doi: 10.1016/j.asoc.2019.106018.

[163] A. K. Bohre, G. Agnihotri, and M. Dubey, "The Butterfly-Particle Swarm Optimization (Butterfly-PSO/BF-PSO) Technique and Its Variables," *Int. J. Soft Comput. Math. Control*, vol. 4, no. 3, pp. 23–39, 2015, doi: 10.14810/ijscmc.2015.4302.

[164] A. Bhadoria and V. K. Kamboj, "Optimal generation scheduling and dispatch of thermal generating units considering impact of wind penetration using hGWO-RES algorithm," *Appl. Intell.*, 2019, doi: 10.1007/s10489-018-1325-9.

[165] M. Wang, A. A. Heidari, M. Chen, H. Chen, X. Zhao, and X. Cai, "Exploratory Differential Ant Lion-based Optimization," *Expert Syst. Appl.*, p. 113548, 2020, doi: 10.1016/j.eswa.2020.113548.

[166] Z. Wang, Q. Luo, and Y. Zhou, *Hybrid metaheuristic algorithm using butterfly and flower pollination base on mutualism mechanism for global optimization problems*, no. 0123456789. Springer London, 2020.

[167] S. Gupta, K. Deep, S. Mirjalili, and J. H. Kim, “A modified Sine Cosine Algorithm with novel transition parameter and mutation operator for global optimization,” *Expert Syst. Appl.*, vol. 154, p. 113395, 2020, doi: 10.1016/j.eswa.2020.113395.

[168] K. Deb and M. Goyal, “A combined genetic adaptive search (GeneAS) for engineering design,” *Comput. Sci. Informatics*, 1996, doi: citeulike-article-id:9625478.

[169] H. Chen, Y. Xu, M. Wang, and X. Zhao, “A balanced whale optimization algorithm for constrained engineering design problems,” *Appl. Math. Model.*, vol. 71, pp. 45–59, 2019, doi: 10.1016/j.apm.2019.02.004.

[170] N. Hansen, S. D. Müller, and P. Koumoutsakos, “Reducing the time complexity of the derandomized evolution strategy with covariance matrix adaptation (CMA-ES),” *Evol. Comput.*, vol. 11, no. 1, pp. 1–18, 2003, doi: 10.1162/106365603321828970.